Phase unbalance on low-voltage electricity networks and its mitigation using static balancers

by

Shiva Beharrysingh

A Doctoral Thesis submitted in partial fulfilment of the requirements for the award of the degree of
Doctor of Philosophy (PhD), at Loughborough University.

31st March, 2014.

CREST (Centre for Renewable Energy Systems Technology),
School of Electronic, Electrical and Systems Engineering,
Loughborough University, Loughborough,
Leicestershire, United Kingdom, LE11 3TU.

CERTIFICATE OF ORIGINALITY

This is to certify that I am responsible for the work submitted in this thesis, that the original work is my own except as specified in acknowledgements or in footnotes, and that neither the thesis nor the original work contained therein has been submitted to this or any other institution for a degree.

……. Shiva Beharrysingh ……. (Signed)

……. 31st March, 2014 ……. (Date)

I. Abstract

Existing low-voltage networks may not accommodate high penetrations of low-carbon technologies. The topic of this thesis is unbalance, which if minimised can delay or avoid the constraining of these technologies or the replacing of still-useful network assets.

Most of the discussion on unbalance, as seen in the standards and the literature, centres on the effects of voltage unbalance on consumer equipment. Its effects on the network are not equally reported. This thesis recognises fundamental differences between the consumer and network perspectives. It can inform distribution network operators on the interpretation of measurements taken on low-voltage networks and guide research on unbalance due to high penetrations of low-carbon technologies.

Much of the work involved simulations of LV networks. Initially, existing 3 x 3 or 5 x 5 approaches to the forward-backward sweep method were thought suitable. After a review of these approaches however, there were doubts as to how accurately they accounted for the shared neutral-earth return path on which the out-of-balance current flows. This led to the derivation of a new 5 x 5 approach using only Kirchhoff's voltage (KVL) and current laws (KCL). Its results are validated thoroughly in the thesis. In addition to satisfying KVL and KCL, they match Matlab SimPowerSystems exactly and are in close agreement with measurements taken on a very unbalanced rural feeder.

This thesis also investigates the mitigation of unbalance using the static balancer. This is a transformer with a single interconnected-star winding. It was used in 1930-1950s to correct unbalance. Contributions are made for its possible re-introduction as a retrofit option. They include a model for use in the forward-backward sweep method, validated by laboratory and field measurements, and the quantification of the static balancer's strengths and weaknesses as this can help identify when it should be used.

Key Words : Current unbalance, Voltage unbalance, forward-backward sweep method, static balancer, low-voltage electricity networks, low-carbon technologies.

II. Table of Contents

III. Acknowledgements

I wish to express my sincere gratitude to my supervisor, Murray Thomson at CREST, Loughborough University, for his excellent guidance, support and encouragement throughout this thesis. During our meetings and discussions you have shown how to supervise and encourage an engineer in research, and I am very grateful for this experience and hope to someday do the same.

I am also very grateful for the guidance and support of my industrial supervisors - Richard Hair (E.ON), Robert Ferris (formerly at Western Power Distribution), Steven Burns, Nigel Johnson and Philip Bale at Western Power Distribution. I also very much appreciated the support of Colin Archer at The Transformer and Electrical Co Ltd.

Very special thanks to Ryan Kavanagh and Dean Allen at E.ON for their support in the field trial.

I would also like to thank my colleagues at CREST, especially Andrew Urquhart and Ian Richardson. I also thank Nathan Oliver-Taylor for assisting in the laboratory experiments.

I am very grateful to be blessed with a supporting and understanding family. To my mother Ranouka, my late father Kenty and my brother Brahma - thank you for your love and support throughout these years, it has sustained me through both masters and this PhD thesis. This thesis is dedicated to my loving family.

This work was financially supported by Western Power Distribution, E.ON Engineering Ltd and the Engineering and Physical Sciences Research Council, UK, within the SUPERGEN Highly Distributed Energy Futures (HiDEF) project (EP/G031681/1).

Shiva Beharrysingh
March 2014.

IV. List of figures

V. List of tables

VI. List of abbreviations

ABC	Aerial Bundled Conductors
AVR	Automatic Voltage Regulator
BST	British Summer Time
DAQ	Data Acquisition Card
EV	Electric Vechicle
GMT	Greenwich Mean Time
HRT	Harmonic Rejection Transformers
HV	High Voltage
IUF	Current Unbalance Factor
KCL	Kirchhoff's Current Law
KVL	Kirchhoff's Voltage Law
LBT	Load Balancing Transformer
LV	Low Voltage
LVUR	Line Voltage Unbalance Ratio
MCB	Main Circuit Breaker
μCHP	Micro-Combined Heat and Power
MEB	Midlands Electricity Board
NCT	Neutral Current Trap
NU	Network Utilisation
OLTC	On-Load Tap Changer
PCC	Point of Common Coupling
pf	Power Factor
PME	Protective Multiple Earth
PRCC	Potential Released Current Capacity
PV	Solar Photovoltaic
PVUR	Phase Voltage Unbalance Ratio
RCD	Residual Current Device
THD	Total Harmonic Distortion
VR	Voltage Regulation
VUF	Voltage Unbalance Factor

1. Introduction

1.1 Unbalance and the low-voltage electricity network

The typical low-voltage distribution feeder in the UK supplies mostly single-phase consumers and has a three-phase, four-wire design with a multi-grounded neutral [1]. The unequal distribution of these consumers amongst the three phases along with variations in their individual consumer demands, results in unequal phase currents on the low-voltage network. This is called “current unbalance”. If significant, this current unbalance can result in several problems as illustrated in Figure 1.1, including voltage unbalance.

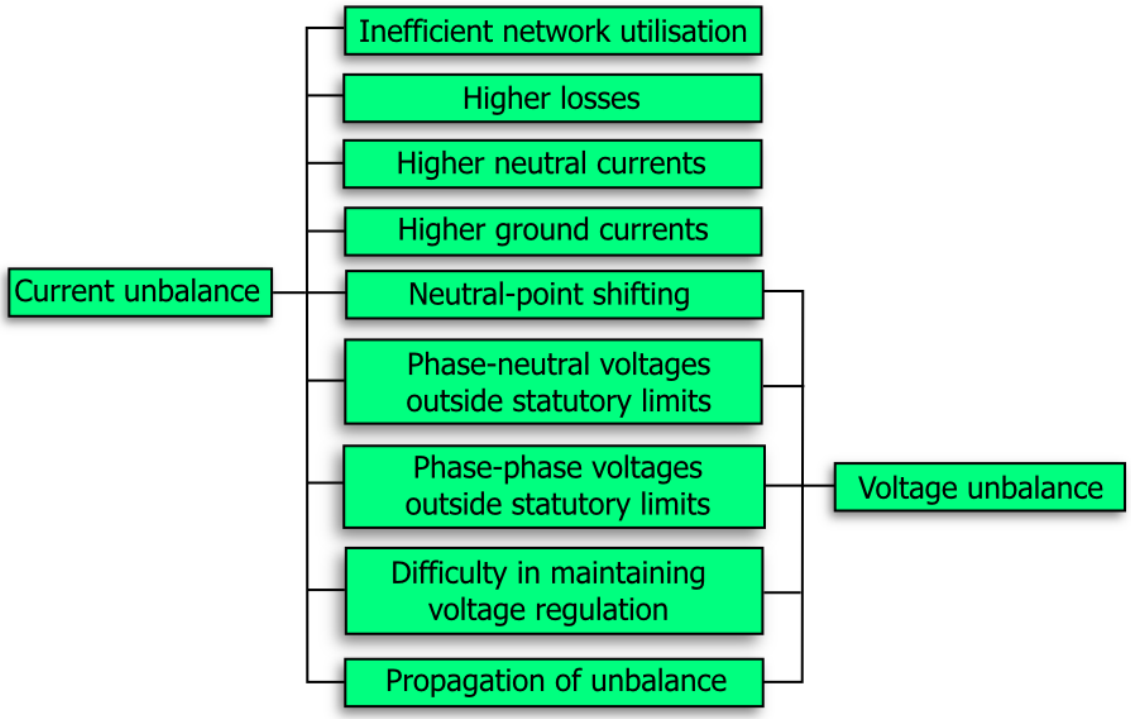

Figure 1.1: Effects of current unbalance

The severity and extent of current unbalance on present-day low-voltage networks are however mostly unknown, as low-voltage monitoring by utilities has been very limited. Recently though, with the availability of cheaper metering and concerns about low-carbon technologies, there has been greater interest in low-voltage monitoring. Some of the monitoring undertaken by distribution network operators (DNOs), as part of the

Low Carbon Network Fund (LCNF) Tier 1 projects, have shown that current unbalance on present-day low-voltage networks may be significant. Examples of current measurements taken by three DNOs - Scottish and Southern Energy as reported in [2] as well as Western Power Distribution [3] and Electricity North West [4] as presented at the 2012 LCNF Conference [5] - are shown in Figure 1.2. All show significant current unbalance with the most heavily loaded phase at times carrying nearly twice the current of the least loaded phase.

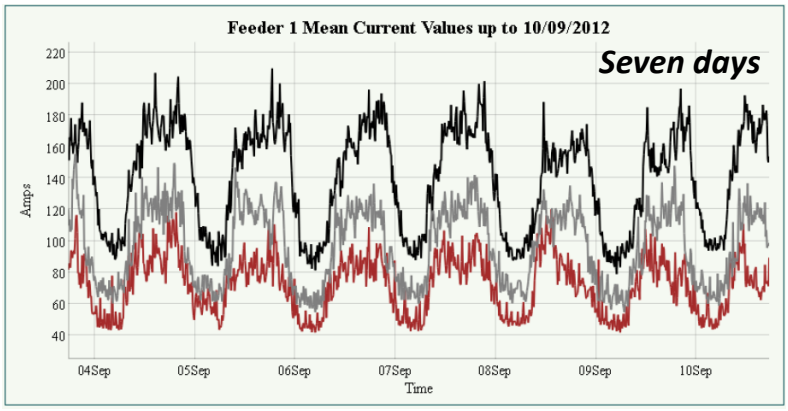

(a)

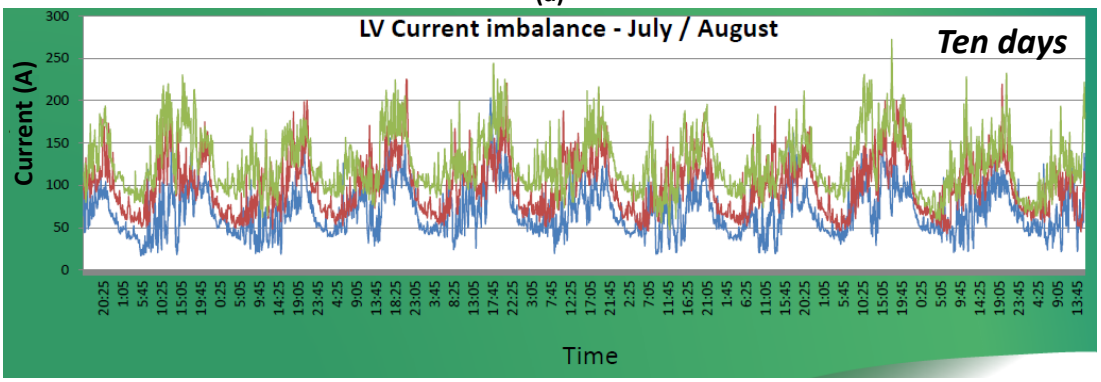

(b)

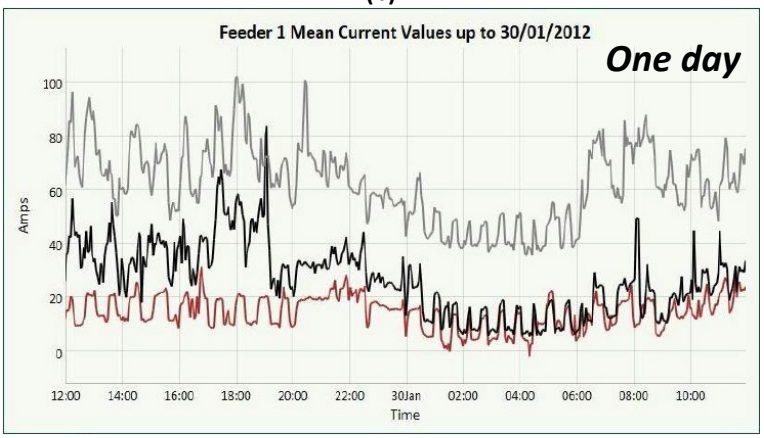

(c)

Figure 1.2: Examples of current measurements taken on low-voltage feeders by (a) Scottish and Southern Energy [2] (b) Western Power Distribution [3] and (c) Electricity North West [4]

1.2 Low-carbon technologies and their influence on unbalance in the future

Low-carbon technologies such as photovoltaic micro-generation, electric vehicles, heat pumps, micro-combined heat and power (μCHP) are being introduced into the low-voltage network. At higher penetrations these low-carbon technologies will influence the current unbalance because:

- **There may be greater possibility for coincident usage by groups of consumers sharing similar low-carbon technologies** [6]**.** This will mean that the usage of certain low-carbon technologies may have a greater influence on the aggregated demand profile of the phase to which they are connected. Presently, appliances with power ratings as high as those of the low-carbon technologies are used at random times and for much shorter periods and so do not significantly influence the aggregated demand profile per phase. An example is the use of electric kettles or electric showers. In contrast, many low-carbon technologies will have longer operating times with potentially greater chance of coincident use between households. An example is where an electric vehicle is charging during the night.
- **There may be less uniformity in the aggregated demand profiles seen across phases because these profiles may be shaped differently depending on the mix of low-carbon technologies on each phase.** This uniformity, seen on present day low-voltage feeders, is reflected in the current flow plots shown in Figure 1.2, with each phase sharing similar valleys and peaks. This becomes increasingly apparent when there are more consumers on each phase. The first two plots for instance, display greater uniformity than the last plot, because they have more consumers on each phase (this can be deduced from the range of current values).

The potential worsening of current unbalance and its effects (Figure 1.1) presents a challenge to distribution network operators (DNOs) as the existing network infrastructure is in financial terms, a substantial long-term investment. Therefore, maximising its use and minimising upgrades whilst not restricting the uptake of low-

carbon technologies are of significant interest to them. This thesis focuses on achieving this by reducing current unbalance using a type of transformer called the static balancer.

1.3 The static balancer and the low-voltage electricity network

The static balancer can be described as an interconnected-star autotransformer for use on low-voltage networks. As shown in Figure 1.3, its construction is similar to a normal oil immersed power transformer except that it has no external secondary bushings. Inside this tank, there is typically a three-limb, common core iron stack and on each limb there are two coils of equal turns (Figure 1.4 (a)). Each phase of the interconnected-star winding is taken from the series connection of two coils wound on different limbs (Figure 1.4 (b)).

Figure 1.3: A static balancer (pole-mounted design)

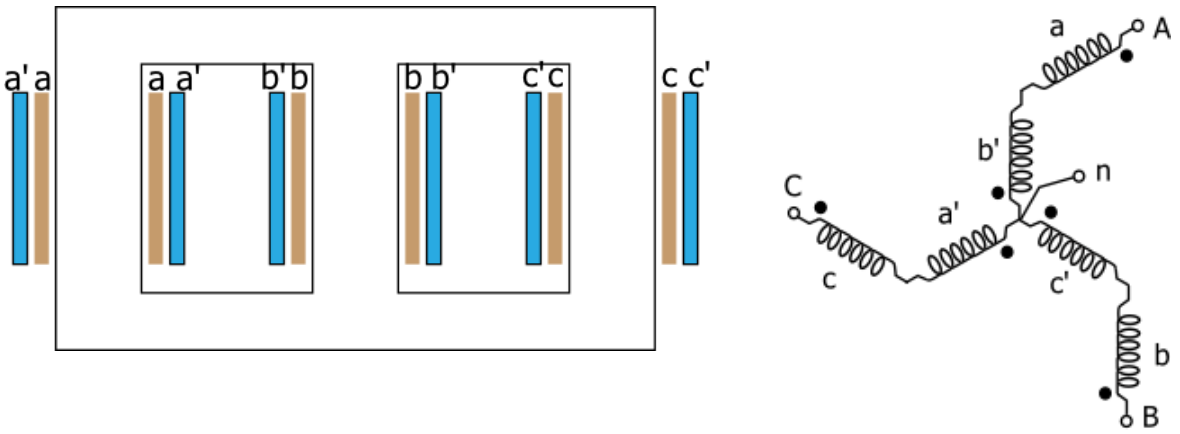

(a) Three-limb, common core iron stack with two coils per limb

(b) The interconnected-star winding formed from coils on two limbs

Figure 1.4: Common core and interconnected-star windings of static balancer

The use of the static balancer on low-voltage networks extends as far back as 1919, as evident from [7], and well into the 1930s to the 1940s, having been covered extensively in early editions of the J&P Transformer Book [8] of that period. Detailed information on its history is sketchy. But its use from the 1910s to the 1920s seems to have been more to provide a neutral point on three-wire low-voltage networks [7] [8]. Eventually, many of these networks would have been upgraded with neutral wires and so its use for this purpose would have declined. It nonetheless continued to be used in the 1930s to the 1960s, but more on low-voltage feeders where unbalance was a problem or where there was a *single* poorly balanced consumer installation [9]. Presently, only a few utilities in the UK including Western Power Distribution (specifically that part which had previously been E.ON Central Networks) and Scottish and Southern Energy continue to use static balancers but just as an interim measure to correct voltage unbalance on rural low-voltage feeders until permanent reinforcement can be done [10].

Much of the knowledge and experience on the use of static balancers on low-voltage networks has been lost over the last few decades. With the imminent introduction of low-carbon technologies and their potential at high penetrations, to worsen current unbalance, there is a need to better understand this technology. Given that it had been used in the past, an investigation into its use would be a good first step. It may also find support with many utilities looking for simple and robust measures to maximise their existing low-voltage network infrastructure. Furthermore, with the relatively short time

horizon for introduction of certain low-carbon technologies such as photovoltaic micro-generation and electric vehicles, the static balancer is a retrofit option with advantages both in cost and time to fit.

1.4 Primary aim and objectives

1.4.1 Primary aim

To reduce current unbalance on low-voltage networks so as to avoid constraints in the uptake of low-carbon technologies and minimise the need for future network upgrades.

1.4.2 Research objectives

(a) *To accurately model and solve very unbalanced low-voltage feeders.*
(b) *To investigate the causes and quantify the effects of current unbalance on low-voltage networks.*
(c) *To investigate the behaviour and quantify the benefits of the static balancer to low-voltage networks.*

1.5 Thesis structure

Chapter 2 is a literature review on current and voltage unbalance covering its causes, effects and mitigation. It concludes with a detailed list of the work needed to achieve the research objectives listed in Section 1.4.2.

Chapter 3 is the first working chapter. It focuses on objective (a), which is a pre-requisite to the other objectives. It is in part a literature review of the existing 3 x 3 and 5 x 5 approaches to the forward-backward sweep unbalanced power flow method, which is typically used to solve radial low-voltage feeders. In that discussion, concerns are raised as to assumptions and approximations which are made. Following from that, a new 5 x 5 approach is developed and its results validated against Matlab SimPowerSystems.

Chapter 4 focuses on objective (b). It starts with a discussion of the mathematical expressions needed to quantify the effects of unbalance identified in Figure 1.1; which were either chosen from the literature or derived. The new 5 x 5 approach to the forward-backward sweep method is then used to solve a representative low-voltage network so as to investigate the relationships of current unbalance to the quantified network effects. The theoretical basis for the use of devices, like the static balancer, which correct the zero sequence current, is an outcome from this investigation. Additionally, the suitability of voltage unbalance factors as measures of unbalance on low-voltage networks is discussed.

Chapter 5 focuses on the modelling of the static balancer and so addresses part of objective (c). It explains the influence of the interconnected-star winding of the static balancer to its low zero sequence impedance. Following that, a representation of the static balancer, suitable for use in the forward-backward sweep method is found. This representation is validated against laboratory measurements of an actual static balancer using impedances determined by a short-circuit test.

Chapter 6 focuses mainly on objective (c) but contributes to objective (b) as well. It presents an analysis of measurements taken during a field trial of the static balancer by Western Power Distribution on one of their rural low-voltage feeders. The main aim of this chapter is to provide quantified evidence of the strengths and weaknesses of the static balancer on low-voltage networks. This was done by quantifying the network effects as identified in Figure 1.1, before and after a static balancer was put into service. Also, power quality meters placed upstream and downstream of the static balancer, gave an opportunity for additional insight into the behaviour of the static balancer on low-voltage networks. Moreover, the representation of the static balancer developed in **Chapter 5** was further validated using these measurements. Observations are also made about the sequence unbalance factors, validating some of the findings from the theoretical analysis of **Chapter 4.** In this regard, this chapter also contributes to objective (b).

Chapter 7 completes objectives (a) and (c). In it, the rural LV feeder is modelled and the solutions found using both the new 5 x 5 approach and the standard 3 x 3 approach to the unbalanced power flow method compared against the voltage and current measurements on the rural feeder without the static balancer. The static balancer model is then included and a similar comparison done against measurements with the static balancer. The benefits found from the network simulations are also compared against those quantified previously in Chapter 6 from field measurements; so as to confirm that the proposed 5 x 5 approach and the representation of static balancer can be used to predict them.

Chapter 8 presents the conclusions of the work and **Chapter 9** provides recommendations for future work.

2. Literature review of current and voltage unbalance

2.1 Basic concepts

2.1.1 Definition of unbalance

Unbalance describes the condition on a three-phase system in which the phasors of voltage or current are either not all of equal magnitude or the angular difference between consecutive phasors are not exactly 120°. Figure 2.1 compares the ideal condition to several unbalanced conditions using a general system of voltage or current phasors - M_a, M_b and M_c.

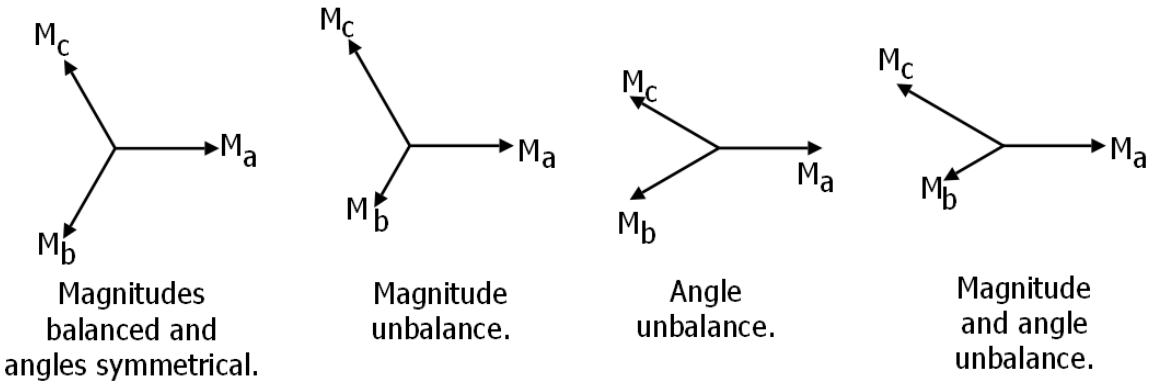

Figure 2.1: General system of phasors showing magnitude and angle unbalance

2.1.2 Relationship between current and voltage unbalance

Current unbalance is related to voltage unbalance through the network impedances which may be either symmetrical or asymmetrical, as shown in Figure 2.2. An asymmetrical network is defined as one with unequal self- and/or mutual-impedances [11]. In Figure 2.2, an example is given of a four-core cable with concentric neutral. With this cable design there will be unequal mutual impedances between phases and between phases and neutral.

Instances in which unequal self-impedances will result include the use of different single-core cables and distribution transformers formed by banks of different single-phase transformers.

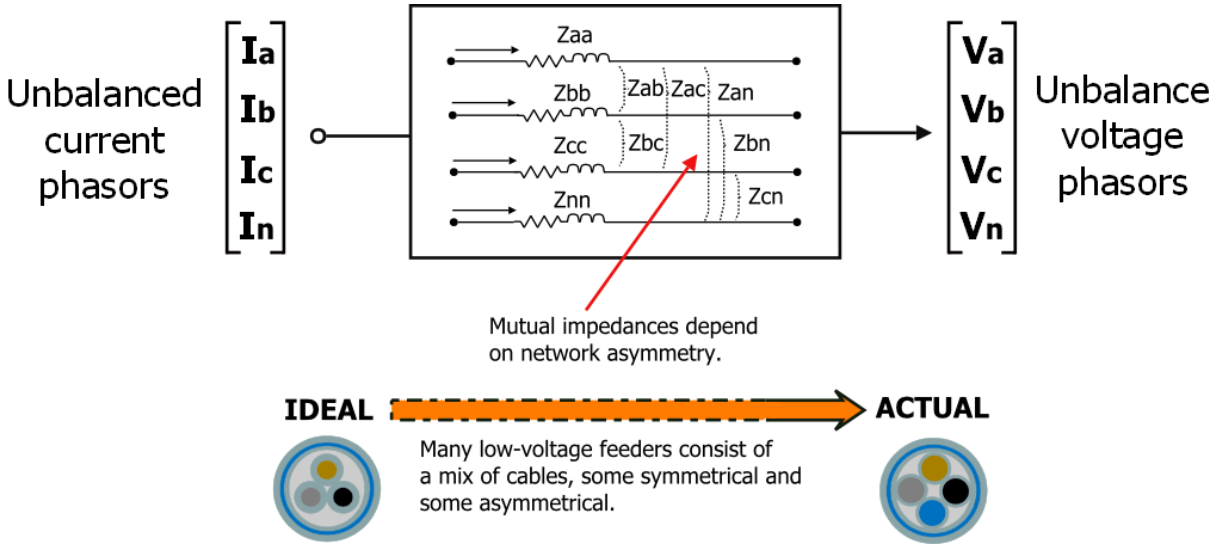

Figure 2.2: Relationship between voltage and current unbalance

2.1.3 Symmetrical components

Symmetrical components, developed by Fortescue in 1918 [12], is a method used to represent any set of unbalanced phasors by three sets of balanced phasors:

- a direct (positive) sequence system in the order (a-b-c);
- an inverse (negative) sequence system in the order (a-c-b); and
- a homopolar (zero) sequence system in the same direction.

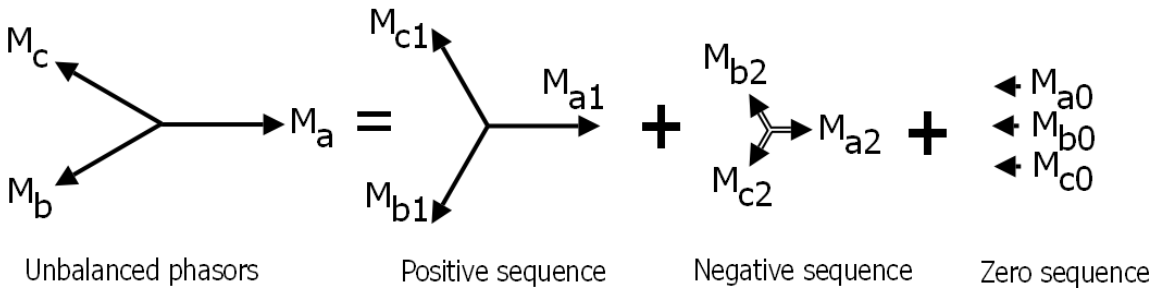

Figure 2.3: Unbalanced set of current phasors represented by symmetrical components

The relationship between the unbalanced phasors and the three balanced sequence systems is expressed mathematically by:

$$\begin{bmatrix} M_0 \\ M_1 \\ M_2 \end{bmatrix} = \frac{1}{3}\begin{bmatrix} 1 & 1 & 1 \\ 1 & a & a^2 \\ 1 & a^2 & a \end{bmatrix}\begin{bmatrix} M_a \\ M_b \\ M_c \end{bmatrix} \quad (2.1)$$

where $a = e^{j.\frac{2}{3}\pi} = 1\angle 120°$

Fundamentally, a balanced group of phasors will translate into a positive sequence system only. And any unbalance resulting from any inequality in magnitude or deviation in angular difference from 120° will give rise to the negative and zero sequence systems of phasors.

An alternative method, p-q theory [13] [14], can also be used to separate unbalanced currents (or voltages) into balanced and unbalanced components. This method though, is the topic of much discussion [15] [16]. The symmetrical components method on the other hand is more widely accepted, being covered by many power system analysis texts such as [17].

2.1.4 Relationship between any sequence voltage and the other sequence currents

On low-voltage networks with asymmetrical network impedances, the sequence networks are not independent. This means that the negative sequence voltage does not depend solely on the negative sequence current, but will also be influenced to some extent by the zero sequence current. This interdependence depends on the asymmetry in the network impedances.

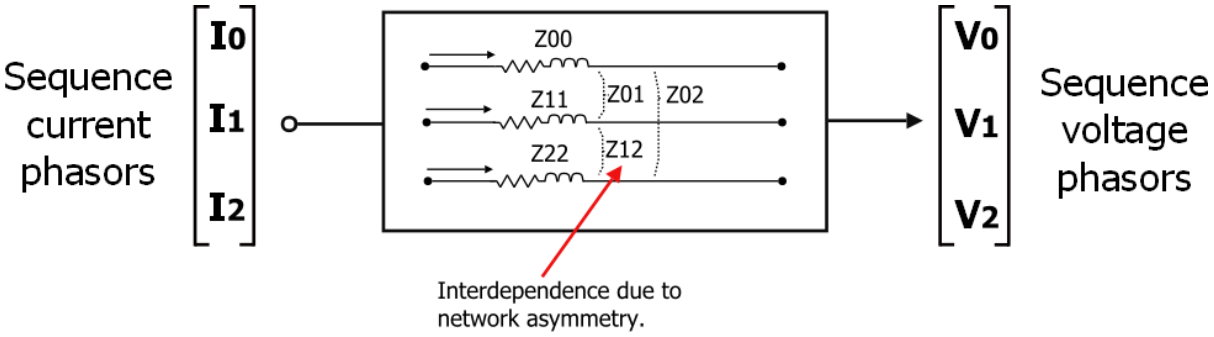

Figure 2.4: Relationship between sequence voltages and currents

2.2 Standards and recommended limits

2.2.1 More emphasis on the voltage unbalance

Most standards are concerned with protecting consumers, and so focus more on voltage unbalance. Several of these standards are not based on symmetrical components, but on the voltage phasor magnitudes. The definitions are varied. Figure 2.5 presents a structured view of the various definitions by categorising them into either the sequence domain or the phase domain. Table 2.1 presents the equations for these definitions. It should be appreciated that the basic form of these definitions may also be adapted for quantifying current unbalance (by instead using current phasor magnitudes).

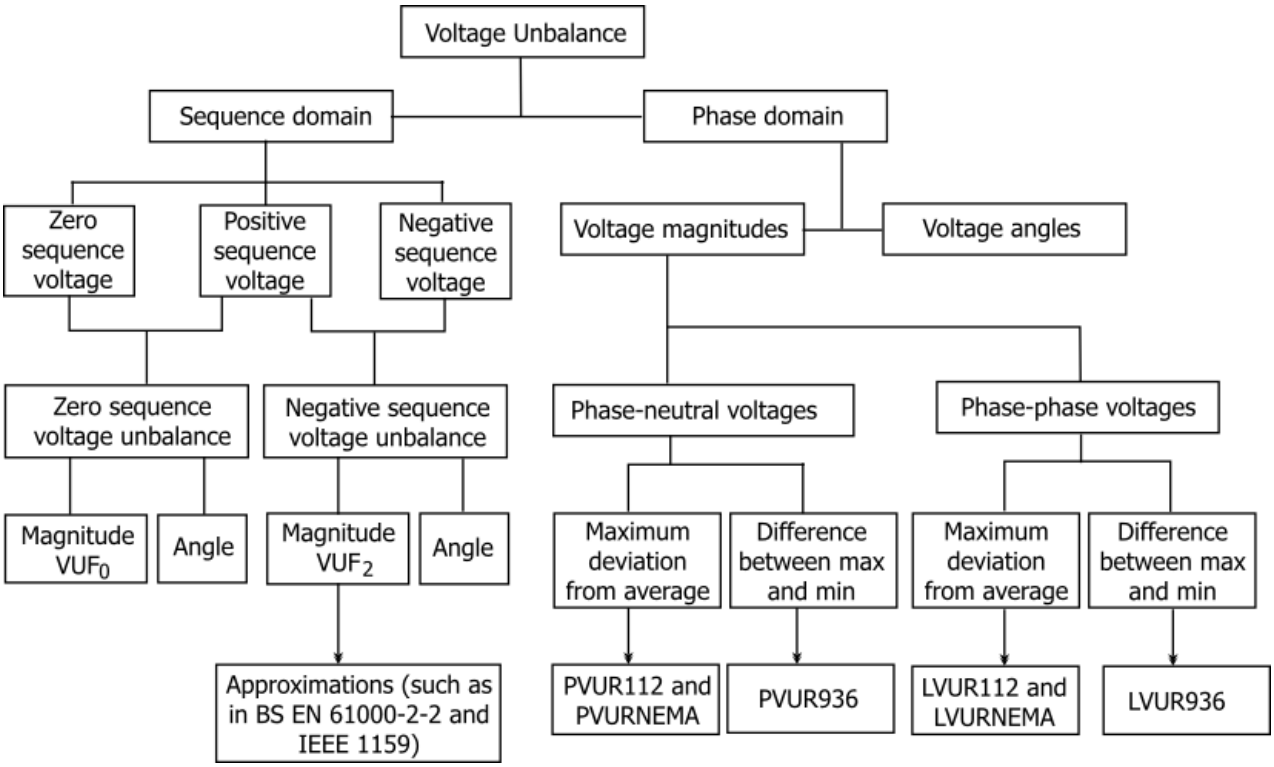

Figure 2.5: The various definitions of unbalance

Phase domain		
	Phase-phase voltages (as required in standards)	**Phase-neutral voltages (as interpreted by some authors [18] , [19] and [20])**
IEEE 112	$\mathbf{LVUR}_{112} = \left(\frac{\boldsymbol{max}(\lvert V_{ab} - V_{pp-avg}\rvert, \lvert V_{bc} - V_{pp-avg}\rvert, \lvert V_{ca} - V_{pp-avg}\rvert)}{V_{pp-avg}}\right)$	$\mathbf{PVUR}_{112} = \left(\frac{\boldsymbol{max}(\lvert V_{an} - V_{pn-avg}\rvert, \lvert V_{bn} - V_{pn-avg}\rvert, \lvert V_{cn} - V_{pn-avg}\rvert)}{V_{pn-avg}}\right)$
NEMA MG 1	Same as $LVUR_{112}$	Same as $PVUR_{112}$
IEEE 936	$\mathbf{LVUR}_{936} = \left(\frac{\boldsymbol{max}(\lvert V_{ab}\rvert, \lvert V_{bc}\rvert, \lvert V_{ca}\rvert) - \boldsymbol{min}(\lvert V_{ab}\rvert, \lvert V_{bc}\rvert, \lvert V_{ca}\rvert)}{V_{pp-avg}}\right)$	$\mathbf{PVUR}_{936} = \left(\frac{\boldsymbol{max}(\lvert V_{an}\rvert, \lvert V_{bn}\rvert, \lvert V_{cn}\rvert) - \boldsymbol{min}(\lvert V_{an}\rvert, \lvert V_{bn}\rvert, \lvert V_{cn}\rvert)}{V_{pn-avg}}\right)$
	where $V_{pp-avg} = (V_{ab} + V_{bc} + V_{ac})/3$	where $V_{pn-avg} = (V_{an} + V_{bn} + V_{cn})/3$
Sequence domain		
	Negative sequence voltage unbalance factor VUF_2	
	Phase-phase voltages	**Phase-neutral voltages**
BS EN 61000-2-2	$\mathbf{Approx.\ VUF}_2 = \sqrt{\left(\frac{6 * (V_{ab}^2 + V_{bc}^2 + V_{ac}^2)}{(V_{ab} + V_{bc} + V_{ac})^2} - 2\right)}$	-
IEEE 1159	$\mathbf{Approx.\ VUF}_2 = \sqrt{\left(\frac{1 - \sqrt{3 - 6\beta}}{1 + \sqrt{3 - 6\beta}}\right)}$	
	where $\beta = \frac{\lvert \mathbf{V_{ab}}\rvert^4 + \lvert \mathbf{V_{bc}}\rvert^4 + \lvert \mathbf{V_{ca}}\rvert^4}{(\lvert \mathbf{V_{ab}}\rvert^2 + \lvert \mathbf{V_{bc}}\rvert^2 + \lvert \mathbf{V_{ca}}\rvert^2)^2}$	where $\beta = \frac{\lvert \mathbf{V_{an}}\rvert^4 + \lvert \mathbf{V_{bn}}\rvert^4 + \lvert \mathbf{V_{cn}}\rvert^4}{(\lvert \mathbf{V_{an}}\rvert^2 + \lvert \mathbf{V_{bn}}\rvert^2 + \lvert \mathbf{V_{cn}}\rvert^2)^2}$ (valid only if there is no zero sequence voltage present)
	Zero sequence voltage unbalance factor VUF_0	
	Phase-phase voltages	**Phase-neutral voltages**
	Requires use of both phase-phase and phase-neutral voltages. No approximations given in standards.	

Table 2.1: Mathematical definitions used in various standards

2.2.2 Standards using symmetrical components define both current and voltage unbalance

Several standards such as the BS EN 50160:2010 [21], BS EN 61000-2-2-2002 [22] and IEEE 1159-2009 [23] define unbalance using symmetrical components. Negative and zero sequence unbalance factors of current and voltage are given. These unbalance factors are ratios of either the negative or zero sequence phasor magnitudes to the positive sequence phasor magnitude.

$$UF_2 = |M_2/M_1| \tag{2.2}$$

$$UF_0 = |M_0/M_1| \tag{2.3}$$

Throughout this thesis the zero and negative sequence current unbalance factors will be denoted by IUF_0 and IUF_2 and the zero and negative sequence voltage unbalance factors by VUF_0 and VUF_2.

2.2.3 Approximations to sequence unbalance factors are not suited to low-voltage networks

The exact calculation of negative and zero sequence voltage unbalance factors using symmetrical components requires either:

1) phase-neutral phasor magnitudes and angles, directly applying equations (2.1) to (2.3); or
2) both phase-neutral and phase-phase voltage magnitudes, using methods described in [11] and [24].

This exact calculation may be beyond the capability of most measurement instruments, as they typically provide the phase-phase or phase-neutral voltage magnitude only. Therefore, standards based on symmetrical components such as [22] and [23] give approximations which require only voltage magnitudes. These standards are however, more suited for use on ungrounded supplies, such as a delta or wye with an isolated neutral because:

- they give approximations of the negative sequence voltage unbalance factor - VUF_2 only; and
- the approximations of VUF_2, as explained by example in [23], are not valid for phase-neutral voltage magnitudes, if there is a zero sequence voltage present.

These standards are therefore less suitable for the low-voltage network because, with its multi-grounded neutral, both negative and zero sequence voltage unbalance are important. Also any approximation used should ideally be valid in the presence of both sequence voltages. For instance, the approximation given in [23] for VUF_2, which necessitates measurements of phase-phase phasor magnitudes in the presence of zero sequence components has the following shortcomings (if applied to the low-voltage network):

- Precludes detection of zero sequence voltage unbalance - VUF_0.
- Limited just to voltages (as there are no phase-phase currents that can be measured on the low-voltage network, if say IUF_2 was a concern).

2.2.4 Phase domain definitions

The phase domain definitions are rather diverse. They are based on phase-phase voltage magnitudes, however some authors such as [18] and [19], have interpreted them to imply phase-neutral voltage magnitudes as well. This ambiguity has resulted in later papers such as [20] also making the same assumption. In Table 2.1, the $LVUR_{936}$, $LVUR_{112}$ and $LVUR_{NEMA}$ are based on phase-phase voltage magnitudes and $PVUR_{936}$, $PVUR_{112}$ and $PVUR_{NEMA}$ on phase-neutral voltages.

2.2.4.1 Problems with using phase domain definitions of voltage unbalance

As can be seen by a simple example of the three triangles shown in Figure 2.6, the phase domain definitions do not give a full picture of voltage unbalance. The use of phase-phase voltage magnitudes can omit changes in the phase-neutral voltage magnitudes (and vice-versa). Both cases do not account for changes in voltage angles.

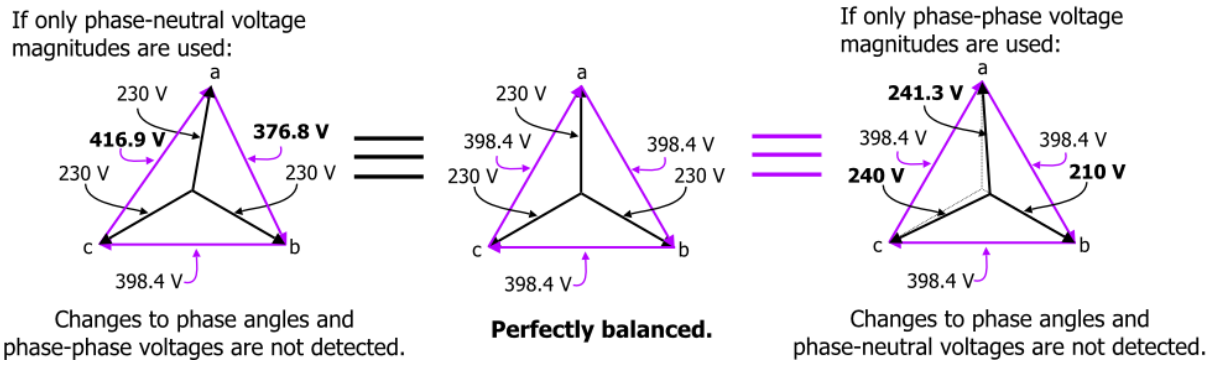

Figure 2.6: Simple example of three triangles.

The use of phase-phase voltage magnitudes will not account for changes in the zero sequence voltage. This may lead one to consider definitions using phase-neutral voltage magnitudes (as changes in both zero and negative sequence voltage can be detected). However, in [19] it was found that values of voltage unbalance calculated using phase-neutral voltage magnitudes varied significantly in the presence of zero sequence voltages. Figure 2.7 shows a plot from [19] which demonstrates the range of values from these definitions for a 2 % negative sequence voltage and a 1.5 % zero sequence voltage. For this graph, the angle of the negative sequence voltage is varied from 0° to 360° to show the range of values from the different definitions – $LVUR_{NEMA}$, $PVUR_{936}$

and $PVUR_{112}$. The $LVUR_{NEMA}$ definition uses phase-phase voltage magnitudes and so was characteristically insensitive to the zero sequence voltage.

Further, the observations made using these phase domain definitions for voltage unbalance, will apply equally if they had been used for current unbalance. This is because they are all attempts to quantify the unbalance of an unbalanced system of phasors using only phasor magnitudes.

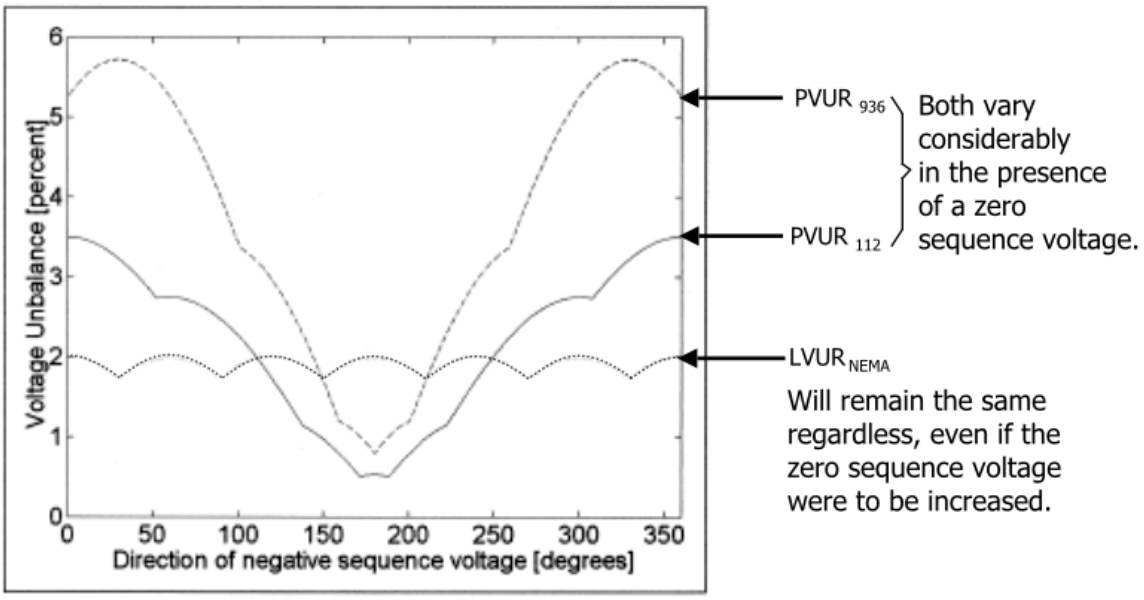

Figure 2.7: Voltage unbalance according to different definitions for 2 % negative sequence voltage and 1.5 % zero sequence voltage. [19]

2.2.5 The choice of definition for this thesis

For the reasons discussed in the previous section, the phase domain definitions - though simpler to measure and calculate - will not be used in this thesis. Instead, the fundamental definition based on symmetrical components will be used for both current and voltage unbalance. This will involve the exact calculation of unbalance factors using phase-neutral phasor magnitudes and angles (i.e. equations (2.1) to (2.3)).

2.2.6 Recommended limits for low-voltage network

Just as the definitions given in the standards focused on voltage unbalance, so too do the recommended limits. Therefore, there are no limits specified for current unbalance.

The standards applicable to the low-voltage network are:

- **BS EN 50160:2010** [21] **and BS EN 61000-2-2:2002** [22]**:** Both require that 95 % of the observations of the negative sequence voltage unbalance factor averaged at ten-minute intervals over any one week period must be below 2 %. A higher limit of 3 % is given for networks in which there is a considerable amount of single-phase and two-phase loads (such as the low-voltage network); and
- **Engineering Recommendation P29 (1990)** [25]**:** These are planning limits (for 132 kV systems and below) specified at the point of common coupling (PCC) of a proposed load. They are not intended for the entire network. The negative sequence voltage unbalance factor is also defined but oddly is approximated using $PVUR_{112}$. As in the previous standards, the limit under normal conditions is also 2 % but taken over a one-minute interval. The length of the observation period is not specified.

There are no recommended limits for the zero sequence voltage unbalance factor. As the standards only recommend a limit on the negative sequence voltage unbalance factor, it might be assumed that that alone would be sufficient and that both negative and zero sequence voltage unbalance factors will vary together. That however, is not the case. Observations made in [6] from field measurements on feeders showed that on some feeders the negative sequence voltage unbalance factor was higher than the zero sequence voltage unbalance factor while on others they were equal.

2.2.7 Summary

- Standards give more focus to voltage unbalance than current unbalance.
- Standards are more suited to three-phase, three-wire consumer supplies which would see only negative sequence voltage unbalance. This is evident in the

approximations and in the recommended limits, which are given for the negative sequence voltage unbalance factor only.

- Standards are less suited to the three-phase, four-wire low-voltage network, in which both negative and zero sequence components of voltage and current will be present because no approximations or recommended limits are given for sequence current unbalance factors or zero sequence voltage unbalance factor.
- Phase domain definitions do not give consistent values in the presence of zero sequence phasors. The fundamental definitions based on symmetrical components are therefore preferable.

2.3 Causes of current and voltage unbalance

The principal causes – (1) to (6) – of current unbalance on present day and future low-carbon low-voltage feeders are illustrated in Figure 2.8. The sections which follow, also labelled (1) to (6) will discuss each of the causes in turn. The close relationship with voltage unbalance, seen through the distribution transformer and network impedances are also shown.

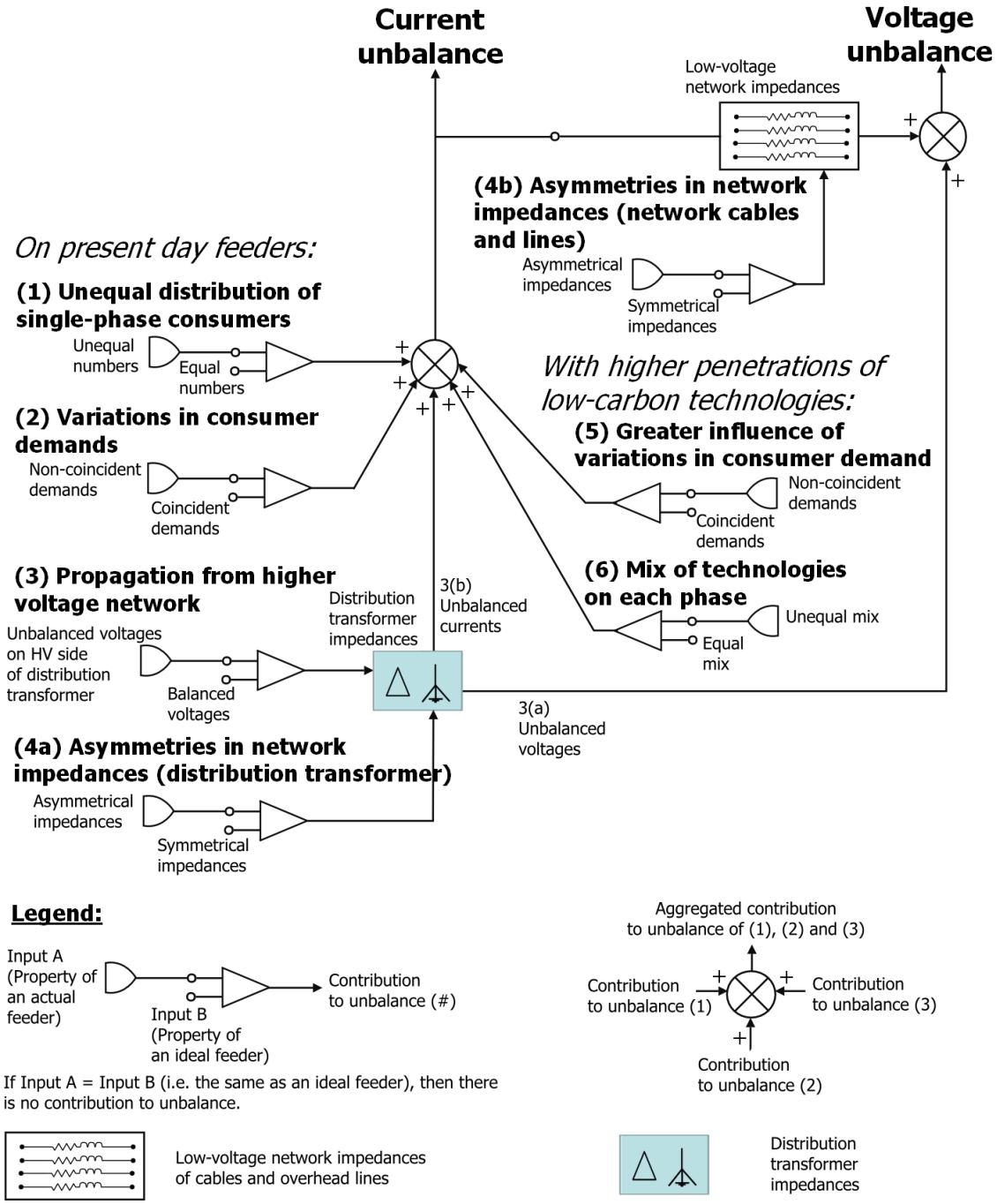

Figure 2.8: The principal causes of current unbalance on present day and future low-carbon, low-voltage feeders

2.3.1 Present day low-voltage feeders

(1) Unequal distribution of single-phase consumers

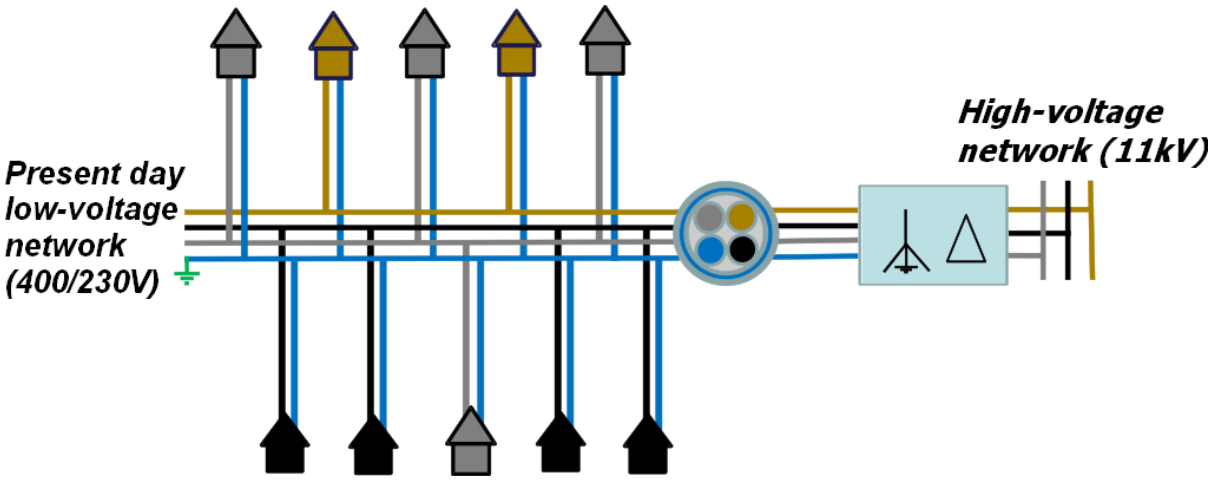

Figure 2.9: Present day low-voltage network showing unequal distribution of consumers

Decades ago, when present day low-voltage feeders were constructed, the distribution network operators would have attempted to connect equal numbers of consumers on each of the phases [10]. Achieving this in practice however, is not an easy task.

Consider as an example, Figure 2.9, which shows a four-core cable laid on one side of a street with ten single-phase consumers. Each house must be connected to two wires – a phase wire and the neutral wire. In Figure 2.9 the tendency, in practice, to use one of the two phase wires closest to the neutral wire is depicted. This means that the phase wire diagonally opposite to the neutral may be the least likely used wire.

Further, in practice no records are kept of the phase to which each consumer is connected or the total number of consumers per phase. This means that the phase chosen for any new consumer may also depend on what is more convenient practically.

(2) Variations in consumer demands

The demand of each single-phase consumer varies minute-to-minute as household appliances are used. The influence of these variations on the aggregated demand per phase is more pronounced when there are fewer consumers (e.g. a rural low-voltage feeder). With more consumers (e.g. an urban low-voltage feeder), the individual

consumer demand variations will have less influence on the aggregated demand per phase.

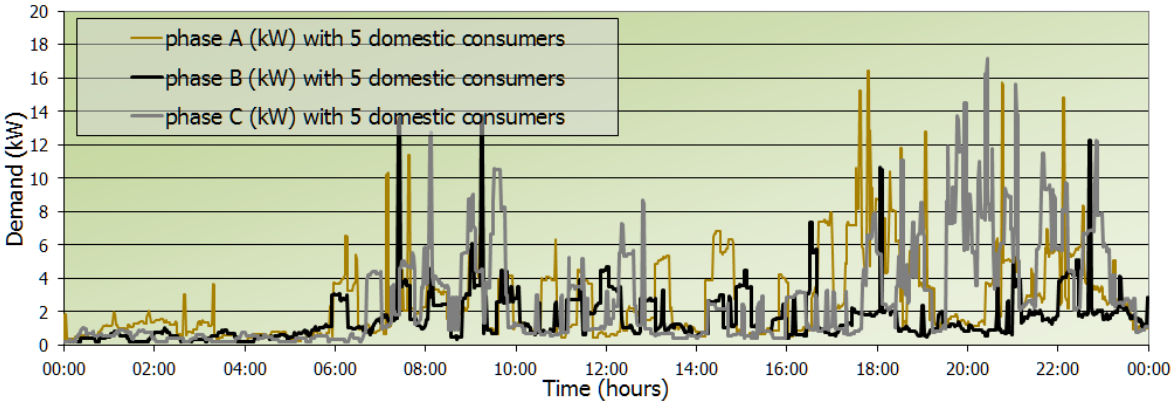

(a)

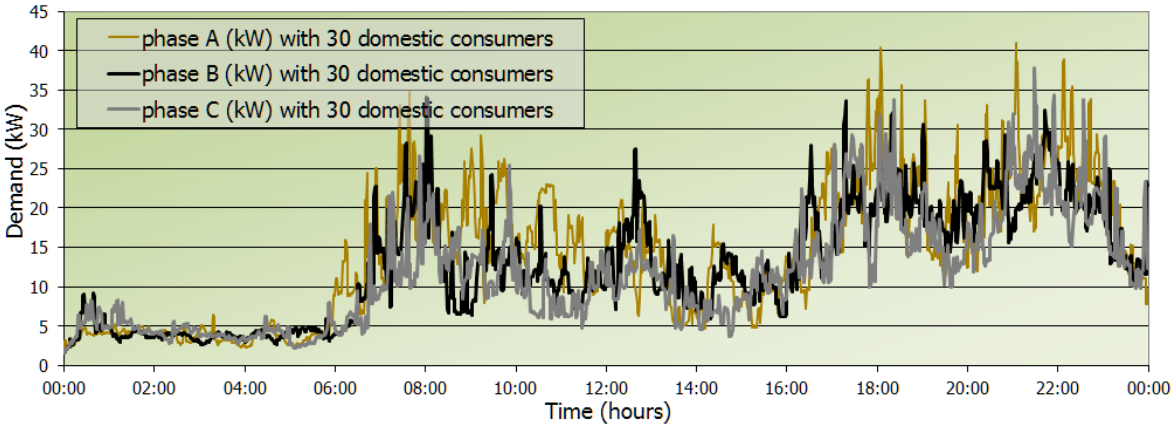

(b)

Figure 2.10: Aggregated demands for (a) five consumers and (b) thirty consumers per phase

This is demonstrated in Figure 2.10 (a) and (b) by aggregating domestic consumer demands generated using the domestic demand model developed in [26]. The aggregated demand of five consumers on each phase is shown in Figure 2.10 (a) and for thirty consumers on each phase in Figure 2.10 (b).

(3) Propagation from higher voltage network

Unbalanced voltages on the higher voltage network will be translated through the windings of the distribution transformer to the low-voltage network (identified by 3(a) in Figure 2.8). Any changes to the phase-neutral voltages will also affect the phase currents on the low-voltage feeder (identified by 3(b) in Figure 2.8).

It should be appreciated that as the higher voltage network is a delta, only negative sequence voltage unbalance will be present and propagated.

(4) Asymmetries in network impedances

As mentioned in section 2.1, current unbalance is related to voltage unbalance through the network impedances. If the network impedances – which includes that of cables and distribution transformer - are asymmetric, voltage unbalance can occur even though the currents are perfectly balanced. The voltage unbalance caused by asymmetric network impedances contributes to a *background voltage unbalance,* which rarely exceeds 0.5 % [25].

2.3.2 Low-voltage feeders with higher penetrations of low-carbon technologies

(5) Greater influence of variations in consumer demand

The demand variations of individual consumers or groups of consumers sharing similar low-carbon technologies may have a greater influence on the aggregated demand per phase. Compared to existing consumer devices many low-carbon technologies have:

- **Higher current ratings.** Single-phase devices of higher current ratings will take up a greater proportion of the total current seen on a given phase of the low-voltage feeder. Their influence will be greatest at times of minimum demand, like early mornings; and
- **Longer operating times.** The longer the operating time of a device, the higher the chances of coincident usage [6]. The influence of devices which have a limited operating window will be greatest. For instance, most consumers will use their electric vehicles during the day (as they do with vehicles now) and charge them in the night. During this limited operating window, there will be a greater possibility of coincident charging. Similarly, the power production from photovoltaic (PV) micro-generation correlates to the solar irradiance and is limited to daylight hours.

(6) Mix of technologies on each phase

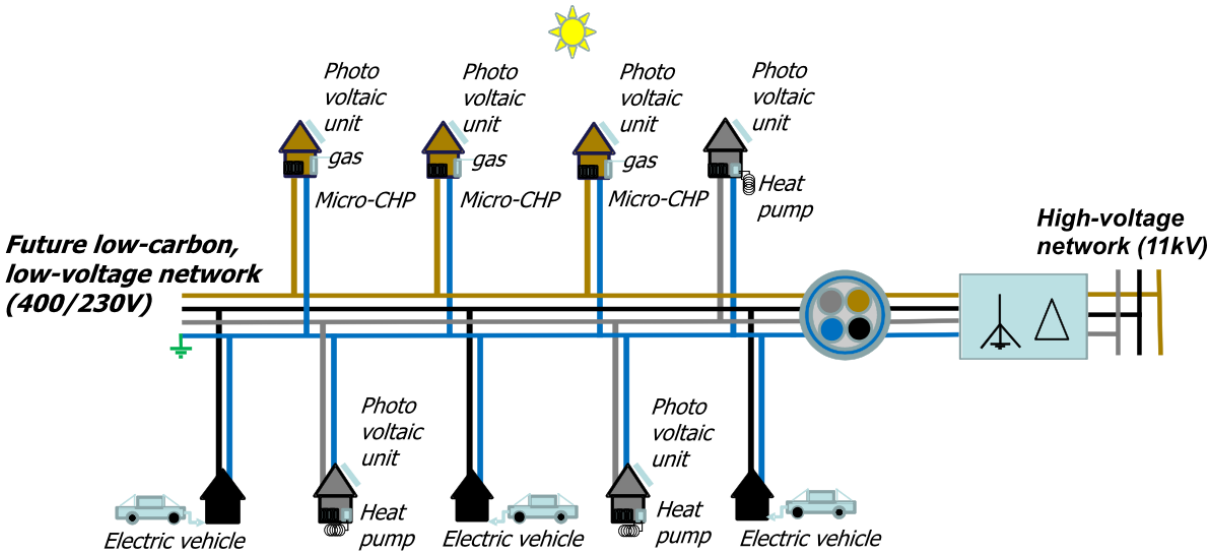

Figure 2.11: Future low-voltage network showing unequal mix of different low-carbon technologies

The uptake of the different low-carbon technologies by domestic consumers cannot be predicted. Different low-carbon technologies can affect the aggregated demand profiles per phase differently – increasing or decreasing the demand at different times of the day. Figure 2.12 illustrates, using the domestic demand model developed in [26], the current unbalance that can be created by the mix of low-carbon technologies depicted in Figure 2.11.

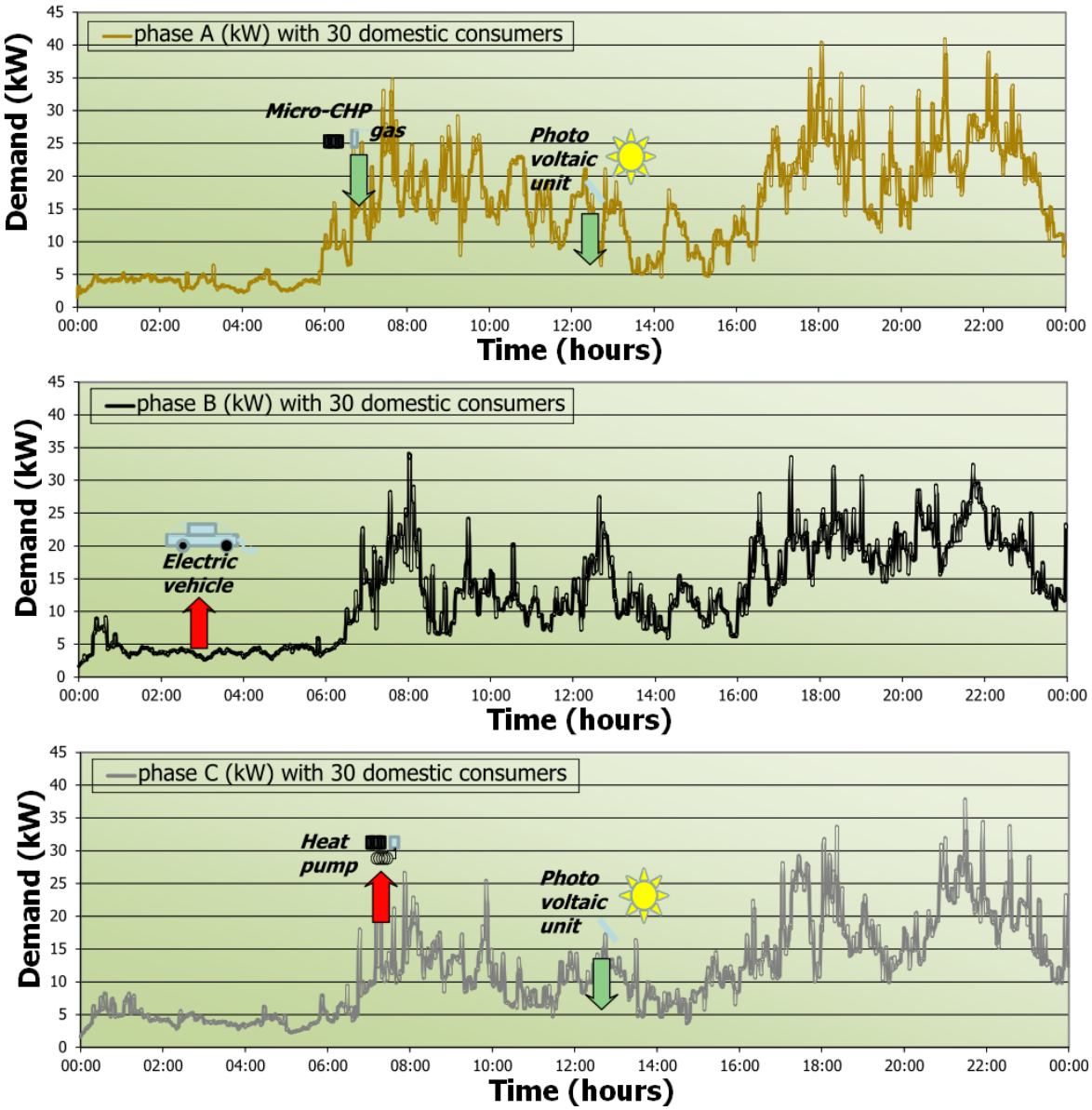

Figure 2.12: Impact on different combinations of low-carbon technologies on the aggregated demand per phase

2.3.3 Summary

- One of the main causes of current unbalance on present-day feeders is the unequal distribution of consumers among the three phases.
- Low-carbon technologies can potentially worsen current unbalance.
- Variations in consumer demands have greater influence when there are fewer consumers on each phase (e.g. a rural low-voltage feeder).

2.4 Effects of current and voltage unbalance

The effects – (a) to (k) – of current unbalance on the low-voltage network and three-phase consumers are illustrated in Figure 2.13. The sections which follow, also labelled (a) to (k) will discuss each effect in turn.

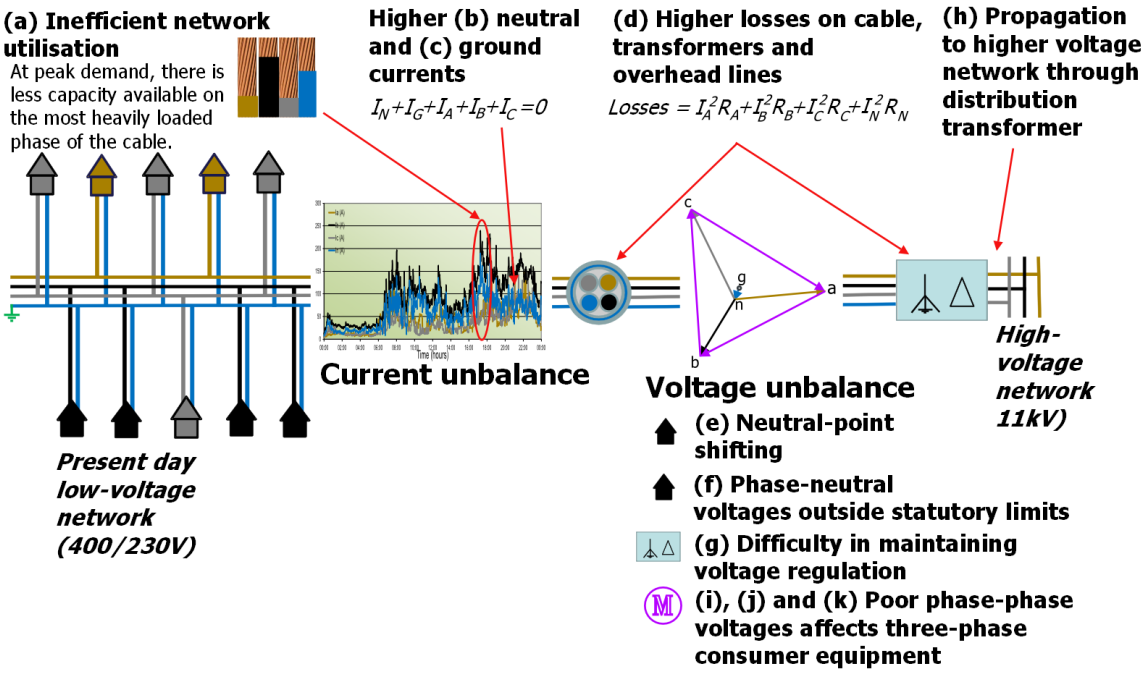

Figure 2.13: The effects of current and voltage unbalance on the low-voltage network

2.4.1 Effects on LV network are due primarily to current unbalance but also voltage unbalance

(a) Inefficient network utilisation

As there is a disproportionate sharing of the total feeder demand, with future growth the more heavily loaded phase may become overloaded while the other phases remain underutilised. This may result in equipment being replaced even though they may be well within their three-phase power rating. Therefore, to the distribution network operator, the investment made in transformer or cable capacity is never fully realised.

(b) Higher neutral currents

As the neutral conductor is the main return path, it carries most of the out-of-balance current (i.e. the phasor sum of phase currents). This can potentially overload the neutral conductor, especially if it is of a lower rating than the phase conductors.

(c) Higher ground currents

Larger out-of-balance currents also result in higher ground currents. This current depends on the relative impedances of the neutral and earth return paths. It affects communications networks and also poses a safety concern [27].

(d) Higher losses in transformers, cables and overhead lines

As losses depend on the square of the currents seen on all wires, they will be higher than under ideal conditions were phase currents are perfectly balanced and the neutral current is zero. This results in:

- an additional cost to supply the same amount of energy (as compared to ideal conditions); and
- reduced life of distribution transformers [28] and underground cables [29] due to additional thermal stresses on insulation.

(e) Neutral-point shifting

Displacement of the neutral voltage is due to neutral currents flowing through the neutral conductor [30]. This can result in the phase-neutral voltage of one phase being decreased while those of the other two phases are increased or the phase-neutral voltage of one phase being increased while the other two are decreased. This can add to the risk of voltages seen by single-phase consumers being outside statutory limits.

(f) Phase-neutral voltages outside statutory limits

Lower phase-neutral voltages result from larger voltage drops on the heavily loaded phases (and likewise higher phase-neutral voltages on the lightly loaded phases) than if

supplying the same total three-phase demand but balanced. This can add to the risk of voltages to the consumer being outside statutory limits.

(g) Difficulty in maintaining voltage regulation

An additional concern, related to (f), is the widening of the difference between phase-neutral voltages of lightly loaded and heavily loaded phases. This can increase the operational complexity of maintaining adequate voltage regulation. On present day low-voltage networks, the tap position of the distribution transformer is set so as to maintain adequate voltages towards the end of the low-voltage feeder. Adjustment of the tap position, which is usually done off-load, raises or lowers all three phase-neutral voltages simultaneously. With this there is a risk that phase-neutral voltages may be improved on some phases but worsened on others. This can result in:

- Increased risk of operators incorrectly setting the distribution transformer tap position, especially if adjustment is based on readings from only one phase on which consumer complaints were received; and
- Possible reductions to the maximum load that the distribution transformer may adequately supply.

(h) Propagation of voltage and current unbalance

The voltage unbalance of one low-voltage feeder may be seen by other low-voltage feeders fed from the same distribution transformer. Additionally, current unbalance can be propagated through the distribution transformer, onto the higher voltage network [31]. This depends on the transformer winding configuration. In a star/star winding configuration for instance, both negative and zero sequence currents will be propagated whilst with a delta/star, only the negative sequence current is propagated. The unbalanced current which does propagate, will result in unbalanced voltages on the higher voltage network. Other low-voltage feeders fed from the same high voltage feeder will then see these unbalanced voltages.

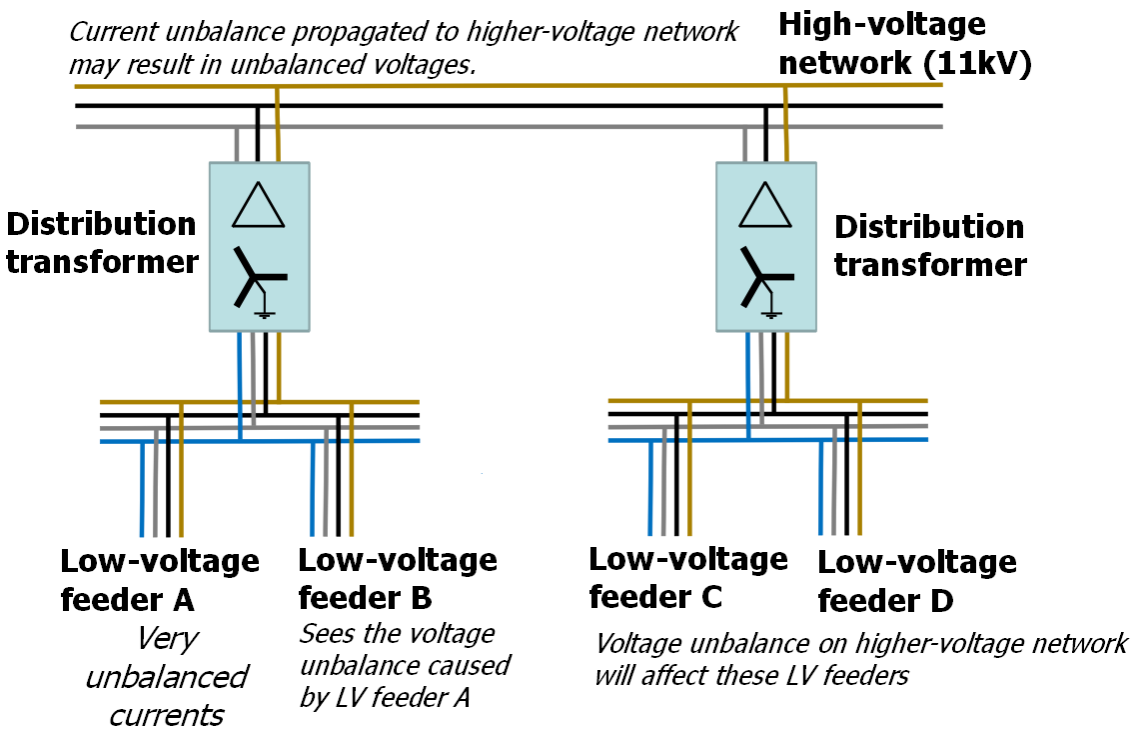

Figure 2.14: Propagation of unbalance to other parts of the electricity network

2.4.2 Effects on consumer three-phase load equipment are due primarily to voltage unbalance

Unequal current flows on the low-voltage feeder also result in unbalanced phase-phase voltages. The effects on three-phase consumer load equipment – such as rotating machines, AC/DC rectifiers and inverters – are mostly the result of the unbalanced phase-phase voltages, as their load equipment are usually supplied in a delta or a wye with an isolated neutral. This is seen as a higher negative sequence voltage unbalance. In fact, the negative sequence voltage unbalance was proposed as a standard definition for unbalance out of concerns over its effects on induction machines in 1954 [32]. Moreover, much of the literature on unbalance actually pertains to induction machines.

(i) Induction machines

The effects on induction machines as summarized in [33], [34] and [35] include:

- Heating effects which result in a reduction in efficiency and faster thermal ageing. Under unbalanced voltage conditions, an induction machine has a very low negative sequence impedance (similar to its starting state) [34] and so draws unbalanced currents. This results in additional heating.

- Reduced speed and torque. The positive sequence voltage is responsible for the useful or productive torque. Under unbalanced conditions, there will also be negative sequence voltages at the terminals of the machine. These result in a reverse torque. Hence a net reduction in torque and speed.

As a result of these effects, standards such as NEMA MG-1 [36] specify de-rating factors if the voltage unbalance, as defined in Table 2.1 by $LVUR_{NEMA}$, is above 1 %. This will mean that larger sized motors must be used. Additionally, protection may be used to detect severe conditions (e.g. the loss of one phase) and disconnect the machine [34].

Additionally, the BS EN 60034-1:2010 [37] gives withstand limits for both negative and zero sequence voltage unbalance factors. It stipulates that any three-phase motor should be capable of withstanding, without having to be de-rated:

- a negative sequence voltage unbalance factor - VUF_2 - of 1 % over a long period or 1.5 % over a short period (in minutes).
- a zero sequence voltage unbalance - VUF_0 - of 1 %.

(j) Three-phase AC/DC rectifiers

AC/DC rectifiers are used in dc motors and as front end rectifiers in inverters. The influence of negative sequence voltage unbalance on these devices is explained and quantified in [38] using an ideal three-phase diode rectifier (Figure 2.15). It is shown to result in:

- unequal phase currents (i_a, $i_b$and i_c);
- less steady dc output voltage ripple (v_d); and
- additional third harmonic currents (i.e. more than what might be expected had the voltages been balanced).

Figure 2.16 shows the waveforms of the dc output voltage and phase currents under balanced voltage conditions. Equal phase currents result because six times in each cycle, the capacitor is charged to the same half-wave peak voltage and subsequently discharged over equal time intervals.

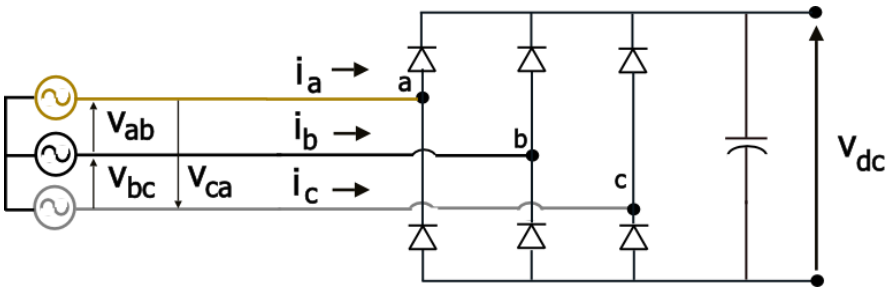

Figure 2.15: Three-phase diode rectifier [38]

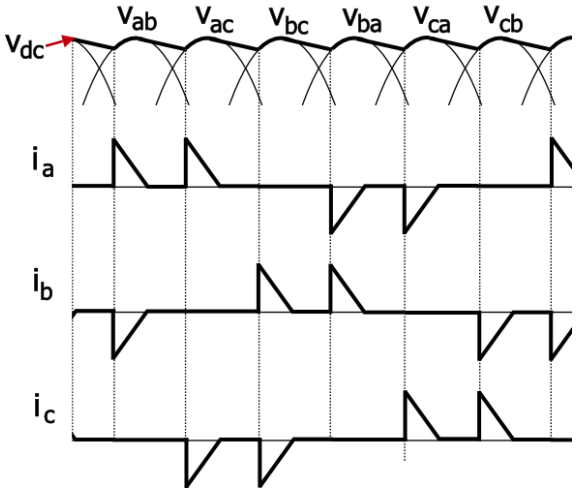

Figure 2.16: Waveforms under balanced voltage conditions [38]

Unbalanced voltages can result in three modes of operation as categorised in [38]. They are referred to as the *six-pulse mode*, the *four-pulse mode* and the *two-pulse mode*, according to the number of half-wave peak voltages appearing in the dc voltage waveform.

An example of a *six-pulse mode* of operation is shown in Figure 2.17. In it, the half-wave peak voltages for V_{ca} are increased slightly. As can be seen the dc output voltage is no longer a steady, uniform ripple. Also, the phase currents are no longer equal (the phase A and C currents differ from that seen under balanced conditions).

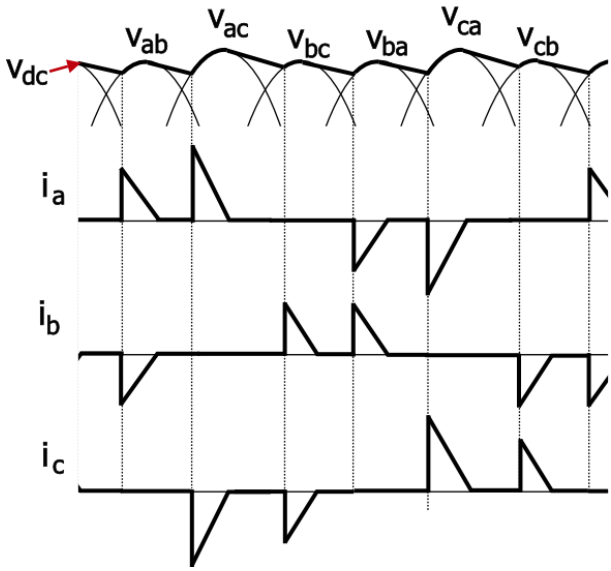

Figure 2.17: Waveforms under unbalanced voltage conditions (six-pulse mode) (adapted from [38])

The four-pulse and two-pulse modes of operation are shown in Figure 2.18 and Figure 2.19 respectively.

In the case of the four-pulse mode, one phase-phase voltage (say V_{ca}) is significantly less than the other two; so much so that the peaks of its half-wave voltages are less than the dc output voltage. The charging current is drawn only on the other four half-wave voltages (i.e. those of V_{ab} and V_{bc}). As can be seen, the dc output voltage is no longer a steady, uniform ripple. Moreover, less current is drawn from phases A and C.

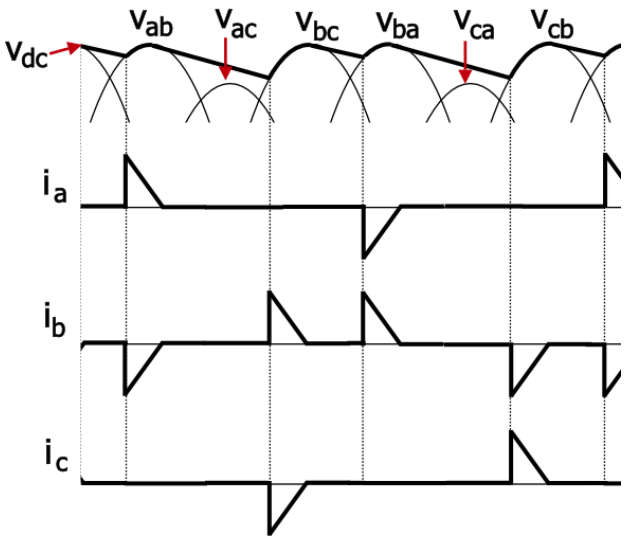

Figure 2.18: Waveforms under unbalanced voltage conditions (four-pulse mode) (adapted from [38])

With the two-pulse mode, one phase-phase voltage (say V_{ab}) is significantly more than the other two, and the capacitor is charged only for its half-wave peak voltages (i.e. V_{ab}

and V_{ba}). This is the same as if a single-phase rectifier was placed across V_{ab}. The result is no current is drawn from phase C.

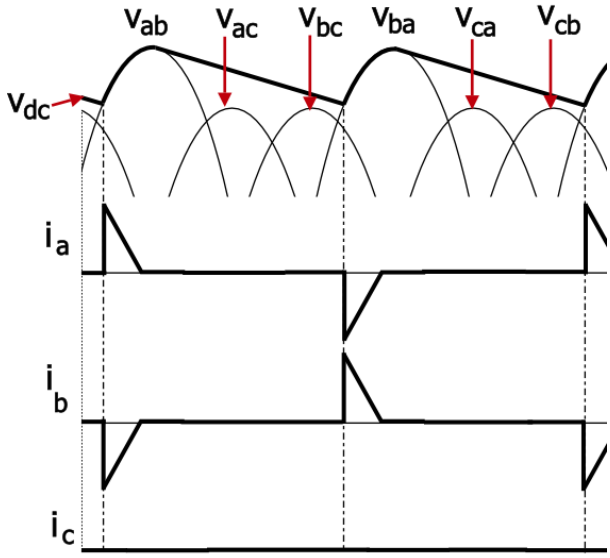

Figure 2.19: Waveforms under unbalanced voltage conditions (two-pulse mode) (adapted from [38])

These unbalanced phase currents affects the rectifier as unequal current flows on the legs of the rectifier circuit increases losses and may damage the rectifier components [38]. To the low-voltage network though, the change in phase currents drawn by the rectifier may actually reduce the current unbalance. For instance, in Figure 2.19 an increased V_{ab} may be the result of either phases A and B being lightly loaded or phase C being heavily loaded. As seen, the rectifier draws current from only the less loaded phases, which may contribute to some extent towards reducing the current unbalance on the network.

Also, as mentioned in [38], these phase currents (which are short duration pulses) contain an additional third harmonic current which they show to be a multiple ($\sqrt{2}$) of the negative sequence current for all three unbalanced modes of operation.

(k) Three-phase inverters

Three-phase inverters, as shown in Figure 2.20, are used to connect low-carbon technologies to the network. The influence of negative sequence voltage unbalance on them is explained and quantified in [39]. There, the underlying principles are revealed with an example which assumes that the gating signals to the converter valves are

equally spaced and commutation is instantaneous. It is shown that, with unbalanced voltages at its terminals, the dc voltage of the three-phase inverter is composed of:

- a $v_{dc}^{+}(t)$ component corresponding to the positive sequence component of the unbalanced voltages at its terminals, which is the same waveform that would exist had the voltages been balanced; and
- a $v_{dc}^{-}(t)$ component corresponding to the negative sequence component of the unbalanced voltages at its terminals.

The latter appears in the dc voltage as a harmonic component of twice the fundamental frequency; the magnitude of which is $3\sqrt{3}/\pi$ times the magnitude of negative sequence voltage and is independent of the converter delay angle. The phase displacement of this ripple is however a function of the difference between the delay angle and the angle of the negative sequence voltage. Also present, but not as dominant, are higher-order harmonics at multiples of twice the fundamental frequency. If the inverter connects an electric machine, this can result in additional losses, torque pulsations and noise issues [40]. This problem can be minimised by using an appropriately sized dc capacitor or a suitable control method for the converter as discussed in [40] [41].

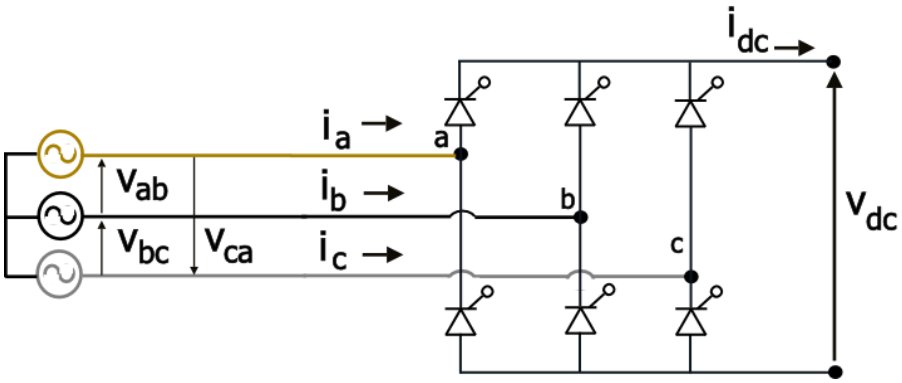

Figure 2.20: Three-phase inverter using thyristers [39]

The harmonics in the dc voltage can also result in harmonics in the dc current, with the 2nd order harmonic being the dominant component, which in turn results in unbalanced phase currents being drawn through the inverter, unless a properly sized smoothing reactor is used [39]. Further, as mentioned in [42], these phase currents will also contain 3rd harmonic components. With phase currents flowing through the inverter being unbalanced and having 3rd harmonic components, additional losses and damage to the inverter components can result. If the inverter is used as part of a photovoltaic

system (or any other low-carbon technology) these additional losses will reduce the average power output of the system.

2.4.3 Summary

- The negative sequence voltage unbalance is particularly important to three-phase consumer load equipment.
- The negative and zero sequence components of both voltage and current unbalance are important to the low-voltage network.
- Voltage unbalance is caused by current unbalance.
- Most of the effects on the low-voltage network are the result of current unbalance.

2.5 Adopting an LV network perspective differs from the consumer focus of the past

The standards have given emphasis to protecting consumer three-phase equipment by focusing on voltage unbalance. This has led to approximations and recommended limits for the negative sequence voltage unbalance factor only. The zero sequence voltage unbalance factor as well as both sequence current unbalance factors are mostly ignored.

This thesis instead gives emphasis to low-voltage network. In doing so, the differences between the two perspectives, must be recognised. They are identified in Table 2.2.

Consumer perspective	LV network perspective
Supply is:	
typically three-wire (no neutral)	four-wire with a multi-grounded neutral
Effects are driven by:	
voltage unbalance	current unbalance
Indicators that are of interest:	
VUF_2	All sequence unbalance factors (IUF_0, IUF_2, VUF_0 and VUF_2)
Locations in which these indicators are of interest:	
consumer's point of common coupling (PCC)	start and at the end of the feeder At start: IUF_0 and IUF_2 most onerous. At end: VUF_0 and VUF_2 most onerous.
Determining the potential source of the unbalance may include:	
LV network or consumer's other loads	HV network, loads of local feeder or other LV feeders from same distribution transformer.
Boundaries of interest (as depicted in* Figure 2.21*):	
consumer only (shaded in blue)	Includes LV network and consumers (shaded in yellow)

Table 2.2: Differences between the consumer and LV network perspectives

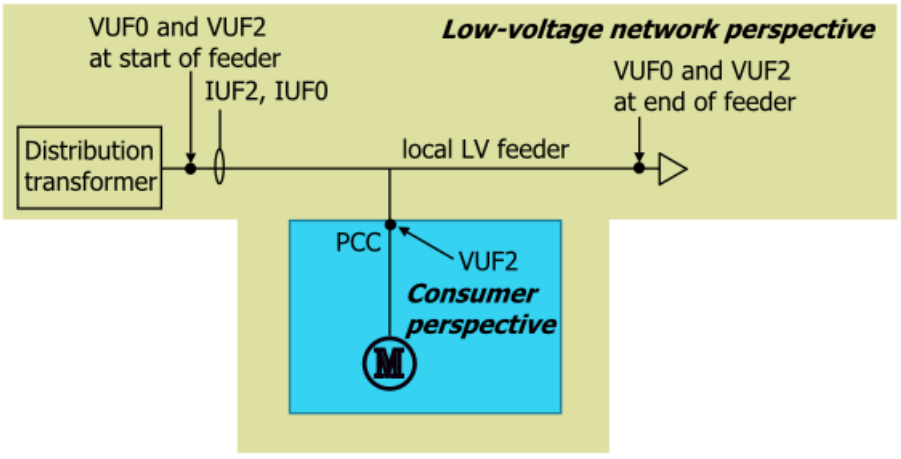

Figure 2.21: Consumer and network perspectives

2.5.1 Localised indicators of unbalance

Two important distinctions of the network perspective are that all the sequence unbalance factors are important and that there are more potential sources of the unbalance. To help understand these indicators, it is useful to categorise them into either localised or non-localised indicators. Localised indicators being those that identify with unbalance originating on the local feeder itself. And non-localised indicators being those which can be influenced by unbalance on other parts of the network (HV network or other LV feeders from the same distribution transformer).

Consider if measurements are taken at the start and at the end of a local feeder, as depicted in Figure 2.22.

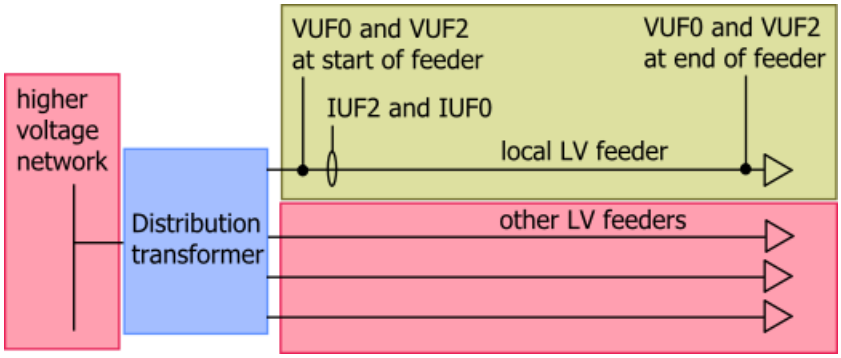

Figure 2.22: Indicators of unbalance on a local LV feeder

Both sequence current unbalance factors depend only on the unbalance of the loads on the local feeder. And so, they are inherently localised indicators of unbalance.

The zero sequence voltage unbalance factor, seen at the start of the feeder, is isolated from the HV network by the delta-star winding of the distribution transformer. It will depend only on the unbalance of loads on all feeders supplied from the distribution transformer. At the end of the rural feeder however, it will depend more on the unbalance of the loads on the local feeder. So at the end of the feeder, it may be a localised indicator.

The negative sequence voltage unbalance factor on the other hand is not isolated from the HV network, as the delta-star winding of the distribution transformer does not block negative sequence voltages. It can therefore be influenced by the negative

sequence voltage unbalance originating from the high-voltage feeder. Also, it is influenced by voltage unbalance on the other low-voltage feeders. Because of this, it cannot be considered a localised indicator of unbalance at any point of the local feeder.

2.6 Mitigation of voltage and current unbalance

Different methods are used to correct unbalance and each can be related to the mitigation of one or several of the effects identified in Figure 2.13. The primary goals though, of most of these methods are to ensure that:

- consumer three-phase equipment are not affected by voltage unbalance; and
- utility equipment at the higher voltages are not affected by unbalance caused at the lower voltages.

The discussion which follows presents mitigation methods either adopted or proposed for electricity networks in several countries. As such, the location of corrective measures may vary depending on the style of the system, which may be either North American or European. The characteristics of both system styles are covered in [43]. For clarity, Figure 2.23 (a) and (b) gives the location of corrective measures for both styles of systems.

The mitigation methods are identified by (A) to (F) in Figure 2.23 (a) and (b). The sections which follow are labelled with the mitigation option – (A) to (F) – to be discussed.

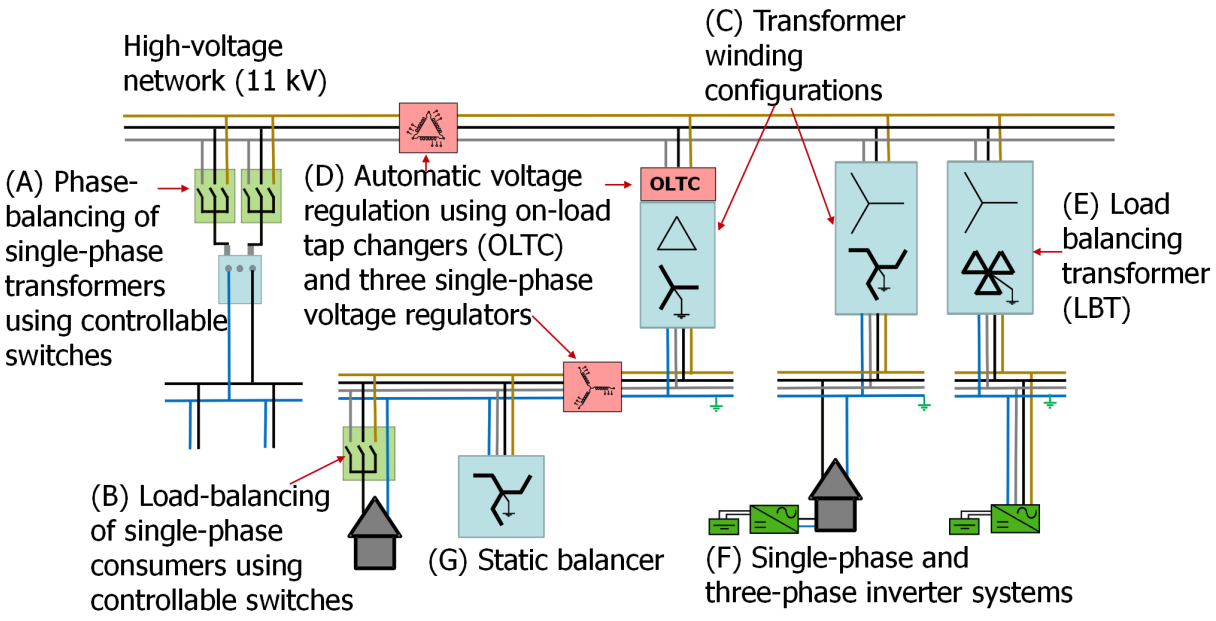

(a)

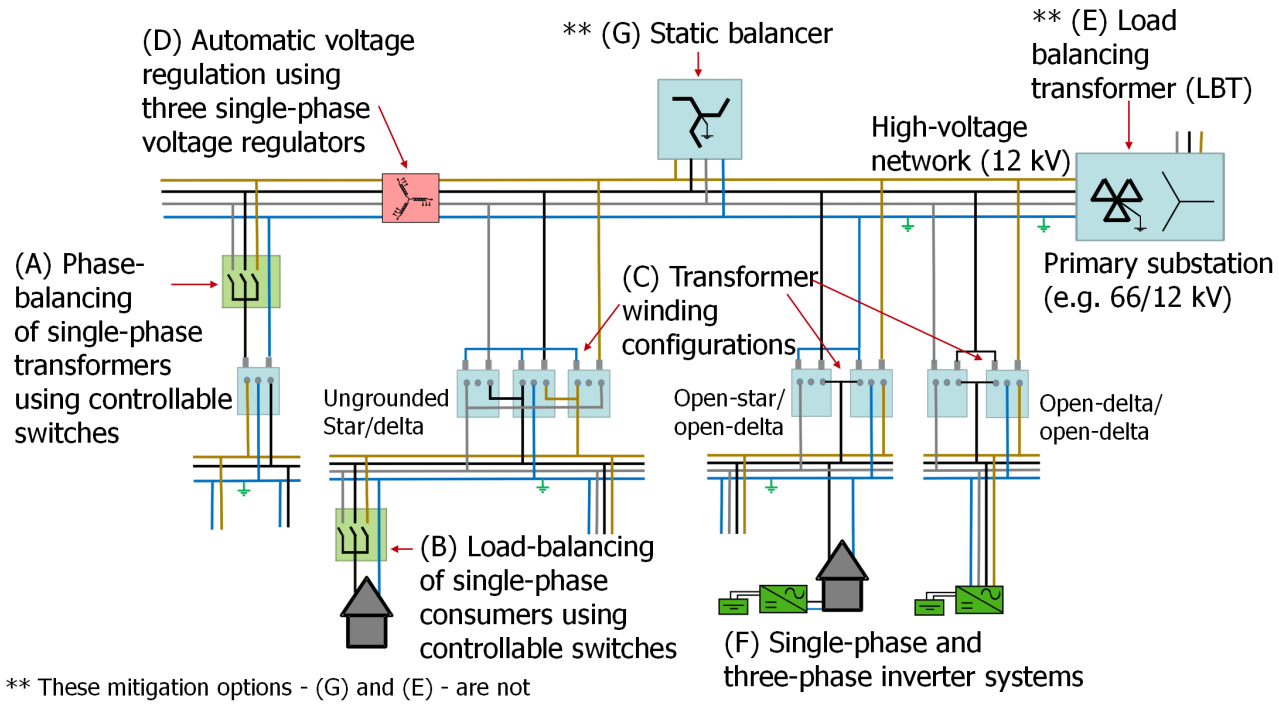

** These mitigation options - (G) and (E) - are not used on North American style systems.
Suitable locations suggested.

(b)

Figure 2.23: Mitigation methods on (a) European and (b) North American system styles

2.6.1 (A) Phase and (B) load balancing as complementary functions to network reconfiguration

Network reconfiguration is a process which can be carried out on the high-voltage network. Its objectives are primarily to minimise losses and relieve overloads [44], [45]. This is done by rearranging sections of the high-voltage network using sectionalizing or tie switches so as to transfer load from heavily loaded to less loaded sections of the network. This method looks at the power losses across sections and does so without catering for the current unbalance on them.

Network reconfiguration can however be complemented by phase and load balancing on the low-voltage network as proposed in [44]. The objective of these complementary functions is to arrive at a more even distribution of loads between the three phases, i.e. the reduction of current unbalance. Phase balancing involves reassigning the connection of single-phase transformers along a high-voltage feeder and load balancing involves reassigning the connection phase of individual consumers. They may be implemented either by:

- ***A manual trial and error approach.*** This traditional approach requires lots of field measurements and analysis to determine which phases to reconnect transformers, which consumers to reassign, or which sections of the low-voltage network to reconfigure. As was mentioned in [44] and [46] though, it rarely succeeded in reducing the unbalance to the extent that would have justified the considerable service interruptions needed to effect the changes and the improvements which may be seen, rarely last for very long. It should be noted as well that this approach is more difficult with underground systems as opposed to overhead line systems, as the consumer's phase is not visible and there are fewer positions available to connect measurement instruments.
- ***Automated distribution networks.*** This provides advantages technically and economically to implement phase and load balancing in real-time. Several techniques have been proposed in [44] and [47]. They include heuristic and neural network algorithms [44], implemented at the high- and low-voltage levels, which seek optimal solutions to problems of phase current balancing and

loss minimisation, respectively. Another algorithm [47] proposes using the principle of superposition to minimise the probabilistic voltage drop on the low-voltage feeder by systematically assigning phases to the individual or grouped consumers at different nodes along the feeder.

Regardless of the algorithm, the solution found determines the statuses (on/off) of controllable static switches strategically located on the network. At the high-voltage, these switches re-arrange the connection between the feeder and single-phase transformers (*phase balancing*). And at the low-voltage level, they assign single-phase loads to the different phases along the low-voltage feeder (*load balancing*). This approach requires more network monitoring and the strategic locating of switches.

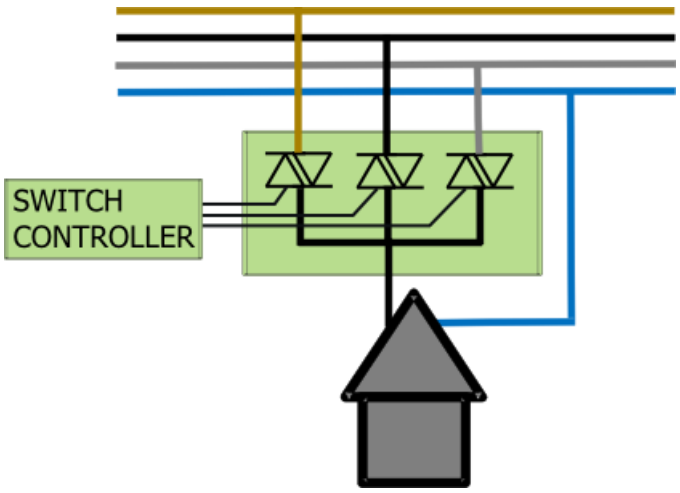

Figure 2.24: Proposed controllable static switch used to connect a consumer to one of the three phases [44]

2.6.2 (C) Transformer winding configurations, ratings and impedances

As shown in Figure 2.23, in North American style systems, three-phase and single-phase loads are supplied through different winding configurations typically having a four-wire delta secondary. The winding configurations used are the star/delta, open-star/open-delta or open-delta/open-delta. Of them the star/delta is best suited to supply single-phase loads. Further, these transformer banks are made by wiring together single-phase transformers. They comprise a larger transformer (called the lighting transformer), which supplies the single-phase loads and at least one other transformer (called the power transformer) which supplies the three-phase loads. The ratings and impedances of these transformers are usually different, resulting in asymmetric impedances (due to differing self-impedances). This, along with the winding configuration results in unbalanced secondary voltages [48], [32]. In some cases, as was shown in [49], high voltage unbalance on the secondary may be corrected by the closing the open-star/open-delta bank with a third single-phase transformer.

On European style systems, mostly three-phase transformers with delta/star winding configurations are used. Although this is well suited to the supply of unbalanced loads, another suitable winding configuration is the star/interconnected-star [8]. This winding configuration is not typically used because it has a larger frame size and so costs more. The use of these windings on distribution transformers as a standard practice is responsible for:

- limiting unbalanced secondary voltages as a result of supplying single-phase loads; and
- blocking the propagation of zero sequence current unbalance onto the higher voltage network [8], [50].

In the mitigation method (E), a third, more recently developed winding configuration is presented.

2.6.3 (D) Automatic voltage regulation

Automatic voltage regulators are typically used for the voltage regulation of all three-phases simultaneously. They can however be configured to regulate individual phase-neutral voltages so as to reduce voltage unbalance.

The use of automatic voltage regulators on the high-voltage network of North American style systems is described in [51]. They consist of three single-phase step-voltage regulators wired together in either star or closed delta configuration. The star configuration is shown in Figure 2.25. Each step-voltage regulator consists of an autotransformer and an on-load tap changer (OLTC). The tap changer is controlled by a line drop compensator which models the voltage drop on the high-voltage feeder. To do this the compensator impedance is calibrated against the actual line impedance.

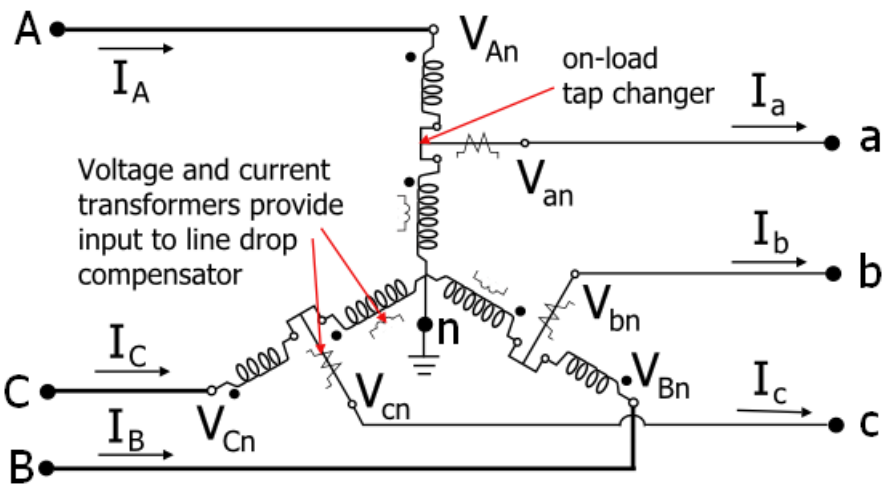

Figure 2.25: Star connected three-phase step-voltage regulators (type B) [51]

When used to improve voltage regulation, the three single-phase step-voltage regulators are gang operated, with all taps controlled by a single compensator circuit.

However, when used to reduce voltage unbalance, the three single-phase regulators are independently operated, each controlled by its own compensator circuit. The taps on each regulator change separately, regulating individual phase-neutral voltages. Examples in [51] demonstrate this and show that with different tap positions on each regulator, the device is capable of balancing phase-neutral voltages. It should be

pointed out however, that from these examples, the improvement in current balance appears limited.

Automatic voltage regulators had been used on the low-voltage networks of European style systems [52]. This included use of both independently operated and gang operated automatic voltage regulators. Their use however, is no longer a standard practice [10]. Even so, they have been included as part of an on-going field trial by Electricity Northwest [53]. The automatic voltage regulators in this field trial are however being used to improve voltage regulation and not to reduce voltage unbalance (i.e. they are gang operated).

2.6.4 (E) The load balancing transformer (LBT)

This is a distribution transformer with an unconventional winding configuration based on a patent [54] by T.J. Reynal in 1996. The original design has been improved upon by others [55] [56] through simulations and experiments undertaken on a 12 kVA laboratory prototype. The novelty in this unconventional winding configuration is that it achieves a better sharing of currents on the primary side of the distribution transformer when serving unbalanced loads. This type of winding configuration can therefore:

- improve the utilisation of distribution transformer capacity; and
- better mitigate the propagation of current unbalance from the low-voltage to high-voltage networks.

This technology is however in an early stage of development.

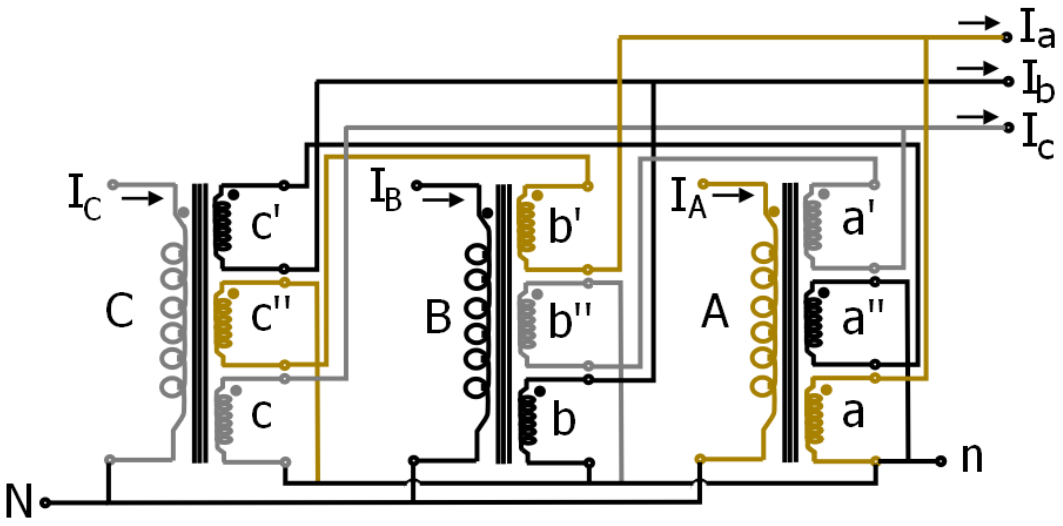

Figure 2.26: The original load balancing transformer (LBT) [54], [55]

Figure 2.26 shows the *original load balancing transformer* (LBT) design [54], [55]. The secondary of each phase consists of three windings connected such that each load current draws two-thirds of its current through one winding and one-third from a set of two windings in series. So for instance, two-thirds of the secondary current I_a is supplied by winding a and one-third by windings b' and c''. In this way each of the secondary load currents are not drawn equally from the three primary phases. This results in a better sharing of currents on the primary side of the distribution transformer. Figure 2.27 gives a comparison of the currents seen on the primary side of the two conventional winding configurations - delta/star and star/interconnected-star - to that of the *original load balancing transformer*. As an example of the benefit to this

sharing of primary current, consider the losses assuming a line resistance of R_L. On the two conventional windings, the total losses will be $2I_P^2R_L$ whilst with the original load balancing transformer it will be $(\frac{3}{2})I_P^2R_L$.

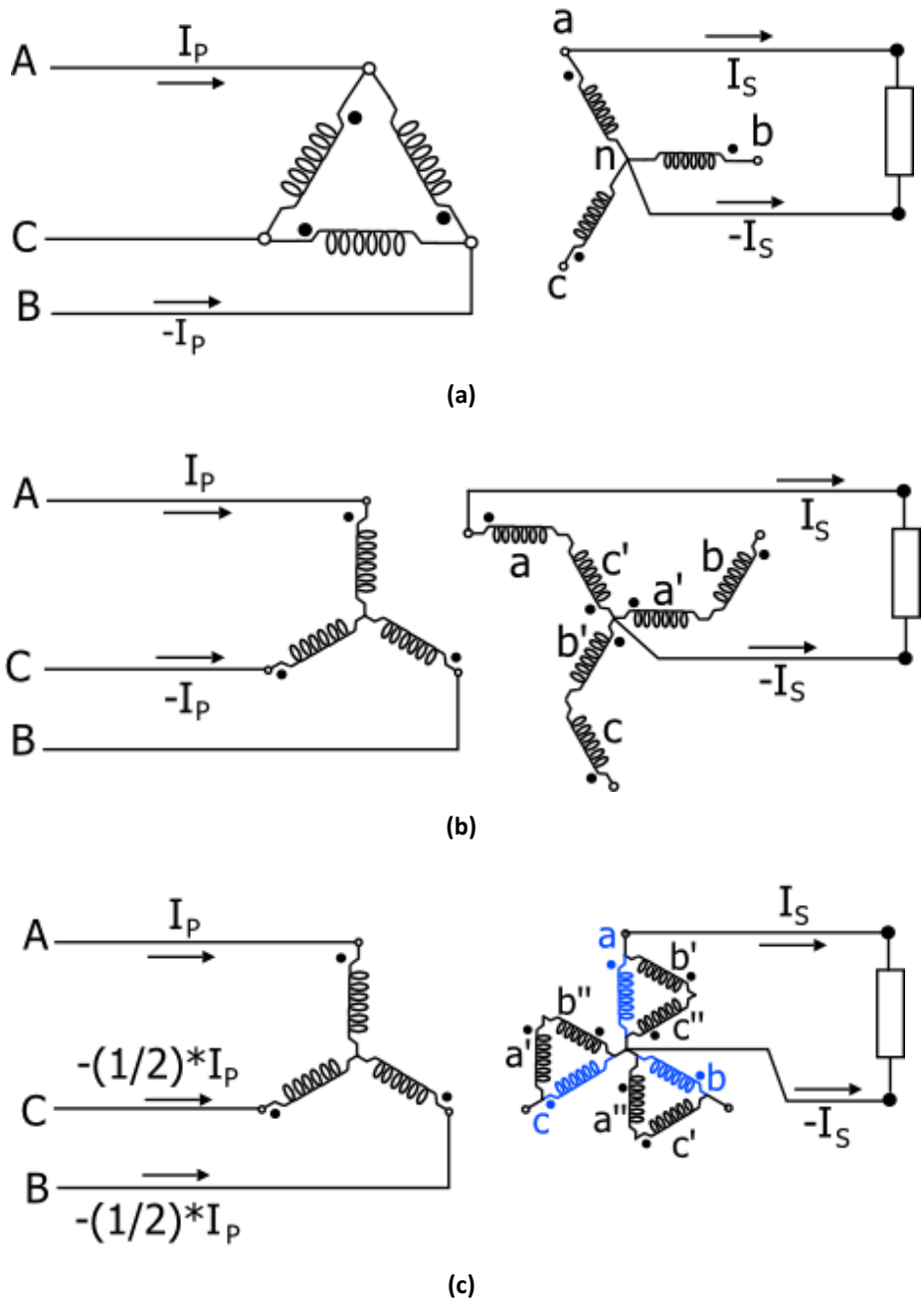

Figure 2.27: Comparison of primary current sharing for several transformer winding configurations (a) Delta/Star, (b) Ungrounded star/interconnected-star and (c) Load balancing transformer [8], [55]

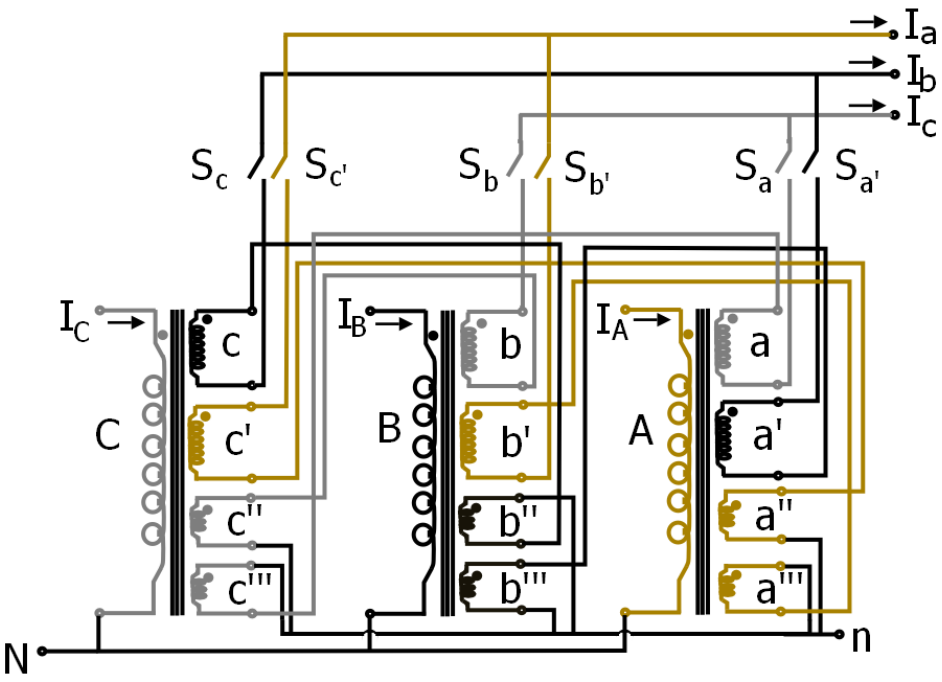

Figure 2.28: Single-stage switch-mode best load balancing transformer (or switch-mode best LBT) [55]

An improved design called the *single-stage switch-mode best load balancing transformer* (or *switch-mode best LBT*) has been developed by Ahmadi and Bina et al [55]. This is shown in Figure 2.28. This design includes additional coupling windings along with six switches (two per phase – one for the series winding and the other for the coupling windings). A controller is used to determine the best possible switching states required to achieve near balanced primary currents by altering the configuration of these secondary windings based on the unbalanced secondary load current present. Simulated and experimental results presented in [55] showed:

- improved transformer capacity utilisation over *original load balancing transformer* (Figure 2.26); and
- Reduced negative and zero sequence components of the primary currents.

There was one disadvantage however, in that even though the *switch-mode best LBT* reduces the zero sequence current considerably, it does not eliminate them as would the *original load balancing transformer* (or any of the conventional winding configurations shown in Figure 2.27). This should however be weighed against the improved transformer capacity utilisation and having a design which is responsive to changes in the unbalanced secondary currents.

2.6.5 (F) DC/AC inverter systems with unbalance compensation as an ancillary function

Inverters are used by low-carbon technologies to interface with the low-voltage network. Most inverters are presently designed to deliver primarily active power and positive sequence currents. They can however be designed with the mitigation of voltage unbalance or current unbalance in mind. The attention here is on those which can do the latter.

Several proposals are presented in the literature for inverters used in photovoltaic micro-generation, fuel cells and energy storage systems. They include both single-phase and three-phase inverter designs.

Three-phase inverter designs

The choice of inverter topology is very important if these systems are to be used for unbalance compensation on low-voltage networks. This is because the inverter must be able to supply both negative and zero sequence currents. In [57] the strengths and weaknesses of three inverter topologies suitable for this application are discussed. These are summarized in Table 2.3. The three-leg split capacitor converter (TLSC), which is most commonly used on low-voltage and medium-voltage networks [57] [58], is shown in Figure 2.29. The dc-bus voltage can be energized by photovoltaic micro-generation, fuel cells and energy storage systems (or other low-carbon technologies).

A disadvantage to the inverter design, in providing unbalance compensation as an ancillary function, is that large dc capacitors are used [58]. This is because of the need to reduce the 2^{nd} harmonic component which appears on the dc voltage when the voltages at the inverters terminals are unbalanced. Also, in the case of the three-leg split capacitor converter (TLSC) shown in Figure 2.29, to cater for harmonic currents flowing through the two capacitors and into the neutral.

Inverter topology	Strengths	Weaknesses
Three-leg split capacitor converter (TLSC)	Control simplicity. Lower cost.	Some limitations to zero sequence voltage and current compensation.
Four-leg full bridge converter (FLFB)	Higher zero sequence currents compensation than (TLSC).	Control very complex and expensive.
Three-bridge four wire converter (TBFW)	Control simplicity. Even higher zero sequence current compensation than (FLFB). Suitable for higher power applications.	Expensive.

Table 2.3: Three-phase inverter topologies suitable for compensating zero sequence currents

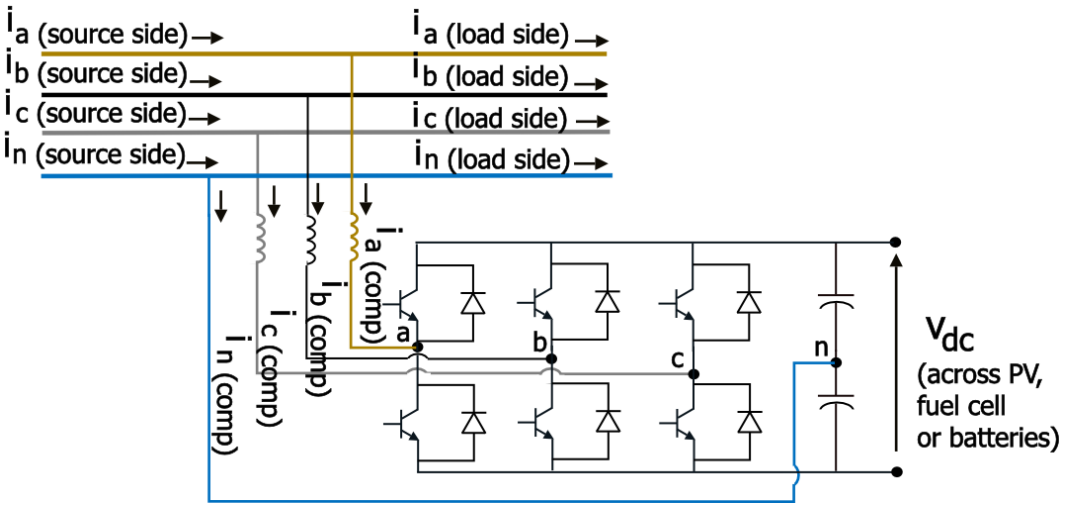

Figure 2.29: Three-leg split capacitor converter (TLSC) [57]

Another important aspect in the design of these systems is the unbalance compensation strategy. Several are presented in [59]. They involve setting reference values for the inverter phase currents, expressed in sequence components, in relation to the voltages at its terminals using two input conductances - g_1 (fundamental input conductance) and g_d(damping input conductance). In one of the strategies presented in [59], *the three-phase damping control strategy*, g_1 was used to control the positive sequence reference current and g_d was used to control the negative and zero sequence reference currents. This was expressed by:

$$\begin{bmatrix} i_0 \\ i_1 \\ i_2 \end{bmatrix} = \begin{bmatrix} g_d & 0 & 0 \\ 0 & g_1 & 0 \\ 0 & 0 & g_d \end{bmatrix} \begin{bmatrix} v_0 \\ v_1 \\ v_2 \end{bmatrix} \quad (2.4)$$

In this way both negative and zero sequence currents were supplied by the inverter. Other strategies can be used which supply positive sequence currents along with:

- the zero sequence current only as in [57]; or
- the negative sequence current only as proposed in [60] for the higher voltage network.

As illustrated in Figure 2.29, supplying zero and/or negative sequence components to the downstream load currents, reduces the current unbalance on the low-voltage network upstream of the inverter system. Further, as shown in [59], the voltage unbalance at the point of interconnection will also be reduced.

Single-phase inverter designs

The use of three-phase inverters on the low-voltage network, in which single-phase connections predominate, can be anticipated to have very limited application without considerable network upgrades and expenditures. Recognizing this, the use of single-phase inverters for unbalance compensation has been proposed for photovoltaic micro-generation [61] and energy storage systems [62].

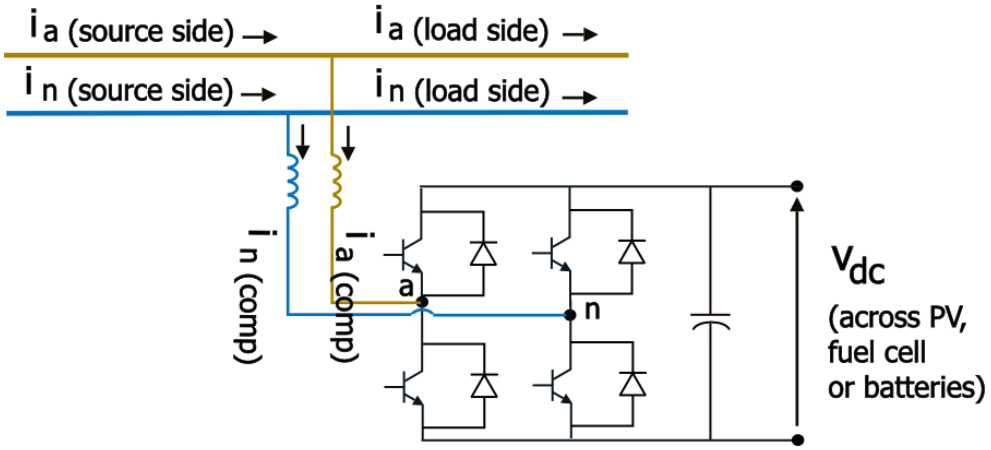

Figure 2.30: Single-phase full-bridge inverter

Several inverter topologies are suitable, including the full-bridge inverter and the half-bridge inverter [63]. The full-bridge inverter is shown in Figure 2.30. The real challenge with having a single-phase connection is in the unbalance compensation strategy. This is because, with only two wires connected to the network, there are limits to the visibility and control of voltages and currents. Two strategies proposed include:

- The adjustment of the active power output from an energy storage system so as to minimize the neutral current monitored on the low-voltage network [62]; and

- The adjustment of reactive power output from a photovoltaic micro-generation system so as to maintain the phase-neutral voltage at some reference value [61].

There are practical limitations to each. In the first, the neutral current (on low-voltage network) must be measured and provided as input to the controller of the energy storage system. In the second, larger capacity inverters are required [61].

In addition to the proposals presented in the literature, there is also a smart grid pilot project presently underway by Scottish and Southern Energy [64], which will investigate both single-phase and three-phase inverter designs with energy storage systems as well as a three-phase inverter design with no energy storage [65]. This latter variant would be the power electronic equivalent to the static balancer.

The use of inverter systems for unbalance compensation may have several disadvantages including:

- In the case of single-phase inverter designs, these may not be owned by the utility. To a distribution network operator, this can introduce uncertainty in low-voltage network planning. The mitigation of unbalance on their low-voltage networks will rely on uptake of these technologies by consumers (an unknown) as opposed to any of the other mitigation options mentioned which they may introduce as required by themselves;
- They may contribute more harmonics to the low-voltage network;
- They would not be able to correct unbalance throughout the day. For instance, if used with photovoltaic micro-generation, the inverter capacity will be available during night hours only;
- They may involve the use of batteries, which in addition to incurring energy losses in charging and recharging, will also have significant environmental costs; and
- They may, as in the case of the two strategies proposed for single-phase inverter systems, involve a renewable energy source either having its active power output constrained to minimize neutral currents or being used to produce reactive power to support the voltage.

2.6.6 (G) The static balancer

Explanations of how the static balancer improves current and voltage unbalance are presented in [8] and [9]. Figure 2.31 shows the static balancer on the low-voltage network with a single-phase load connected to phase B. It is assumed that the single-phase load has unity power factor and the phase and neutral wires are resistances R_L and R_N, respectively. The influence of the static balancer is best appreciated by looking at the phasor diagrams of current (Figure 2.32) and voltage (Figure 2.33) with and without the static balancer.

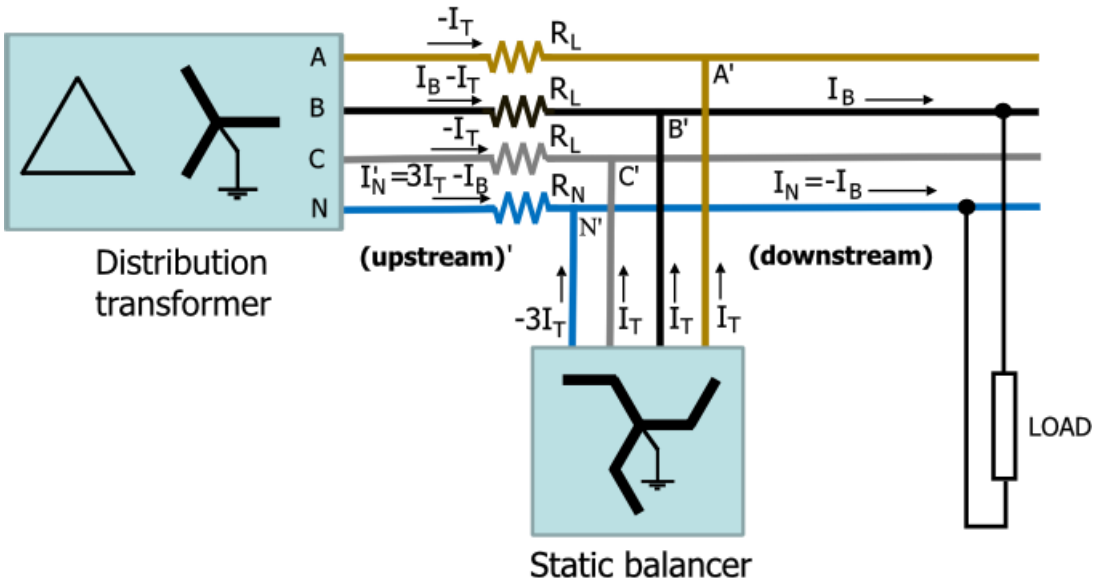

Figure 2.31: Simple example explaining influence of static balancer using a single-phase load on phase B

(a) Without static balancer **(b) With static balancer**

Figure 2.32: Current phasors with and without static balancer connected

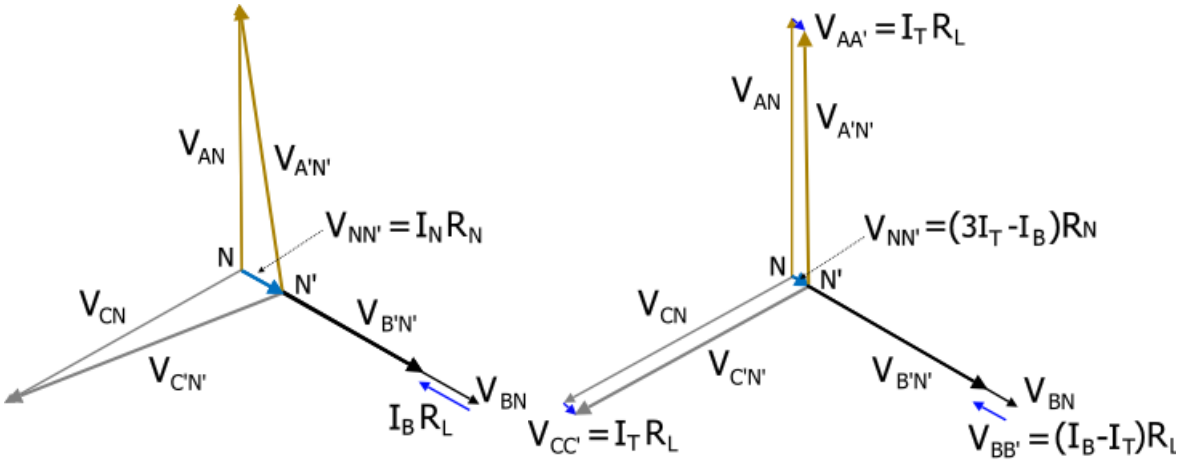

(a) Without static balancer **(b) With static balancer**

Figure 2.33: Voltage phasors with and without static balancer connected

Without the static balancer connected the total load current flows on phase B and is returned on the neutral. The net result is that:

- the phase-neutral voltage on the loaded phase V_{BN} is decreased by the flow of I_B
  - along the line, which results in a voltage drop $I_B R_L$, as well as
  - its return along the neutral ($I_N = -I_B$), which results in the movement of the neutral in same direction as loaded phase.
- the phase-neutral voltages on the unloaded phases V_{AN} and V_{CN} are increased by
  - the movement of the neutral.

The static balancer once connected, draws some of the neutral current (because it has a low zero sequence impedance) and shares it equally onto the three phases. The result of this redistribution is that:

- the phase-neutral voltage on the loaded phase V_{BN} is improved as the voltage drops on the line - $(I_B - I_T)R_L$ - as well as on the neutral – $(3I_T - I_B)R_N$ - are decreased; and
- the phase-neutral voltages on the unloaded phases V_{AN} and V_{CN} are improved because the voltage drops, which now appear on them, move in the same direction as that on the neutral.

Specification

For the static balancer to perform effectively it must be properly specified in relation to the low-voltage feeder. Several key items are:

- *Impedance (ohms).* The proportion of the neutral current drawn by the static balancer depends on its impedance in relation to that of the network. If it is set too high then less of the neutral current will be shared amongst the phases;
- *Rating (kVA).* This will determine the maximum current that can be drawn by the static balancer. It should be greater than the maximum neutral current anticipated on the low-voltage feeder; and
- *Iron losses (kW) and winding resistance (ohms).* They determine the losses on the static balancer which should ideally work out less than the reduction in losses due to its mitigation of current unbalance.

Deployment

In the Midlands Electricity Board (MEB) Notes on the static balancer [9] it is stated that in deciding the position of the static balancer on the low-voltage feeder, the following should be kept in mind:

- the voltage drop on the neutral for an unbalanced load located downstream of the static balancer will be greater than if the same unbalanced load was placed exactly the same distance away but upstream of the static balancer.
- the voltage drop due to the unbalanced load increases rapidly with distance from the static balancer.

This, it is argued, leads to the recommendation that the most suitable position for the static balancer is at the end of the low-voltage feeder. This recommendation applies to a straightforward radial low-voltage feeder as shown in Figure 2.34 (a). For branched low-voltage feeders as shown in Figure 2.34 (b) and (c), the recommended position and number of static balancers will vary depending on the length of the tee-offs and the severity of the current unbalance on them. In (c), two static balancers are recommended if the current unbalance is severe.

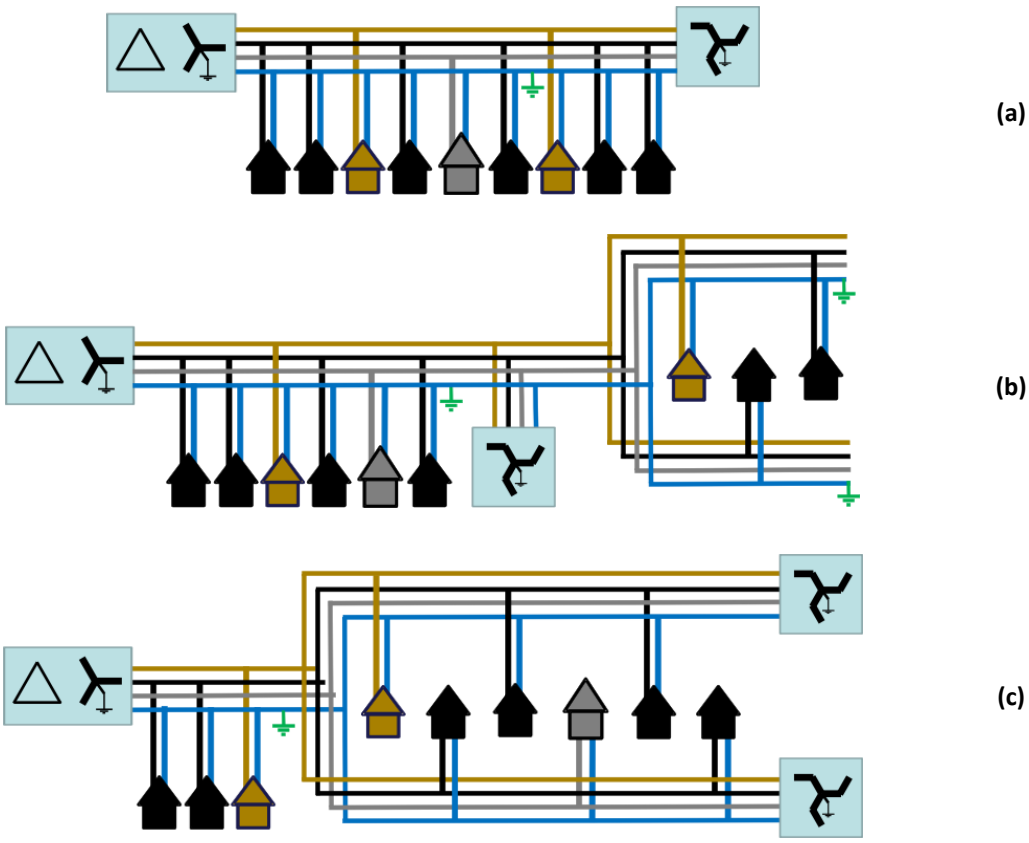

Figure 2.34: Recommended positions on low-voltage feeders as given in [9]

Modelling of static balancer

Existing representations of the static balancer [7] [8] were developed prior to modern computing. They include:

1. A method for constructing a circular chart to determine the current distribution on the upstream side of a static balancer when used to provide a neutral point on a three-wire, low-voltage feeder [7]. *(1919)*; and
2. The solution of a simple circuit comprising the static balancer, network impedances and distribution transformer [8]. This representation is useful for illustrating the ability of the static balancer to reduce unbalance. *(1930s)*

Both representations were the basis of several parts of [8].

Use of static balancers alongside automatic voltage regulators

There are opposing views to this in the literature. In [52], the combined use of these devices is discussed. It is argued that a smaller and thus cheaper automatic voltage regulator is required if installed alongside a static balancer. This is because as the static

balancer reduces the voltage drop on the neutral, there is also a reduction in the voltage variation between lightly loaded and heavily loaded phases (i.e. effect (g) of Figure 2.13). This minimises the job required of the automatic voltage regulator, which per kVA is more expensive.

The combined use of both devices was however, not favoured by the Midlands Electricity Board (MEB) [9]. The main reason given was that the need for static balancers usually arises long before that for automatic voltage regulators and the position chosen for the static balancer, which as recommended in [9] would usually be towards the end of the low-voltage feeder, may not be the most ideal for an automatic voltage regulator (which is usually placed upstream of the loads).

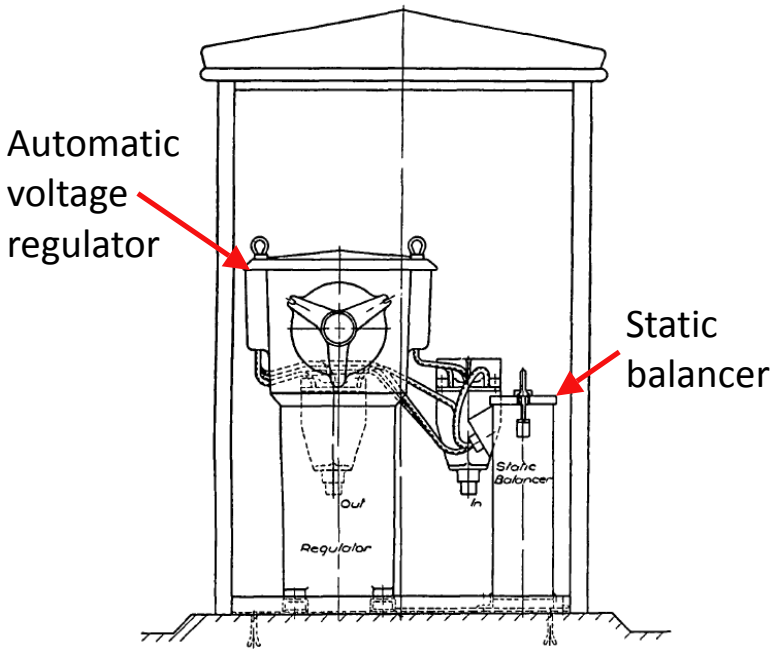

Figure 2.35: Automatic voltage regulator and static balancer in a kiosk [52]

An additional benefit

The interconnected-star winding of the static balancer also enables it to reduce voltage and current harmonics. Several transformer manufacturers [66] [67] market *3rd Harmonic Rejection Transformers (HRT)* or *Neutral Current Traps (NCT)* for reducing harmonics at industrial and commercial sites. These devices also have an interconnected-star winding and are therefore very similar to the static balancer.

This benefit is advantageous considering that in addition to worsening unbalance, low-carbon technologies using inverter systems will also add to the harmonics on the low-voltage network. For the distribution network operator this means that a single network device can be used to solve both problems. This will translate not only into savings but practical benefits, such as minimising the number of locations on low-voltage feeders required to place new equipment.

It was felt, in the early stages of this work, that to discuss and examine both concepts – unbalance and harmonics - in parallel would have taken away from the narrative and depth of work in each topic. The issue of unbalance was identified by the industrial supervisors as the immediate concern, given its effect on network utilisation, and so was given preference.

2.6.7 Summary

- Methods which correct current unbalance also improve voltage unbalance.
- The mitigation methods may grouped depending on if their emphasis is on reducing:
    - *Current unbalance:* (a) phase-balancing, (b) load balancing, (g) the static balancer and (f) inverter systems.
    - *Voltage unbalance:* (c) transformer winding configuration, (e) load balancing transformer and (d) automatic voltage regulation.
    - *Propagation of unbalance onto the higher voltage network:* (c) transformer winding configuration and (e) load balancing transformer.

  These groupings are linked to the effects of unbalance in Figure 2.36.
- Table 2.4 summarises the merits and demerits to each mitigation method. It can be seen that:
    - Three methods – load balancing, inverter systems and static balancer – will correct both voltage and current unbalance on low-voltage networks.
    - The static balancer has many advantages, making it worthy of closer investigation.
    - The single-phase inverter systems are one of the less favoured methods, mainly because they may not be utility owned. That may not be the case with three-phase inverter systems, and for that reason they are a more favoured option.
    - The load balancing method is also a good option for low-voltage networks. Its main drawback is that it may add complexity.

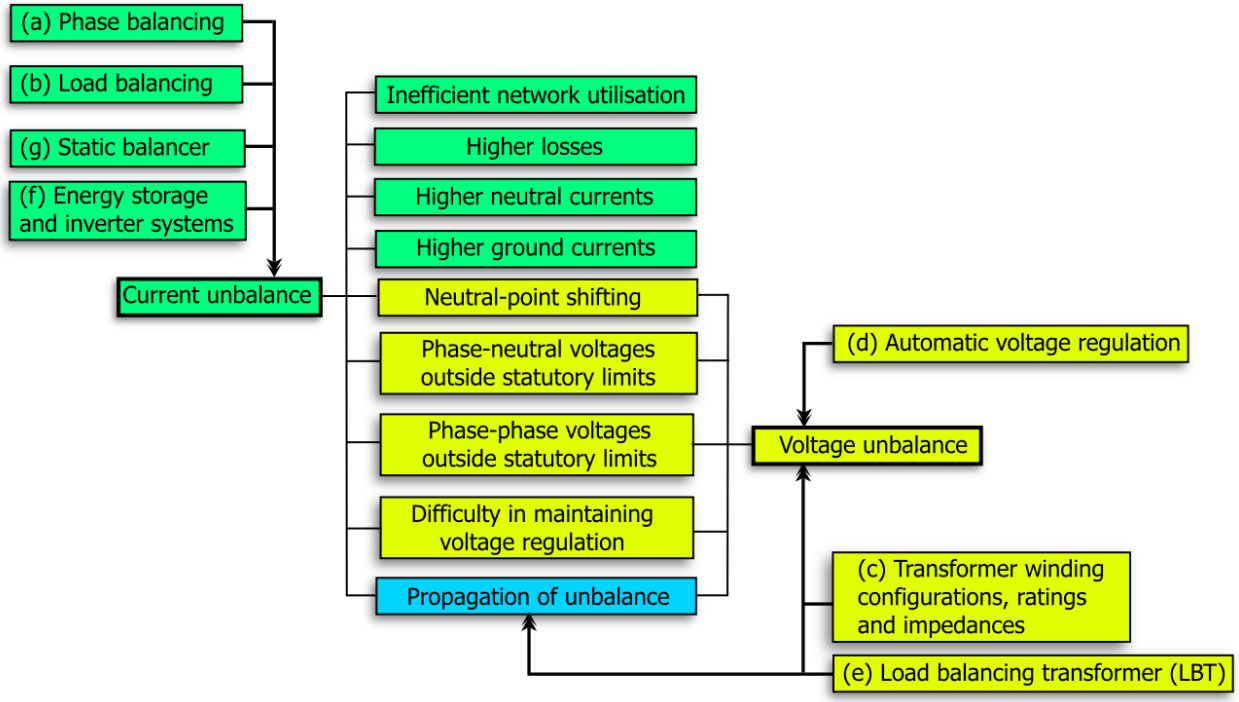

Figure 2.36 : Effects of voltage and current unbalance linked to mitigation measures

		(A) Phase balancing	(B) Load balancing	(C) Transformer winding configurations	(D) Automatic voltage regulation	(E) Load balancing transformer		(F) Inverter systems		(G) Static balancer
						Orig.	Impr.	3ph	1ph	
Reduces current unbalance	HV	+		+		+	+			
	LV		+					+	+	+
Reduces voltage unbalance	HV	+			+					
	LV		+	+	+	+	+	+	+	+
Involves retrofit only (as opposed to replacement)		+	+	-	+	-	-	+	+	+
Reduces harmonics				+/-		+	+	+/-	+/-	+
Preserves simplicity		-	-	+	-	+	-	-	-	+
Utility ownership		+	+	+	+	+	+	+	-	+
Total		+++	+++	+++	+++	++++	++	+++	+	++++++

Legend : + improves +/- depends on design - worsens

Table 2.4: Table of merits and demerits for the various mitigation methods

2.7 Conclusions of literature review

The unequal distribution of consumers and variations in consumer demands during the day are the dominant causes of unbalance on the low-voltage network. It leads to current unbalance which has a variety of effects on the low-voltage network. The standards however focus on only one of these effects, voltage unbalance. They also give particular emphasis to the negative sequence voltage unbalance factor. This is adequate when unbalance is viewed from a consumer perspective where its effects on three-phase induction motors and AC/DC rectifiers are of concern. Adopting a low-voltage network perspective however requires that both voltage and current unbalance be given emphasis in investigating and quantifying the effects of unbalance. It also means that both sequence components – negative and zero – must be considered.

Mitigation methods which focus on correcting current unbalance will lead to a greater benefit to the low-voltage network. Several mitigation methods were considered and of them, the static balancer was the most favoured method. In addition to correcting both current and voltage unbalance, it has other merits including preserving simplicity and reducing harmonics which make it a very good choice. Unlike the other mitigation options though, it has not been covered in recent literature.

2.8 Objectives and elucidated tasks

The primary aim and objectives, outlined in section 1.4, are restated below. Each objective is now broken down into tasks. They centre upon furthering the understanding of:

- unbalance from a low-voltage network perspective; and
- the ability of the static balancer to mitigate unbalance.

The working chapters in which these tasks are covered are identified.

2.8.1 Primary aim

To reduce current unbalance on low-voltage networks so as to avoid constraints in the uptake of low-carbon technologies and minimise the need for future network upgrades.

2.8.2 Research objectives with elucidated tasks

Objective (a): To accurately model and solve very unbalanced low-voltage feeders.

Theory

Task (a.1): Review the approaches used to solve radial low-voltage networks in terms of their suitability for the study of unbalance and its effects. *(Chapter 3)*

Network simulations and Field

Task (a.2): Model an actual low-voltage feeder (cables and lines) and validate network simulation results (voltages and currents) against field measurements. *(Chapter 7)*

Objective (b): To investigate the causes and quantify the effects of current unbalance on low-voltage networks.

Theory and Network simulations

Task (b.1): Solve a representative low-voltage feeder so as to investigate and quantify the relationships of each sequence current unbalance to effects on the network. *(Chapter 4)*

Field

Task (b.2): Demonstrate from field measurements the relationships between the effects of unbalance and the unbalance factors. *(Chapter 6)*

Objective (c): To investigate the behaviour and quantify the benefits of the static balancer to low-voltage networks.

Theory

Task (c.1): Develop a static balancer model for use in an unbalanced power flow method. *(Chapter 5)*

Laboratory

Task (c.2): Validate the static balancer model by experiments in the laboratory. *(Chapter 5)*

Field

Task (c.3): Validate the static balancer model by measurements taken on an actual low-voltage feeder. *(Chapter 6)*

Task (c.4): Investigate the behaviour of the static balancer on an actual low-voltage feeder. *(Chapter 6)*

Task (c.5): Quantify the benefits to an actual low-voltage feeder of using the static balancer. *(Chapter 6)*

Network simulations

Task (c.6): Compare the benefits found from network simulations with the static balancer model to those from field measurements. *(Chapter 7)*

3. Low-voltage network modelling and analysis

3.1 Objectives and tasks

This chapter supports ***Objective (a)*** by fulfilling:

Task (a.1): *Review the approaches used to solve radial low-voltage networks in terms of their suitability for the study of unbalance and its effects.*

It is a pre-requisite to the simulations needed in ***Objectives (b) and (c)***.

3.2 Overview

This chapter starts with a description of the typical low-voltage feeder circuit to be solved. It gives the nomenclature to be used throughout the thesis. The basic assumptions of the typical low-voltage feeder circuit are also given.

Next, the unbalanced power flow problem is stated, identifying the inputs and outputs for its solution. Its solution typically involves using a forward-backward sweep method. There are several approaches to using this method. These approaches are presented, identifying challenges, assumptions and approximations typically made. In each approach, the costs of simplification are identified. In this way, these approaches, which might be used in most off-the-shelf software and literature, are ruled out.

A new approach is then proposed; it solves the typical low-voltage feeder circuit described without further assumptions or approximations, especially with regard to the neutral and ground paths. This new approach to the forward-backward sweep method is then validated by a series of tests to show that its results satisfy Kirchhoff's voltage

and current laws (KVL and KCL) and are a match to Matlab Simulink SimPowerSystems. As will be seen later in the thesis, this however is the first stage in the validation, as a comparison with actual field measurements on a rural low-voltage feeder follows later in Chapter 7.

Additionally, the results from the new approach are compared against those from the standard 3 x 3 approach, so as to confirm that it delivers an improvement in accuracy.

An overview of the chapter is shown in Figure 3.1.

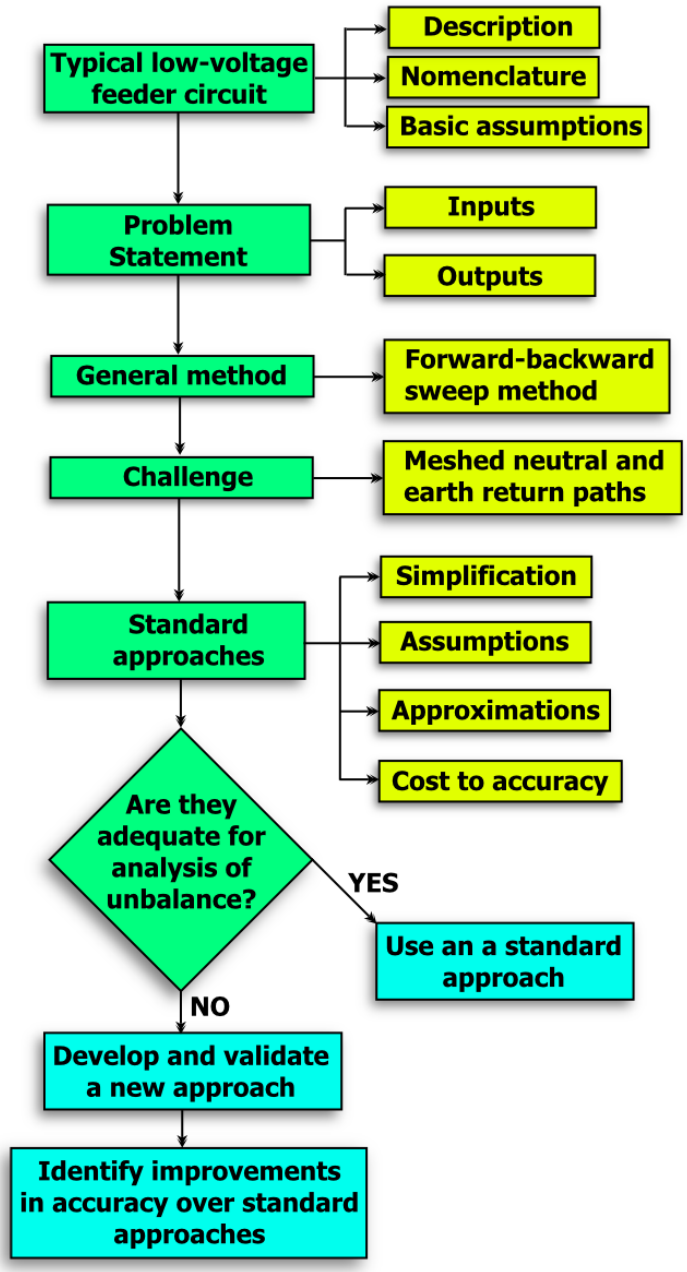

Figure 3.1: Overview of Chapter 3

3.3 A typical low-voltage feeder circuit

The topology of a radial low-voltage feeder with a multi-grounded neutral is illustrated by a typical low-voltage feeder shown in Figure 3.2. It consists of a main feeder backbone branching out with laterals and then from laterals, sub-laterals and so on. Figure 3.3 provides a closer look at the circuits which represent its general components. They include (a) the start of the feeder, (b) a junction node # with load, (c) a generic sub-lateral off junction node # (d) a generic branch segment l and (e) a generic load at node j.

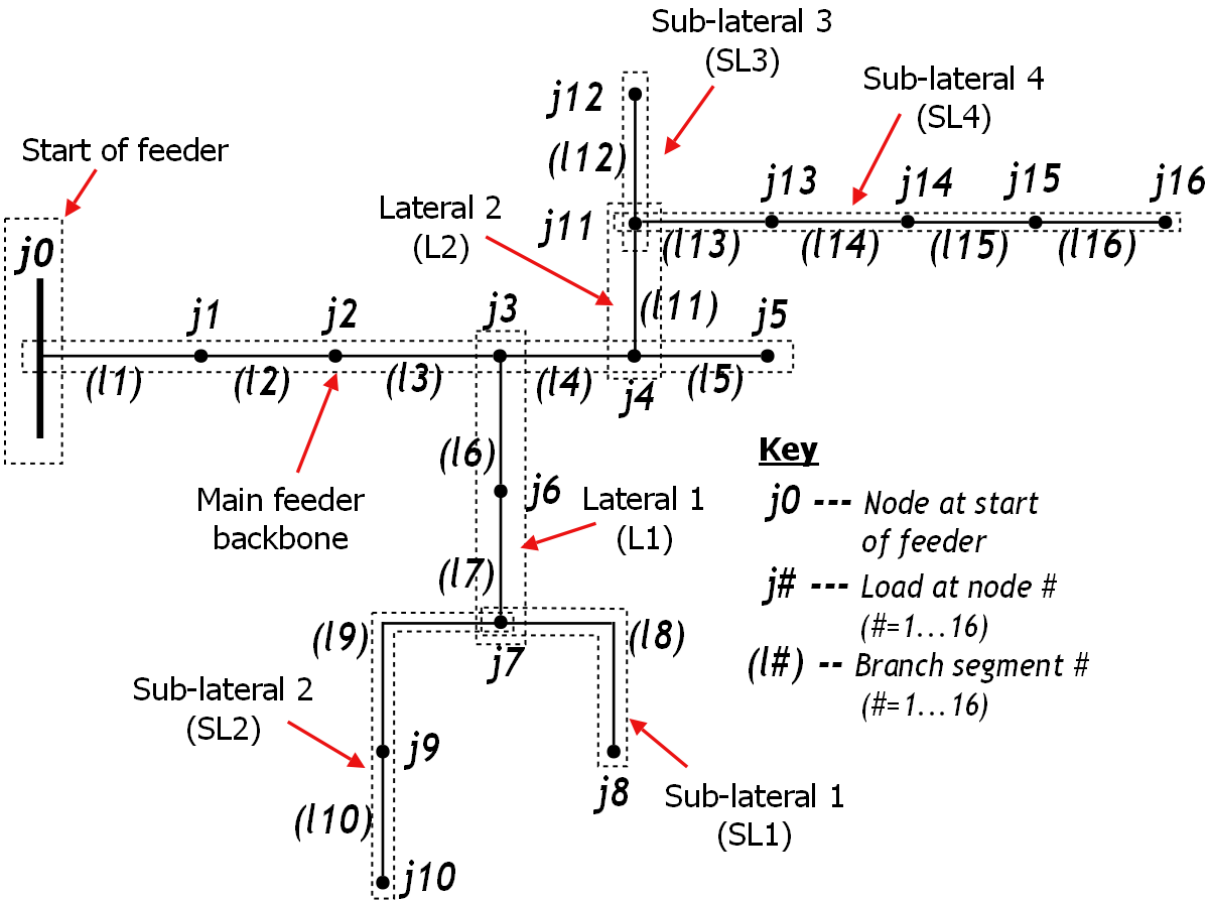

Figure 3.2: Typical low-voltage feeder circuit showing main feeder backbone, laterals and sub-laterals.

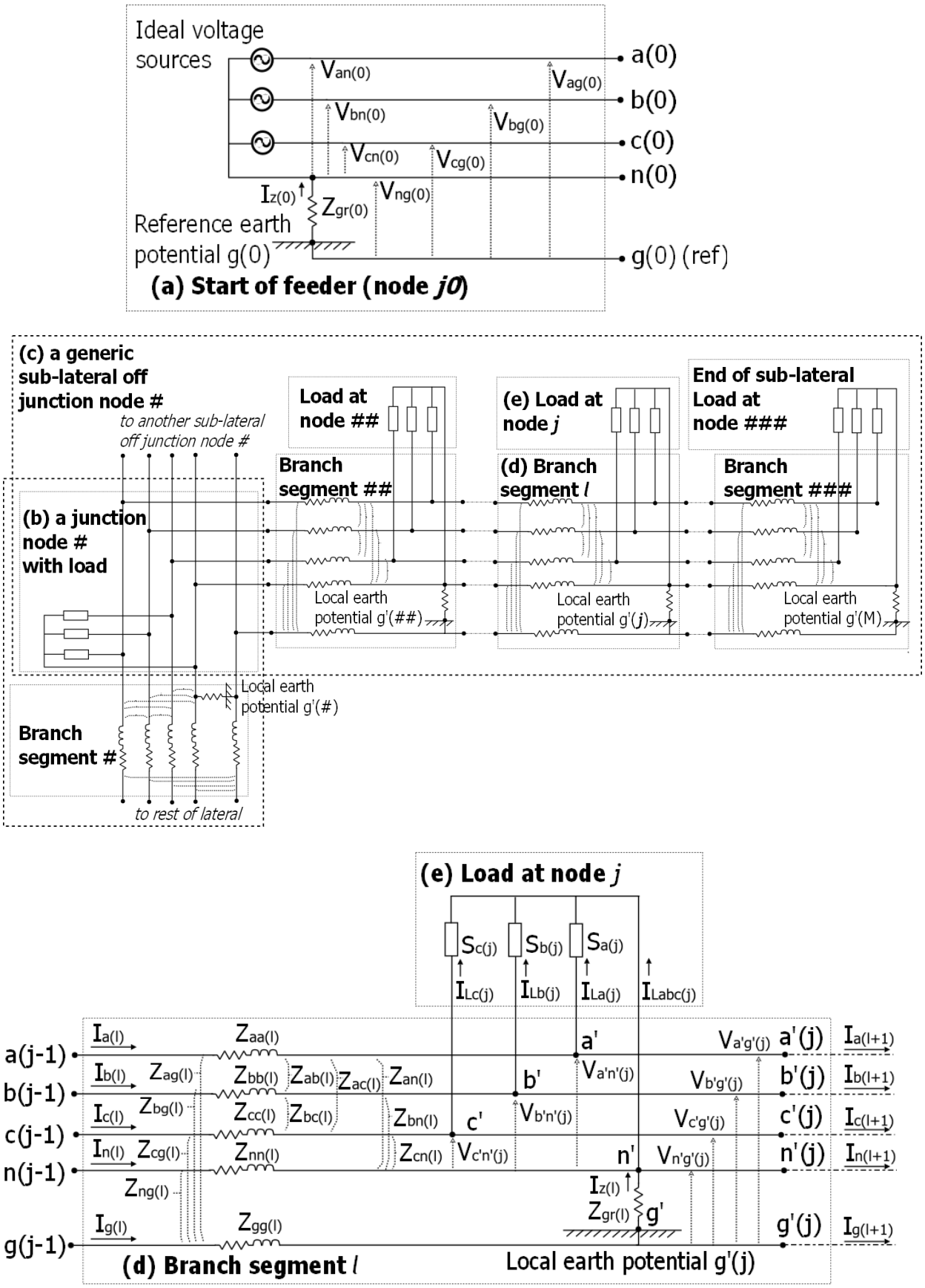

Figure 3.3: More detailed view of (a) start of feeder (*j*0), (b) a junction node # with load, (c) a generic sub-lateral off junction node #, (d) a generic branch segment *l* and (e) a generic load at node *j*.

3.3.1 Description

The following are descriptions of these general circuit components.

Start of the feeder

The voltages at the start of the feeder are set by ideal voltage sources connected between phase and neutral. They represent the voltages at the terminals of the distribution transformer.

The earth point $g(0)$, is taken as the reference for all other voltages on the feeder.

Start of laterals or sub-laterals

These are the junction nodes from which laterals or sub-laterals emerge. The junction nodes of Figure 3.2 are nodes 3, 4, 7 and 11.

Branch segments l

The branch segment l represents the cable impedances along with Carson's assumed earth return [68] [69]. Primitive self and mutual impedances, as defined in [70], are used to represent all phase, neutral and assumed ground wires. The impedance calculation method covered in [70], which is based on Carson's papers [68]and [69], are applied in Appendix A for several typical cable designs.

Branch segment l is represented by a 5 x 5 series impedance matrix. Recognising the reciprocity of the mutual impedances within a cable ($Z_{ab} = Z_{ba}$ etc.), this is given by:

$$Z_{abcng} = \begin{bmatrix} Z_{aa} & Z_{ab} & Z_{ac} & Z_{an} & Z_{ag} \\ Z_{ab} & Z_{bb} & Z_{bc} & Z_{bn} & Z_{bg} \\ Z_{ac} & Z_{bc} & Z_{cc} & Z_{cn} & Z_{cg} \\ Z_{an} & Z_{bn} & Z_{cn} & Z_{nn} & Z_{ng} \\ Z_{ag} & Z_{bg} & Z_{cg} & Z_{ng} & Z_{gg} \end{bmatrix} \quad (3.1)$$

where:

$Z_{aa}, Z_{bb}, Z_{cc} =$ self impedances of phase wires.

$Z_{ab}, Z_{ac}, Z_{bc} =$ mutual impedances between phase wires.

Z_{nn} = self impedance of neutral wire.

Z_{an}, Z_{bn}, Z_{cn} = mutual impedances between phase and neutral wires.

Z_{gg} = self impedance of assumed earth wire.

$Z_{ag}, Z_{bg}, Z_{cg}, Z_{ng}$ = mutual impedances between assumed earth wire and phase and neutral wires.

Earthing resistances

Connected between the neutral and earth, at the start of the feeder and at the receiving end of each branch l, are earthing resistances $Z_{gr(0)}$ and $Z_{gr(l)}$. They represent the resistances of the earth electrodes connected to the neutral at multiple points along the low-voltage feeder as well as the earth connections which may be made to metal work at consumer premises. As normal utility practice, earth electrodes – which would have a lower earthing resistance than the connections made to metal work - are located at the start and at the end of the low-voltage feeder.

Load at nodes j

At the end of branch segment l is node j. Connected between phases and neutral of node j, are three single-phase loads (or equally a three-phase load). They represent the consumer power demands. The behaviour of these loads may fit either one or a combination of load types including - constant power, constant impedance or constant current. The complex power demands are denoted by $S_{La(j)}, S_{Lb(j)}, S_{Lc(j)}$, impedances by $Z_{La(j)}, Z_{Lb(j)}, Z_{Lc(j)}$ and load currents by $I_{La(j)}, I_{Lb(j)}$ and $I_{Lc(j)}$.

Further, the total out-of-balance current at node j, given by the phasor sum of the load currents is denoted by $I_{Labc(j)}$.

3.3.2 Basic assumptions

The basic assumptions for the typical low-voltage feeder circuit are as follows:

- All voltages and currents are perfectly sinusoidal and at 50 Hz.
- The assumed earth wire is based on Carson's papers [68] [69], where the earth is assumed to be an infinite solid with uniform resistivity.

Both assumptions are typically made in the analysis of electricity networks [51] [70] [17]. The first assumption means that the model does not account for the influence of non-linear loads on rms voltages and currents. The second assumption is the basis for impedance calculations of cables and overhead lines with an earth return [70], which are presented in Appendix A. As mentioned in [71] there is a general acceptance of Carson's equations based on satisfactory results from many sources that have used them over the decades since they were published in 1926 but there is also an absence in the literature of follow-up work to prove or expand the theory behind his equations. For this thesis, it is recognised that adopting this assumption will affect the accuracy of the calculated earth and neutral currents as well as the movement of the neutral voltage with respect to earth reference $g(0)$. The validity of both assumptions will be seen later in Chapter 7 when simulations results are compared against measurements on an actual low-voltage feeder.

3.4 Problem statement

For the analysis of the effects of unbalance on the low-voltage network (depicted in Figure 2.13) the unbalanced power flow problem for the typical low-voltage feeder circuit may be stated as follows:

"Given the network impedances, the three phase-neutral voltages at the start of the feeder, the demands of all loads and their load type (constant power, constant impedance or constant current) solve the low-voltage network for the phase-neutral and neutral-ground voltage magnitudes and angles at all nodes and the phase, neutral and ground current magnitudes and angles on all branches."

The input and output terms are explicitly listed in Table 3.1 for a low-voltage feeder having M branches and N nodes.

	Input	Output
Impedances	$\begin{bmatrix} Z_{aa} & Z_{ab} & Z_{ac} & Z_{an} & Z_{ag} \\ Z_{ab} & Z_{bb} & Z_{bc} & Z_{bn} & Z_{bg} \\ Z_{ac} & Z_{bc} & Z_{cc} & Z_{cn} & Z_{cg} \\ Z_{an} & Z_{bn} & Z_{cn} & Z_{nn} & Z_{ng} \\ Z_{ag} & Z_{bg} & Z_{cg} & Z_{ng} & Z_{gg} \end{bmatrix}$ **For branches** $l = 1 \dots M$	
Loads	**Constant power:** $S_{La(j)}, S_{Lb(j)}, S_{Lc(j)}$ **Constant impedance:** $Z_{La(j)}, Z_{Lb(j)}, Z_{Lc(j)}$ **Constant current:** $I_{La(j)}, I_{Lb(j)}, I_{Lc(j)}$ **For nodes** $j = 1 \dots N$	
Voltages	$\begin{bmatrix} V_{an(0)} \\ V_{bn(0)} \\ V_{cn(0)} \end{bmatrix}$ **At start of feeder, node** $j = 0$.	$\begin{bmatrix} V_{a'n'(j)} \\ V_{b'n'(j)} \\ V_{c'n'(j)} \end{bmatrix}$, $V_{ng(0)}$ **and** $V_{n'g(j)}$. **For nodes** $j = 1 \dots N$
Currents		$\begin{bmatrix} I_{a(l)} \\ I_{b(l)} \\ I_{c(l)} \\ I_{n(l)} \\ I_{g(l)} \end{bmatrix}$ **For branches** $l = 1 \dots M$

Table 3.1: Input and output terms of unbalanced power flow solution

It should be appreciated that at node j, phase-neutral voltages are required as consumers and network devices are connected to the neutral and not to the earth point reference $g(0)$ at the start of the feeder nor any of the local earths $g(j)$, which in reality are all inaccessible.

The network is however more conveniently solved with voltages given with respect to $g(0)$. Determining phase-neutral voltages will require determining the neutral voltages accurately by finding $V_{ng(0)}$ and $V_{n'g(j)}$.

3.5 Overview of the general method

3.5.1 Overview

The forward-backward sweep method as described in [51] is typically used to solve the power flow problem on unbalanced, radial low-voltage feeders. It gives better convergence characteristics compared to the other, perhaps more familiar methods, such as the Newton Raphson or Gauss-Seidel methods which are typically used to solve the power flow problem on transmission networks.

The forward-backward sweep method traverses the feeder, from end to start and then start to end, one circuit component at a time - first finding currents and then voltages. In this manner first KCL and then KVL are applied to each circuit component. Due to the nonlinearity of the loads (constant power), this process is repeated iteratively until voltages converge. Using Figure 3.2 to demonstrate, each iteration consists of:

- **a forward sweep *(towards start of feeder or laterals/sub-laterals)* in which voltages are used to find load currents and then branch currents using KCL.**
  This goes from the sub-laterals, then to the laterals and lastly to the main feeder backbone. For the typical low-voltage feeder circuit of Figure 3.2, the forward sweep of sub-laterals are carried in the order of say – SL1, SL2, SL3 then SL4. It begins from the end node of the sub-lateral and moves towards its junction node. The currents found on the branches just downstream of the junction nodes 7 and 11 (to the sub-laterals) are then used in the forward sweep of the laterals L1 and L2. In a similar manner, the currents on the branches just downstream of junction nodes 3 and 4 (to the laterals) are used in forward sweep of the main feeder backbone. In this manner, all branch currents are estimated.
- **a backward sweep *(towards end of feeder or laterals/sub-laterals)* in which branch currents and sending end voltages are used to find the receiving end voltages using KVL.**
  This goes from the main feeder backbone, then to laterals and lastly to sub-laterals. On the main feeder backbone, the sending end voltages of the first

branch are set at the *start of the feeder* by the ideal voltage sources. In the backward sweep of the main feeder backbone, receiving end voltages for each of the branches are then found in turn using the branch currents found in the forward sweep. The voltages found for the junction nodes 3 and 4 (to the laterals) are used in the backward sweep of laterals L1 and L2. And similarly, the voltages found on the junction nodes 7 and 11 (to the sub-laterals) are used in the backward sweep of the sub-laterals.

3.5.2 The challenge – the currents through branch segment l

Looking at Figure 3.3 ((d) and (e)), it can be appreciated that in the forward sweep, the currents on the phase wires into branch segment l can be found easily by summating load currents with downstream branch currents. This is clear from the first three rows of equation (3.2).

$$\begin{bmatrix} I_{a(l)} \\ I_{b(l)} \\ I_{c(l)} \\ I_{n(l)}? \\ I_{g(l)}? \end{bmatrix} = \begin{bmatrix} I_{La(j)} \\ I_{Lb(j)} \\ I_{Lc(j)} \\ I_{Ln(j)} = (?/?)I_{Labc(j)} \\ I_{Lg(j)} = (?/?)I_{Labc(j)} \end{bmatrix} + \begin{bmatrix} I_{a(l+1)} \\ I_{b(l+1)} \\ I_{c(l+1)} \\ I_{n(l+1)} \\ I_{g(l+1)} \end{bmatrix} \tag{3.2}$$

Determining the neutral and ground current flows ($I_{n(l)}$ and $I_{g(l)}$) from the out-of-balance current of the load at node j ($I_{Labc(j)} = -\left(I_{La(j)} + I_{Lb(j)} + I_{Lc(j)}\right)$) and the downstream neutral and ground current flows ($I_{n(l+1)}$ and $I_{g(l+1)}$), however is not as straightforward. This will depend on the meshed neutral and earth return paths both upstream and downstream of node j.

In the backward sweep, the neutral and ground currents $I_{n(l)}$ and $I_{g(l)}$ are used to find the receiving end voltages. Therefore, if they are not determined correctly, the receiving end voltages will also be inaccurate and the network will more than likely not converge.

This problem is avoided in standard approaches to the forward-backward sweep method. In the next section these standard approaches are examined in detail. They

involve changes to the representation of branch segment l which affect the fourth and fifth rows of equation (3.2).

3.6 Standard approaches

3.6.1 Network simplification

This is explained in [51] and [70]. In the following sections, the 5 x 5 representation of Figure 3.4 is reduced first to a 4 x 4 and then to a 3 x 3 matrix representation.

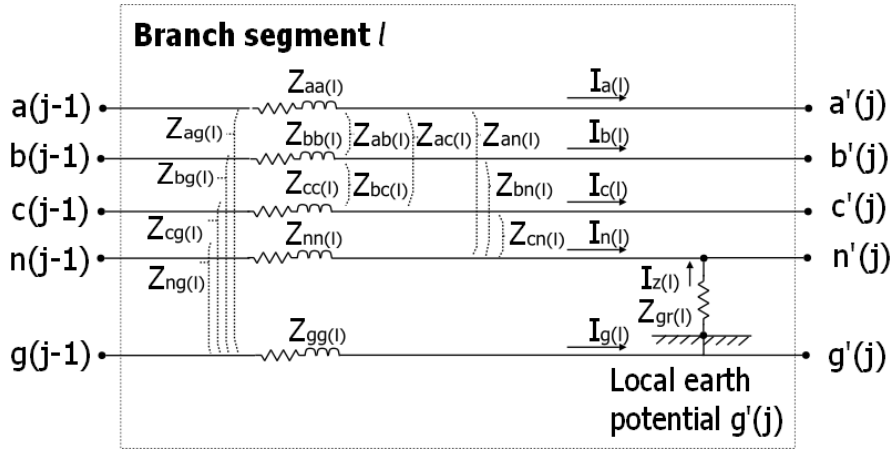

Figure 3.4: A closer look at a branch segment l between nodes $j-1$ and j

Reduction to a 4 x 4 matrix representation

The voltage drops across the phases, neutral and assumed earth wires are given by:

$$\begin{bmatrix} V_{aa\prime(l)} \\ V_{bb\prime(l)} \\ V_{cc\prime(l)} \\ V_{nn\prime(l)} \\ V_{gg\prime(l)} \end{bmatrix} = \begin{bmatrix} Z_{aa} & Z_{ab} & Z_{ac} & Z_{an} & Z_{ag} \\ Z_{ab} & Z_{bb} & Z_{bc} & Z_{bn} & Z_{bg} \\ Z_{ac} & Z_{bc} & Z_{cc} & Z_{cn} & Z_{cg} \\ Z_{an} & Z_{bn} & Z_{cn} & Z_{nn} & Z_{ng} \\ Z_{ag} & Z_{bg} & Z_{cg} & Z_{ng} & Z_{gg} \end{bmatrix} \begin{bmatrix} I_{a(l)} \\ I_{b(l)} \\ I_{c(l)} \\ I_{n(l)} \\ I_{g(l)} \end{bmatrix} \tag{3.3}$$

From Kirchhoff's current law (KCL):

$$I_{g(l)} = -\left(I_{a(l)} + I_{b(l)} + I_{c(l)} + I_{n(l)}\right) \tag{3.4}$$

Substituting this to eliminate $I_{g(l)}$ in equation (3.3) gives:

$$\begin{bmatrix} V_{aa\prime(l)} \\ V_{bb\prime(l)} \\ V_{cc\prime(l)} \\ V_{nn\prime(l)} \\ V_{gg\prime(l)} \end{bmatrix} = \begin{bmatrix} Z_{aa}-Z_{ag} & Z_{ab}-Z_{ag} & Z_{ac}-Z_{ag} & Z_{an}-Z_{ag} & 0 \\ Z_{ab}-Z_{bg} & Z_{bb}-Z_{bg} & Z_{bc}-Z_{bg} & Z_{bn}-Z_{bg} & 0 \\ Z_{ac}-Z_{cg} & Z_{bc}-Z_{cg} & Z_{cc}-Z_{cg} & Z_{cn}-Z_{cg} & 0 \\ Z_{an}-Z_{ng} & Z_{bn}-Z_{ng} & Z_{cn}-Z_{ng} & Z_{nn}-Z_{ng} & 0 \\ Z_{ag}-Z_{gg} & Z_{bg}-Z_{gg} & Z_{cg}-Z_{gg} & Z_{ng}-Z_{gg} & 0 \end{bmatrix} \begin{bmatrix} I_{a(l)} \\ I_{b(l)} \\ I_{c(l)} \\ I_{n(l)} \\ -\left(I_{a(l)} + I_{b(l)} + I_{c(l)} + I_{n(l)}\right) \end{bmatrix} \tag{3.5}$$

Applying Kirchhoff's voltage law (KVL):

$$\begin{bmatrix} V_{ag(j-1)} \\ V_{bg(j-1)} \\ V_{cg(j-1)} \\ V_{ng(j-1)} \end{bmatrix} = \begin{bmatrix} V_{aa'(l)} \\ V_{bb'(l)} \\ V_{cc'(l)} \\ V_{nn'(l)} \end{bmatrix} + \begin{bmatrix} V_{a'n'(j)} + V_{n'g'(j)} \\ V_{b'n'(j)} + V_{n'g'(j)} \\ V_{c'n'(j)} + V_{n'g'(j)} \\ V_{n'g'(j)} \end{bmatrix} - \begin{bmatrix} V_{gg'(l)} \\ V_{gg'(l)} \\ V_{gg'(l)} \\ V_{gg'(l)} \end{bmatrix} \quad (3.6)$$

Substituting the voltage drops given in equation (3.5):

$$\begin{bmatrix} V_{ag(j-1)} \\ V_{bg(j-1)} \\ V_{cg(j-1)} \\ V_{ng(j-1)} \end{bmatrix} = \begin{bmatrix} Z'_{aa} & Z'_{ab} & Z'_{ac} & Z'_{an} \\ Z'_{ab} & Z'_{bb} & Z'_{bc} & Z'_{bn} \\ Z'_{ac} & Z'_{bc} & Z'_{cc} & Z'_{cn} \\ Z'_{an} & Z'_{bn} & Z'_{cn} & Z'_{nn} \end{bmatrix} \begin{bmatrix} I_{a(l)} \\ I_{b(l)} \\ I_{c(l)} \\ I_{n(l)} \end{bmatrix} + \begin{bmatrix} V_{a'n'(j)} + V_{n'g'(j)} \\ V_{b'n'(j)} + V_{n'g'(j)} \\ V_{c'n'(j)} + V_{n'g'(j)} \\ V_{n'g'(j)} \end{bmatrix} \quad (3.7)$$

where

$Z'_{pq} = Z_{pq} - Z_{pg} - Z_{qg} + Z_{gg}$; $p = a, b, c, n$ and $q = a, b, c, n$

This new branch segment l' is shown in Figure 3.5 within the solid red block. Up to this point, it should be noted, no assumptions have been made. However, equation (3.7) cannot yet be solved because $I_{n(l)}$ remains unknown.

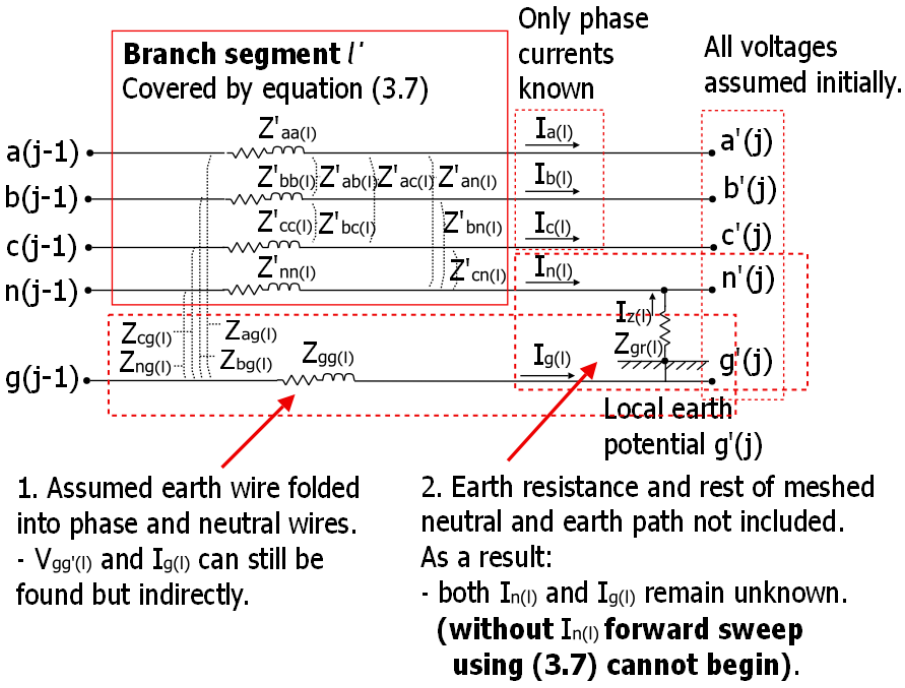

Figure 3.5: New branch segment l' represented by the 4 x 4 matrices.

The 4 x 4 representation as given by equation (3.7) can however be used, with no further assumptions, to solve an ungrounded low-voltage network ($Z_{gr(l)}$ effectively replaced by an open circuit). In that case, the current on the neutral depends only on the out-of-balance current $I_{Labc(j)}$ and the neutral current on the downstream branch $I_{n(l+1)}$. Equation (3.2) becomes:

$$\begin{bmatrix} I_{a(l)} \\ I_{b(l)} \\ I_{c(l)} \\ I_{n(l)} \\ I_{g(l)} \end{bmatrix} = \begin{bmatrix} I_{La(j)} \\ I_{Lb(j)} \\ I_{Lc(j)} \\ I_{Ln(j)} = I_{Labc(j)} \\ 0 \end{bmatrix} + \begin{bmatrix} I_{a(l+1)} \\ I_{b(l+1)} \\ I_{c(l+1)} \\ I_{n(l+1)} \\ I_{g(l+1)} \end{bmatrix} \quad (3.8)$$

The current flow on the assumed earth wire $I_{g(l)}$, though not given in equation (3.7) can be determined indirectly using equation (3.4). After which, $V_{gg'(l)}$ can be found from the fifth row of equation (3.3). For an ungrounded network, both $I_{g(l)}$ and $V_{gg'(l)}$are due to the mutual reactances between the assumed earth wire and the phase and neutral wires only. The out-of-balance current $I_{Labc(j)}$ which flows on the neutral wire, therefore influences them, but indirectly through the mutual reactance Z_{ng}.

For a multi-grounded low-voltage network for which the solution is being sought however, $I_{g(l)}$ is more directly related to $I_{Labc(j)}$, as identified in equation (3.2). The extent of this influence will depend in part on the earth resistances of meshed neutral and earth return paths.

Reduction to a 3 x 3 matrix representation

Reduction to a 3 x 3 representation is covered in [51]. This is the typical approach taken for multi-grounded low-voltage networks. It begins with equation (3.7) in which the assumed earth wire has already been *folded* into the phase and neutral wires. The neutral and earth return paths which are not fully accounted for are typically [51] dealt with by making two assumptions:

- ***Assumption 1:*** The **neutral is solidly connected to the local earths** on both sides of the branch segment l' making $V_{ng(j-1)} = V_{n'g'(j)} = 0$. The premise for this is that the low-voltage network is multi-grounded and so both voltages may be expected to be small.
- ***Assumption 2:*** $g(j-1)$ and $g'(j)$ are connected by a **perfect earth conductor**. The basis for this is that $V_{nn'(l)}$and $V_{gg'(l)}$are small by comparison to both phase-neutral or phase-ground voltages. All voltages are now said to be with respect to $g(0)$.

Both assumptions are depicted in Figure 3.6.

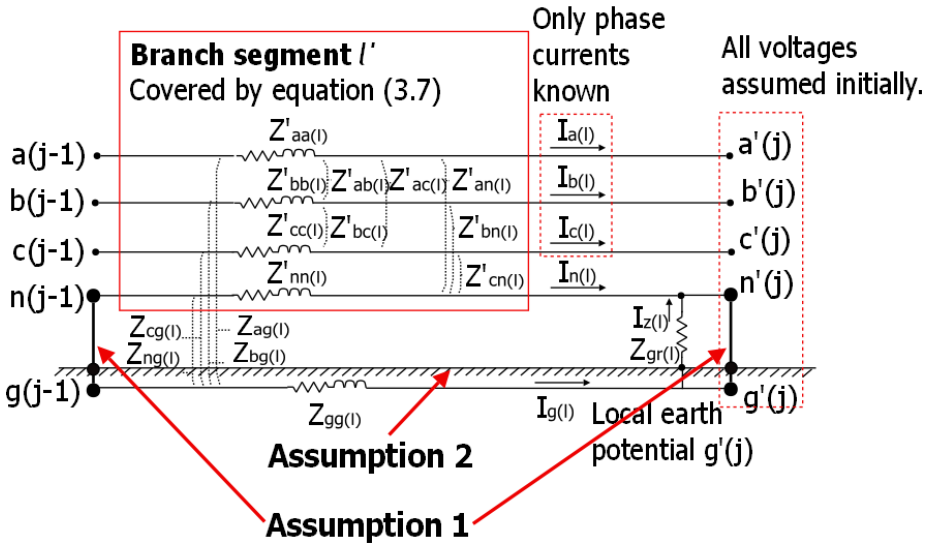

Figure 3.6: Assumptions made to branch segment *l'* to allow its reduction to a 3 x 3 representation.

Using Assumption 1 (neutral is solidly connected to local earths):

Letting $V_{ng(j-1)} = V_{n'g'(j)} = 0$ in equation (3.7) and partitioning the matrices:

$$\begin{bmatrix} V_{ag(j-1)} \\ V_{bg(j-1)} \\ V_{cg(j-1)} \end{bmatrix} = \begin{bmatrix} Z'_{aa} & Z'_{ab} & Z'_{ac} \\ Z'_{ab} & Z'_{bb} & Z'_{bc} \\ Z'_{ac} & Z'_{bc} & Z'_{cc} \end{bmatrix} \begin{bmatrix} I_{a(l)} \\ I_{b(l)} \\ I_{c(l)} \end{bmatrix} + \begin{bmatrix} V_{a'n'(j)} \\ V_{b'n'(j)} \\ V_{c'n'(j)} \end{bmatrix} + \begin{bmatrix} Z'_{an} \\ Z'_{bn} \\ Z'_{cn} \end{bmatrix} \left[I_{n(l)} \right] \tag{3.9}$$

$$[0] = [Z'_{an} \quad Z'_{bn} \quad Z'_{cn}] \begin{bmatrix} I_{a(l)} \\ I_{b(l)} \\ I_{c(l)} \end{bmatrix} + [0] + [Z'_{nn}] \left[I_{n(l)} \right] \tag{3.10}$$

Eliminating $I_{n(l)}$ from (3.9) by substituting (3.10) and taking into account that n and g at node $j-1$ are now at the same potential:

$$\begin{bmatrix} V_{an(j-1)} \\ V_{bn(j-1)} \\ V_{cn(j-1)} \end{bmatrix} = \begin{bmatrix} Z''_{aa} & Z''_{ab} & Z''_{ac} \\ Z''_{ab} & Z''_{bb} & Z''_{bc} \\ Z''_{ac} & Z''_{bc} & Z''_{cc} \end{bmatrix} \begin{bmatrix} I_{a(l)} \\ I_{b(l)} \\ I_{c(l)} \end{bmatrix} + \begin{bmatrix} V_{a'n'(j)} \\ V_{b'n'(j)} \\ V_{c'n'(j)} \end{bmatrix} \tag{3.11}$$

where

$$Z''_{pq} = Z'_{pq} - \frac{Z'_{pn} Z'_{qn}}{Z'_{nn}};\ p = a, b, c, n \text{ and } q = a, b, c, n$$

Equation (3.11) can be used in a forward-backward sweep method. This approach has avoided the need to determine $I_{n(l)}$ and $I_{g(l)}$ as they have both been eliminated from equation (3.11). It has basically simplified equation (3.2) to:

$$\begin{bmatrix} I_{a(l)} \\ I_{b(l)} \\ I_{c(l)} \\ I_{n(l)} + I_{g(l)} \end{bmatrix} = \begin{bmatrix} I_{La(j)} \\ I_{Lb(j)} \\ I_{Lc(j)} \\ I_{Ln(j)} + I_{Lg(j)} = I_{Labc(j)} \end{bmatrix} + \begin{bmatrix} I_{a(l+1)} \\ I_{b(l+1)} \\ I_{c(l+1)} \\ I_{n(l+1)} + I_{g(l+1)} \end{bmatrix} \quad (3.12)$$

This simplification however, comes at a cost. The following are several of its disadvantages:

- $I_{n(l)}$ and $I_{g(l)}$ cannot be individually determined accurately. Only their sum is available from the phase currents using KCL $\left(I_{g(l)} + I_{n(l)}\right) = -\left(I_{a(l)} + I_{b(l)} + I_{c(l)}\right)$. It is recognised that after finding the phase currents, equation (3.10) can be used to find $I_{n(l)}$ (as was done in [72]). However, this will not give realistic values as it would be based on the assumption that neutral is solidly connected to the local earths (i.e. as if the neutral and assumed earth wire are bundled).
- $V_{nn\prime(l)}$ and $V_{gg\prime(l)}$ cannot be determined.
- The movement of the neutral $V_{n\prime g(j)}$ with respect to a common earth reference $g(0)$ is unknown.

It must also be appreciated that this is an extreme condition in that it effectively replaces $Z_{gr(l)}$ (and $Z_{gr(l-1)}$ on the downstream branch) by short circuits.

Using Assumption 2 (perfect earth conductor):

From equation (3.11) it can be seen that the sending and receiving end voltages are found with respect to the local neutral or equally the local earths (as they are assumed to be shorted). In [51] a perfect earth conductor is shown connecting $g(j-1)$ and $g'(j)$. By doing this both sending and receiving end voltages are instead defined with respect to the same reference, which effectively is $g(0)$. Equation (3.11) becomes:

$$\begin{bmatrix} V_{ag(j-1)} \\ V_{bg(j-1)} \\ V_{cg(j-1)} \end{bmatrix} = \begin{bmatrix} Z''_{aa} & Z''_{ab} & Z''_{ac} \\ Z''_{ab} & Z''_{bb} & Z''_{bc} \\ Z''_{ac} & Z''_{bc} & Z''_{cc} \end{bmatrix} \begin{bmatrix} I_{a(l)} \\ I_{b(l)} \\ I_{c(l)} \end{bmatrix} + \begin{bmatrix} V_{a\prime g(j)} \\ V_{b\prime g(j)} \\ V_{c\prime g(j)} \end{bmatrix} \quad (3.13)$$

It should be appreciated that the basis for this assumption (i.e. $V_{nn\prime(l)}$and $V_{gg\prime(l)}$ are both small) need not be valid, especially on networks with significant neutral and ground currents.

The new branch segment l'' given by equation (3.13) is shown in Figure 3.7.

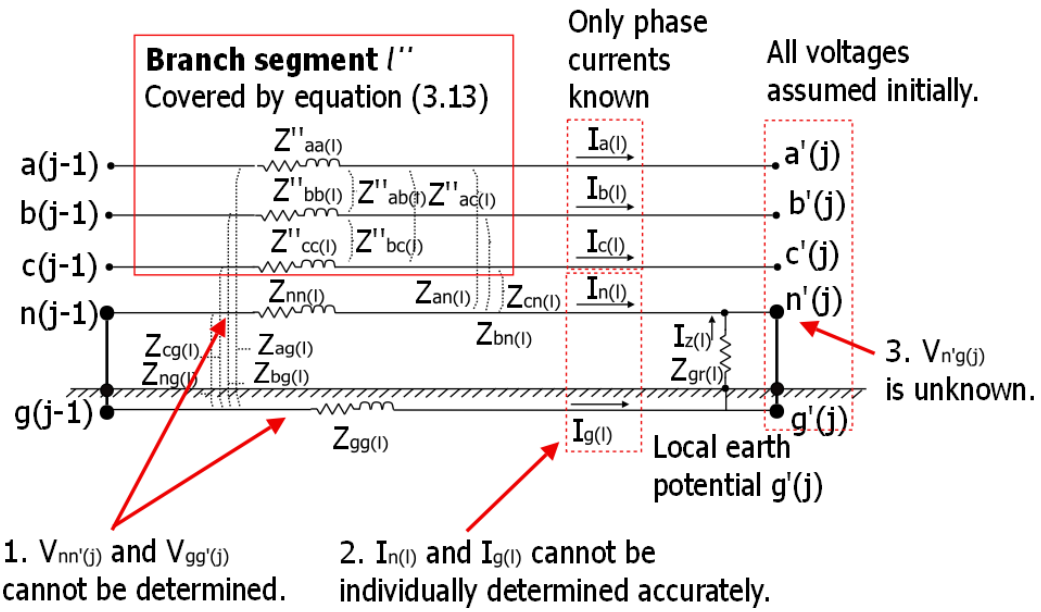

Figure 3.7: New branch segment l'' represented by the 3 x 3 matrices.

These assumptions and the analysis of the effects of unbalance

On highly unbalanced low-voltage networks the neutral current may at times be as high as the phase currents. These high neutral currents and the resulting neutral voltage drop will have as significant an influence on voltage unbalance and its effects (such as the phase-neutral voltages seen by consumers) as the voltage drops on the phase wires. The high neutral current in of itself will be a significant contributor to the total losses on the cable. Therefore, to make assumptions which involve bundling neutral and assumed earth wires (such that neither current can be separated accurately) or as to how small $V_{ng(j-1)}, V_{n'g'(j)}, V_{nn'(l)}$ or $V_{gg'(l)}$ might be, will not be ideal for the analysis of the effects of unbalance. These assumptions would, for the very least, result in:

- Incalculable currents and voltages such as $I_{n(l)}$ and $V_{n'g(j)}$ important to effects of unbalance;
- Questionable phase-neutral and phase-ground voltages; and
- Questionable phase currents (because for constant power and constant impedance loads they will depend on the phase-neutral voltages).

In fact, comparisons carried out in [27] between results found using PSpice for Windows (used to solve a North American style four-wire 11 kV feeder with earth and

neutral wires explicitly represented) and this standard method have shown that these assumptions will lead to inaccurate results for unbalanced load conditions.

Summary

- For multi-grounded low-voltage networks, either 3 x 3, 4 x 4 or 5 x 5 representations may be used.
    - The 3 x 3 offers simplification but at a cost to accuracy and calculable voltages and currents. The assumptions involved are unsuitable if the effects of unbalance are to be investigated accurately.
    - If solutions are to be found using 5 x 5 or 4 x 4 representations the meshed neutral and earth return paths must be accounted for so as to determine $I_{n(l)}$ and $I_{g(l)}$.
    - An advantage of the 5 x 5 representation over the 4 x 4 representation is that $I_{g(l)}$ and $V_{gg'(l)}$ can be determined directly.
- For ungrounded low-voltage networks, the 4 x 4 representation is suitable and can be used without the need for further assumptions.

In the next section, a well-cited 5 x 5 approach is discussed.

3.6.2 An approach using a 5 x 5 matrix representation

An approach to the forward-backward sweep method using 5 x 5 matrices is given in [73]. This approach was initially considered for use in this thesis. However, it had to be ruled out after convergence problems under unbalanced loadings were recognised even for simple low-voltage networks, such as a single branch segment with three single-phase loads at the end. Upon closer inspection of the equations presented in [73] it was realised that an assumption and certain approximations were made.

Assumption

The model solved is very close to the typical multi-grounded low-voltage network model described in Figure 3.2 and Figure 3.3, except that it appears to assume that the voltages at the local earth points $g'(j)$ and $g(j-1)$ at the end of all branch segments are the same as the reference earth point $g(0)$. It therefore uses **assumption 2 (perfect earth conductor)** as was done in the 3 x 3 reduction. A generic sub-lateral is shown in Figure 3.8 with this assumption.

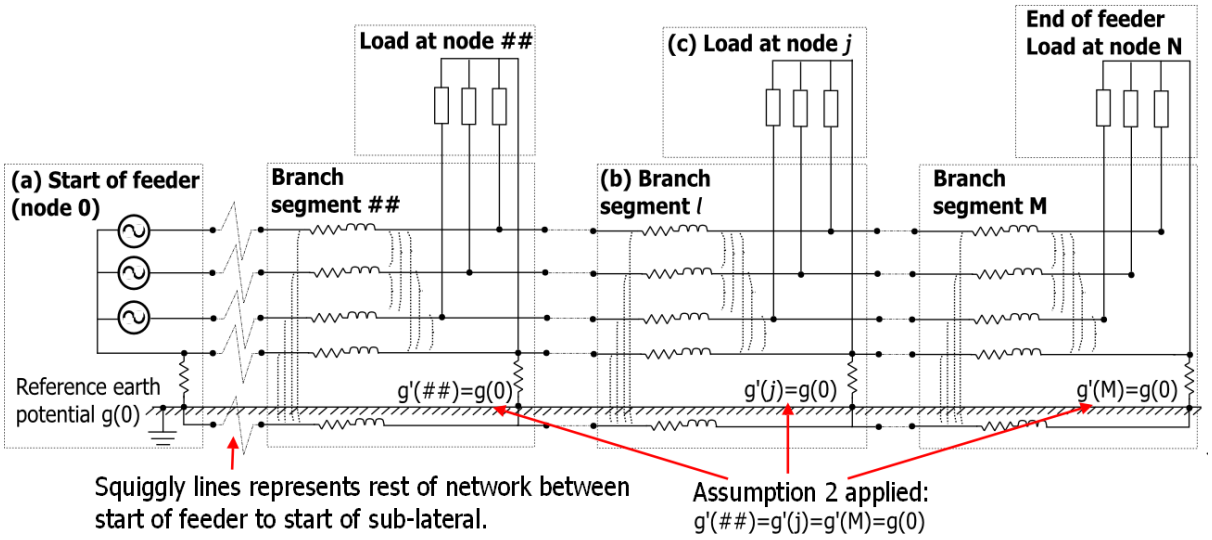

Figure 3.8: Generic sub-lateral as would be used in [73]

Approximations

Further, though not stated, an approximation is made for the sharing of the out-of-balance current of the loads:

$$I_{Ln(j)} = -\frac{(Z_{gr(l)}+Z_{gg(l)})}{Z_{nn(l)}+(Z_{gr(l)}+Z_{gg(l)})}\left(I_{La(j)} + I_{Lb(j)} + I_{Lc(j)}\right) \quad (3.14)$$

$$I_{Lg(j)} = -\frac{Z_{nn(l)}}{Z_{nn(l)}+(Z_{gr(l)}+Z_{gg(l)})}\left(I_{La(j)} + I_{Lb(j)} + I_{Lc(j)}\right) \quad (3.15)$$

With these approximations $I_{n(l)}$ and $I_{g(l)}$ can be determined using equation (3.2). These are the equations of a current divider. They basically reduce the earth and neutral return paths to two parallel impedances as shown by Figure 3.9, seen between the neutral point n' of node j and the reference earth $g(0)$.

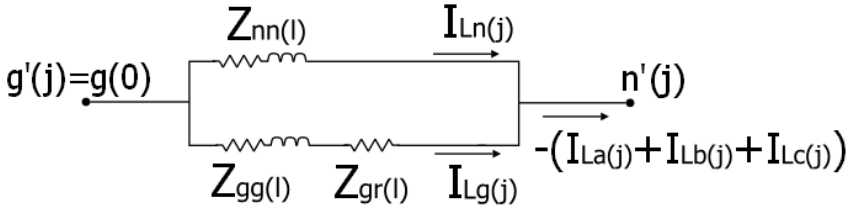

Figure 3.9: Implied reduction of earth and neutral return paths to a current divider circuit

It must be stated that any current divider approximation (such as Figure 3.9) will not account for the effect of mutual impedances between phases, neutral and assumed earth wire on these currents.

Also, the sharing of the out-of-balance current at neutral point n' will be influenced by both upstream and downstream neutral impedances and earth resistances (for example a portion may flow through $Z_{nn(l+1)}$ of the upstream branch segment and not just $Z_{nn(l)}$ as in Figure 3.9). This is also not accounted for in the current divider approximation.

Continuing, the equations (3.14) and (3.15), used as an approximation in the iterative solution, also involve a further step in which the voltages across the earth electrodes - $V_{n'g'(j)}$ - undergo a correction:

$$V_{n'g'(j)} = I_{g(l)}Z_{gr(l)} \quad (3.16)$$

This equation raises a concern in that it multiplies a branch current - $I_{g(l)}$ – which flows on the assumed earth wire with the earth electrode resistance (and not the current flowing through the earth electrode itself, represented here by $I_{z(l)}$). This is a second approximation.

Summary

There are concerns over this method. They include use of:

- **Assumption 2 (perfect earth conductor)** which ignores the voltages at the local earths $g'(j)$.
- Approximations - equations (3.14) to (3.16) - to determine $I_{n(l)}$, $I_{g(l)}$ and $V_{n'g'(j)}$. The voltage drops found using these currents even with the voltage correction will not satisfy KVL for the earth and neutral paths as they ignore the mutual impedances.

In the next section, exact equations based on KVL and KCL are derived to account for the sharing of the neutral and ground currents.

3.7 Proposed approach

The following proposed approach to solve multi-grounded low-voltage networks, makes no further assumptions, as was done for the 3 x 3 solution and the 5 x 5 solution of [73]. Furthermore, unlike [73] it makes no approximations. Instead it uses KVL and KCL to determine $I_{n(l)}$ and $I_{g(l)}$ (for equation (3.2)) exactly.

3.7.1 Neutral and ground currents on a branch segment l using KVL and KCL

Figure 3.10 shows three branch segments of the typical low-voltage feeder circuit as was shown in Figure 3.2 and Figure 3.3.

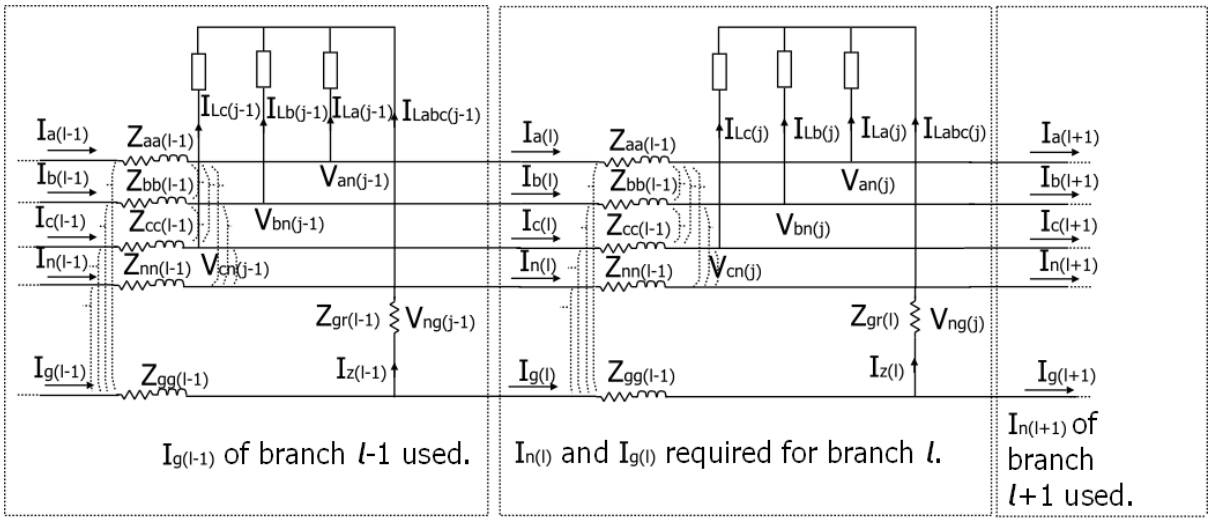

Figure 3.10: Parts of three branch segments used to determine neutral and ground currents on branch l.

The following gives the derivation of expressions for the neutral current $I_{n(l)}$ on branch segment l in terms of:

- the out-of-balance current $I_{Labc(j)}$ of the load connected to its receiving end (node j);
- the neutral current $I_{n(l+1)}$ seen on the next branch segment $(l+1)$; and
- the ground current $I_{g(l-1)}$ seen on the previous branch segment $(l-1)$.

This is found by the solution of the loop circuit shown in Figure 3.11 which includes the voltages induced on the neutral and assumed ground wire of branch l.

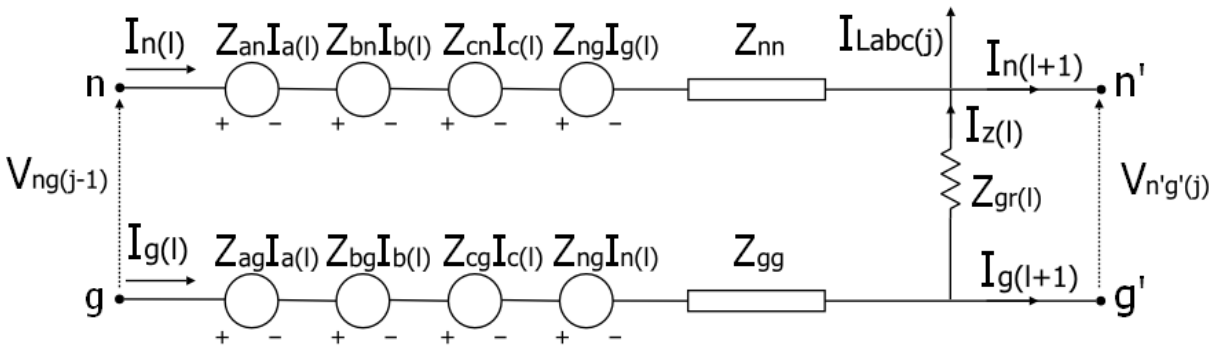

Figure 3.11: Loop circuit of neutral and assumed ground wires of branch l.

Applying Kirchhoff's voltage law:

$$V_{ng(j-1)} = Z_{an}I_{a(l)} + Z_{bn}I_{b(l)} + Z_{cn}I_{c(l)} + Z_{ng}I_{g(l)} + Z_{nn}I_{n(l)} + V_{n'g'(j)} - \left(Z_{ag}I_{a(l)} + Z_{bg}I_{b(l)} + Z_{cg}I_{c(l)} + Z_{ng}I_{n(l)} + Z_{gg}I_{g(l)}\right) \quad (3.17)$$

Using Kirchhoff's current law:

$$I_{a(l)} + I_{b(l)} + I_{c(l)} + I_{n(l)} + I_{g(l)} = 0 \quad (3.18)$$

To substitute for $I_{g(l)}$ gives:

$$V_{ng(j-1)} = Z'_{an}I_{a(l)} + Z'_{bn}I_{b(l)} + Z'_{cn}I_{c(l)} + Z'_{nn}I_{n(l)} + V_{n'g'(j)} \quad (3.19)$$

where

$$Z'_{pn} = Z_{pn} - Z_{pg} - Z_{ng} + Z_{gg}; p = a, b, c, n$$

Now the voltage drop across the earth electrode at the receiving end is given by:

$$V_{n'g'(j)} = -I_{z(l)}Z_{gr(l)} = -\left(I_{n(l+1)} - I_{n(l)} + I_{Labc(j)}\right)Z_{gr(l)} \quad (3.20)$$

where $I_{Labc(j)} = -\left(I_{La(j)} + I_{Lb(j)} + I_{Lc(j)}\right)$.

And the voltage drop across the earth electrode at the sending end is given by:

$$V_{ng(j-1)} = -I_{z(l-1)}Z_{gr(l-1)} = -\left(I_{g(l-1)} - I_{g(l)}\right)Z_{gr(l-1)} \quad (3.21)$$

Substituting equations (3.20) and (3.21) into (3.19):

$$-\left(I_{g(l-1)} - I_{g(l)}\right)Z_{gr(l-1)} = (Z'_{an})I_{a(l)} + (Z'_{bn})I_{b(l)} + (Z'_{cn})I_{c(l)} + (Z'_{nn})I_{n(l)} - \left(I_{n(l+1)} - I_{n(l)} + I_{Labc(j)}\right)Z_{gr(l)} \quad (3.22)$$

Using KCL (equation (3.18)) to find $I_{n(l)}$ gives:

$$I_{n(l)} = \frac{\left[(-I_{g(l-1)})Z_{gr(l-1)}+(I_{n(l+1)}+I_{Labc(j)})Z_{gr(l)}-\left[(Z'_{an}+Z_{gr(l-1)})I_{a(l)}+(Z'_{bn}+Z_{gr(l-1)})I_{b(l)}+(Z'_{cn}+Z_{gr(l-1)})I_{c(l)}\right]\right]}{(Z'_{nn}+Z_{gr(l)}+Z_{gr(l-1)})} \quad (3.23)$$

Equation (3.23) is general and would apply to any branch segment on the network. Some simplifications should be noted though if:

- l is the only branch: $I_{La(j)} = I_{a(l)}$,$I_{Lb(j)} = I_{b(l)}$,$I_{Lc(j)} = I_{c(l)}$ and $I_{Labc(j)} = I_{n(l)} + I_{g(l)}$ (3.24a)
- l is the last branch: $I_{n(l+1)} = 0$ and $I_{g(l+1)} = 0$. (3.24b)
- l is the first branch: $I_{g(l-1)} = 0$ and $Z_{gr(l-1)} = Z_{gr(0)}$. (3.24c)

The current flow on the assumed ground wire - $I_{g(l)}$- is then found using equation (3.18).

3.7.2 Overview of forward-backward sweep method with proposed approach

The following is an overview of the forward-backward sweep method with the proposed approach. It can be used to solve a radial low-voltage network of the general topology depicted in Figure 3.2 and Figure 3.4.

Initially the phase voltages of all nodes are set to nominal values and the neutral and ground voltages to zero, then for iteration k:

Forward sweep

This starts from the last node of the sub-lateral/lateral or main feeder backbone.

Load model

1. The nodal load currents are first calculated:

$$\begin{bmatrix} I_{La(j)} \\ I_{Lb(j)} \\ I_{Lc(j)} \end{bmatrix}^{(k)} = \begin{bmatrix} \left(\frac{S_{a(j)}}{V_{a'n'(j)}^{(k-1)}} \right)^* \\ \left(\frac{S_{b(j)}}{V_{b'n'(j)}^{(k-1)}} \right)^* \\ \left(\frac{S_{c(j)}}{V_{c'n'(j)}^{(k-1)}} \right)^* \end{bmatrix} \tag{3.25}$$

   Equation (3.25) applies to constant power loads. Equations for constant impedance and constant current loads can be found in [51].

Branch model

2. The phase currents on the branch segment l are then found:

$$\begin{bmatrix} I_{a(l)} \\ I_{b(l)} \\ I_{c(l)} \end{bmatrix}^{(k)} = \begin{bmatrix} I_{La(j)} \\ I_{Lb(j)} \\ I_{Lc(j)} \end{bmatrix}^{(k)} + \begin{bmatrix} I_{a(l+1)} \\ I_{b(l+1)} \\ I_{c(l+1)} \end{bmatrix}^{(k)} \tag{3.26}$$

   where $l+1$ is the branch segment downstream of node j.

3. Next, the current flow $I_{n(l)}^{(k)}$ on the neutral wire is found by applying equation (3.23):

$$I_{n(l)}^{(k)} = \frac{\left[\left(-I_{g(l-1)}^{(k)}\right)Z_{gr(l-1)}+\left(I_{n(l+1)}^{(k)}+I_{Labc(j)}^{(k)}\right)Z_{gr(l)}-\left[\left(Z'_{an}+Z_{gr(l-1)}\right)I_{a(l)}^{(k)}+\left(Z'_{bn}+Z_{gr(l-1)}\right)I_{b(l)}^{(k)}+\left(Z'_{cn}+Z_{gr(l-1)}\right)I_{c(l)}^{(k)}\right]\right]}{\left(Z'_{nn}+Z_{gr(l)}+Z_{gr(l-1)}\right)} \quad (3.27)$$

where

$Z'_{pn} = Z_{pn} - Z_{pg} - Z_{ng} + Z_{gg}; p = a, b, c, n$

4. Using Kirchhoff's current law the ground current $I_{g(l)}^{(k)}$ is then found and the current flows on branch segment l are then expressed fully as:

$$\begin{bmatrix} I_{a(l)} \\ I_{b(l)} \\ I_{c(l)} \\ I_{n(l)} \\ I_{g(l)} \end{bmatrix}^{(k)} = \begin{bmatrix} I_{a(l)}^{(k)} \\ I_{b(l)}^{(k)} \\ I_{c(l)}^{(k)} \\ I_{n(l)}^{(k)} \\ -\left(I_{a(l)}^{(k)} + I_{b(l)}^{(k)} + I_{c(l)}^{(k)} + I_{n(l)}^{(k)}\right) \end{bmatrix} \quad (3.28)$$

5. Steps 1 to 4 are repeated for each branch segment until $l = 1$.

Backward sweep

This starts from the first node of the main feeder backbone and then progresses through the laterals and then sub-laterals.

6. The phase-neutral voltages at the first node 0 are fixed with respect to the neutral (for $j = 0$, only). However, as $V_{ng(0)}^{k}$ changes with $I_{g(l=1)}^{k}$, they will vary with respect to g. This is given by:

$$\begin{bmatrix} V_{ag(0)} \\ V_{bg(0)} \\ V_{cg(0)} \\ V_{ng(0)} \\ V_{gg(0)} \end{bmatrix}^{(k)} = \begin{bmatrix} V_{an(0)} \\ V_{bn(0)} \\ V_{cn(0)} \\ 0 \\ 0 \end{bmatrix} + \begin{bmatrix} V_{ng(0)} \\ V_{ng(0)} \\ V_{ng(0)} \\ V_{ng(0)} \\ 0 \end{bmatrix}^{(k)} \quad (3.29)$$

where $V_{ng(0)}^{k} = I_{g(l=1)}^{k} Z_{gr(0)}$.

7. The voltages at the receiving end of the branch segments are then found by:

$$\begin{bmatrix} V_{a\prime g(j)} \\ V_{b\prime g(j)} \\ V_{c\prime g(j)} \\ V_{n\prime g(j)} \\ V_{g\prime g(j)} \end{bmatrix}^{(k)} = \begin{bmatrix} V_{ag(j-1)} \\ V_{bg(j-1)} \\ V_{cg(j-1)} \\ V_{ng(j-1)} \\ V_{gg(j-1)} \end{bmatrix}^{(k)} - \begin{bmatrix} Z_{aa} & Z_{ab} & Z_{ac} & Z_{an} & Z_{ag} \\ Z_{ab} & Z_{bb} & Z_{bc} & Z_{bn} & Z_{bg} \\ Z_{ac} & Z_{bc} & Z_{cc} & Z_{cn} & Z_{cg} \\ Z_{an} & Z_{bn} & Z_{cn} & Z_{nn} & Z_{ng} \\ Z_{ag} & Z_{bg} & Z_{cg} & Z_{ng} & Z_{gg} \end{bmatrix} \begin{bmatrix} I_{a(l)} \\ I_{b(l)} \\ I_{c(l)} \\ I_{n(l)} \\ I_{g(l)} \end{bmatrix}^{(k)} \quad (3.30)$$

8. The phase-neutral voltages, supplying the single-phase loads at node j are then found:

$$\begin{bmatrix} V_{a\prime n\prime(j)} \\ V_{b\prime n\prime(j)} \\ V_{c\prime n\prime(j)} \end{bmatrix}^{(k)} = \begin{bmatrix} V_{a\prime g(j)} \\ V_{b\prime g(j)} \\ V_{c\prime g(j)} \end{bmatrix}^{(k)} - V_{n\prime g(j)}^{k} \tag{3.31}$$

9. Steps 6 to 8 are repeated, finding the receiving end voltages of each branch segment until $l = M$. All voltages are found with respect to g at the first node ($j = 0$). Step 6 is repeated only if $j = 0$.

Convergence criteria

10. At the end of the iteration, the real and imaginary power mismatches (denoted as $\Delta P_p^{(k)}$ and $\Delta Q_p^{(k)}$ where $p = a, b, c$) of the single-phase loads are found by:

$$\Delta S_{a(j)}^{(k)} = V_{a\prime n\prime(j)}^{(k)} \left(I_{a(j)}^{(k)}\right)^{*} - S_{a(j)} \tag{3.32a}$$

$$\Delta S_{b(j)}^{(k)} = V_{b\prime n\prime(j)}^{(k)} \left(I_{b(j)}^{(k)}\right)^{*} - S_{b(j)} \tag{3.32b}$$

$$\Delta S_{c(j)}^{(k)} = V_{c\prime n\prime(j)}^{(k)} \left(I_{c(j)}^{(k)}\right)^{*} - S_{c(j)} \tag{3.32c}$$

11. Additionally, the voltages of iteration k are compared to those of $k-1$:

$$\Delta Vmag_{(j)}^{(k)} = max\left(\left| \begin{bmatrix} V_{a\prime g(j)} \\ V_{b\prime g(j)} \\ V_{c\prime g(j)} \\ V_{n\prime g(j)} \\ V_{g\prime g(j)} \end{bmatrix}^{(k)} \right| - \left| \begin{bmatrix} V_{a\prime g(j)} \\ V_{b\prime g(j)} \\ V_{c\prime g(j)} \\ V_{n\prime g(j)} \\ V_{g\prime g(j)} \end{bmatrix}^{(k-1)} \right| \right) \tag{3.33a}$$

$$\Delta Vang_{(j)}^{(k)} = max\left(\begin{bmatrix} \delta_{a\prime g(j)} \\ \delta_{b\prime g(j)} \\ \delta_{c\prime g(j)} \\ \delta_{n\prime g(j)} \\ \delta_{g\prime g(j)} \end{bmatrix}^{(k)} - \begin{bmatrix} \delta_{a\prime g(j)} \\ \delta_{b\prime g(j)} \\ \delta_{c\prime g(j)} \\ \delta_{n\prime g(j)} \\ \delta_{g\prime g(j)} \end{bmatrix}^{(k-1)} \right) \tag{3.33b}$$

where $\delta_{a\prime g(j)}$, $\delta_{b\prime g(j)}$, $\delta_{c\prime g(j)}$, $\delta_{n\prime g(j)}$ and $\delta_{g\prime g(j)}$ are the respective angles of voltages $V_{a\prime g(j)}, V_{b\prime g(j)}, V_{c\prime g(j)}, V_{n\prime g(j)}$ and $V_{g\prime g(j)}$.

12. The solution converges when these mismatches are all less than the set limits $Vmag_{tol}, Vang_{tol}, P_{tol}$ and Q_{tol}.

3.8 Validation of proposed 5 x 5 approach

The proposed 5 x 5 approach to the forward-backward sweep method was written as a script function in Matlab. Its results – voltages and currents - were validated using the test network shown in Figure 3.12 for three sets of test input data (which are given in Appendix B). The validation involved several checks to ensure that the results satisfied Kirchhoff's voltage and current laws. These KVL and KCL checks are described in the sections which follow. Appendix B gives the results confirming that the proposed 5 x 5 approach passed these checks.

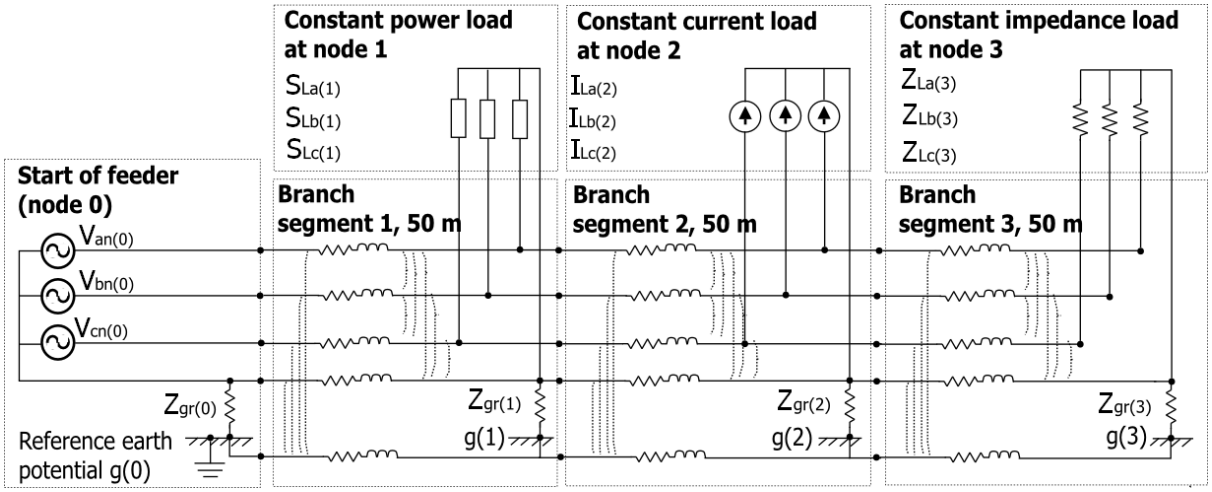

Figure 3.12: Test network used for validation

The results also matched those from a model of this test network built in Matlab Simulink SimPowerSystems and solved using its phasor solution method. As explained in [74], for this method Matlab Simulink SimPowerSystems replaces its state-space model (differential equations relating resistive, inductive and capacitive elements) of the circuit by a complex transfer matrix which defines network algebraic equations relating the voltage and current phasors at fundamental frequency. It then solves these algebraic equations using one of its continuous variable-step solvers. The results found using Matlab Simulink SimPowerSystems are included in Appendix B alongside those of the proposed 5 x 5 approach. Both are in very good agreement.

Also given in Appendix B are the computation times for Matlab Simulink SimPowerSystems and the proposed 5 x 5 approach. For Matlab Simulink SimPowerSystems they range between 4 to 6 seconds whilst for the proposed 5 x 5

approach they are less than 0.3 seconds. The longer computation time of Matlab Simulink SimPowerSystems precludes its potential use for the simulation of practical low-voltage feeders.

3.8.1 KVL check

The *KVL check* ensured that the voltages drops calculated for loops, such as the *phase A loop* identified in Figure 3.13, sum to zero. The equation verified (for the *phase A loop* shown) is:

$$-V_{an(0)} - V_{ng(0)} + V_{aa\prime(1)} + V_{aa\prime(2)} + V_{aa\prime(3)} + V_{an(3)} + V_{ng(3)} - V_{gg\prime(3)} - V_{gg'(2)} - V_{gg'(1)} = 0 \quad (3.34)$$

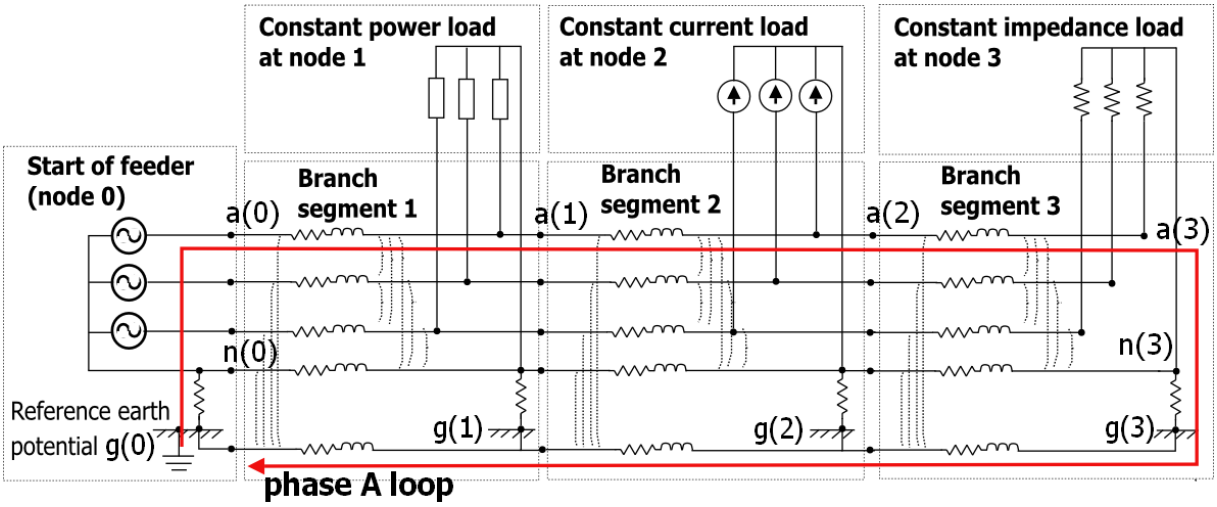

Figure 3.13: KVL check (*phase A loop* shown).

3.8.2 KCL check 1

KCL check 1 verified that the sum of the branch currents on each segment is zero. This is identified in Figure 3.14.

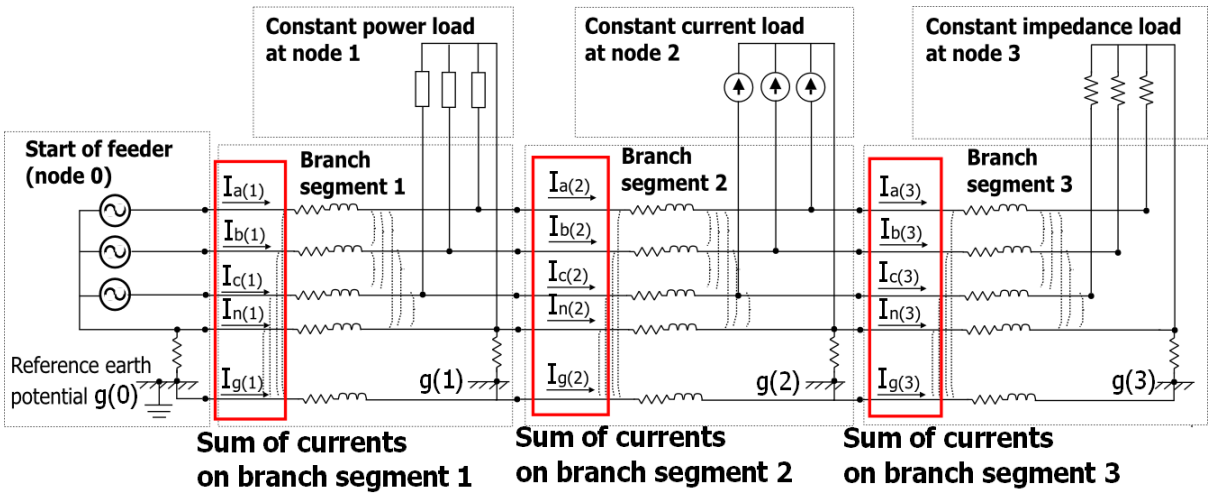

Figure 3.14: KCL check 1 of the sum of branch currents.

3.8.3 KCL check 2

KCL check 2 looked more closely at the sum of currents at each node. This is shown in Figure 3.15. As an example, for *node 1*, the equation verified is:

$$I_{a(1)} - I_{La(1)} - I_{a(2)} = 0$$

$$I_{b(1)} - I_{Lb(1)} - I_{b(2)} = 0$$

$$I_{c(1)} - I_{Lc(1)} - I_{c(2)} = 0$$

$$I_{n(1)} - I_{Labc(1)} - I_{n(2)} = \left(I_{g(2)} - I_{g(1)}\right) \qquad (3.35)$$

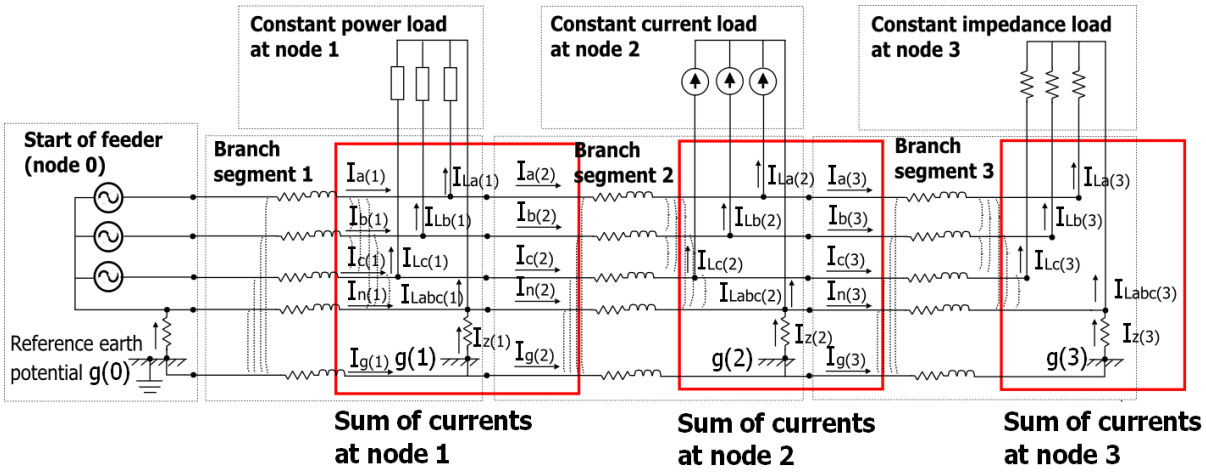

Figure 3.15: KCL check 2 of the sum of currents at each node.

3.9 Comparisons of results from the different approaches

The test network was also used to compare results found using the proposed 5 x 5 approach to those from the standard 3 x 3 approach. This was done using the input data given in Figure 3.16. As can be seen, the loading on the phases were made very unbalanced, with the total load on phase C being twice that of the other two phases (similar to the current measurements shown in Figure 1.2).

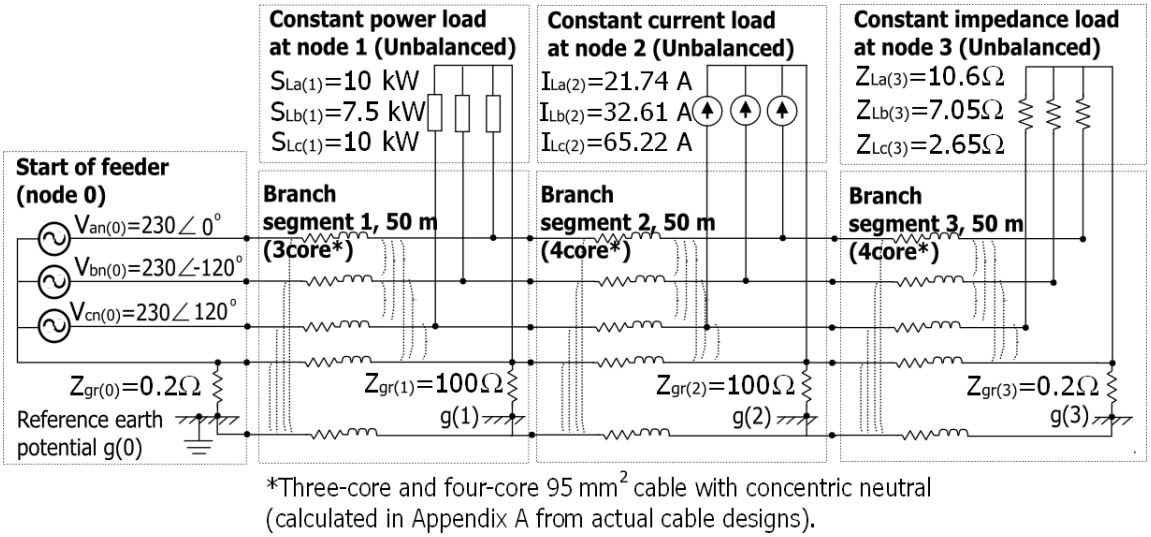

Figure 3.16: Test network showing the input data used to compare both approaches

It was found that with the exception of the phase-neutral voltages and the zero sequence voltage unbalance, the results from both approaches were in general, a good match. To give an example, the results at node 3 are compared in Table 3.2.

	Proposed 5 x 5 approach		3 x 3 approach	
	Mag (A)	Ang (°)	Mag (A)	Ang (°)
$V_{an(3)}$	229.85	-0.75	228.73	-0.13
$V_{bn(3)}$	227.69	-119.27	226.17	-119.82
$V_{cn(3)}$	219.87	119.48	222.53	119.42
	Mag (%)	Ang (°)	Mag (%)	Ang (°)
VUF_0	2.14	-44.61	1.11	-22.47

Table 3.2: Comparison of phase-neutral voltages and zero sequence voltage unbalance as calculated at node 3 (end of feeder)

These differences are because of the assumption made in the 3 x 3 approach that the neutral is solidly connected to local earths. In doing so, the movement of the neutral is not fully captured as it is in the proposed 5 x 5 approach.

Differences were also observed in the neutral currents and in the losses, but they appeared to be minor.

3.10 Chapter conclusions

A new 5 x 5 approach to the forward-backward sweep method has been developed. It differs from the standard approaches [51], [73] in that it makes no unnecessary assumptions or approximations in dealing with the meshed neutral and earth return paths. Instead, it solves this meshed path using KCL and KVL. The results from this new 5 x 5 approach to the forward-backward sweep method were validated by a series of checks to confirm that they satisfied KVL and KCL. Further, as presented in Appendix B, these results are in very good agreement with Matlab Simulink SimPowerSystems. Additionally, it was observed that the computation time of the new 5 x 5 approach was significantly faster than Matlab Simulink SimPowerSystems.

Additionally, it was found that even though results from the 3 x 3 approach and the proposed 5 x 5 approach were in good agreement, differences may be expected in the phase-neutral voltages and the zero sequence voltage unbalance. The potential significance of this in practice will be examined further in chapter 7.

4. Quantifying the effects of current unbalance on the low-voltage network

4.1 Objectives and tasks

This chapter is part of ***Objective (b)***:

To investigate the causes and quantify the effects of current unbalance on low-voltage networks.

It supports this objective by fulfilling:

Task (b.1): *Solve a representative low-voltage feeder so as to investigate and quantify the relationships of each sequence current unbalance to effects on the network.*

4.2 Overview

The mathematical expressions which quantify the effects on the low-voltage network (i.e. effects (a) to (g)) as identified in Figure 2.13 are first presented. A representative low-voltage network is then used to investigate and quantify the relationships between current unbalance and these effects. This is done by looking at three cases - current magnitude unbalance and current angle unbalance separately and then current magnitude and angle unbalance together (Figure 2.1). The analysis of the results leads to several key findings as highlighted in Figure 4.1.

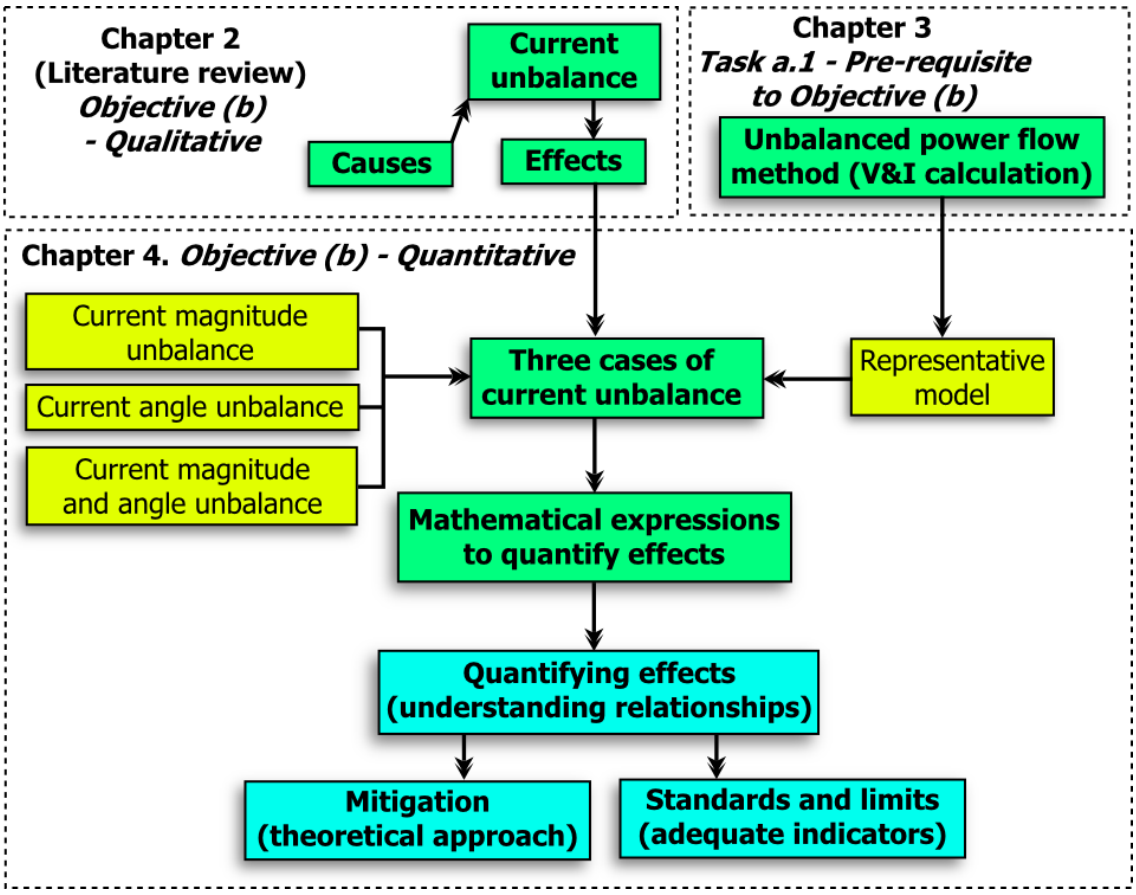

Figure 4.1: Overview of Chapter 4

4.3 Mathematical expressions to quantify effects

The following sections labelled (a) to (g) correspond to the effects on the low-voltage network identified in Figure 2.13. Some effects – voltages and currents - are found directly from the unbalanced power flow solution whilst others must be quantified using mathematical expressions.

4.3.1 (a) Network utilisation

Network utilisation has to do with how well the existing network assets are being utilised. It may be interpreted and therefore quantified in several ways depending on the concerns for:

1. The additional capacity that is wasted in supplying loads unbalanced and which could better be used to cater for future demand growth from consumers. ***(Future demand growth)***

2. The efficient utilisation of network assets for the distribution of balanced power (which can be considered unavoidable) as opposed to unbalanced power (which can be considered avoidable). ***(Efficient use of network capacity)***

Neglecting these concerns can lead to several negative financial implications including:

- investment in assets not achieving their full value as the maximum power served may be much less than the rated power of equipment purchased.
- consumer demand (and potential revenue) being needlessly curtailed.
- early and perhaps unnecessary investment in replacing or upgrading network capacity.

The following sections give mathematical expressions which can be used to quantify each concern.

(1) Potential released current capacity for future demand growth

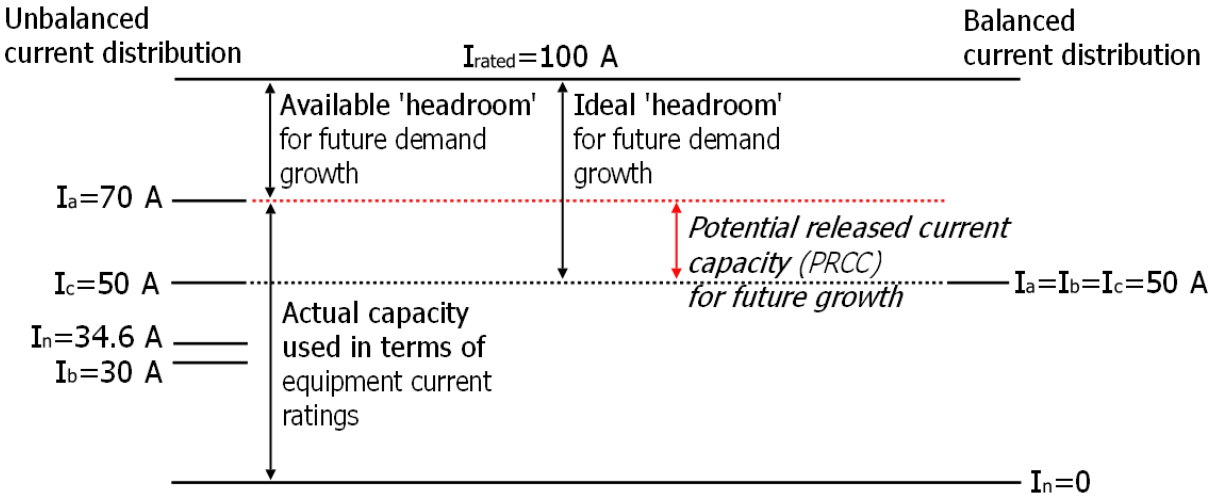

Figure 4.2: Example of potential released current capacity (PRCC) for non-ideal and ideal current distributions

Figure 4.2 gives an example of the potential current capacity which can be released for future demand growth. It shows the currents on a cable rated 100 A under non-ideal and ideal current distributions:

- *Non-ideal:* $I_{a(l)} = 70\ A;\ I_{b(l)} = 30\ A;\ I_{c(l)} = 50\ A$ resulting in $I_{n(l)} = 34.6\ A$ (assuming all loads have unity power factor).

- *Ideal:* the phases would be balanced ($I_{a(l)} = I_{b(l)} = I_{c(l)} = 50\ A$) and $I_{n(l)} = 0\ A$.

Phase A is important as it is the most heavily loaded and likely carries the most consumers. As a result it will also see a greater share of future increases in consumer demand and be the first phase to overload its upstream fuse. The difference between phase A under ideal and non-ideal current distributions can therefore be used as a measure of how inadequately the low-voltage network is being used to serve unbalanced loads. This potential released current capacity can be used as a measure of network utilisation by:

$$NU\_PRCC(\%) = \frac{PRCC}{I_{rated(l)}} \times 100 \quad (4.1)$$

where $PRCC = \left(I_{max(l)} - I_{avg(l)}\right)$ with $I_{max(l)} = \max(|I_{a(l)}|, |I_{b(l)}|, |I_{c(l)}|)$ and $I_{avg(l)} = (|I_{a(l)}| + |I_{b(l)}| + |I_{c(l)}|)/3$.

(2) Efficient use of network capacity

In balanced three-phase power systems, power factor is used as a measure of network utilisation, irrespective of the equipment rating. For a branch element, load or generator it indicates the proportion of the total or apparent power (S) that is used to carry out useful work or active power (P). The total power is called the apparent power because it corresponds to the active power which would have the same apparent voltage and current impact on the network. For single-phase and balanced three-phase power systems, apparent power is clearly understood and defined as the product of rms voltage and rms current [75]. For unbalanced three-phase power systems however, the mathematical definition is not as clear and has been the subject of much discussion [76], [77] and [78].

In this thesis, the definition of apparent power and power factor recommended in the IEEE 1459 [75] is used. They are referred to as the effective apparent power and effective power factor. As described in [78], this definition finds the active power that if transmitted under balanced conditions will result in the same current impact (i.e. losses) and voltage impact (i.e. insulation effects and no-load losses). This effective

apparent power is defined as the product of an equivalent voltage V_e and an equivalent current I_e:

$$S_e = 3 \cdot V_e \cdot I_e \tag{4.2}$$

which are given by:

$$I_e = \frac{1}{\sqrt{3}} \sqrt{\left|I_{a(l)}\right|^2 + \left|I_{b(l)}\right|^2 + \left|I_{c(l)}\right|^2 + \rho\left|I_{n(l)}\right|^2} \tag{4.3}$$

$$V_e = \sqrt{\frac{1}{9(1+\xi)}\left\{3\left(\left|V_{an(j-1)}\right|^2 + \left|V_{bn(j-1)}\right|^2 + \left|V_{cn(j-1)}\right|^2\right) + \xi\left(\left|V_{ab(j-1)}\right|^2 + \left|V_{bc(j-1)}\right|^2 + \left|V_{ca(j-1)}\right|^2\right)\right\}} \tag{4.4}$$

with:

$\rho =$ is the ratio of the resistance of the neutral wire to the phase wires. The recommended value of $\rho = 1$ will be used [75].

$\xi =$ is a weighting factor used to account for the different contributions to the no-load losses of phase-phase voltages (P_Δ) and phase-neutral voltages (P_Y). For simplicity, equal losses (i.e. $P_\Delta = P_\mathrm{Y}$) are assumed and the recommended [75] value of $\xi = 1$ will be used.

Finally, the useful or active power into the branch segment at node $j-1$ is:

$$P_{TFR} = re\left(V_{ag(j-1)}I^*_{a(l)} + V_{bg(j-1)}I^*_{b(l)} + V_{cg(j-1)}I^*_{c(l)} + V_{ng(j-1)}I^*_{n(l)}\right) \tag{4.5}$$

And the effective power factor is therefore:

$$PF_e = P_{TFR}/S_e \tag{4.6}$$

These terms are illustrated by the example of Figure 4.3. This definition differs from that of NU_PRCC in that it places emphasis on:

- the transfer of active power. This means that to achieve an ideal effective power factor of unity would involve not just the balancing of loads amongst phases but also the compensation of reactive power; and
- the impact of unbalance on a comparatively longer time scale. It is driven by losses rather than equipment rating.

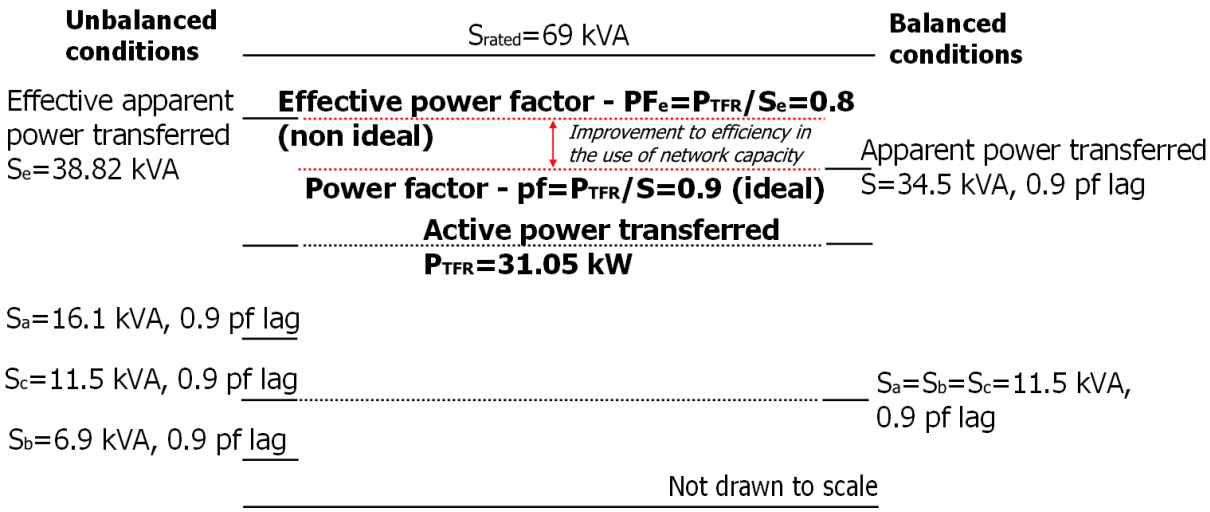

Figure 4.3: Example of effective power factor for non-ideal and ideal current distributions

4.3.2 (b) Neutral and (c) ground currents

Both $I_{n(l)}$ and $I_{g(l)}$ are calculated directly from the unbalanced power flow solution developed in Chapter 3.

4.3.3 (d) Real power losses

The total real power loss on a branch segment l is given simply by:

$$P_{loss(l)} = re\left(V_{aa'}I^*_{a(l)} + V_{bb'}I^*_{b(l)} + V_{cc'}I^*_{c(l)} + V_{nn'}I^*_{n(l)} + V_{gg'}I^*_{g(l)}\right) \quad (4.7)$$

4.3.4 (e) Neutral-point shifting

The displacement of the neutral voltage at each node with respect to a common reference point $g(0)$ is given by $V_{n'g(j)}$. In the case of network simulations, this can be calculated directly from the unbalanced power flow solution developed in Chapter 3. For field measurements however, as will be looked at later the thesis, $V_{n'g(j)}$ is not measureable. In its place, the zero sequence voltage (found from phase-neutral voltages) can be used:

$$V_{0(j)} = \frac{1}{3}\left(V_{an'(j)} + V_{bn'(j)} + V_{cn'(j)}\right) \quad (4.8)$$

4.3.5 (f) Phase-neutral voltages

The voltages seen by consumers and network devices are the phase-neutral voltages – $V_{a'n'(j)}$, $V_{b'n'(j)}$ and $V_{c'n'(j)}$ (as opposed to phase-ground voltages). They are also calculated directly from the unbalanced power flow solution of Chapter 3.

4.3.6 (g) Voltage regulation

Voltage regulation is defined in [79] as the *'percent voltage drop of a line with reference to the receiving end voltage'*. This is given as:

$$VR = \frac{(|V_s| - |V_r|)}{|V_r|} \times 100 \qquad (4.9)$$

Where V_s and V_r are the phase-neutral voltages at the start and at the end of the low-voltage feeder, respectively.

This equation, stated on a single-phase basis, assumes that at the start of the feeder (and at the end of the feeder) the voltages on the individual phases are fairly close and an average can be used. Clearly, this assumption is not suitable for the concerns being addressed here; since at both ends the phase-neutral voltages may be significantly different.

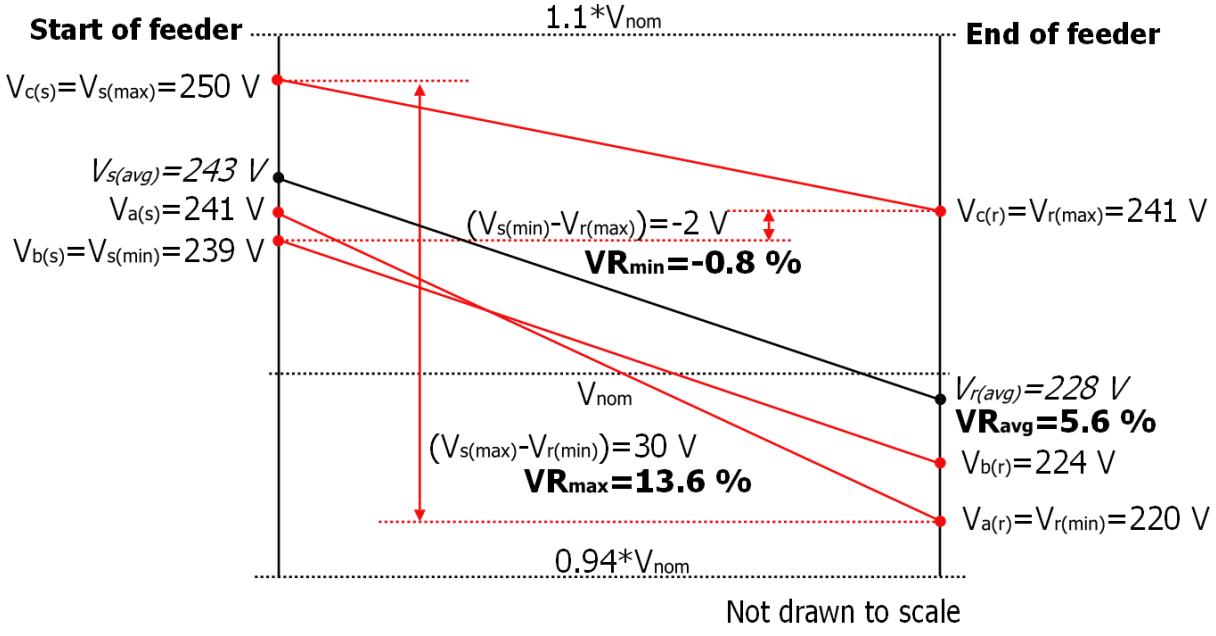

Figure 4.4: Example of voltage regulation

Now the concern, as illustrated in Figure 4.4, is whether the difference between phase-neutral voltages at the receiving end is wide enough such that voltage violations will result when ganged corrections are made to all three phases at the start of the low-voltage feeder. The following sections discuss the situations of concern.

Concern over ganged raising of voltages at start of feeder because of low voltages at end of feeder

- Arises if $V_{r(min)} < 0.94V_{nom}$: Can $V_{r(min)}$ be increased without $V_{s(max)}$ exceeding $1.1V_{nom}$?

  It is required that the following inequality is satisfied:

  $$\left(1.1V_{nom} - V_{s(max)}\right) + V_{r(min)} \geq 0.94V_{nom}$$

  $$\left(V_{s(max)} - V_{r(min)}\right) \leq 0.16V_{nom} \quad (4.10)$$

  where

  $V_{s(max)} = max\left(|V_{an(s)}|, |V_{bn(s)}|, |V_{cn(s)}|\right)$ and

  $V_{r(min)} = min\left(|V_{an(r)}|, |V_{bn(r)}|, |V_{cn(r)}|\right)$.

  Dividing both sides by $V_{r(min)}$ and multiplying by 100:

  $$VR_{max} \leq \frac{16V_{nom}}{V_{r(min)}} \quad (4.11)$$

  where a maximum voltage regulation VR_{max} is defined as:

  $$VR_{max} = \frac{\left(V_{s(max)} - V_{r(min)}\right)}{V_{r(min)}} \times 100 \quad (4.12)$$

Concern over ganged lowering of voltages at start of feeder because of high voltages at end of feeder

- Arises if $V_{r(max)} > 1.1V_{nom}$: Can $V_{r(max)}$ be decreased without $V_{s(min)}$ going below $0.94V_{nom}$?

  This requires that the following inequality is satisfied:

  $$V_{r(max)} - \left(V_{s(min)} - 0.94V_{nom}\right) \leq 1.1V_{nom}$$

  $$\left(V_{s(min)} - V_{r(max)}\right) \geq -0.16V_{nom} \quad (4.13)$$

  where

$V_{s(min)} = min(|V_{an(s)}|, |V_{bn(s)}|, |V_{cn(s)}|)$ and

$V_{r(max)} = max(|V_{an(r)}|, |V_{bn(r)}|, |V_{cn(r)}|)$.

Dividing both sides by $V_{r(max)}$ and multiplying by 100:

$$VR_{min} \leq \frac{16V_{nom}}{V_{r(max)}} \quad (4.14)$$

where a minimum voltage regulation VR_{min} is defined as:

$$VR_{min} = \frac{(V_{s(min)} - V_{r(max)})}{V_{r(max)}} \times 100 \quad (4.15)$$

Therefore if either concern were to arise, it is necessary to ensure that VR_{max} and VR_{min} satisfy inequalities (4.11) and (4.14).

It is also important to appreciate that even if $V_{r(min)} < 0.94V_{nom}$ and $V_{r(max)} > 1.1V_{nom}$ do not arise, VR_{max} and VR_{min} can still be used to quantify how severely voltage unbalance at the end of the feeder impacts the voltage regulation ability of in situ equipment such as off-load tap changing transformers. Considering that under ideal conditions, with balanced voltages at both ends of the low-voltage feeder, VR_{max} and VR_{min} are equal; the difference between them can be used to quantify how far off the voltages at both ends are from ideal conditions. This may be expressed as:

$$VR_{indicator} = \frac{(|VR_{max} - VR_{min}|)}{|VR_{avg}|} \quad (4.16)$$

where VR_{avg}, used as a base, is basically equation (4.9):

$$VR_{avg} = \frac{(|V_{s(avg)}| - |V_{r(avg)}|)}{|V_{r(avg)}|} \times 100 \quad (4.17)$$

where

$V_{s(avg)} = (|V_{an(s)}| + |V_{bn(s)}| + |V_{cn(s)}|)/3$ and

$V_{r(avg)} = (|V_{an(r)}| + |V_{bn(r)}| + |V_{cn(r)}|)/3$.

4.4 Developing a representative model and analysis procedure

This section describes the approach taken to allow a clearer understanding through quantification, of the relationships between current unbalance and its effects.

4.4.1 A representative model

A radial low-voltage feeder such as the one depicted previously in Figure 3.2, is essentially a number of branch segments connected together according to the topology of the feeder. The approach taken here is to examine in detail, the behaviour of a single branch segment in response to unbalanced loads (or downstream branch currents) at its receiving end, so as to understand and anticipate the behaviour of an entire low-voltage feeder under similar unbalanced loading conditions. This avoids unnecessary complexities which may mask the relationships between current unbalance and its effects. Moreover, the basic principles underlying these relationships can be easily recognised.

So as to reveal these underlying principles, the representative model must be capable of considering changes in the branch currents so as to look at:

- current magnitude and angle unbalance separately and together; and
- negative and zero sequence current unbalance separately and together.

Representative low-voltage feeder

The representative low-voltage feeder is shown in Figure 4.5. It consists of a single branch segment (1) terminated by three single-phase loads.

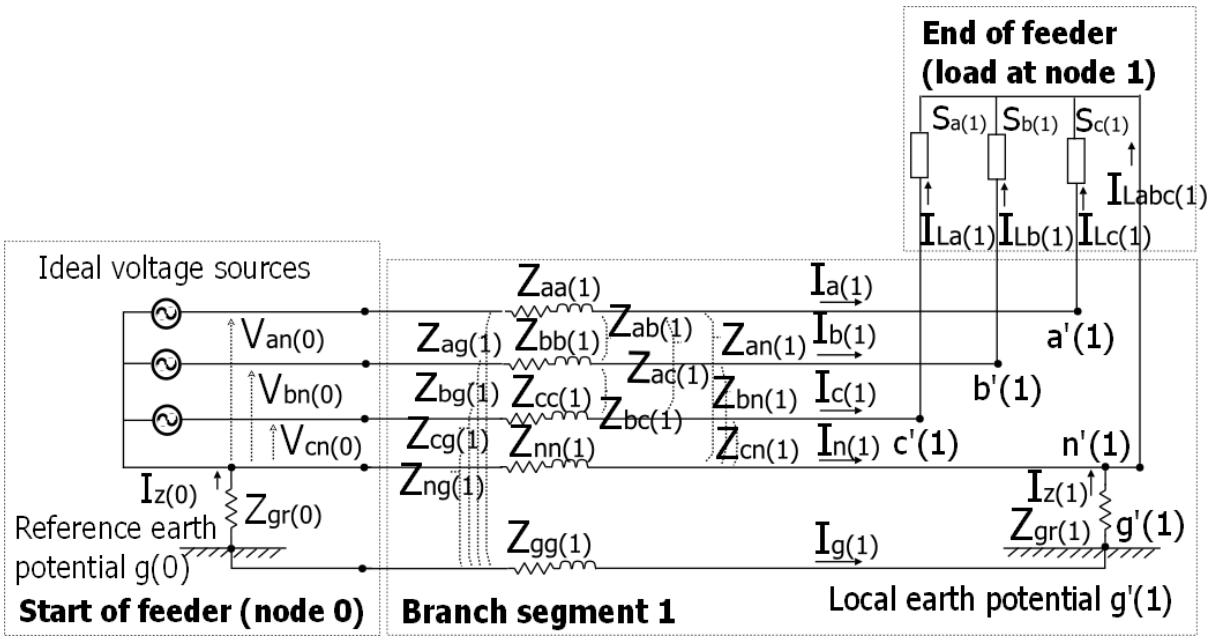

Figure 4.5: Representative low-voltage feeder comprising a single branch segment (1)

Model data, dependent and independent variables of representative low-voltage feeder

These are identified in Table 4.1.

Input or Model data	Dependent variables	Independent variables
Branch segment impedances: $\begin{bmatrix} Z_{aa} & Z_{ab} & Z_{ac} & Z_{an} & Z_{ag} \\ Z_{ab} & Z_{bb} & Z_{bc} & Z_{bn} & Z_{bg} \\ Z_{ac} & Z_{bc} & Z_{cc} & Z_{cn} & Z_{cg} \\ Z_{an} & Z_{bn} & Z_{cn} & Z_{nn} & Z_{ng} \\ Z_{ag} & Z_{bg} & Z_{cg} & Z_{ng} & Z_{gg} \end{bmatrix}$ These values are for a four-core 95 mm^2 cable with a concentric neutral as calculated in Appendix A using actual cable designs. The feeder length is 100 m. ***Earth electrode resistances:*** $Z_{gr(0)} = 6\ \Omega$ and $Z_{gr(1)} = 6\ \Omega$. *(Unless otherwise stated).* **Voltages at start of feeder:** $\begin{bmatrix} V_{an(0)} \\ V_{bn(0)} \\ V_{cn(0)} \end{bmatrix} = \begin{bmatrix} 230\angle 0° \\ 230\angle -120° \\ 230\angle 120° \end{bmatrix}$ *(Unless otherwise stated).*	***Branch currents:*** $\begin{bmatrix} I_{a(1)} \\ I_{b(1)} \\ I_{c(1)} \\ I_{n(1)} \\ I_{g(1)} \end{bmatrix}$ ***Voltages at receiving end:*** $\begin{bmatrix} V_{a'n'(1)} \\ V_{b'n'(1)} \\ V_{c'n'(1)} \end{bmatrix}$, $V_{ng(0)}$ and $V_{n'g(1)}$.	***Three single-phase loads:*** **Constant power:** $S_{La(1)}, S_{Lb(1)}, S_{Lc(1)}$ *(Unless otherwise stated).*

Table 4.1: Table of inputs, dependent and independent variables

The next section gives the analysis procedure. It will explain the variation of the independent variables.

4.4.2 Analysis procedure

This section develops the analysis procedure for the representative low-voltage feeder which will achieve **Objective (b)**. It considers several aspects, as summarised in Figure 4.6.

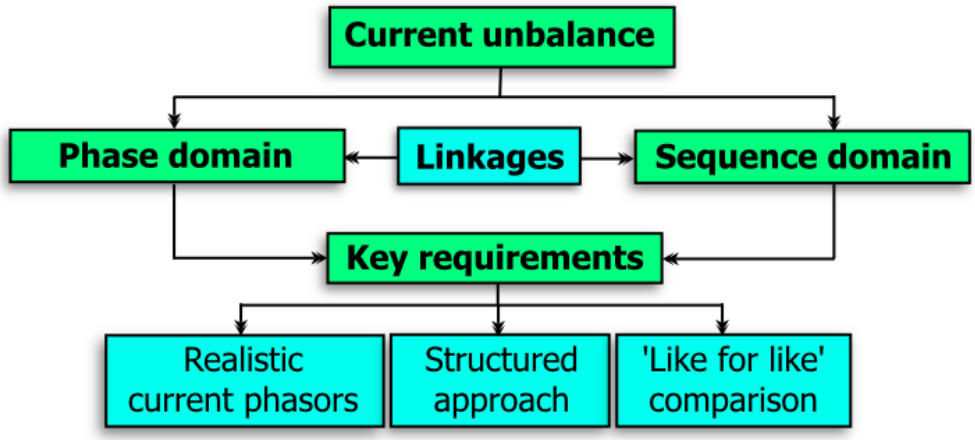

Figure 4.6: Concerns in developing an analysis procedure

Firstly, it should be recognised that current unbalance can be investigated either from the phase domain or the sequence domain. As highlighted, it is important that the changes in the current unbalance be **structured** and the variations in current phasors are **realistic**. Additionally, comparisons should be **like for like**, that is, the total three-phase apparent power of the single-phase loads should be the same regardless of variations to the system of current phasors. Additionally, the approach should allow comparisons of effects for equal active power transfers under different unbalanced loading conditions.

A combined approach which gives precedence to the phasor domain but which uses the method of symmetrical components to help explain the underlying principles is favoured. This is because even though realistic current phasors can be generated with both approaches, it is more straightforward to do so in phasor domain. Also, regardless of which domain is used, transformation can be done easily and the linkages between the two, which can be shown by systems of phasors, will also reveal certain underlying principles. For these reasons a combined approach is followed.

It is appreciated that any structured approach is ultimately simplistic when compared to the vast multitude of permutations of magnitudes and angles of current phasors relative to each other which might be seen on actual low-voltage feeders. However, the aim here is to gain a clear understanding of the relationships and for that reason, a structured and albeit simplistic approach to the variation is in fact preferable at this point. In later chapters though, analysis of field measurements from an actual low-voltage feeder will be carried out, examining these same relationships.

Further, it is important that calculated current and voltage phasors are realistic. To ensure this, the total three-phase apparent power demand was chosen so as not to exceed the current ratings of the cable used (i.e. 235 A assuming they are directly buried [80]). Further, a cable length (100 m) was chosen to ensure that even with all the demand on one phase, the phase-neutral voltages remained within UK statutory limits (230 V -6%/+10%).

The approach was structured into three cases, as described in the next section.

Case descriptions

These cases are created with the aim of distinguishing the important aspects of current unbalance in both the phase and sequence domains. In the phase domain, these aspects are current magnitude unbalance and current angle unbalance. And in the sequence domain, they are negative sequence current unbalance and zero sequence current unbalance. The aim of this approach is to relate these differing aspects to the effects on the low-voltage network and determine their relative contributions.

Three cases are described in the following sections. The first is current magnitude unbalance only, the second is current angle unbalance only and the third is a combination of both current magnitude and angle unbalance. There are similarities and differences between them in terms of the resulting sequence currents and active power transfers which are highlighted with phasors and plots shown for nominal voltages. In all cases the total three-phase apparent power was 45 kVA. At the end of this section all similarities and differences are summarised.

Case L1-mag: Current magnitude unbalance only

Current magnitude unbalance was created by gradually increasing the demand of the single-phase load on phase A from 0 kW to 45 kW whilst the demands on the other two single-phase loads on phases B and C were decreased equally from 22.5 kW to 0 kW. In this way, the total active power transferred was maintained at 45 kW, unity power factor. The anticipated current phasors are shown in Figure 4.7 (a) for nominal voltages.

The effects, which will be examined in section 4.5, can be better understood by first appreciating the variation of the anticipated sequence currents. This is shown in Figure 4.7 (b) and Figure 4.8. For current magnitude unbalance, it can be seen that $|I_0| = |I_2|$ as demands of the three single-phase loads deviate from the balanced condition. Also, sequence currents on either side of the balanced condition will mirror each other (i.e. equal magnitude but opposite direction) up to the point that phase A is loaded to 66.7 % of the total demand. Beyond this, the sequence currents continue to increase and are at their highest when all demand is on phase A.

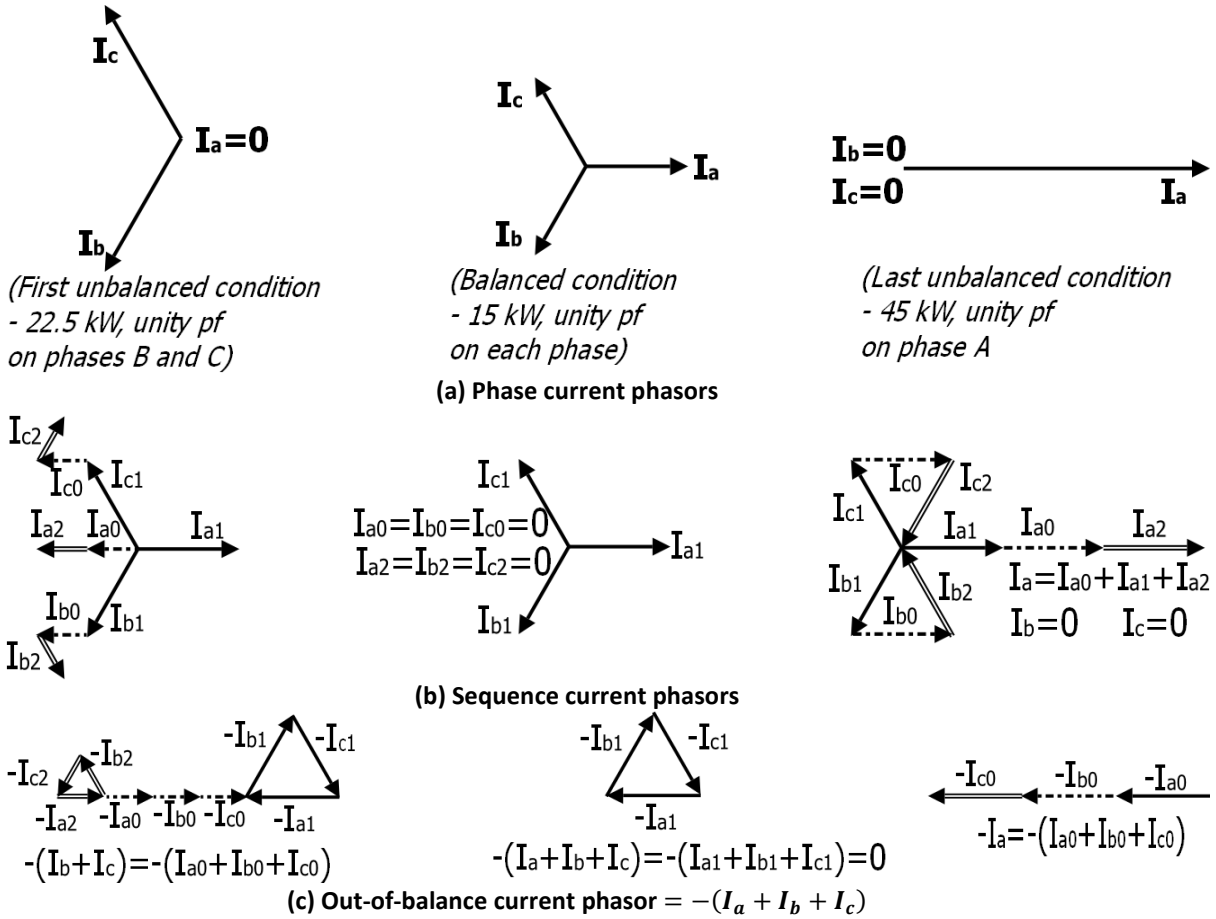

Figure 4.7: Phase, sequence and out-of-balance current phasors for *L1-mag*

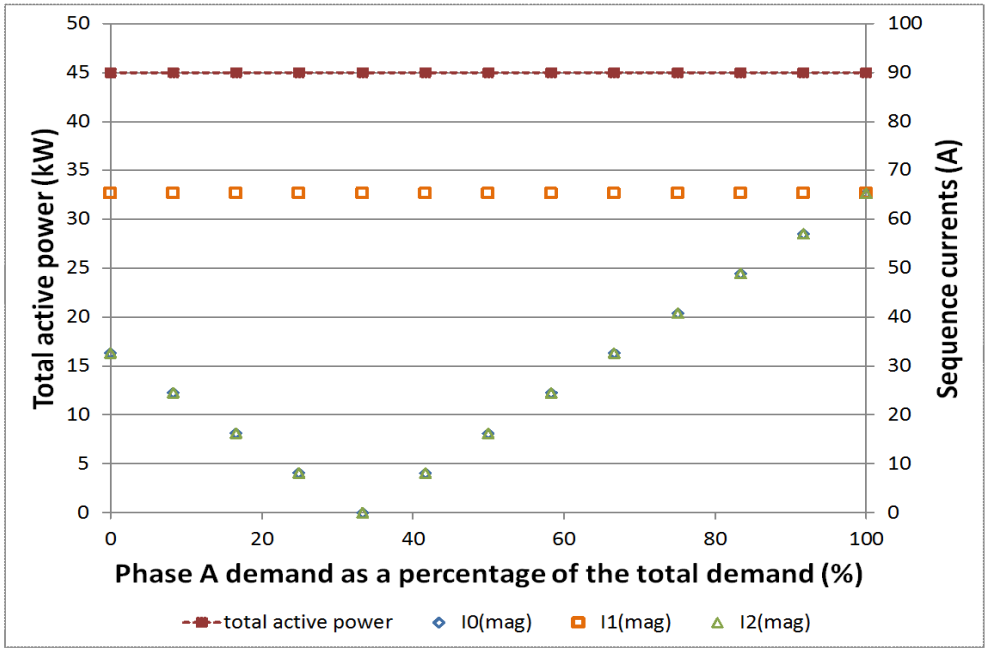

Figure 4.8: Resulting variation of active power transferred and sequence currents for *L1-mag*

Also, very important is the out-of-balance current shown in Figure 4.7 (c). It can be seen that as the I_1 and I_2 components form closed triangles, the out-of-balance current will consist of I_0 components only. Its direction will depend on the power factors of all three single-phase loads, which for this case, all equal to unity.

Case L1-ang: Current angle unbalance only

Current angle unbalance was created by gradually varying the power factor of phase C from 0.866 leading to 0.866 lagging and that of phase B from 0.866 lagging to 0.866 leading whilst keeping the apparent power demand on each phase constant and equal (15 kVA). The single-phase load on phase A is kept at 15 kW, unity power factor. In doing this, the total active power transferred varies but is mirrored equally on either side of the balanced condition, as shown in Figure 4.10.

The anticipated current phasors are shown in Figure 4.9 (a) for nominal voltages. As can be seen, varying the power factors on phases B and C results in the current angle between both these phases increasing from 60° to 180°. The current magnitudes on all phases are equal.

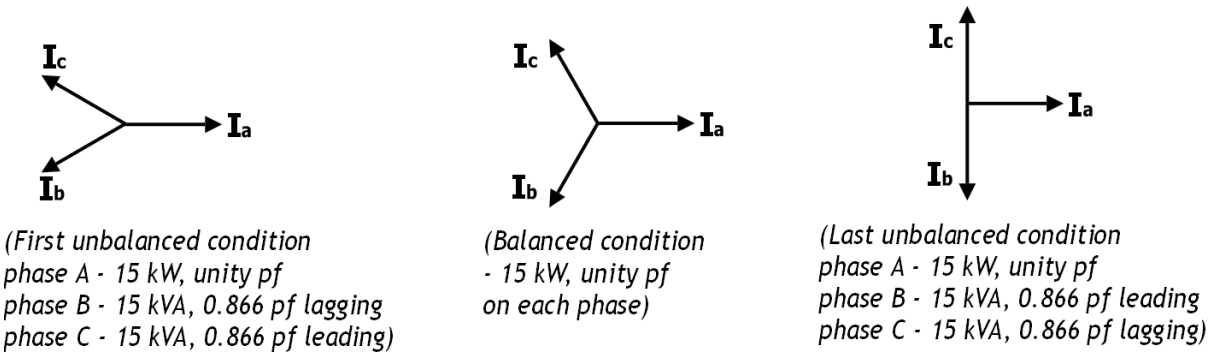

(a) Phase current phasors

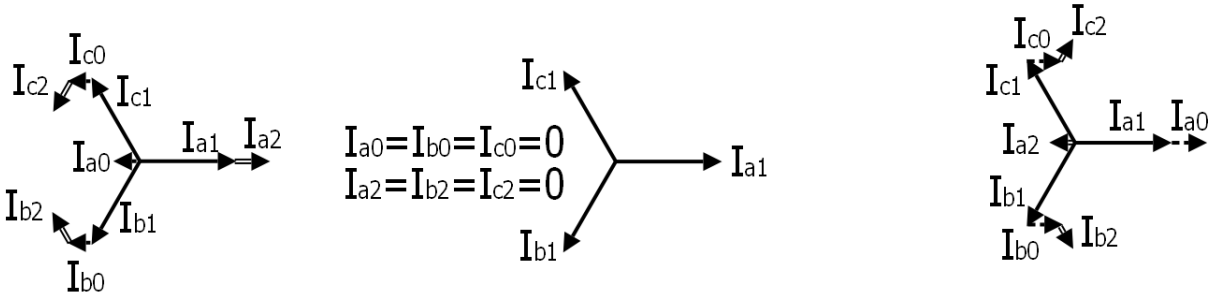

(b) Sequence current phasors

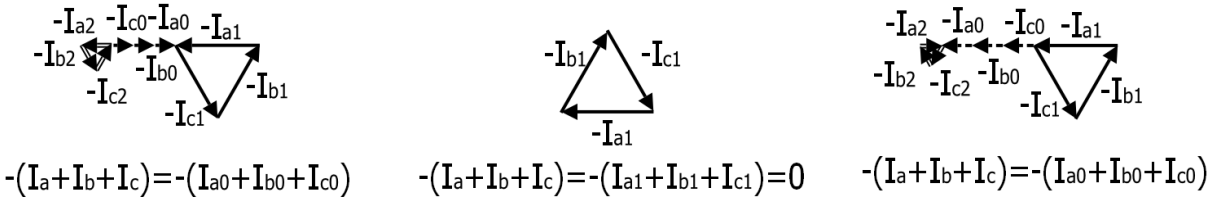

(c) Out-of-balance current phasor $= -(\boldsymbol{I_a} + \boldsymbol{I_b} + \boldsymbol{I_c})$

Figure 4.9: Phase, sequence and out-of-balance currents for *L1-ang*

Transforming to the sequence domain gives the sequence current phasors shown in Figure 4.9 (b). The variations in their magnitudes are shown in Figure 4.10 (for nominal voltages). Unlike the ***L1-mag*** case, the sequence currents are not equal. The positive sequence current (which corresponds to active power) varies and is mirrored equally on either side of the balanced condition. The negative and zero sequence current vary as follows:

- $|\boldsymbol{I_2}| \geq |\boldsymbol{I_0}|$ whilst current angle between phase B and C is decreased from 120° to 60°. It can be appreciated that the closer the phase B and C current phasors become, the nearer they are to swapping over. If that were to happen the phase rotation will change from ABC to ACB i.e. a system of negative sequence phasors.
- $|\boldsymbol{I_0}| \geq |\boldsymbol{I_2}|$ whilst current angle between phase B and C is increased from 120° to 180°. As phase B and C current phasors move closer to the phase A current

phasor, all three current phasors will become homopolar i.e. a system of zero sequence phasors.

Additionally, it can be seen that $|\boldsymbol{I_0}|$ equals $|\boldsymbol{I_2}|$ on the opposite side of the balanced condition (and vice-versa). As $|\boldsymbol{I_1}|$ is mirrored equally, this means that for the same active power transfer, the magnitudes of IUF_0 and IUF_2 also swap around on opposite sides of the balanced condition.

Finally, as shown in Figure 4.9 (c) the out-of-balance current consists of $\boldsymbol{I_0}$ only. It can be seen that for the same three single-phase loads on either side of the balanced condition, significantly different $\boldsymbol{I_0}$ and out-of-balance currents arise, simply by swapping the loads on the B and C phases. Both its direction and magnitude will depend on the power factors of all three single-phase loads relative to each other.

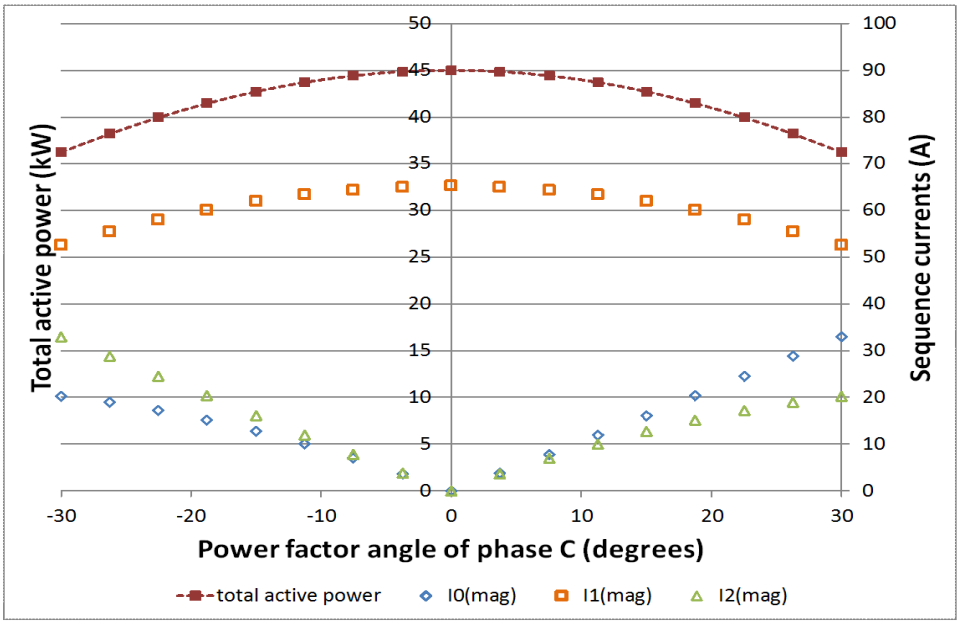

Figure 4.10: Resulting variation of active power transferred and sequence currents for *L1-ang*

Case L1-mag-ang: Current magnitude and angle unbalance

This case combines both current magnitude and angle unbalance. It borrows from the differing $|\boldsymbol{I_0}|$ and $|\boldsymbol{I_2}|$ created by current angle unbalance but takes it to extreme conditions in which either $|\boldsymbol{I_0}|$ or $|\boldsymbol{I_2}|$ equals zero while the other is at a maximum. For this case the maximum created is for the particular sequence current to equal $|\boldsymbol{I_1}|$. It should be noted though, that more severe conditions can be created by combining current magnitude and angle unbalance in which either $|\boldsymbol{I_0}|$ or $|\boldsymbol{I_2}|$ exceeds $|\boldsymbol{I_1}|$.

For ***L1-mag-ang***, the power factor of phases B and C was varied in the same manner as in ***L1-ang***. The demand of phases B and C are however first decreased from 22.5 kVA to 15 kW as their power factors approach unity whilst the demand on phase A is increased from 0 kW to 15 kW. After the balanced condition is reached, the demand on phases B and C are increased to 22.5 kVA and the demand on phase A is decreased to 0 again. As in ***L1-ang***, the active power varies but is mirrored on either side of the balanced condition. This is shown in Figure 4.12.

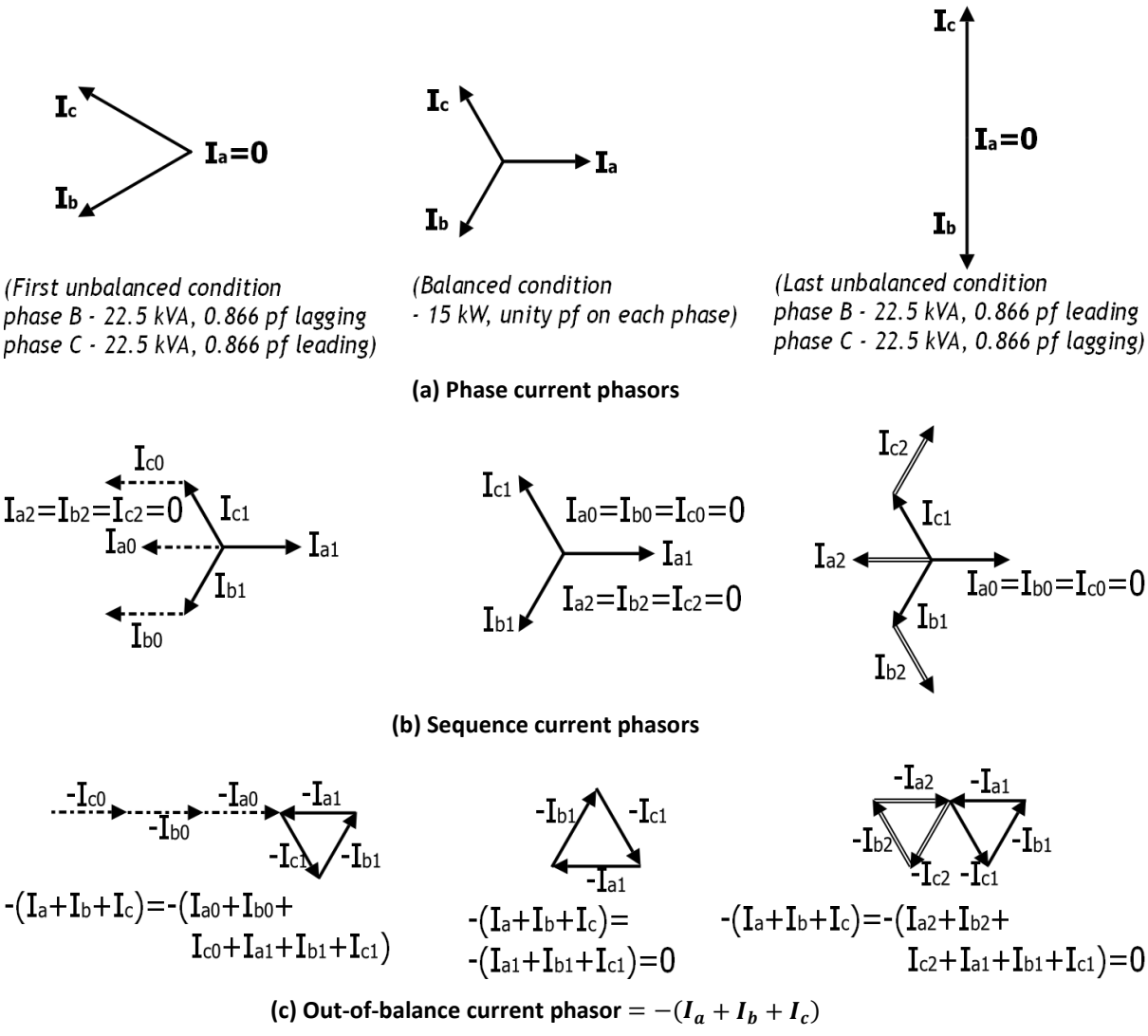

Figure 4.11: Phase, sequence and out-of-balance currents for *L1-mag-ang*

The resulting current phasors are shown in Figure 4.11 (for nominal voltages). It can be seen that the current angle between phase B and C increases from 60° to 120° whilst the current magnitudes of phases B and C decrease and that of phase A increases. After the balanced condition is reached, the current angle between phase B and C continues

its increase from 120° to 180° but the current magnitude on phase A decreases while that on phase B and C increase.

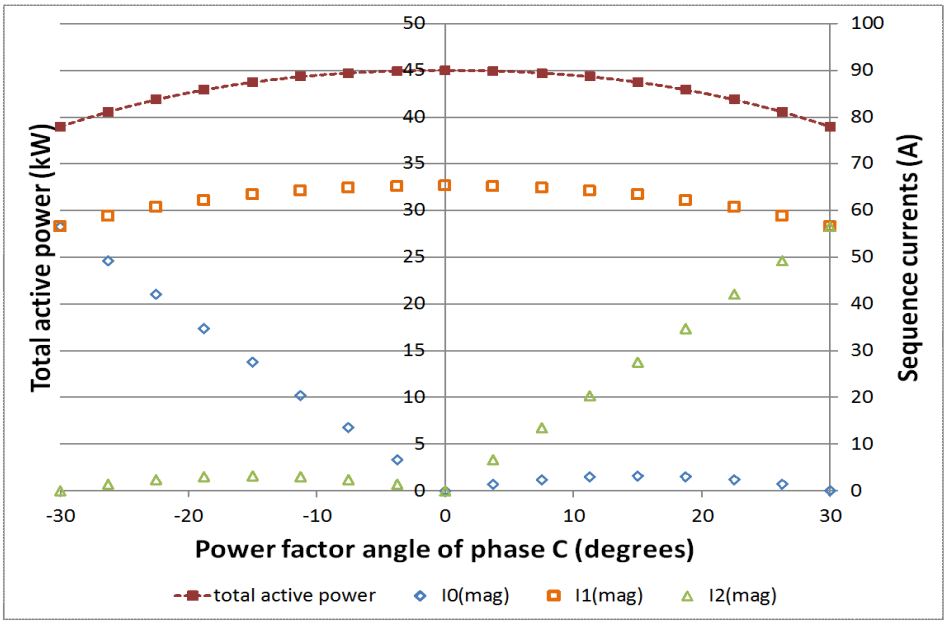

Figure 4.12: Resulting variation of active power transferred and sequence currents for *L1-mag-ang*

The sequence current phasors are shown in Figure 4.11 (b) and the variations in their magnitudes in Figure 4.12 (for nominal voltages). As can be seen the sequence currents are not equal. The positive sequence current (which corresponds to active power) varies and is mirrored equally on either side of the balanced condition. The negative and zero sequence current vary as follows:

- $|\boldsymbol{I_0}| \gg |\boldsymbol{I_2}|$ whilst the angle between phase B and C is decreased from 120° to 60° and the current magnitude of phase A is decreased. From Figure 4.11 (a) it can be appreciated that as the angle between phase B and C approaches 60°, the $\frac{1}{3}a^2 I_\mathrm{b}$ and $\frac{1}{3}aI_\mathrm{c}$ components of the negative sequence current phasor $\left(I_2 = \frac{1}{3}I_a + \frac{1}{3}a^2 I_\mathrm{b} + \frac{1}{3}aI_\mathrm{c}\right)$ are moved closer to being opposite each other. With I_a being decreased at the same time, the resultant negative sequence current phasor remains small. It goes to zero when $I_a = 0$ and $\frac{1}{3}a^2 I_\mathrm{b}$ and $\frac{1}{3}aI_\mathrm{c}$ are opposite each other.
- $|\boldsymbol{I_2}| \gg |\boldsymbol{I_0}|$ whilst the angle between phase B and C is increased from 120° to 180° and the current magnitude of phase A is decreased.

As in ***L1-ang***, $|\boldsymbol{I_0}|$ equals $|\boldsymbol{I_2}|$ on the opposite side of the balanced condition (and vice-versa). And for the same active power transfer, the magnitudes of IUF_0 and IUF_2 also swap around on opposite sides of the balanced condition.

As shown in Figure 4.11, just like ***L1-ang*** the out-of-balance current consists of $\boldsymbol{I_0}$ only and its direction and magnitude are influenced by the power factors of the individual single-phase loads relative to each other.

Summary

Case	Sequence currents	Total active power
L1-mag	$\|\boldsymbol{I_0}\| = \|\boldsymbol{I_2}\|$.	**Constant**
L1-ang	**LHS :** $\|\boldsymbol{I_2}\| > \|\boldsymbol{I_0}\|$ **RHS :** $\|\boldsymbol{I_0}\| > \|\boldsymbol{I_2}\|$ $\|\boldsymbol{I_0}\|$ *mirrors* $\|\boldsymbol{I_2}\|$ *on the opposite side of the balanced condition (and vice-versa).*	**Mirrored equally.**
L1-mag-ang	**LHS :** $\|\boldsymbol{I_0}\| \gg \|\boldsymbol{I_2}\|$ **RHS :** $\|\boldsymbol{I_2}\| \gg \|\boldsymbol{I_0}\|$ $\|\boldsymbol{I_0}\|$ *mirrors* $\|\boldsymbol{I_2}\|$ *on the opposite side of the balanced condition (and vice-versa).*	**Mirrored equally.**
LHS: *Current angle between phase B and C varied from 120° to 60° or power factor angle of phase C varied between -30° to 0° (i.e. leading).* ***RHS:*** *Current angle between phase B and C varied from 120° to 180° or power factor angle of phase C varied between 0° to 30° (i.e. lagging).*		

Table 4.2: Similarities and differences between cases

The L1-ang and L1-mag-ang cases show a less recognised cause of unbalance

The ***L1-ang*** and ***L1-ang-mag*** cases have revealed a subtle but fundamental cause of unbalance which is not among the widely recognised causes given in the literature (which were organised and presented in Figure 2.8).

In both cases, it was seen that for the same three single-phase loads, simply swapping the loads on the B and C phases, resulted in significantly different zero and negative sequence currents. They demonstrate that the power factors of the individual single-phase loads relative to each other, is a cause of current unbalance.

4.5 Analysis of the three current unbalance cases

The objectives of this analysis are to develop a clear understanding of:

1. the quantitative relationships between current unbalance and its effects;
2. the recognition of these effects using either sequence voltage or sequence current unbalance factors as indicators; and
3. the theoretical approach for the reduction of these effects demonstrated with an ideal sequence current compensator.

These objectives are addressed in the sections which follow.

4.5.1 The quantitative relationships between current unbalance and its effects

In this section, the representative low-voltage network is solved for cases ***L1-mag, L1-ang*** and ***L1-mag-ang*** using the proposed 5 x 5 approach to the forward-backward sweep method derived in chapter 3. The aim here is to investigate quantitatively the relative contribution of both sequence components to network effects as identified in Figure 2.13. These simulations were carried out using the input and model data of Table 4.1.

The sections that follow compare the network effects for each case.

(a) Network utilisation

Effective power factor

The effective power factor is shown in Figure 4.13 alongside the sequence current unbalance factors for the three cases. In each case it can be seen that the effective power factor is inversely proportional to both sequence unbalance factors and has maximum points corresponding to the balanced condition.

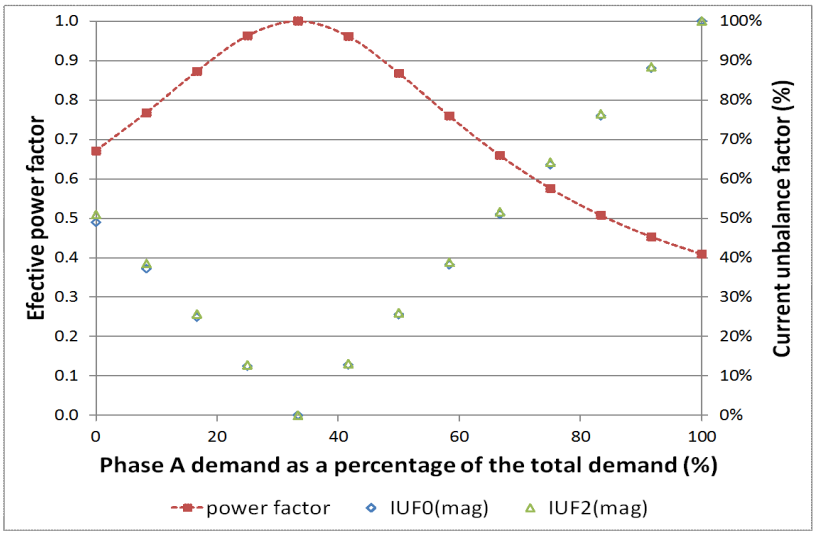

(a)

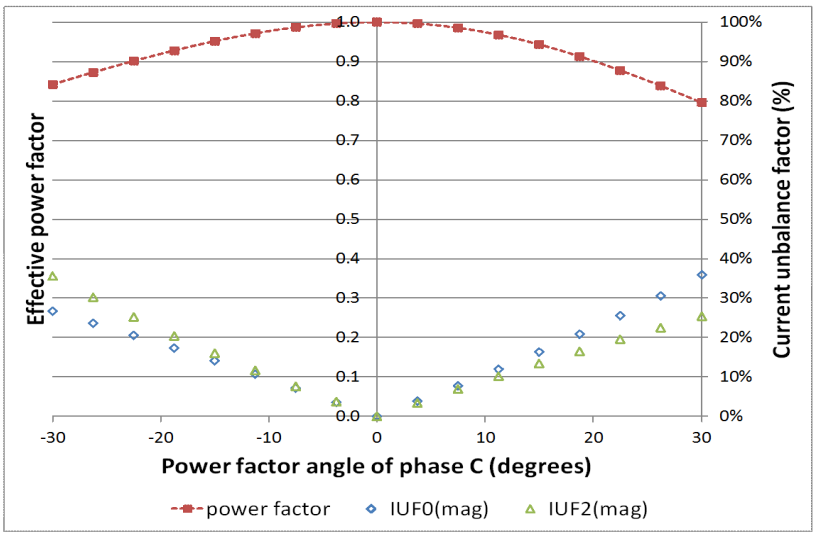

(b)

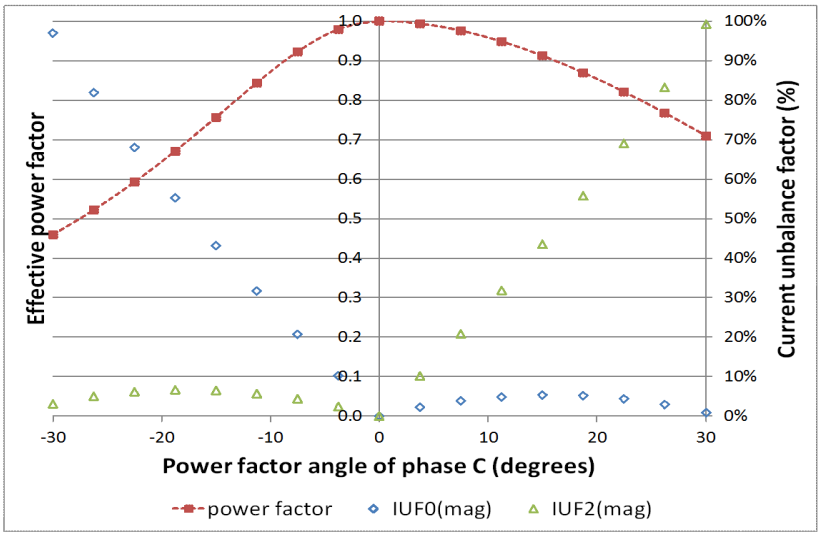

(c)

Figure 4.13: Effective power factor for (a) *L1-mag*, (b) *L1-ang* and (c) *L1-mag-ang*

For the ***L1-mag case***, with equal IUF_0 and IUF_2 there is no discernible difference in the relative contribution of each. The gradient of the curve on either side of this maximum point is equal, as it can be seen that with $IUF_0 = IUF_2 = 0.5$ at both 0 % and 66.7 %, the effective power factors are nearly equal (0.67).

For the other two cases however, it is clear that the effective power factor declines more sharply with IUF_0 than with IUF_2. This is more evident in ***L1-mag-ang***, where for $IUF_0 \gg IUF_2$ the effective power factor decreases from unity to 0.45 compared to 0.71 for $IUF_2 \gg IUF_0$. Clearly, IUF_0 has a much greater impact on effective power factor.

Potential released current capacity

The potential released current capacity depends on how closely the maximum phase current is to the average phase current as defined by their magnitudes in equation (4.1). Therefore, it depends only on current magnitude unbalance. This is evident from the plot for the ***L1-ang*** case (Figure 4.14 (b)), in which there is no current magnitude unbalance and as can be observed the NU_PRCC remained at 0 %.

Now, the ***L1-mag*** and ***L1-mag-ang*** cases both consider current magnitude unbalance.

For the ***L1-mag*** case (Figure 4.14 (a)), where the phase A current is increased by twice as much as phases B and C are decreased by, the gradient of NU_PRCC is twice as steep from 33.3 % to 100 % than from 0 to 33.3 %.

For the ***L1-mag-ang*** case (Figure 4.14 (c)), the maximum phase current is increased equally on either side of the balanced condition and as a result NU_PRCC increases by the same amount on either side.

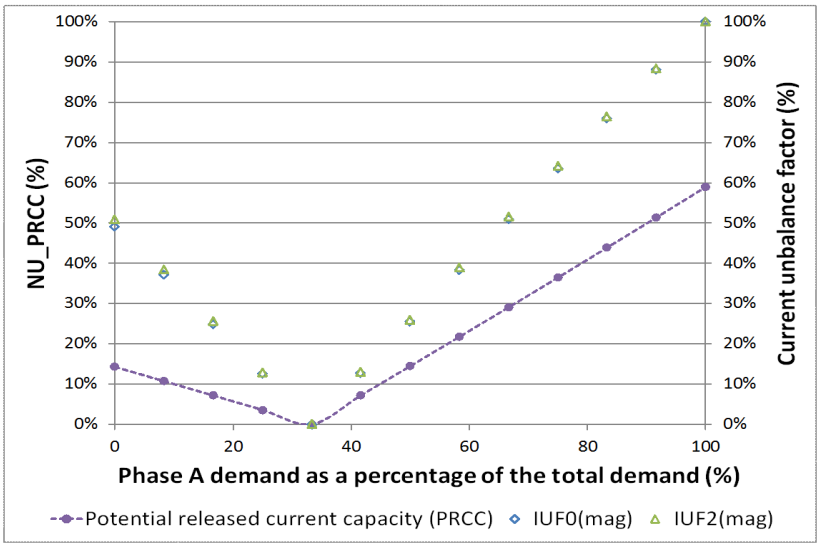

(a)

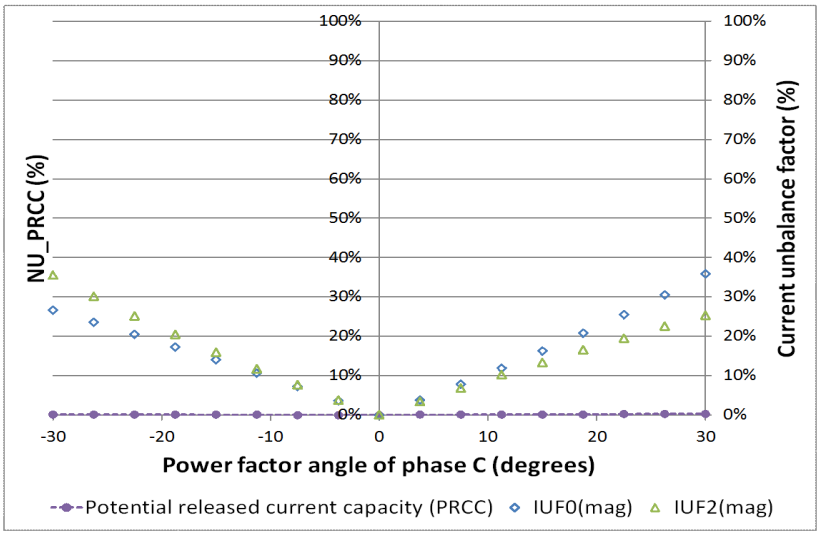

(b)

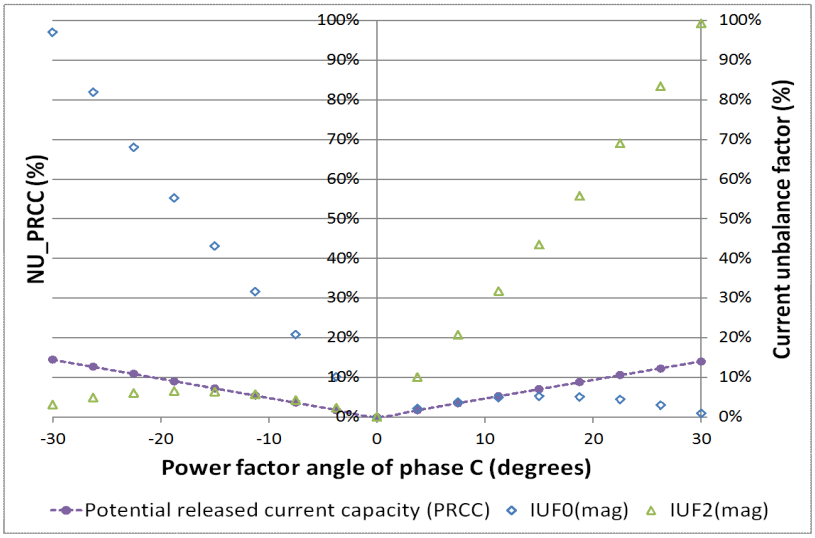

(c)

Figure 4.14: NU_PRCC for (a) *L1-mag*, (b) *L1-ang* and (c) *L1-mag-ang*

(b) Neutral and (c) earth currents

In all three cases the neutral and earth currents were directly proportional to the zero sequence current unbalance factor. Also, as would be expected, the earth currents were much less than the neutral currents.

Both currents are not related to IUF_2. This is very clear from the results of the ***L1-mag-ang*** case shown in Figure 4.15, where even with IUF_2 increasing to 100 % there was no change in either current.

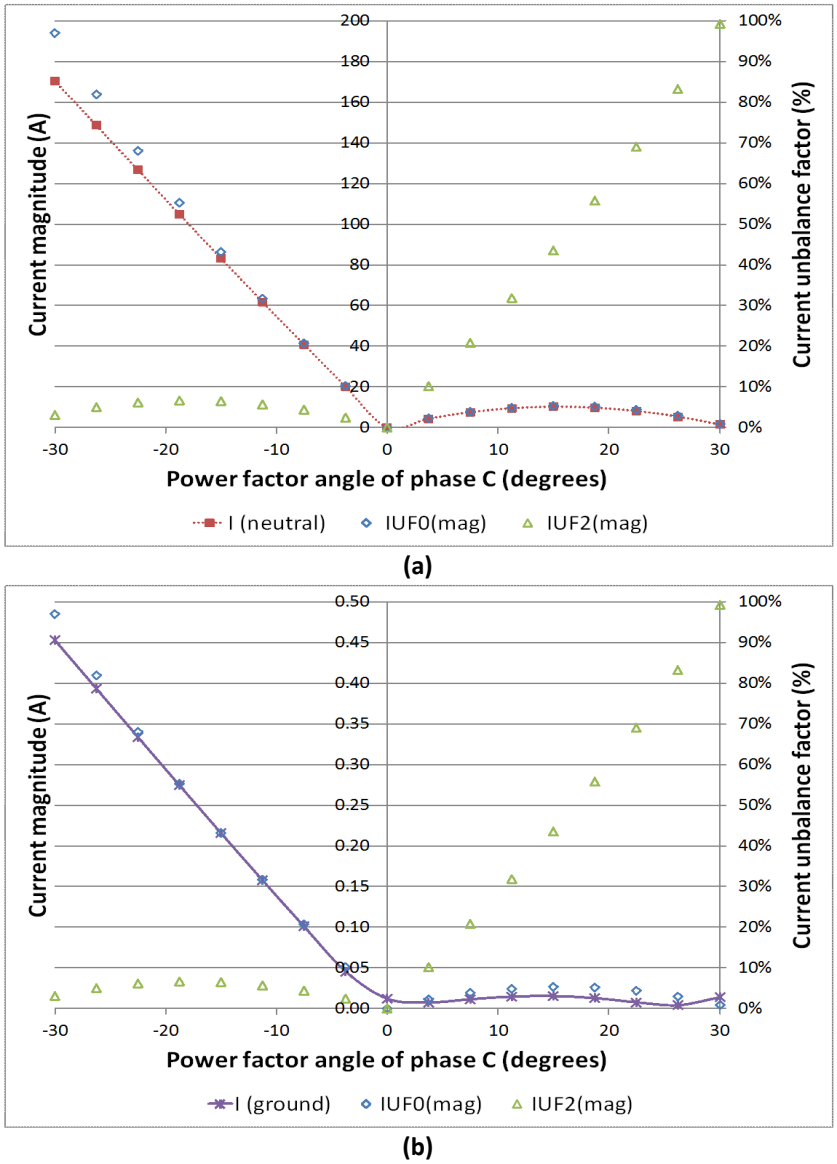

Figure 4.15: (a) Neutral and (b) earth currents for *L1-mag-ang*

Also of interest are the significantly higher neutral currents that arise due to the power factors of the individual single-phase loads relative to each other. As mentioned in

section 4.4, this is a less recognised cause of current unbalance. It can be demonstrated in the results from the ***L1-ang*** case as shown in Figure 4.16. It can be seen that simply by swapping the loads on the B and C phases on either side of the balanced condition, the neutral current can either be 48 A or 65 A.

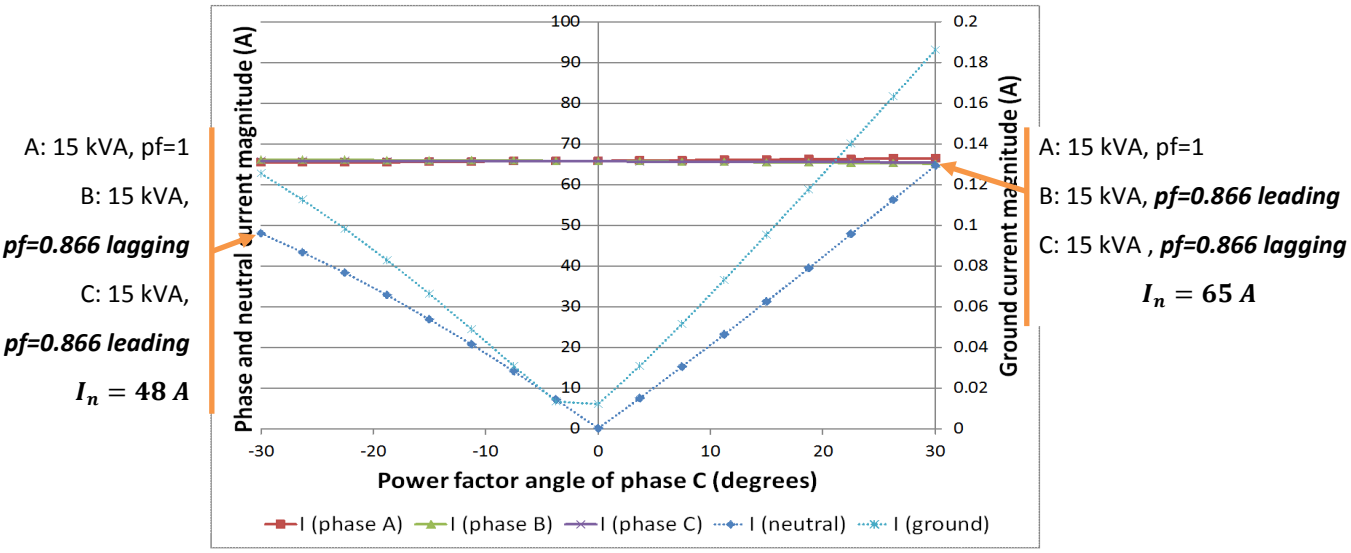

Figure 4.16: Difference in neutral and ground currents for *L1-ang*

(d) Losses

Figure 4.17 shows that for all three cases losses increase with both zero and negative sequence current unbalance factors. Looking at the results for the ***L1-ang*** and ***L1-mag-ang*** cases, it can be seen however, that the zero sequence current unbalance factor has a much greater influence. This is mostly because of its relationship to the neutral current, a fourth source of heating. The negative sequence current unbalance factor on the other hand, affects only the phase currents. This is evident looking at the losses per phase and neutral conductors for the ***L1-mag-ang*** case, shown in Figure 4.18.

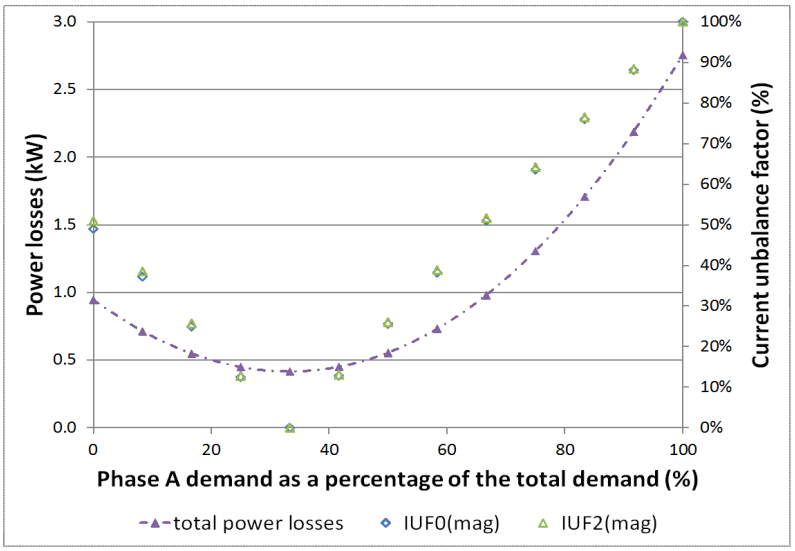

(a)

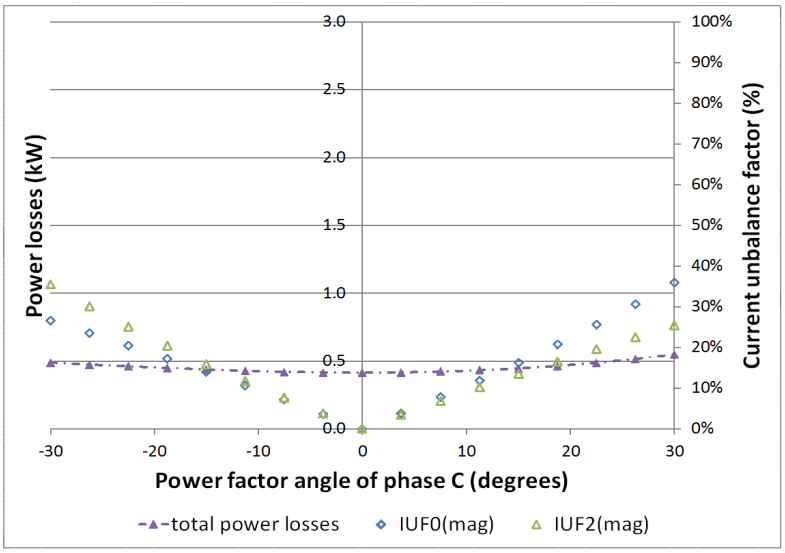

(b)

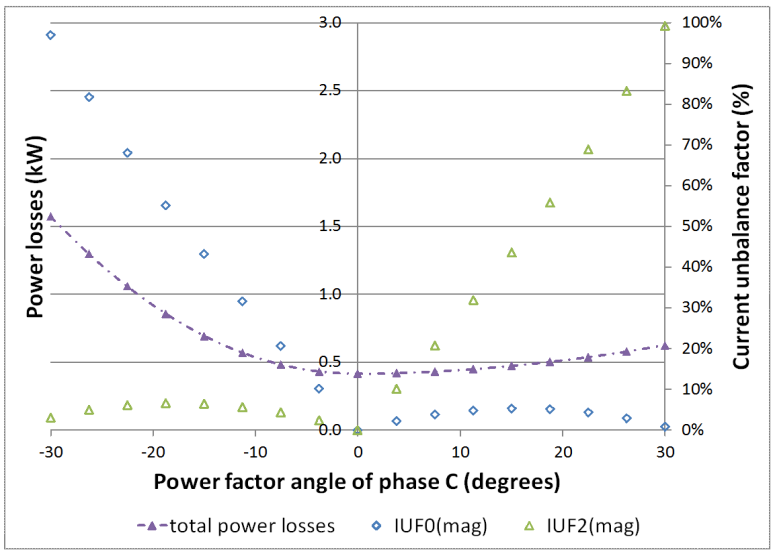

(c)

Figure 4.17: Losses for (a) *L1-mag*, (b) *L1-ang* and (c) *L1-mag-ang*

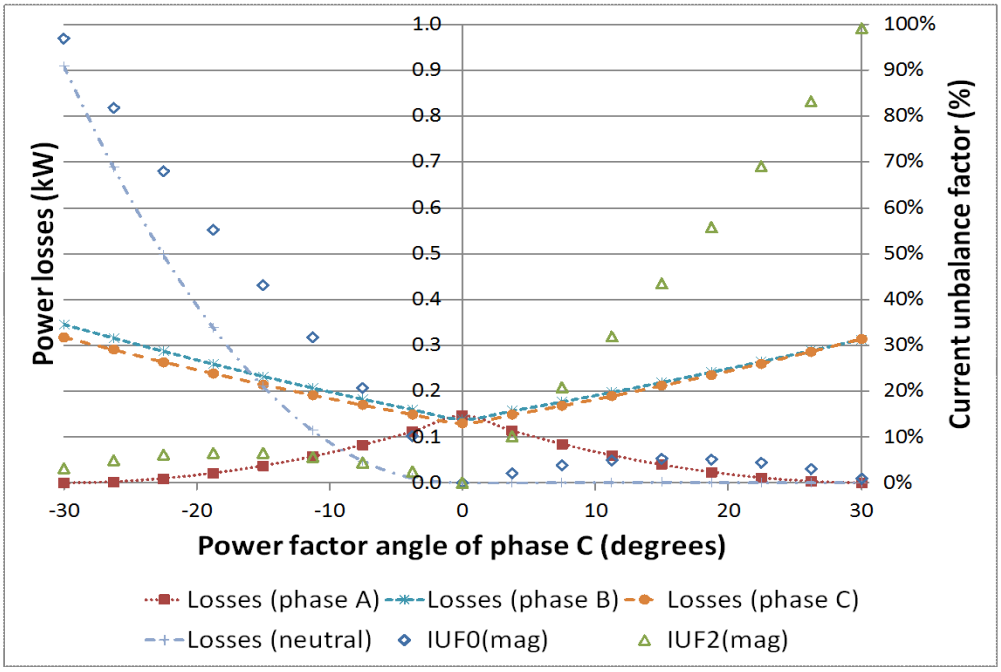

Figure 4.18: Losses per phase and neutral conductors for the *L1-mag-ang* case

(e) Neutral-point shifting

Both the neutral to ground voltages and the zero sequence voltage are for all cases, influenced more by the zero sequence current unbalance factor. Again, this is seen most clearly for the ***L1-mag-ang*** case, shown in Figure 4.19.

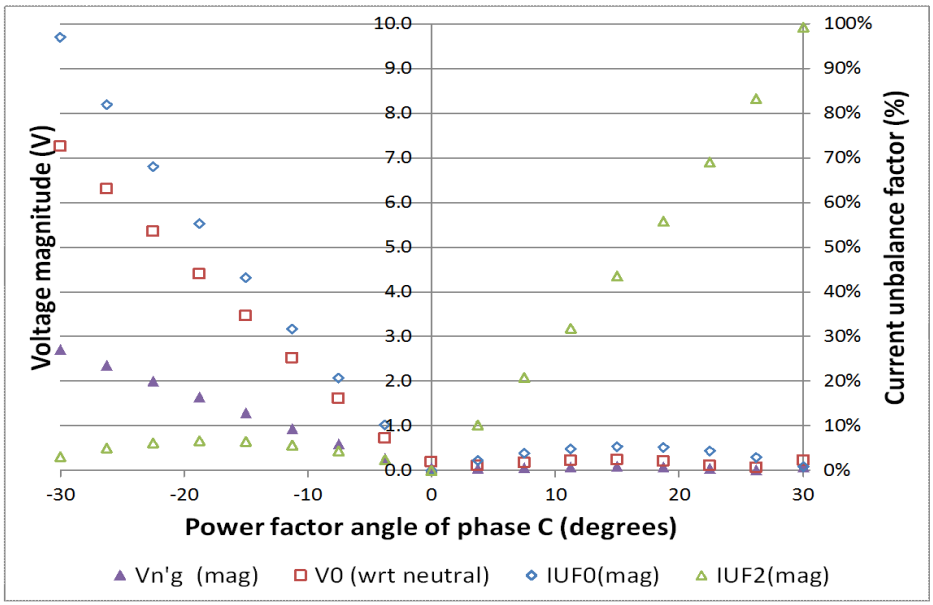

Figure 4.19: Neutral-point shifting for *L1-mag-ang*

(f) Phase-neutral voltages

The starting point of the phase-neutral voltage phasors is the neutral point. If it is displaced then the relative position of all three phase-neutral voltages to each other is affected. From the results shown in Figure 4.20 it can be seen that the sensitivity of the neutral voltage to the IUF_0 was translated to the phase-neutral voltages in all three cases. In each it can be seen that as IUF_0 increased, so too does the separation between the phase-neutral voltage magnitudes. This separation, it must be appreciated, can lead to voltages on some phases going outside statutory limits, considering that the voltages at the start of an actual low-voltage feeder are rarely balanced or at nominal voltage (as was assumed for these cases).

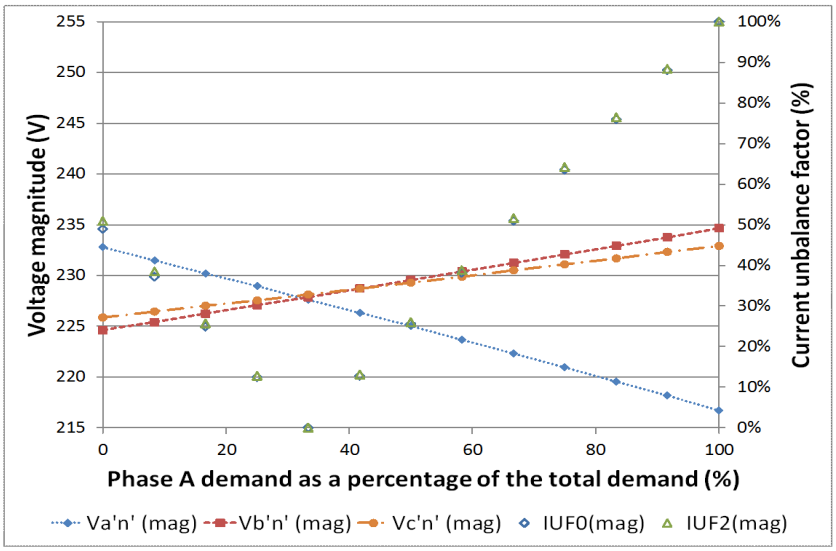

(a)

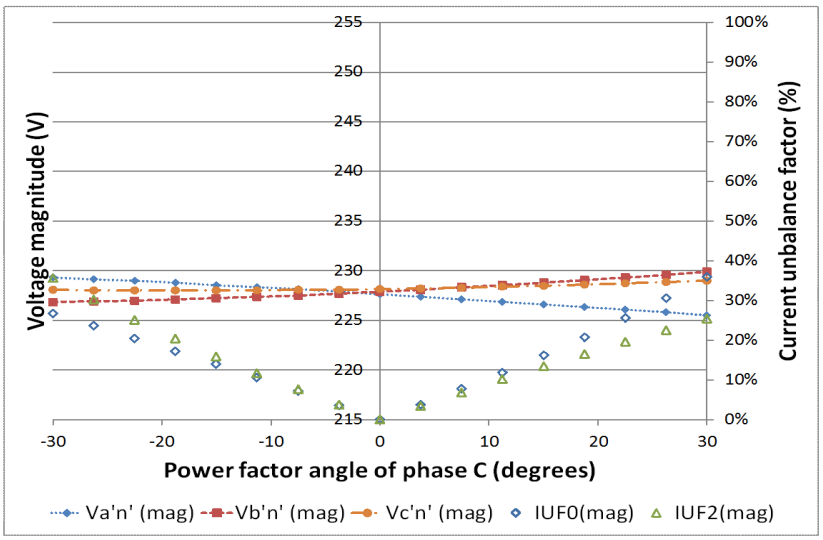

(b)

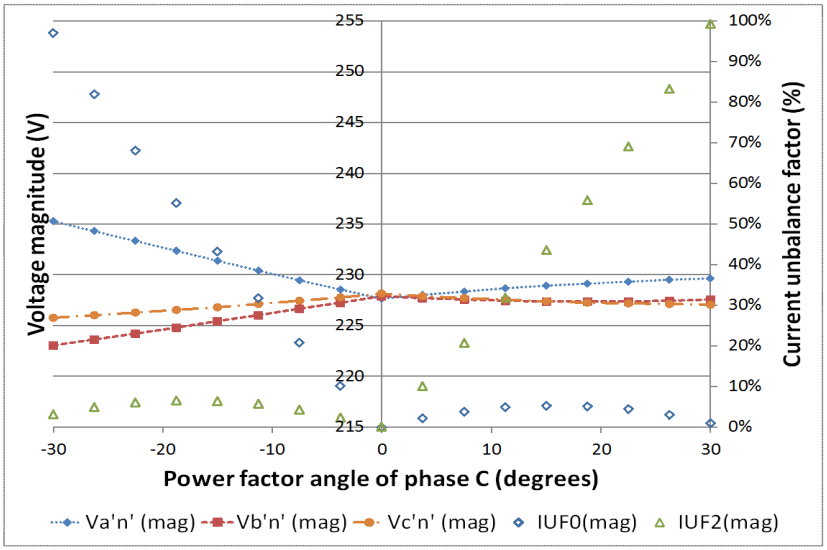

(c)

Figure 4.20: Phase-neutral voltages for (a) *L1-mag*, (b) *L1-ang* and (c) *L1-mag-ang*

(g) Voltage regulation

For all three cases, the separation of the phase-neutral voltages was reflected in the voltage regulation indicator - $VR_{indicator}$. The standard definition - VR_{avg} (given by equation (4.17)) - as expected, did not account for this separation and so remained constant and less than 1 % for all three cases.

Using the results of ***L1-mag-ang*** case (Figure 4.21) to illustrate, it can be seen that the $VR_{indicator}$ gives values:

- close to zero at the balanced condition. It is not exactly zero because a four-core cable (Table 4.1) with asymmetrical impedances was used for this representative low-voltage network; and
- which increase with IUF_0 (which as mentioned in the previous section results in a greater separation in phase-neutral voltages).

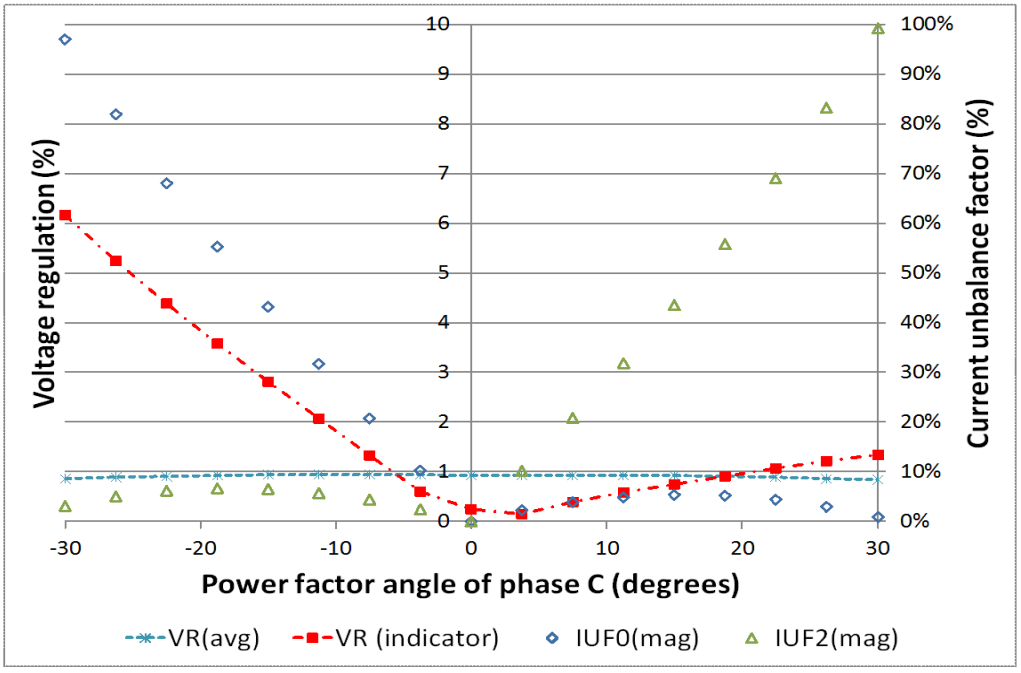

Figure 4.21: Voltage regulation for *L1-mag-ang* case

Summary

Network effect:		IUF_0	IUF_2
(a) Poorer network utilisation			
	(a)(1) effective power factor	->>>-	->-
	(a)(2) potential released current capacity	->- *(note 1)*	->- *(note 1)*
(b) Higher neutral current		->>>-	---
(c) Higher ground current		->>>-	---
(d) Higher losses		->>>-	->-
(e) Greater neutral-point shifting		->>>-	---
(f) Poorer phase-neutral voltages		->>>-	->-
(g) Poorer voltage regulation		->>>-	->-
Legend: --- no effect ->- worsens ->>>- worsens significantly			
Note 1: With current magnitude unbalance only.			

Table 4.3: Relative contributions of zero and negative sequence current unbalance to network effects

4.5.2 The recognition of these effects using sequence voltage and current unbalance factors as indicators

Current unbalance factors

The analysis carried out using the representative low-voltage network has thus far shown that there are close relationships between IUF_0 and many of the effects identified in Figure 2.13. This makes IUF_0 a good indicator of unbalance on low-voltage networks. The relationships between these effects and IUF_2 on the other hand, has been shown to not be as strong. To illustrate this, Figure 4.22 and Figure 4.23 show the correlation between losses to IUF_0 and to IUF_2 using the data points of all three cases. From Figure 4.22, it can be seen that the relationship between losses to IUF_0 appears to take a form similar to that of an I^2R curve. The relationship between losses to IUF_2 however seems more random (Figure 4.23). The only points which appear to fit a form similar to an I^2R curve happen to be the ones for ***L1-mag*** in which $IUF_2 = IUF_0$.

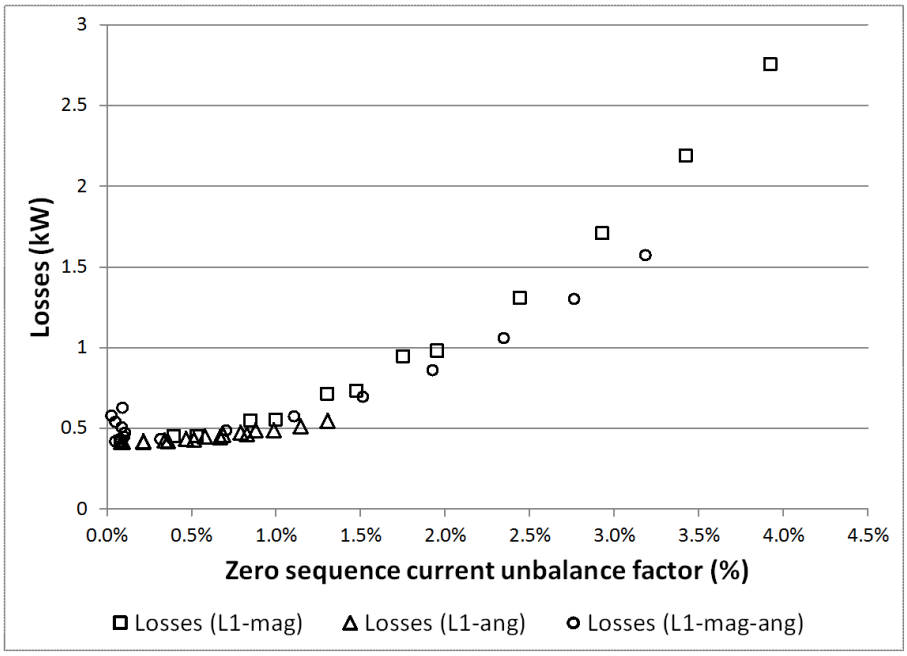

Figure 4.22: Correlation of losses to the zero sequence current unbalance factor

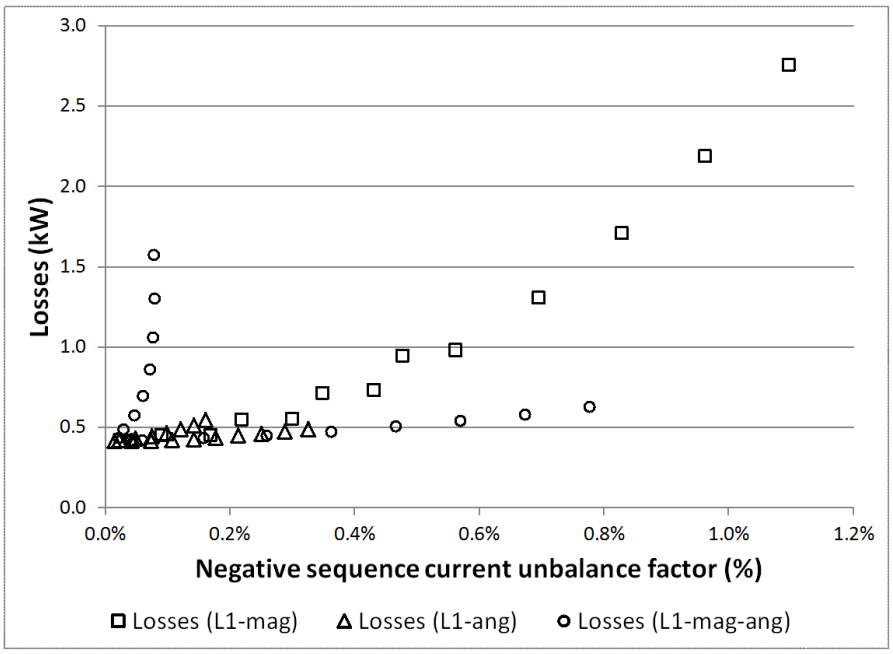

Figure 4.23: Correlation of losses to the negative sequence current unbalance factor

Similarly close relationships can be shown for the other network effects to IUF_0.

Voltage unbalance factors

As mentioned in chapter 2, many standards such as the BS EN 50160 place emphasis on VUF_2. This was because of its importance to three-phase consumer equipment. Apart from that, it has the advantage that unlike VUF_0 it does not require both phase-neutral and phase-phase voltage measurements.

The adequacy of VUF_2 as the only indicator (which is typically logged by most power quality meters and for which standards give a recommended limit) should however be questioned in light of the fact that IUF_0 contributes significantly more to network effects than IUF_2. Now, it is accepted that unbalanced low-voltage networks with asymmetrical network impedances will not have independent sequence networks (as discussed in section 2.1 and illustrated in Figure 2.4), meaning that it can be argued that increases to IUF_0 will in general also be reflected in VUF_2 and so the use of the VUF_2 alone should be sufficient. A closer look into the correlation between sequence current unbalance factors and sequence voltage unbalance factors is however needed to qualify such an argument. These results can give some insight into this as they are for a four-core cable with asymmetrical impedances (Table 4.1).

Figure 4.24 and Figure 4.25 shows both sequence current unbalance factors for all three cases against VUF_0 and VUF_2 respectively. In Figure 4.24 it can be seen that there is a clear correlation between IUF_0 and VUF_0 (hollow shapes) but little correlation between IUF_2 and VUF_0 (solid shapes). Figure 4.25 gives a similar story, with clear correlation between IUF_2 and VUF_2 (solid shapes) but little correlation between IUF_0 and VUF_2 (hollow shapes). Therefore, it cannot be assumed that the sequence networks are linked to the extent that increases in IUF_0 will be reflected in VUF_2. Moreover, given the significance of IUF_0 to network effects and its clear correlation to VUF_0, VUF_0 cannot be ignored.

Also, Figure 4.25 shows that despite the severe network effects associated with higher values of IUF_0, the value of VUF_2 neither changed significantly nor exceeded the recommended limit of 2 % (or 3 %) given in BS EN 50160. The VUF_2 by itself therefore, is not an adequate indicator of unbalance on the low-voltage network.

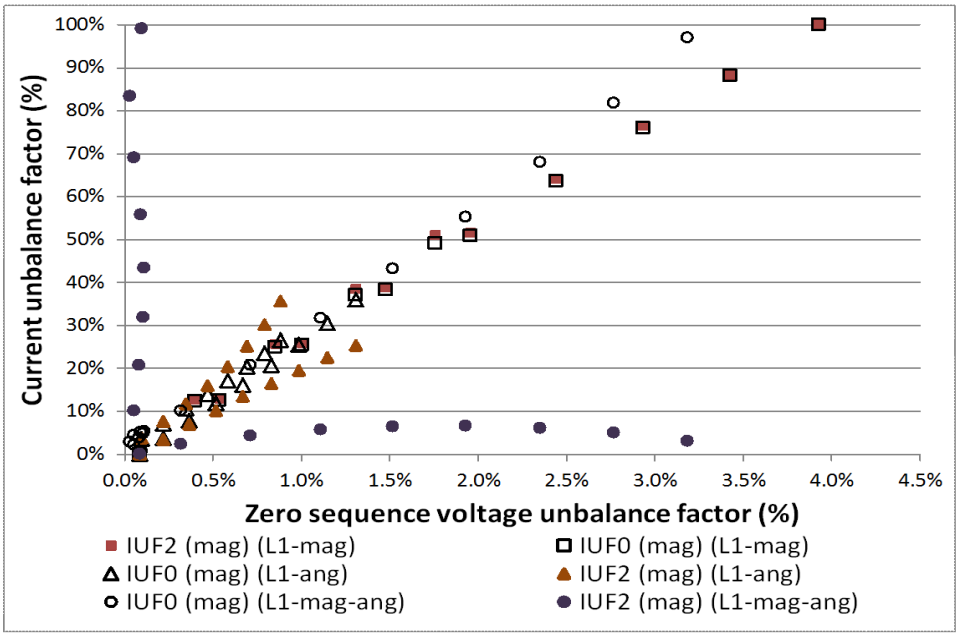

Figure 4.24: Correlation of sequence current unbalance factors to the zero sequence voltage unbalance factor

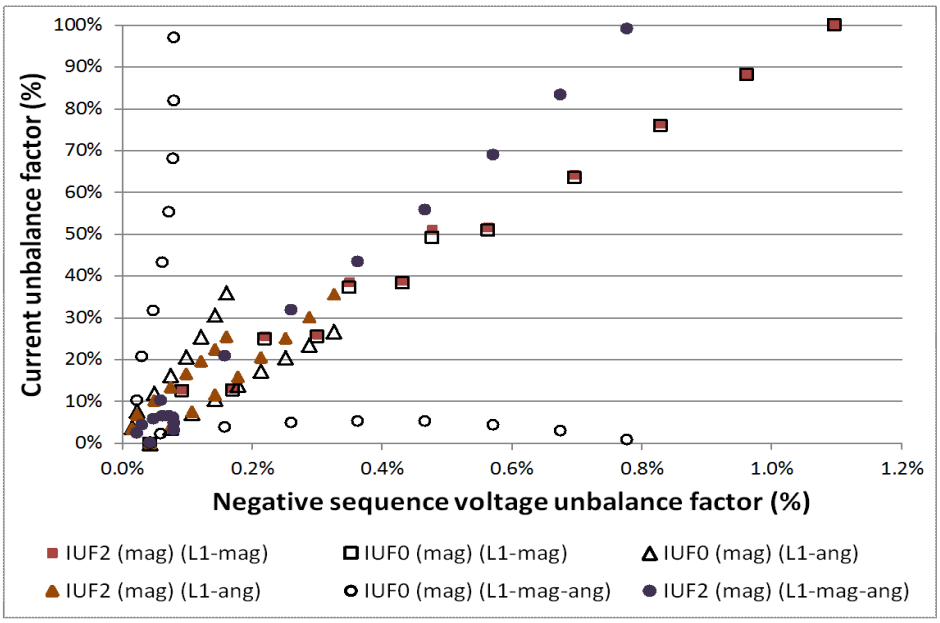

Figure 4.25: Correlation of sequence current unbalance factors to the negative sequence voltage unbalance factor

Summary

- Most of the effects on the network are strongly associated with IUF_0 and this is therefore a good indicator of unbalance on the low-voltage network. Additionally, there is a strong correlation between IUF_0 and VUF_0 which also makes VUF_0 a good indicator.
- IUF_2 and likewise VUF_2 by themselves are not adequate indicators of unbalance on low-voltage networks since neither can be strongly associated with most of the effects on the network. The VUF_2 remains important though, but for three-phase consumer equipment connected to the network.

4.5.3 The theoretical basis for the reduction of these effects

A sequence current compensator will be used to examine the theoretical approaches to mitigation. It can compensate either the negative or the zero sequence current seen on branch segment (1) without altering the power delivered to the three single-phase loads at node (1). The total active and reactive powers on either side are the same, only the per phase active and reactive powers differ as a result of the redistribution of the downstream load currents onto the upstream branch segment (1) currents. The representative low-voltage feeder is shown with the sequence current compensator in Figure 4.26.

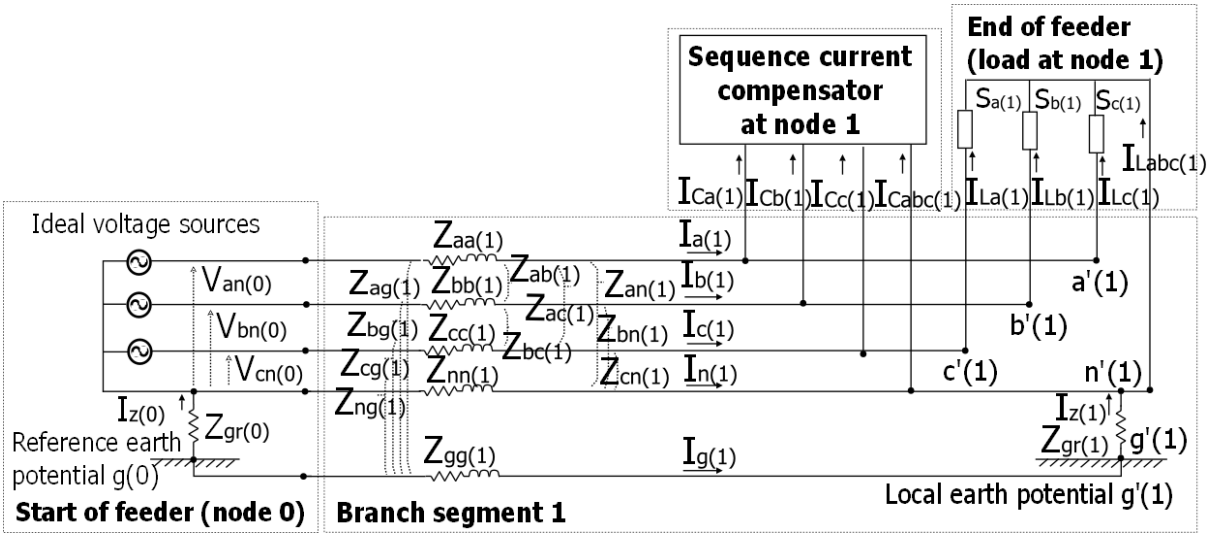

Figure 4.26: Representative low-voltage feeder comprising a single branch segment (1) and sequence current compensator

The next section presents the modelling of this device within the forward-backward sweep method. Following that, it is used to compare the effectiveness of mitigating either negative or zero sequence current unbalance.

Modelling a sequence current compensator

The following refers to a generic branch segment l shown in Figure 4.27 with three single-phase loads and a sequence current compensator at node j. For such a branch segment, equations (3.26) and (3.27) of the overview of the proposed approach given in section 3.7 are replaced by equations (4.21) and (4.22) which follow.

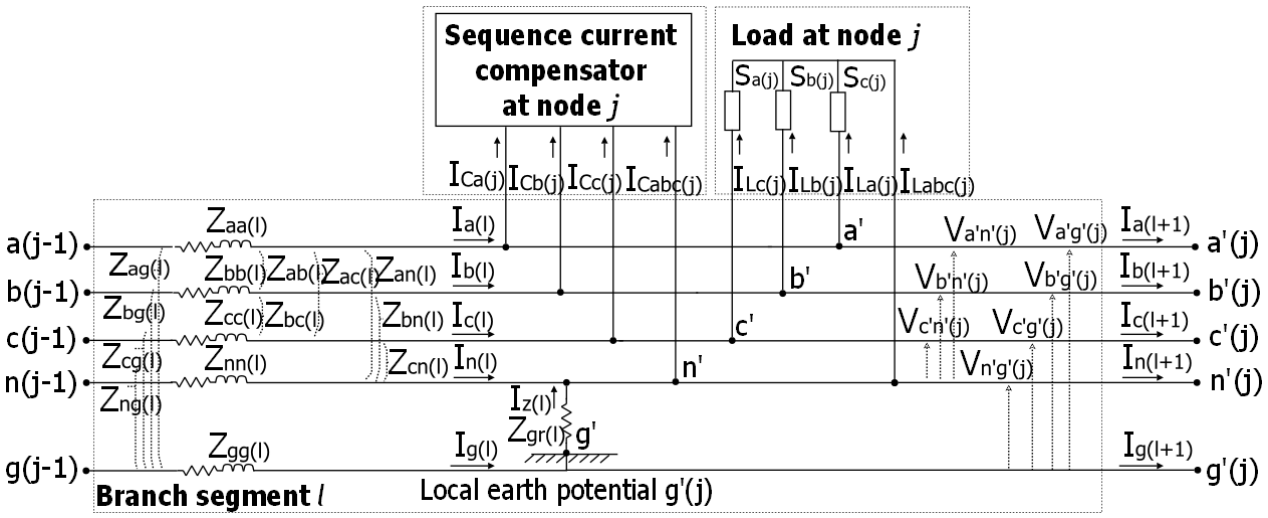

Figure 4.27: Generic branch segment l with load and sequence current compensator at node j

For iteration k, the current drawn by the sequence current compensator depends on the total sequence currents of the load at node j and the downstream branch segment $l+1$. This is given by:

$$\begin{bmatrix} I_0 \\ I_1 \\ I_2 \end{bmatrix} = \frac{1}{3}\begin{bmatrix} 1 & 1 & 1 \\ 1 & a & a^2 \\ 1 & a^2 & a \end{bmatrix}\left[\begin{bmatrix} I_{La(j)} \\ I_{Lb(j)} \\ I_{Lc(j)} \end{bmatrix} + \begin{bmatrix} I_{a(l+1)} \\ I_{b(l+1)} \\ I_{c(l+1)} \end{bmatrix}\right]^{(k)} \tag{4.18}$$

If the sequence current compensator reduces the zero sequence current by a factor C_0, the current drawn is given by:

$$\begin{bmatrix} I_{Ca(j)} \\ I_{Cb(j)} \\ I_{Cc(j)} \end{bmatrix}^{(k)} = \begin{bmatrix} 1 & 1 & 1 \\ 1 & a^2 & a \\ 1 & a & a^2 \end{bmatrix}\begin{bmatrix} -C_0 \cdot I_0 \\ 0 \\ 0 \end{bmatrix} \tag{4.19}$$

And if it reduces the negative sequence current by a factor C_2:

$$\begin{bmatrix} I_{Ca(j)} \\ I_{Cb(j)} \\ I_{Cc(j)} \end{bmatrix}^{(k)} = \begin{bmatrix} 1 & 1 & 1 \\ 1 & a^2 & a \\ 1 & a & a^2 \end{bmatrix}\begin{bmatrix} 0 \\ 0 \\ -C_2 \cdot I_2 \end{bmatrix} \tag{4.20}$$

With this the phase currents on branch segment l are found by:

$$\begin{bmatrix} I_{a(l)} \\ I_{b(l)} \\ I_{c(l)} \end{bmatrix}^{(k)} = \begin{bmatrix} I_{La(j)} \\ I_{Lb(j)} \\ I_{Lc(j)} \end{bmatrix}^{(k)} + \begin{bmatrix} I_{Ca(j)} \\ I_{Cb(j)} \\ I_{Cc(j)} \end{bmatrix}^{(k)} + \begin{bmatrix} I_{a(l+1)} \\ I_{b(l+1)} \\ I_{c(l+1)} \end{bmatrix}^{(k)} \tag{4.21}$$

And the current flow $I_{n(l)}^{(k)}$ on the neutral wire by:

$$I_{n(l)}^{(k)} = \frac{\left[\left(-I_{g(l-1)}^{(k)}\right)Z_{gr(l-1)}+\left(I_{n(l+1)}^{(k)}+I_{Labc(j)}^{(k)}+I_{Cabc(j)}^{(k)}\right)Z_{gr(l)}-\left[\left(Z'_{an}+Z_{gr(l-1)}\right)I_{a(l)}^{(k)}+\left(Z'_{bn}+Z_{gr(l-1)}\right)I_{b(l)}^{(k)}+\left(Z'_{cn}+Z_{gr(l-1)}\right)I_{c(l)}^{(k)}\right]\right]}{\left(Z'_{nn}+Z_{gr(l)}+Z_{gr(l-1)}\right)} \quad (4.22)$$

where $Z'_{pn} = Z_{pn} - Z_{pg} - Z_{ng} + Z_{gg}; p = a, b, c, n$

and $I_{Cabc(j)} = -\left(I_{Ca(j)} + I_{Cb(j)} + I_{Cc(j)}\right)$.

It should be appreciated that this theoretical model, when reducing the upstream zero sequence current, behaves like an ideal static balancer, if $C_0 = 1$. For a real static balancer, the current drawn will depend on the voltages at its terminals and its impedance.

Comparison of zero and negative sequence current compensation

Since zero sequence current unbalance contributes more to the effects of unbalance than negative sequence current unbalance, it can be anticipated that its reduction will also bring greater benefit to the low-voltage network. To illustrate this, all three cases were simulated with the sequence current compensator in the following modes:

- ***L1:*** $(C_0 = 0; C_2 = 0)$. No reduction to either sequence component. Same as results presented thus far. *(base for comparison)*
- ***L2:*** $(C_0 = 1; C_2 = 0)$. Zero sequence current eliminated with negative sequence current unchanged.
- ***L3:*** $(C_0 = 0; C_2 = 1)$. Negative sequence current eliminated with zero sequence current unchanged.

In all three cases where either $IUF_0 = IUF_2$ or $IUF_0 > IUF_2$ it was found that the ***L2 mode*** resulted in a far greater reduction of effects ***(a)(1)*** and ***(b)*** to ***(g)*** than the ***L3 mode.*** This can be seen in the plots shown in Figure 4.28 of several network effects for the ***L1-mag*** case. Additionally, it can be seen that the difference between the results of the ***L2 mode*** and those at the balanced condition (both IUF_0 and IUF_2 eliminated) are relatively small. For voltage regulation shown in Figure 4.28 (c), the $VR_{indicator}$ for the ***L2 mode*** even goes below its value at balanced condition, negating the undesirable effect of the asymmetrical impedances of the four-core cable.

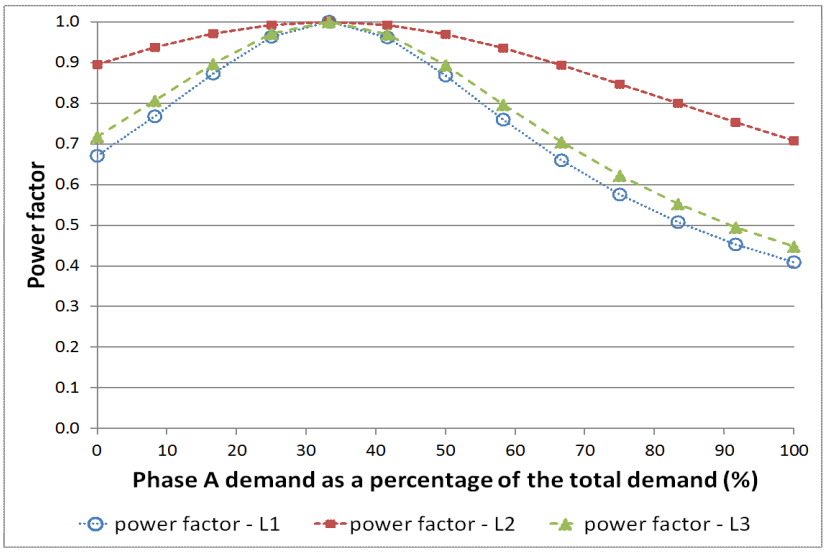

(a)

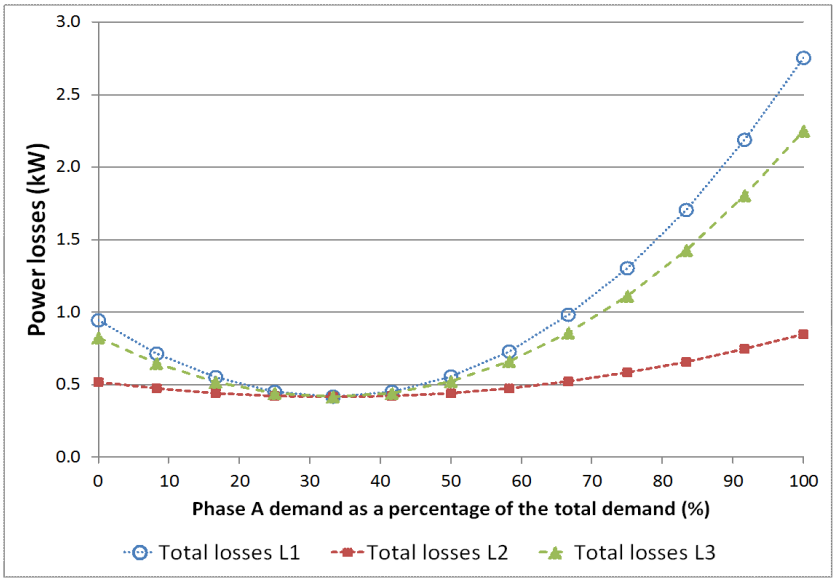

(b)

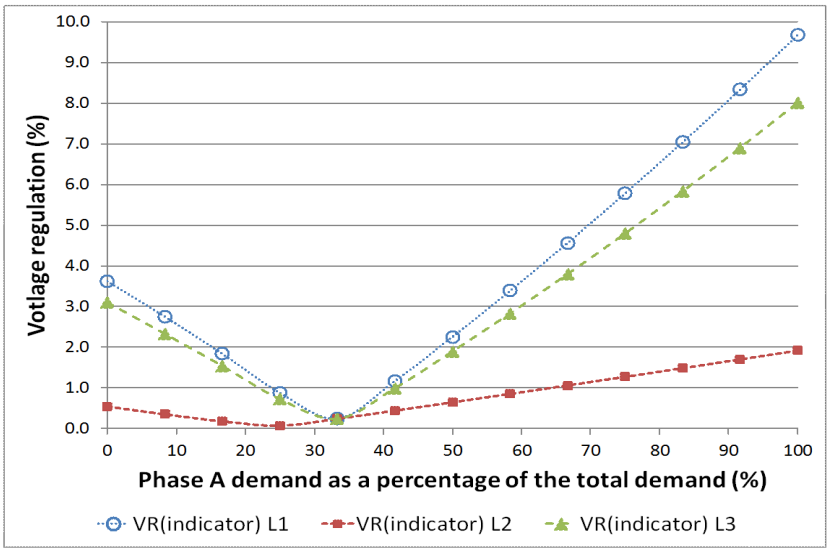

(c)

Figure 4.28: Plots of (a) effective power factor, (b) losses and (c) voltage regulation for the *L1-mag* case using sequence current compensator

In the ***L1-mag-ang*** case, in which $IUF_2 \gg IUF_0$ to the right of the balanced condition,IUF_0 was already very small and so further reduction would have made little difference to any of the effects. To the left of the balanced condition however, where $IUF_0 \gg IUF_2$, the ***L2 mode*** resulted in significant reductions. This can be seen by comparing the losses to the left of the balanced condition for the ***L1*** and ***L2 modes*** shown in Figure 4.29. Similar plots can be shown of the other effects.

It should be noted that the losses for the ***L2 mode*** (to the left) and ***L3 mode*** (to the right) both appear less than at the balanced condition. This is because with one sequence current reduced and the other eliminated, the losses incurred are due to the transfer of active power only, which for this case decreases equally on both sides of the balanced condition (as was shown in Figure 4.12). Hence, the losses will appear less than it is at the balanced condition.

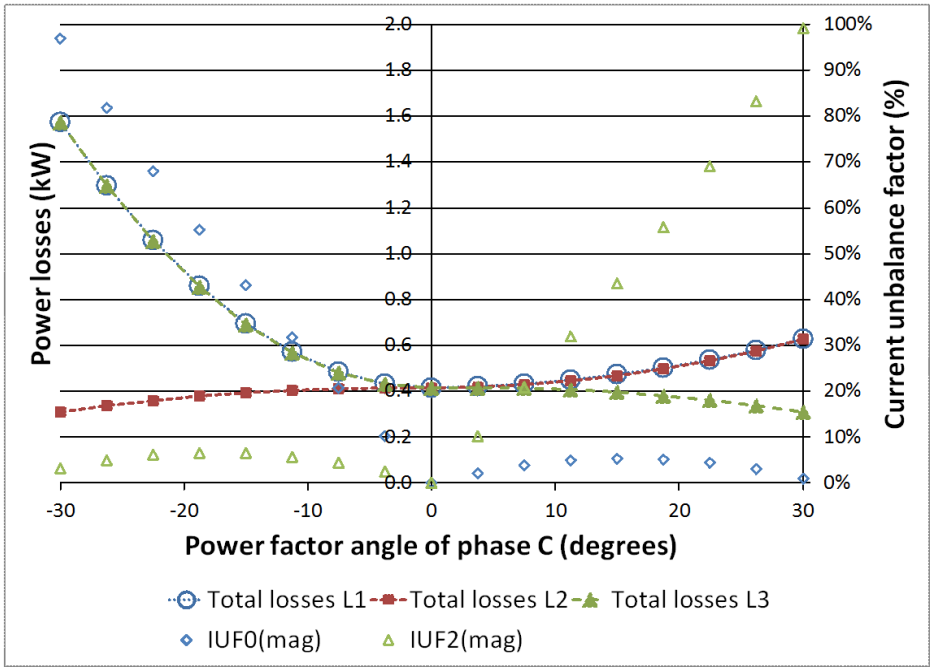

Figure 4.29: Plot of losses for the *L1-mag-ang* case using sequence current compensator

Lastly, it was found that the network utilisation as measured by – NU_PRCC - improved by the same amount for both ***L2*** and ***L3 modes***. The reason for this is that similar reductions in either IUF_0 or IUF_2 result in near equal reductions to phase current magnitudes. This is seen most clearly in the results of NU_PRCC for the ***L1-mag*** case shown in Figure 4.30.

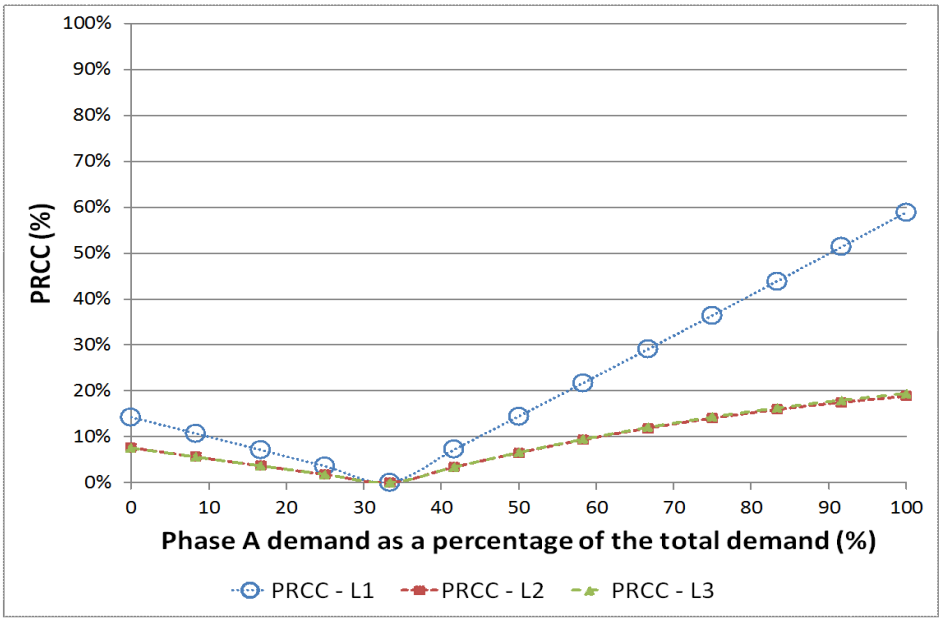

Figure 4.30: Plot of NU_PRCC for the *L1-mag* case using the sequence current compensator

Summary

- Reduction of IUF_0 brings much greater benefit to the low-voltage network than reduction of IUF_2.
- The additional benefit of reducing both IUF_0 and IUF_2 is small.

4.6 Chapter conclusions

It has been shown that IUF_0 contributes to a much greater extent than IUF_2 to most of the effects of current unbalance identified in Figure 2.13. The only exception is the potential released current capacity, which is dependent on the maximum phase current and not sequence currents. Both IUF_0 and IUF_2 influence the maximum phase current and contribute equally to a worsening of the potential released current capacity.

Further, VUF_2 by itself has been shown to not be a good enough indicator of unbalance on low-voltage networks. This is because VUF_2 shares very little correlation with IUF_0 and so does not reflect changes to most of the effects of current unbalance on the low-voltage network. Moreover, the results have shown that in all three cases analysed VUF_2 did not even exceed the recommended limit of 2 % (or 3 %) given in BS EN 50160.

The need for emphasis on VUF_0 has been established based on the significance of IUF_0 to effects on the low-voltage network. Therefore the use of both VUF_2 and VUF_0 is proposed. Of equal importance are IUF_2 and IUF_0.

The ***L1-ang*** and ***L1-ang-mag*** cases have demonstrated that the power factors of the single-phase loads relative to each other is a cause of current unbalance. This subtle but fundamental cause of unbalance is not widely recognised in the literature.

The mitigation of current unbalance was also investigated using a sequence current compensator. The results have shown that mitigation methods, such as the static balancer, which focus on reduction of zero sequence current only, can be justified over methods which focus on reduction of negative sequence current only. Additionally, the incremental benefit of reducing both sequence currents and achieving perfect current balance has been shown to be relatively small.

5. The static balancer – modelling, laboratory experiments and validation

5.1 Objectives

This chapter is part of ***Objective (c):***

To investigate the behaviour and quantify the benefits of the static balancer to low-voltage networks.

It focuses on the first two tasks of this objective, which are:

Task (c.1): *Develop a static balancer model for use in an unbalanced power flow method.*

Task (c.2): *Validate the static balancer model by experiments in the laboratory.*

5.2 Overview

The static balancer as described in Chapter 1 consists of an interconnected-star winding, typically wound on a three-limb, iron core. Its ability to mitigate current and voltage unbalance on low-voltage networks as explained in Chapter 2 is attributed to its low zero sequence impedance, which allows it to draw the neutral current and redistribute it onto the three phases. In this chapter the influence of the interconnected-star winding to its low zero sequence impedance will be explained.

A static balancer model will also be presented. This model will be used in the forward-backward sweep method developed in Chapter 3. It is based on the description of the

static balancer given in [8] which consists of three single-phase transformers; each represented by their short-circuit impedances (denoted by Z_T) and connected together in an interconnected-star. These leakage impedances are then calculated from the design sheets provided by the manufacturer of the static balancer, The Transformer and Electrical Company (TEC) [81].

The results from the model were then validated by carrying out voltage unbalance tests on a static balancer in the laboratory. The test bench and laboratory experiments devised are presented. A short-circuit test was also carried out to confirm the short-circuit impedances. The sensitivity of the results from the model to the short-circuit impedance will also investigated.

Firstly though, the requirements of the static balancer model in this forward-backward sweep method must be defined. In the next section, the structure of the generalised matrix equation needed to describe the static balancer as well as how it will be used in the forward-backward sweep method will be explained.

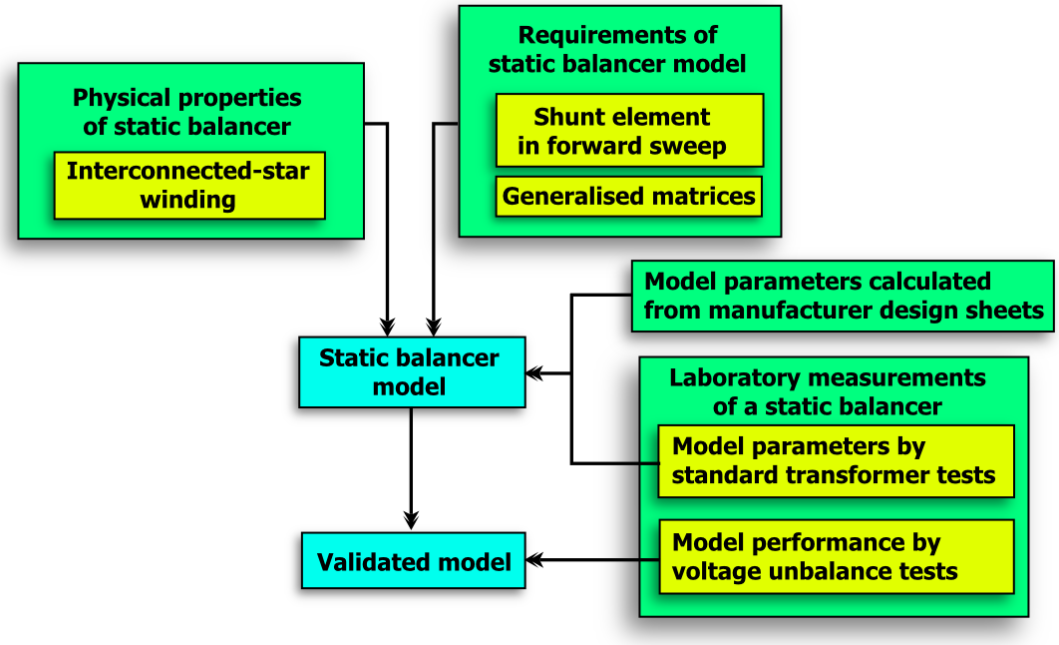

Figure 5.1: Overview of Chapter 5

5.3 Phase-frame model requirements

5.3.1 Series network elements

In the forward-backward sweep method, series elements are represented by generalised phase-frame matrix equations of the form:

$$\left[V_{p,g(j)}\right]^{(k)} = [A]\left[V_{pg(j-1)}\right]^{(k)} + [B]\left[I_{p(l)}\right]^{(k)} \quad (5.1)$$

$$\left[I_{p(l)}\right]^{(k)} = [C]\left[V_{pg(j)}\right]^{(k)} + [D]\left[I_{p(l+1)}\right]^{(k)} \quad (5.2)$$

where $p = a, b, c, n, g$

Equations like (5.1) are used in the backward sweep to find voltages at the receiving end of series elements and equations like (5.2) are used in the forward sweep to find the currents entering series elements. Equations (5.1) and (5.2), it should be noted, are similar to equations (3.30) and (3.28) used in Chapter 3 to represent a generic branch segment l. Generalised matrix equations like this can also be derived for distribution transformers of many standard winding configurations [51].

5.3.2 Shunt network elements

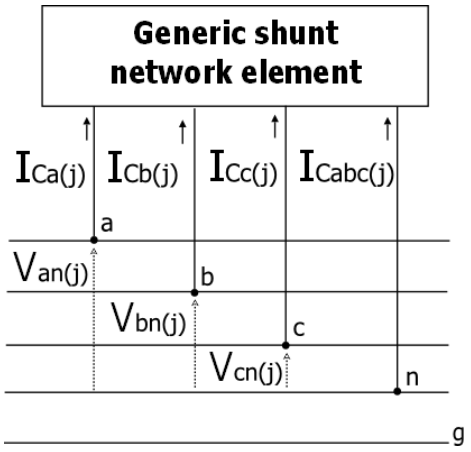

Figure 5.2: A generic shunt network element (like the static balancer)

Shunt network elements, such as loads and capacitor banks appear only in the forward sweep. The currents drawn by these shunt network elements, as shown in Figure 5.2 will depend on the phase-neutral voltages at their terminals. They are also represented by generalised matrix equations of the form:

$$\left[I_{Cp(j)}\right]^{(k)} = [E]\left[V_{pn(j)}\right]^{(k)} \quad (5.3)$$

where $p = a, b, c$ and

$$I_{Cabc(j)} = -\left(I_{Ca(j)} + I_{Cb(j)} + I_{Cc(j)}\right) \quad (5.4)$$

In the case of loads, the currents drawn will vary so long as its composition includes either constant power or constant impedance loads. Capacitor banks are similar to constant impedance loads in that the currents drawn will vary whilst its susceptances are constant.

The static balancer, though a transformer, is shunt connected (as it is auto-wound with no secondary terminals). Its model will therefore take the form of equation (5.3) and be used in the forward sweep. The current drawn by the static balancer will depend on its short-circuit impedance which, as will be explained in the next section on the interconnected-star winding, will dominate its relatively low zero sequence impedance.

5.4 Influence of interconnected-star winding

Consider three ideal single-phase transformers connected together in an interconnected-star as shown in Figure 5.3. To understand the influence on the zero sequence impedance, homopolar or zero sequence currents I_{Ca0}, I_{Cb0} and I_{Cc0} are injected at each terminal by three ideal zero sequence current sources. The neutral of the static balancer is connected to these ideal current sources as shown in Figure 5.3.

The induced zero sequence voltages between each phase (denoted by nodes u, v and w) and neutral (denoted by node n) are given by:

$$\begin{aligned} E_{un0} &= (E_{a0} - E_{b'0}) \\ E_{vn0} &= (E_{b0} - E_{c'0}) \\ E_{wn0} &= (E_{c0} - E_{a'0}) \end{aligned} \quad (5.5)$$

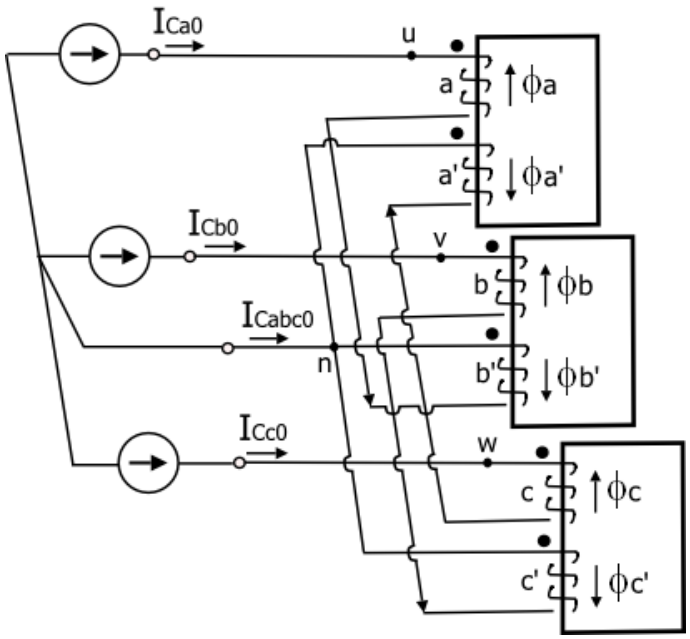

Figure 5.3: Three identical single-phase core type transformers connected in an interconnected-star and injected with homopolar currents

The three zero sequence currents flow through two coils (or half windings) located on separate cores. The zero sequence magnetomotive force from each half winding opposes that of the other half winding on the same core and so the net zero sequence magnetomotive force will be zero. The induced zero sequence voltage across each phase winding, consisting of two half windings, will also be zero:

$$E_{un0} = E_{vn0} = E_{wn0} = 0 \tag{5.6}$$

Therefore, in the case of these three ideal single-phase transformers, the zero sequence impedance will be zero. For three real single-phase transformers though, the zero sequence impedance of the interconnected-star winding will be small, given by the transformer impedances of two half windings in series.

5.5 The static balancer model

This section presents a static balancer model as a generalised matrix equation conforming to equation (5.3).

5.5.1 Description

The model, shown in Figure 5.4, is based on the description of the static balancer given in [8]. It consists of three single-phase transformer models wired in an interconnected-star. Each single-phase transformer model is represented by the short-circuit impedance Z_T, consisting of the winding resistance R_T and leakage reactance X_T.

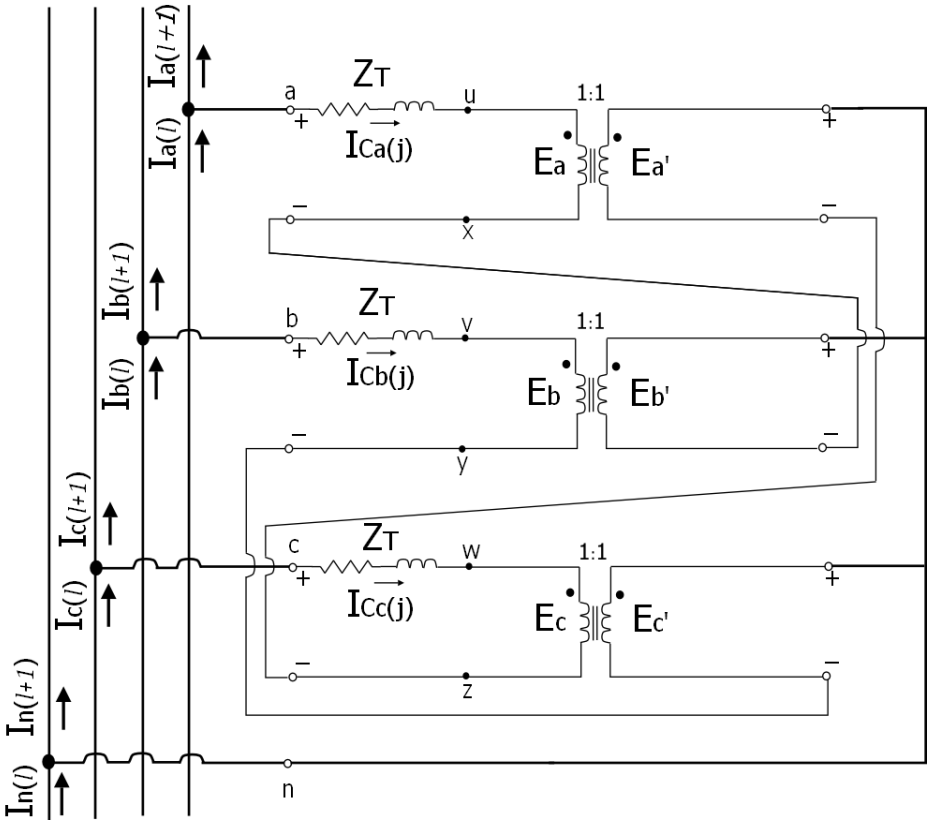

Figure 5.4: Static balancer model (short-circuit impedances only)

5.5.2 Basic assumptions

It assumes that:

- all three phase windings are identical;
- the magnetizing currents are small and can be ignored;

- the static balancer's iron losses are constant and can be accounted for separately using the design sheets provided by the manufacturer [81]; and
- all voltage and currents are perfectly sinusoidal and at 50 Hz.

It should be mentioned that an open-circuit test carried out on the static balancer confirmed that the magnetising currents were small, 0.5 A on phases A and B and 0.8 A on phase C. The slight difference on phase C was because this static balancer had a three-limb iron core, as was shown in Figure 1.4, with only the phase C winding having both its coils (c and a') wound on outer limbs.

5.5.3 Derivation of generalised matrix equation

Now, the phase-neutral voltages at terminals are:

$$\begin{bmatrix} V_{an(j)} \\ V_{bn(j)} \\ V_{cn(j)} \end{bmatrix} = \begin{bmatrix} E_{un} \\ E_{vn} \\ E_{wn} \end{bmatrix} + \begin{bmatrix} Z_T & 0 & 0 \\ 0 & Z_T & 0 \\ 0 & 0 & Z_T \end{bmatrix} \begin{bmatrix} I_{Ca(j)} \\ I_{Cb(j)} \\ I_{Cc(j)} \end{bmatrix} \quad (5.7)$$

where the voltages across the two half windings of each phase are $E_{un} = E_a - E_{b'}$, $E_{vn} = E_b - E_{c'}$ and $E_{wn} = E_c - E_{a'}$.

Because the interconnected-star results in a very low zero sequence impedance, it is assumed that regardless of the phase-neutral voltages at its terminals, the compensating currents drawn by the static balancer are completely homopolar:

$$I_{Ca(j)} = I_{Cb(j)} = I_{Cc(j)} \quad (5.8)$$

Summing the phase-neutral voltages of equation (5.7) and substituting equation (5.8) gives:

$$\left(V_{an(j)} + V_{bn(j)} + V_{cn(j)}\right) = (E_{un} + E_{vn} + E_{wn}) + 3Z_T I_{Ca(j)} \quad (5.9)$$

Applying equation (5.6) for the interconnected-star winding gives:

$$V_{an(j)} + V_{bn(j)} + V_{cn(j)} = 3Z_T I_{Ca(j)} \quad (5.10)$$

This can be expressed as a generalised matrix equation:

$$\begin{bmatrix} I_{Ca(j)} \\ I_{Cb(j)} \\ I_{Cc(j)} \end{bmatrix} = \frac{1}{3Z_T} \begin{bmatrix} 1 & 1 & 1 \\ 1 & 1 & 1 \\ 1 & 1 & 1 \end{bmatrix} \begin{bmatrix} V_{an(j)} \\ V_{bn(j)} \\ V_{cn(j)} \end{bmatrix} \quad (5.11)$$

Equation (5.11) shows that the compensating currents drawn by the static balancer are determined by its short-circuit impedance Z_T and by one-third the phasor sum of the phase-neutral voltages at its terminals (i.e. the zero sequence voltage at its terminals). Now, for a given set of unbalanced phase-neutral voltages at the static balancer's terminals, it should be appreciated that:

- the magnitude of the short-circuit impedance, $|Z_T|$ determines the magnitude of the compensating currents; and
- the angle of the short-circuit impedance θ_T, which equals $tan^{-1}(X_T/R_T)$, determines the phase angle of the compensating currents.

On an actual feeder, as explained in section 2.6.6, the phasor sum of these compensating currents and the unbalanced downstream currents will determine the currents upstream of the static balancer. In this way, both the magnitude and angle of short-circuit impedance Z_T can influence how well the static balancer compensates unbalance.

5.6 Calculation of short-circuit impedance from manufacturer design sheets

The short-circuit impedance was calculated from data provided in the manufacturer's design sheet [81]. This is summarised in Table 5.1.

Rated voltage and current	
Rated voltage, V_{rated}	240 V
Rated current, I_{rated}	30.346
Short-circuit impedance, $Z_{T(pu)}$	
Winding resistance, $R_{T(pu)}$	2.12 %
Leakage reactance, $X_{T(pu)}$	2.085 %
Total losses	
Winding losses, P_{Cu}	381 W
Iron losses, P_{Fe}	118.2 W

Table 5.1: Data provided in design sheet [81]

The winding resistance (in ohms) can be found from the winding losses per phase ($P_{Cu}/3$) and the rated current:

$$R_T = (P_{Cu}/3)/I_{rated}^2 \tag{5.12}$$

With this and the ratio of $X_{T(pu)}/R_{T(pu)}$ the leakage reactance (in ohms) can then be found:

$$X_T = R_T\left(X_{T(pu)}/R_{T(pu)}\right) \tag{5.13}$$

The calculated short-circuit impedance is given in Table 5.2.

Winding resistance, R_T	Leakage reactance, X_T	Short-circuit impedance	
		Magnitude, $\lvert Z_T \rvert$	Angle, θ_T
0.138 Ω	0.136 Ω	0.193 Ω	44.6°

Table 5.2: Calculated short-circuit impedance

In the next section, this value is compared to results from a short-circuit test on an actual static balancer in the laboratory.

5.7 Laboratory experiments to validate the static balancer model

5.7.1 The test bench

The general arrangement of the test bench is shown in Figure 5.5 and a photo in Figure 5.6. It consists of an arrangement of circuit breakers (MCBs), variacs and measurement devices. Different wiring arrangements were devised for the variacs to allow variation of either voltage magnitude or voltage angle at the static balancer terminals. The measurement devices included an Ametek power quality recorder (PQR) and a LabVIEW PC with a data acquisition card (DAQ) connected to voltage and current probes. Much of the results were taken from the Ametek PQR. The LabVIEW program was developed as part of an MEng project by Oliver-Taylor [82]. It provided the ability to view and store current and voltage waveforms.

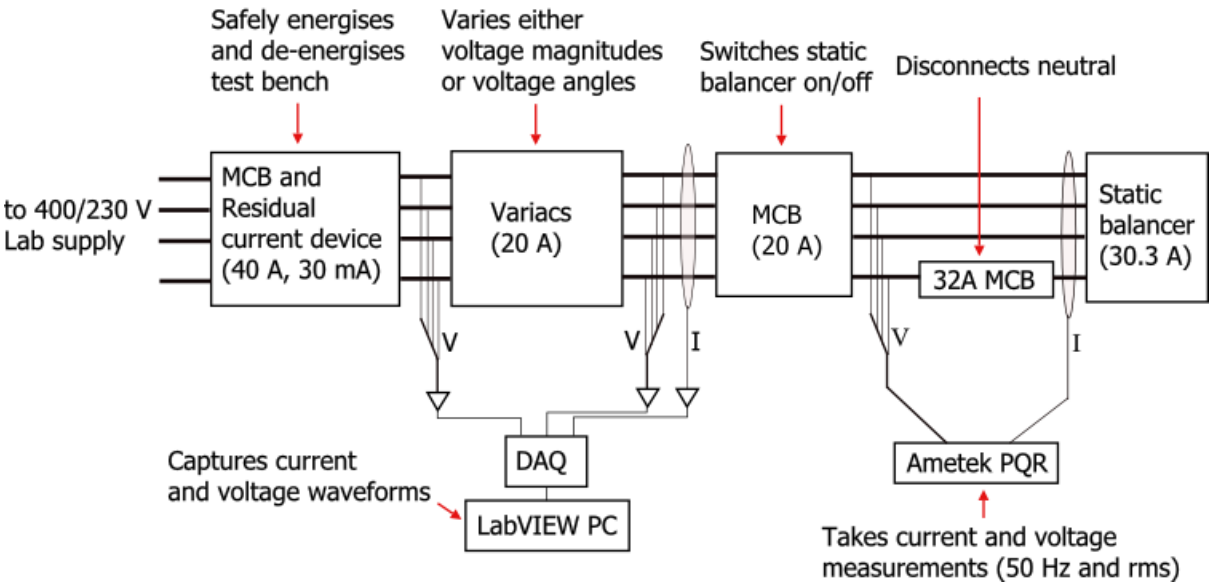

Figure 5.5: General arrangement of test bench

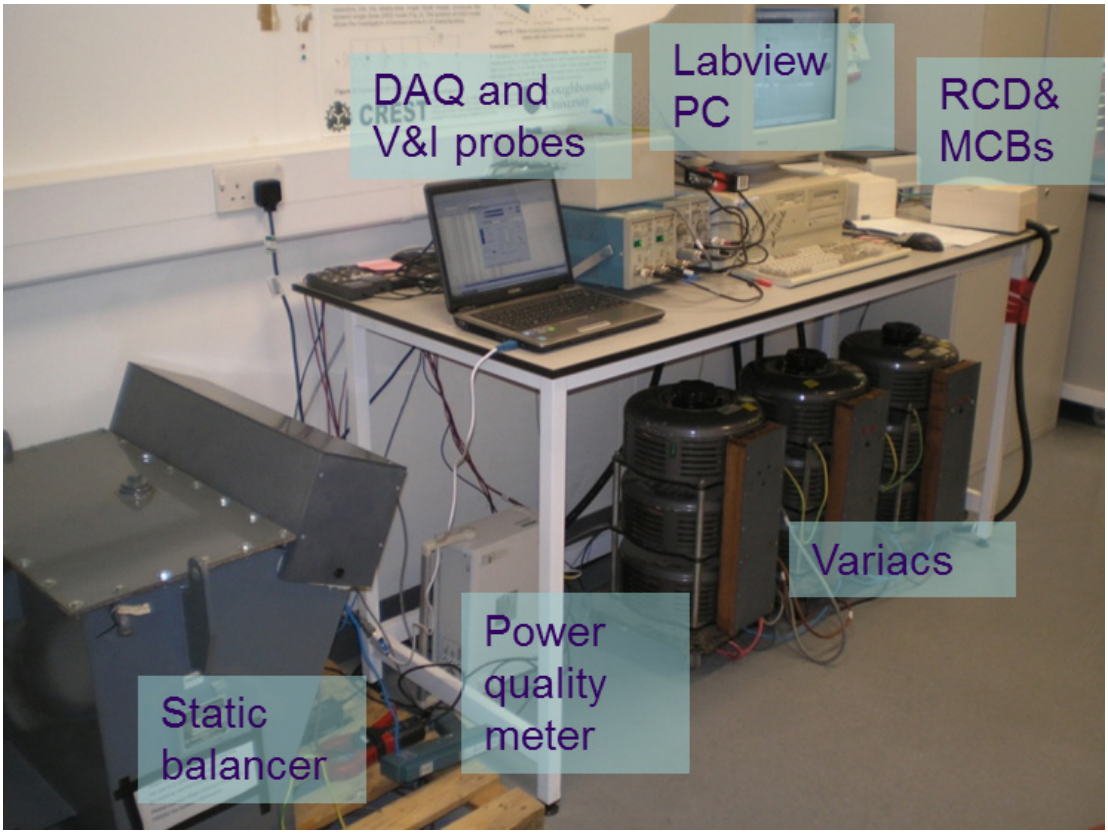

Figure 5.6: Photo of test bench

5.7.2 Short-circuit test

This test determines the short-circuit impedance (Z_T) of the static balancer. It is carried out with the static balancer's phase terminals shorted, as shown in Figure 5.7. Ideally, the voltage across the shorted phase terminals and the neutral terminal would be gradually increased until rated phase current is drawn, which for this static balancer was 30.346 A. This however was not possible, because the variacs available were rated only to 20 A. Instead, several readings were taken just below 20 A; one of them is shown in Figure 5.8.

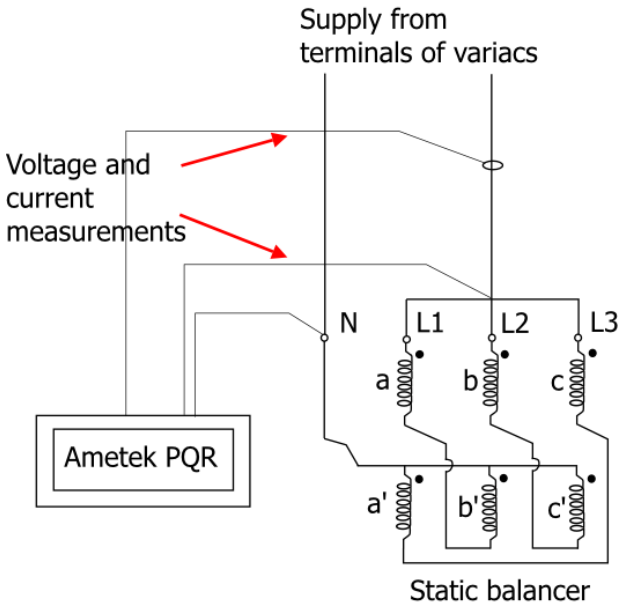

Figure 5.7: Short-circuit test

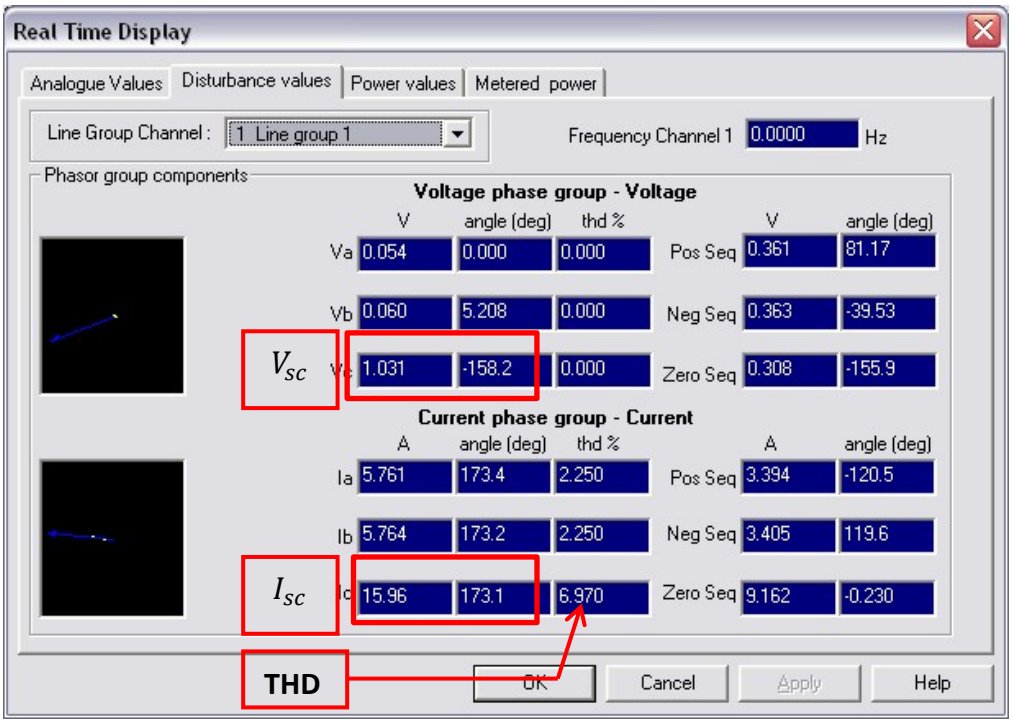

Figure 5.8: Screenshot from Ametek PQR Real Time Display

The equivalent circuit of the static balancer under short-circuit test conditions is shown in Figure 5.9. The short-circuit impedance Z_T is given by:

$$Z_T = V_{sc}/(I_{sc}/3) \tag{5.14}$$

The short-circuit impedance found is given in Table 5.3. The magnitude of Z_T is close to that calculated from the design sheet (Table 5.2) but the winding resistance R_T and leakage reactance X_T are different. The angle of the short-circuit impedance θ_T is therefore different as well.

Winding resistance, R_T	Leakage reactance, X_T	Short-circuit impedance	
		Magnitude, $\|Z_T\|$	Angle, θ_T
0.170 Ω	0.093 Ω	0.194 Ω	28.7°

Table 5.3: Measured short-circuit impedance

It should be pointed out that other readings were taken for slightly higher short circuit currents but they had higher total harmonic distortion (THD) levels (greater than 20 %), as the laboratory supply voltage was slightly less than ideal. They gave short-circuit impedances in the range of 0.23 to 0.28 Ω.

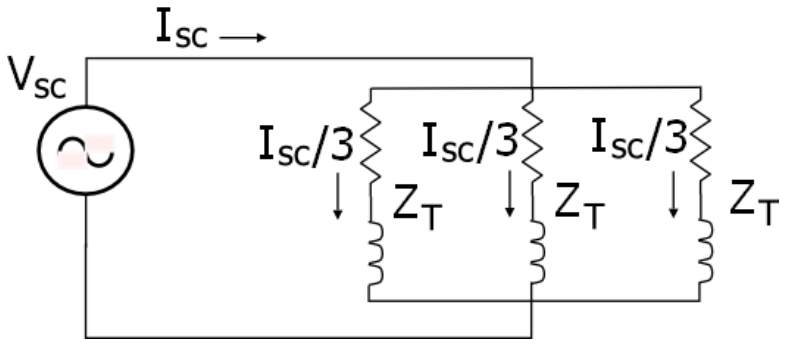

Figure 5.9: Equivalent circuit of static balancer under short-circuit test conditions

5.7.3 Validation of static balancer model by voltage magnitude unbalance experiments

The voltage magnitude unbalance experiment involved varying the phase-neutral voltage magnitude of phase C from 224 V to 238 V whilst keeping the other two phases at 230 V. This was done using three 20 A variacs, as shown in Figure 5.10.

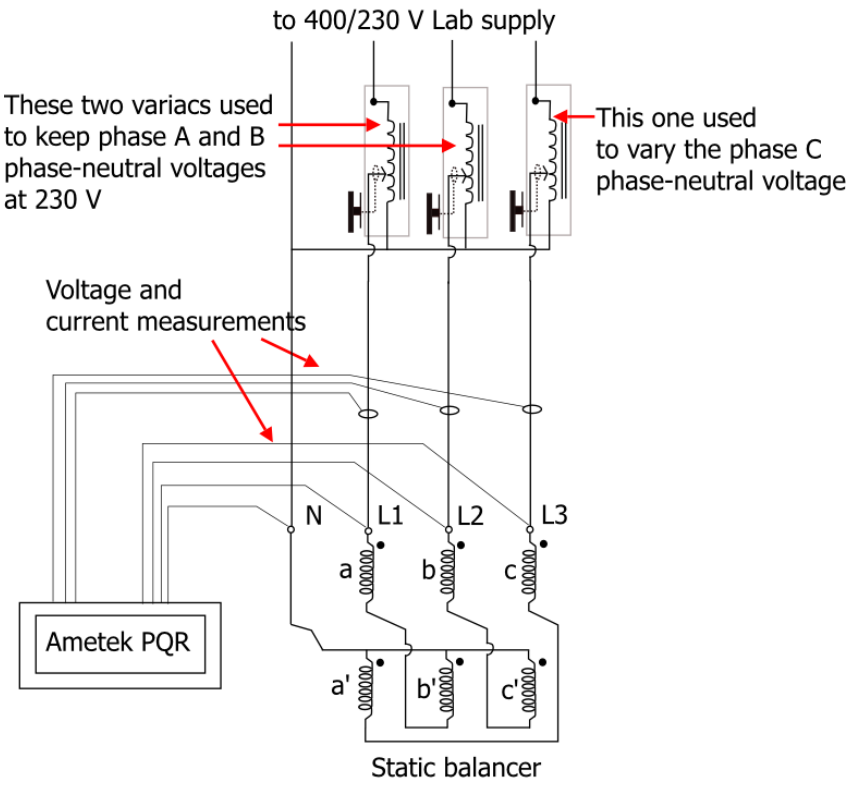

Figure 5.10: Arrangement of variacs used in voltage magnitude unbalance experiments

The phase and neutral currents drawn were measured using the Ametek PQR. Figure 5.11 and Figure 5.12 compare the measured phase and neutral currents against those calculated with the generalised matrix equation (5.11) using the measured short-circuit impedance. It is evident that there is very close agreement. Results found using the short-circuit impedance calculated from the design sheets were a similar match.

The average difference between measured and calculated values for phase and neutral currents were 0.7 A and 1.7 A, respectively. These differences are relatively small and in fact very reasonable, considering that the phase-neutral voltage angles available in the laboratory were not controlled and so would have varied slightly (creating some voltage angle unbalance that would have influenced the currents drawn).

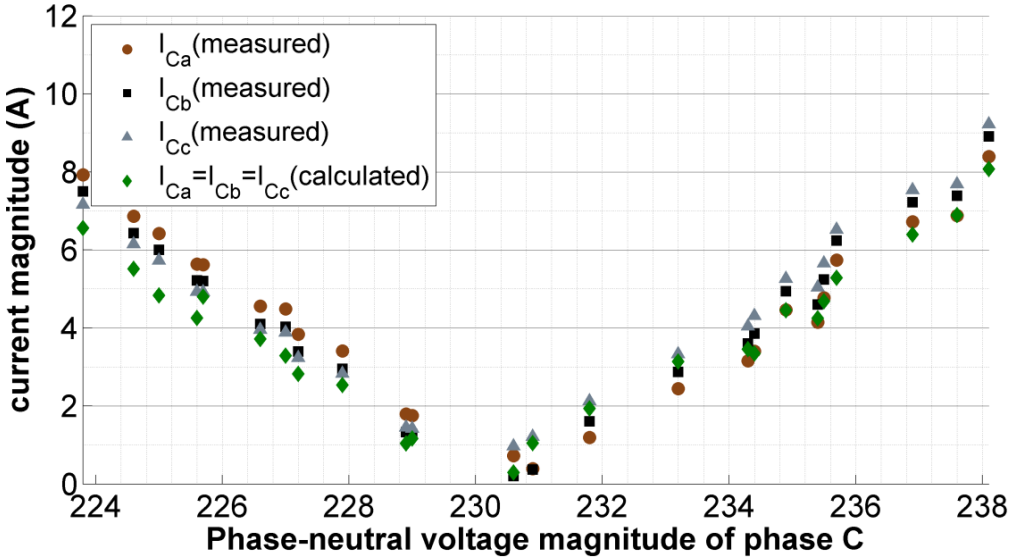

Figure 5.11: Comparison of measured and calculated phase current magnitudes as the voltage magnitude of phase C was varied from 224 V to 238 V (found using the measured short-circuit impedance)

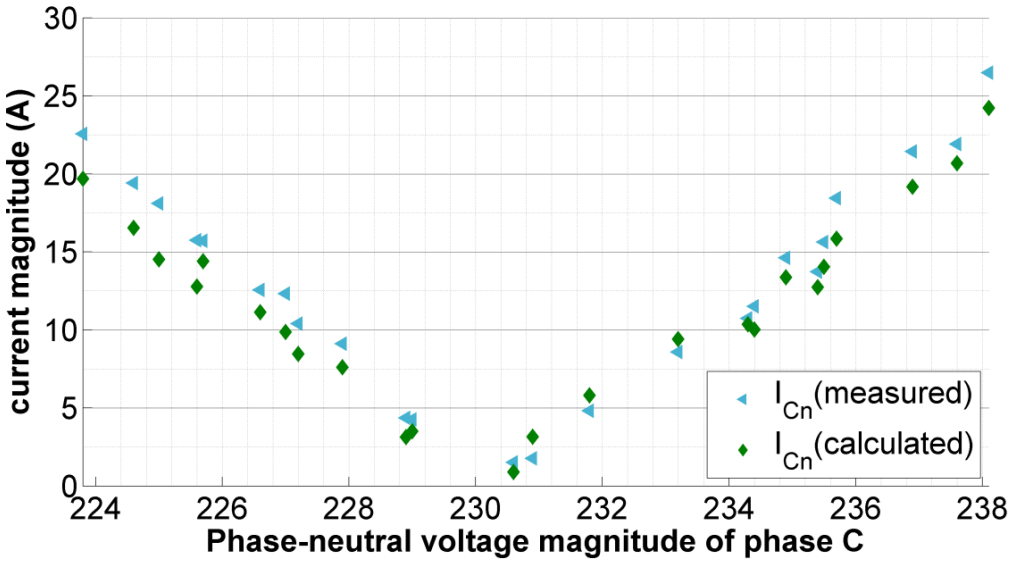

Figure 5.12: Comparison of measured and calculated neutral current magnitudes as the voltage magnitude of phase C was varied from 224 V to 238 V (found using the measured short-circuit impedance)

Continuing, both measured and calculated results show that with balanced voltages at the terminals of the static balancer, the phase and neutral currents drawn are at a minimum. And as the phase-neutral voltages become more unbalanced both phase and neutral currents then increase.

Also, the neutral currents are approximately three times that of the phase currents. This indicates that they are mostly homopolar. This can be seen clearly in the measured current phasors shown in Figure 5.13 for (a) $V_c = 224\ V$ and (b) $V_c = 238\ V$.

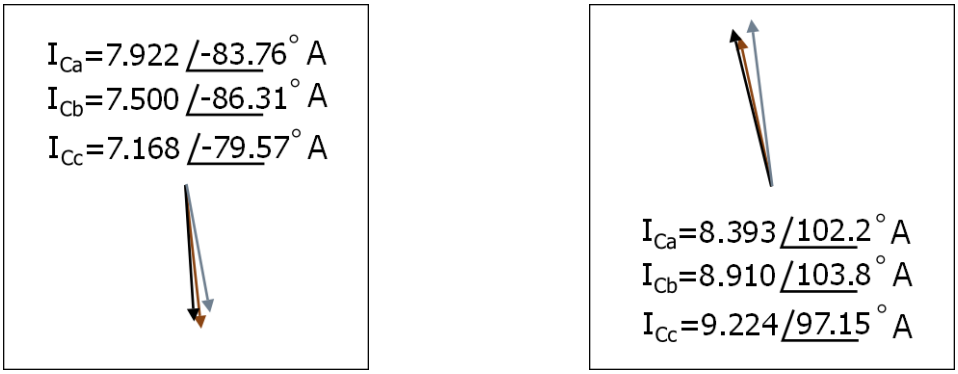

Figure 5.13: Measured current phasors for (a) $V_c = 224\ V$ and (b) $V_c = 238\ V$

The calculated and measured angles of the phase and neutral currents are shown in Figure 5.14 and Figure 5.15, respectively. The calculated angles were found using the measured short-circuit impedance. The difference between calculated and measured angles, which can be observed as the voltages become more balanced, will not have much influence considering that the current magnitudes are at that point approaching minimum (nearly zero). The current angles at the extremities however (i.e. when the voltage unbalance is more severe) are very important as the current magnitudes are much larger. At these extremities, the calculated and measured current angles are in very close agreement.

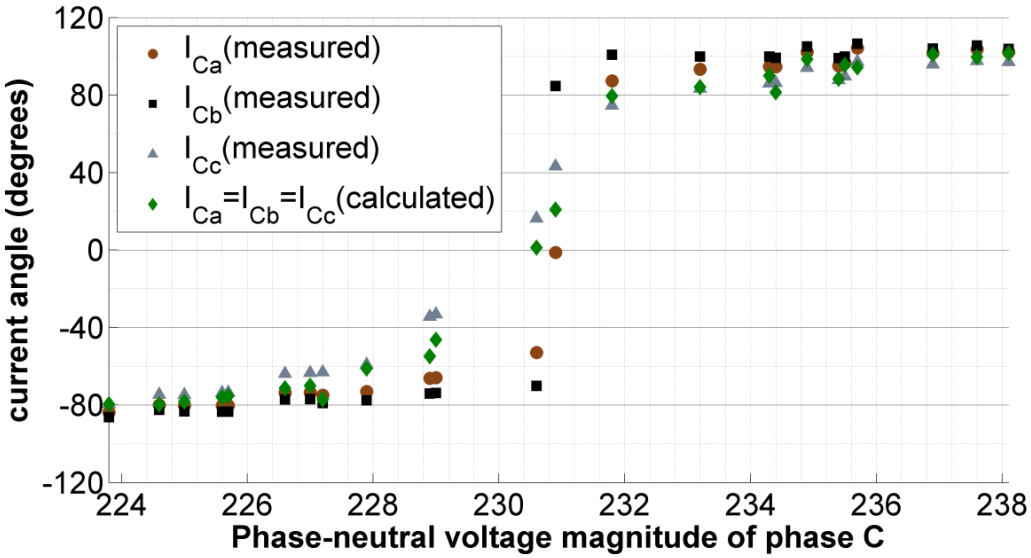

Figure 5.14: Comparison of measured and calculated phase current angles as the voltage magnitude of phase C was varied from 224 V to 238 V (found using the measured short-circuit impedance)

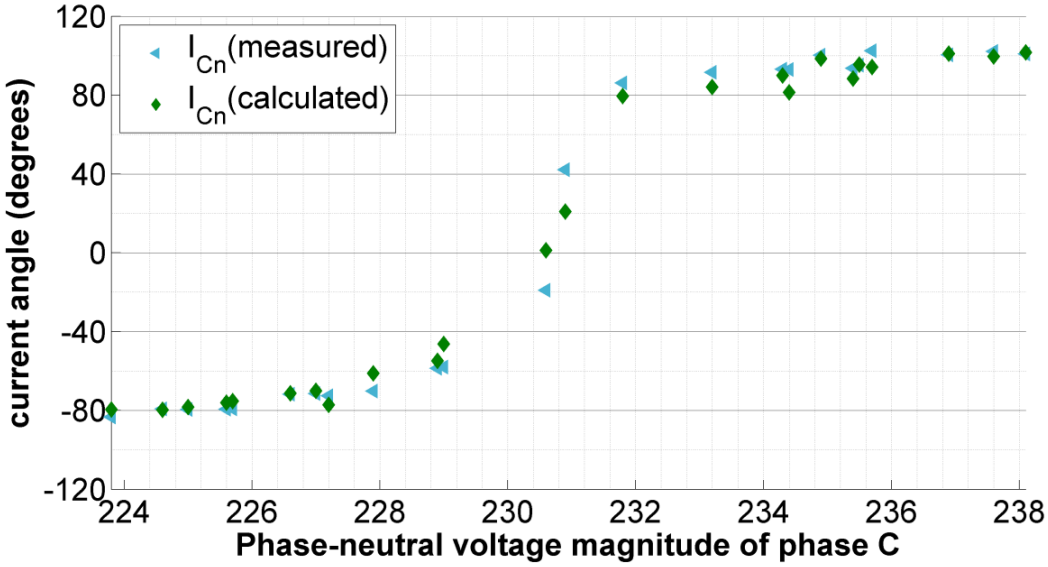

Figure 5.15: Comparison of measured and calculated neutral current angles as the voltage magnitude of phase C was varied from 224 V to 238 V (found using the measured short-circuit impedance)

Now, it was observed that the phase and neutral current angles found using the short-circuit impedance calculated from the design sheets were less of a match compared to those found using the measured short-circuit impedance. They are shown in Figure 5.16 and Figure 5.17. There is a difference of almost 20° between the calculated and measured current angles at the extremities. This may be attributed to the differences in the angles of short-circuit impedances observed in Table 5.2 and Table 5.3. An investigation into the sensitivity of the results to both the magnitude and angle of the short-circuit impedance follows in section 5.8.

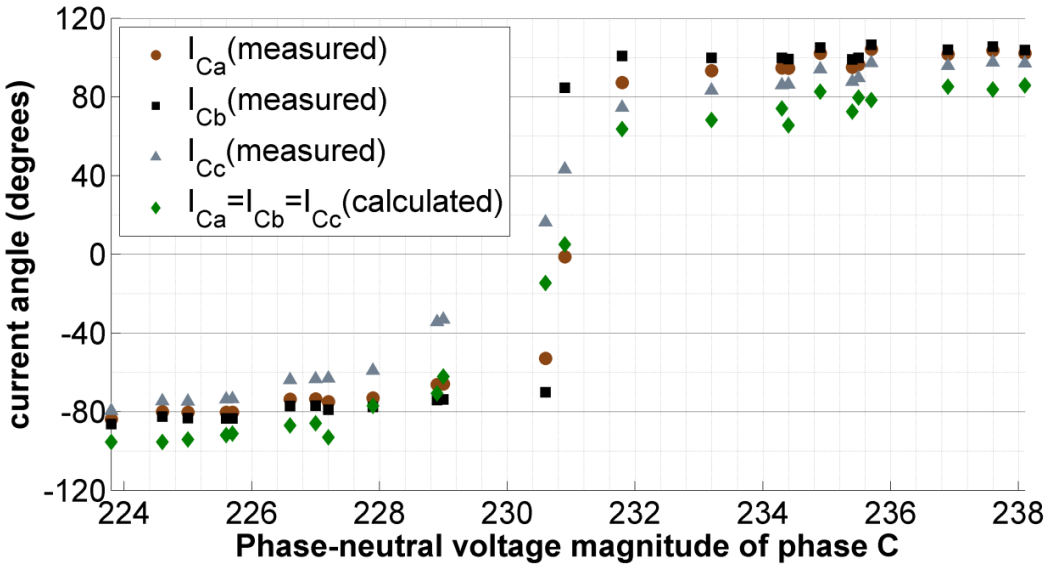

Figure 5.16: Comparison of measured and calculated phase current angles as the voltage magnitude of phase C was varied from 224 V to 238 V (found using the short-circuit impedance calculated from the design sheet)

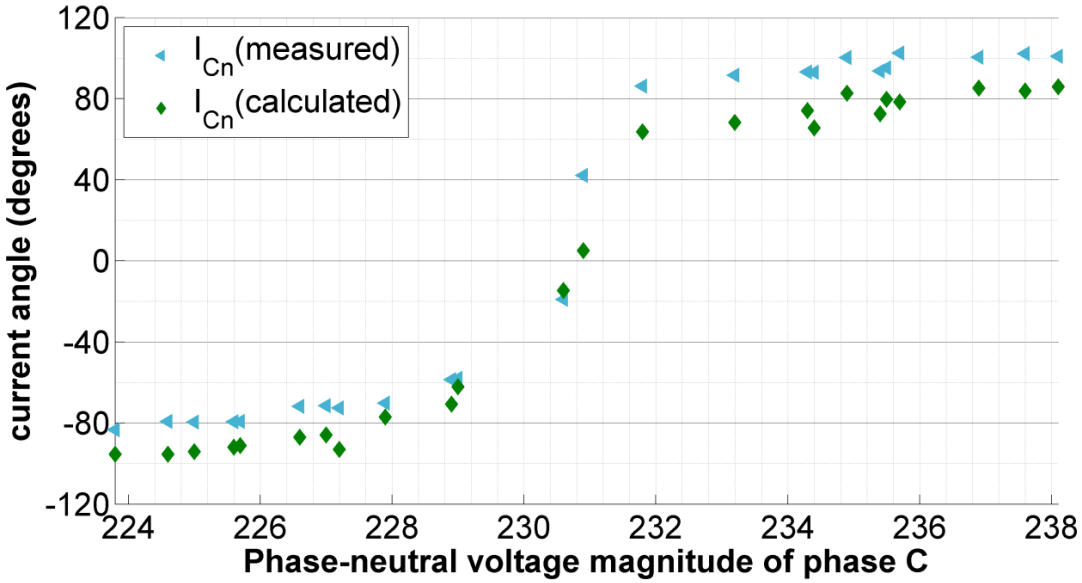

Figure 5.17: Comparison of measured and calculated neutral current angles as the voltage magnitude of phase C was varied from 224 V to 238 V (found using the short-circuit impedance calculated from the design sheet)

Finally, it should be mentioned that further voltage magnitude unbalance experiments were also carried out. They involved:

- increasing the voltage magnitudes of phase B and C together from 221 V to 237 V whilst keeping the voltage magnitude of phase A at 230 V.
- increasing the voltage magnitude of phase B from 230 V to 235 V and decreasing that of phase C from 230 V to 225 V simultaneously whilst keeping the voltage magnitude of phase A at 230 V.

Though not presented, these experiments also showed close agreement between the calculated and measured current magnitudes and angles.

5.8 Sensitivity of results to the short-circuit impedance

It is clear from the generalised matrix equation (5.11) that the short-circuit impedance determines the current drawn by the static balancer. The sensitivity of the results of the model to the magnitude $|Z_T|$ and angle θ_T of the short-circuit impedance can be seen in Figure 5.18 and Figure 5.19, respectively.

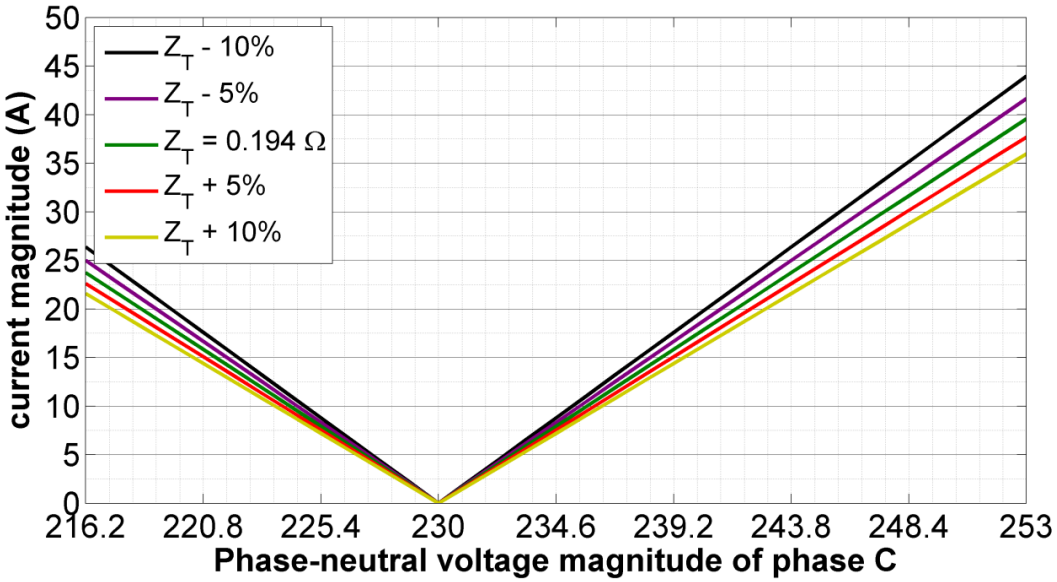

Figure 5.18: Sensitivity of calculated phase current magnitude to the magnitude of the short-circuit impedance

In Figure 5.18, the magnitudes of the phase current drawn by the static balancer were found for the voltage magnitude unbalance experiment described in section 5.7.2 with the model using a range of $|Z_T|$ values and θ_T equal to the measured value of 28.7° (Table 5.3). The current angles do not vary with $|Z_T|$ and are therefore not shown. The plots, which cover the statutory range of variation of the phase C voltage magnitude (230 V -6%/+10%), show that a 10 % change in $|Z_T|$ can result in, at most, a ± 4 A difference in the calculated phase current magnitude.

Similarly Figure 5.19 shows the calculated phase current angles with the model for θ_T ranging from 25° to 65° and $|Z_T|$ equal to the measured value of 0.194 Ω (Table 5.3). The current magnitudes do not vary with θ_T and are therefore not shown. It can be seen that the difference between the curves with $\theta_T = 25°$ (similar to the measured angle of Table 5.3) and $\theta_T = 45°$ (similar to the angle calculated from the design sheet as given in Table 5.2), results in a 20° change in the calculated phase current angle. It is therefore important to accurately determine the angle of the short-circuit impedance.

These sensitivities should be kept in mind in the analyses of Chapters 6 and 7, where the static balancer installed on the rural feeder could not be tested prior to its installation and so the short-circuit impedance calculated from the design sheets was assumed.

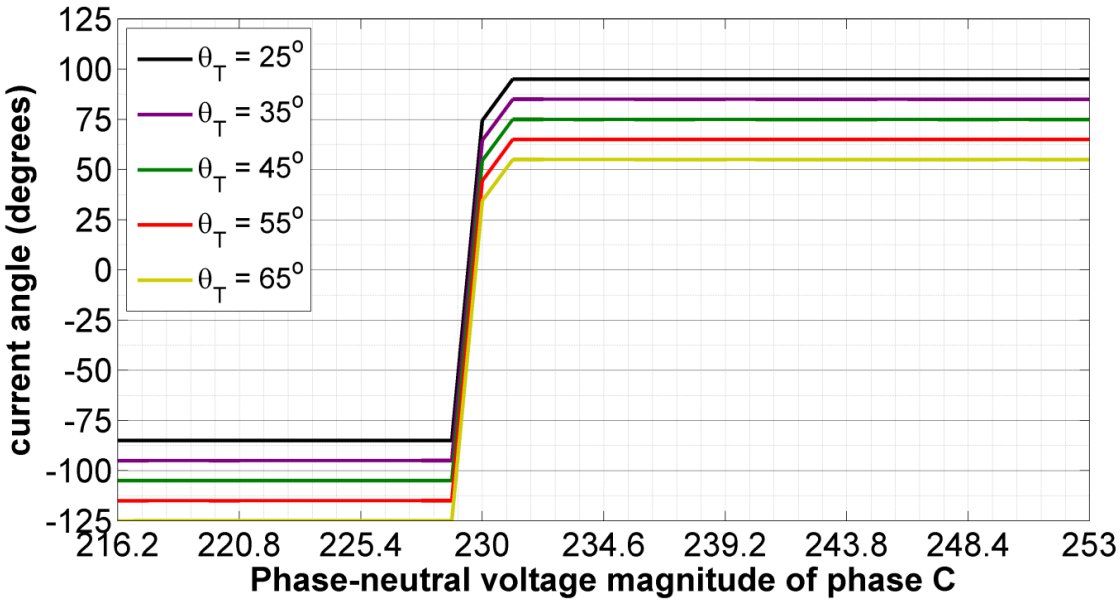

Figure 5.19: Sensitivity of calculated phase current angle to the angle of the short-circuit impedance

5.9 Chapter conclusions

The interconnected-star winding accounts for the low zero sequence impedance of the static balancer. With this physical property as its basis, a static balancer model has been derived from a circuit consisting of three equivalent transformer circuits. The results of this model have been validated by laboratory measurements on an actual static balancer.

This model is suitable for use in the forward-backward sweep method. It will be used in the network simulations of an actual rural low-voltage feeder later on in this thesis.

6. Field trial of the static balancer on a rural LV feeder

6.1 Objectives

This chapter covers the field elements of ***Objective (b)*** and ***Objective (c)***:

Objective (b): *To investigate the causes and quantify the effects of current unbalance on low-voltage networks.*

Objective (c): *To investigate the behaviour and quantify the benefits of the static balancer to low-voltage networks.*

It fulfils the following tasks:

Objective (b)

Task (b.2): *Demonstrate from field measurements the relationships between the effects of unbalance and the unbalance factors.*

Objective (c)

Task (c.3): *Validate the static balancer model by measurements taken on an actual low-voltage feeder.*

Task (c.4): *Investigate the behaviour of the static balancer on an actual low-voltage feeder.*

Task (c.5): *Quantify the benefits to an actual low-voltage feeder of using the static balancer.*

6.2 Overview

The theoretical basis for compensating zero sequence currents was established in Chapter 4 using the concept of a sequence current compensator. It was shown that doing so brought considerable benefits to a representative low-voltage network by way of reducing many of the effects of unbalance identified in Figure 2.13. In Chapter 5, it was explained that the interconnected-star winding of the static balancer resulted in it having a very low zero sequence impedance. And that this, as seen from voltage unbalance experiments in the laboratory, results in the static balancer drawing mostly homopolar currents; thus behaving in a manner similar to the zero sequence current compensator of Chapter 4. The difference being that with the static balancer the current drawn depends on the voltages at its terminals and its impedance.

This chapter aims to provide tangible evidence of the benefits of compensating zero sequence currents using a static balancer. These benefits, which correspond to reductions in the effects identified in Figure 2.13, are quantified after an analysis of field measurements taken on an actual rural low-voltage feeder before and after a static balancer was put into service. This field trial was carried out on the Western Power Distribution (WPD) low-voltage network with their assistance. The low-voltage feeder studied had been selected by them after initial measurements, shown in Figure 6.1, suggested that it was potentially unbalanced. Even though these initial measurements were done for less than a full week, they showed that VUF_2 was greater than 2 % for more than 504 minutes i.e. 5 % of the week. The VUF_2 , as mentioned in Chapter 2, is the only sequence unbalance factor for which there is a recommended limit in the BS EN 50160 [83]. Also shown in Figure 6.1 is the VUF_0, which as stressed in Chapter 4, is of greater importance to the low-voltage network. The change in the indicators of unbalance (which includes not just these sequence voltage unbalance factors but also sequence current unbalance factors) will also be examined from these field measurements. Also, in Figure 6.1 it is clear that both sequence unbalance factors differ. This was also observed by [6] in field measurements taken on feeders in Germany. The reason for the differences in both sequence unbalance factors will be investigated using these field measurements.

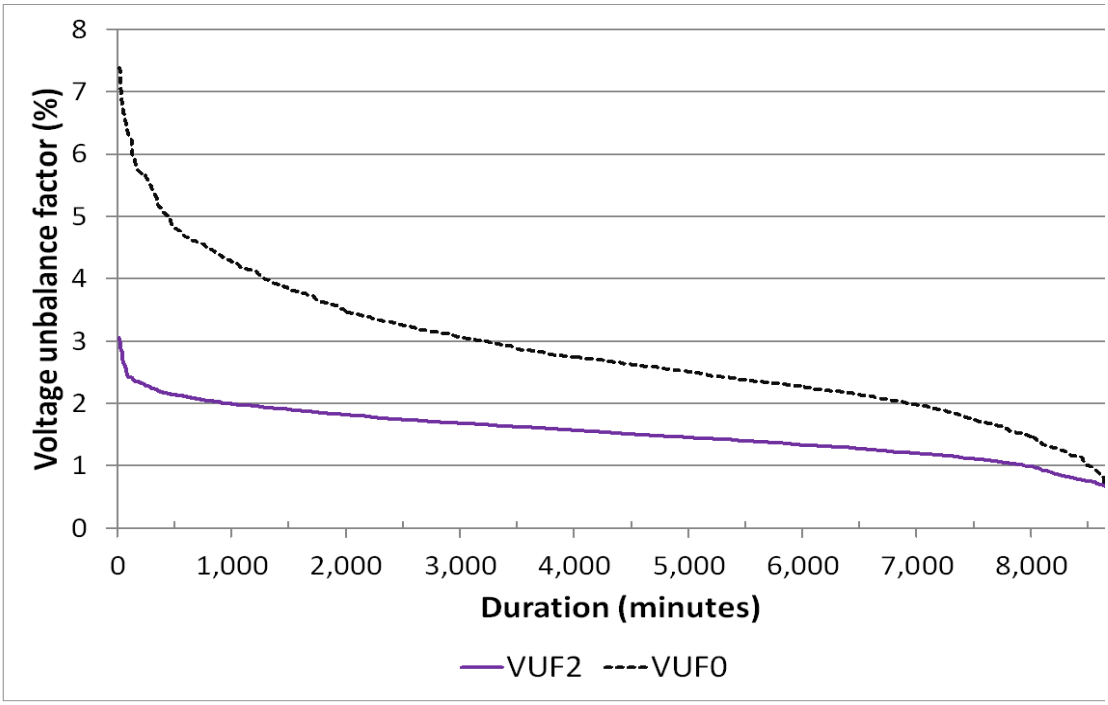

Figure 6.1: Voltage unbalance factors taken at the end of the rural low-voltage feeder (preliminary measurements)

Also, the field measurements presented in this chapter will be compared to network simulations of the rural low-voltage feeder later on in Chapter 7. There, a comparison of voltages, currents and quantified benefits will be used to validate the forward-backward sweep method developed in Chapter 3 as well as the static balancer model developed in Chapter 5.

An overview of this chapter is depicted in Figure 6.2. The rural low-voltage feeder is first introduced. Following that is a discussion of the considerations that went into the choice of locating the different power quality meters on the rural low-voltage feeder. This took into account the capabilities of the power quality meters and field conditions at the different positions on the rural low-voltage feeder. Additional practical challenges encountered are also discussed before presenting a timeline of all the datasets obtained from the meters. Several important aspects related to the processing of the field measurements are also covered.

The analysis sections then follow.

Firstly, the influence of the static balancer on the feeder is studied by looking at the currents upstream and downstream of it. This confirms and then builds on the existing knowledge of its behaviour. After that, the measured upstream currents are also used to validate the static balancer model.

Next, the sequence unbalance factors are examined in relation to one another and to magnitude and angle unbalance. This is a verification of the theoretical discussions presented earlier in Chapter 4 using instead field measurements.

The final section, investigates the benefits of using the static balancer on this rural low-voltage feeder. It quantifies all the effects of unbalance as identified in Figure 2.13, before and after the static balancer was energised.

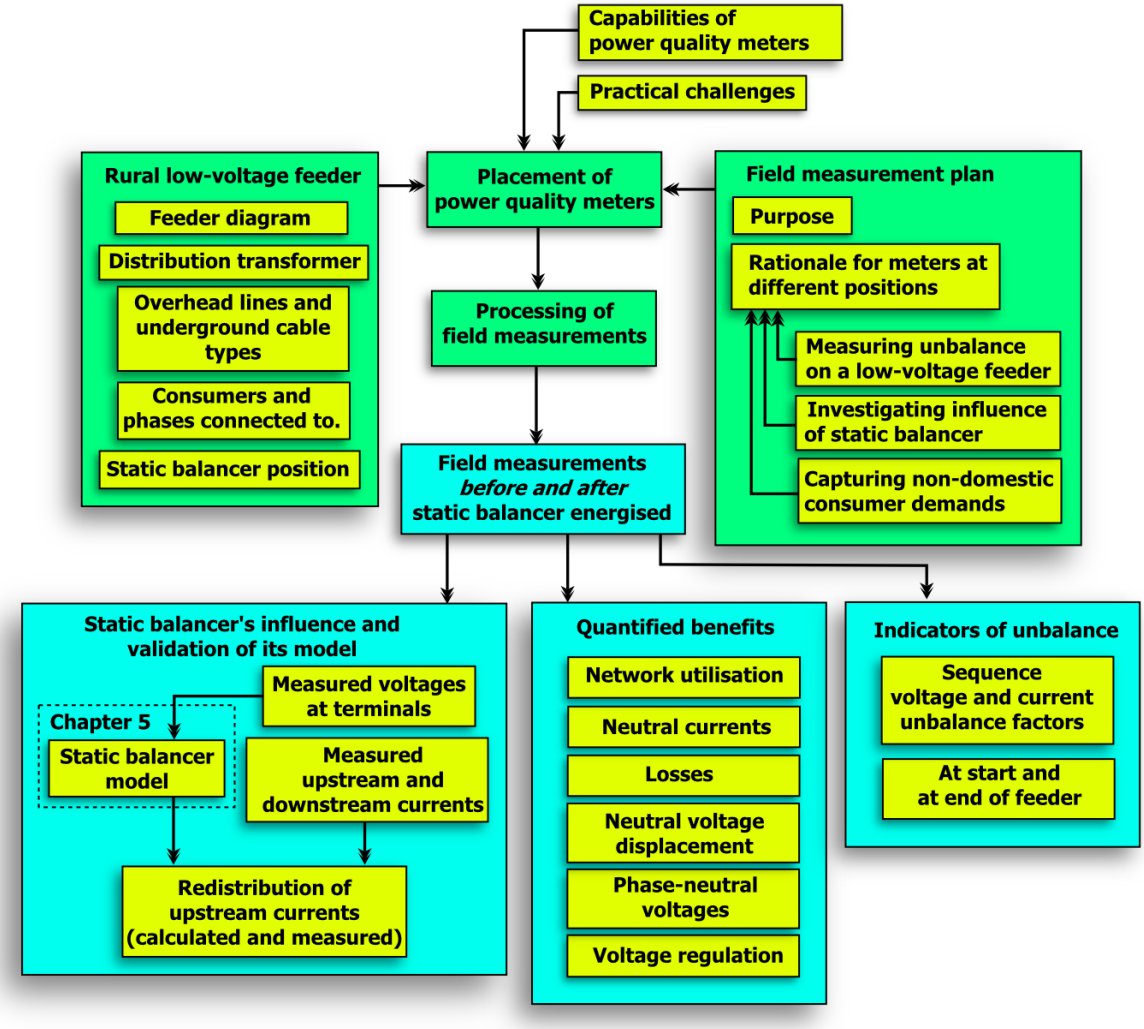

Figure 6.2: Overview of Chapter 6

6.3 The rural low-voltage feeder

6.3.1 Description

The rural low-voltage feeder studied is shown geographically in Figure 6.3 and as a single-line diagram in Figure 6.4. It is one of three low-voltage feeders from the 315 kVA, 11 kV/415 V pole-mounted distribution transformer that supplies the village. Included among the other two rural low-voltage feeders (not studied) is a dedicated underground cable which supplies a restaurant/bar, located opposite the post office shown in Figure 6.3. The third rural low-voltage feeder is mostly overhead line and it supplies a school and domestic consumers on the other side of the village.

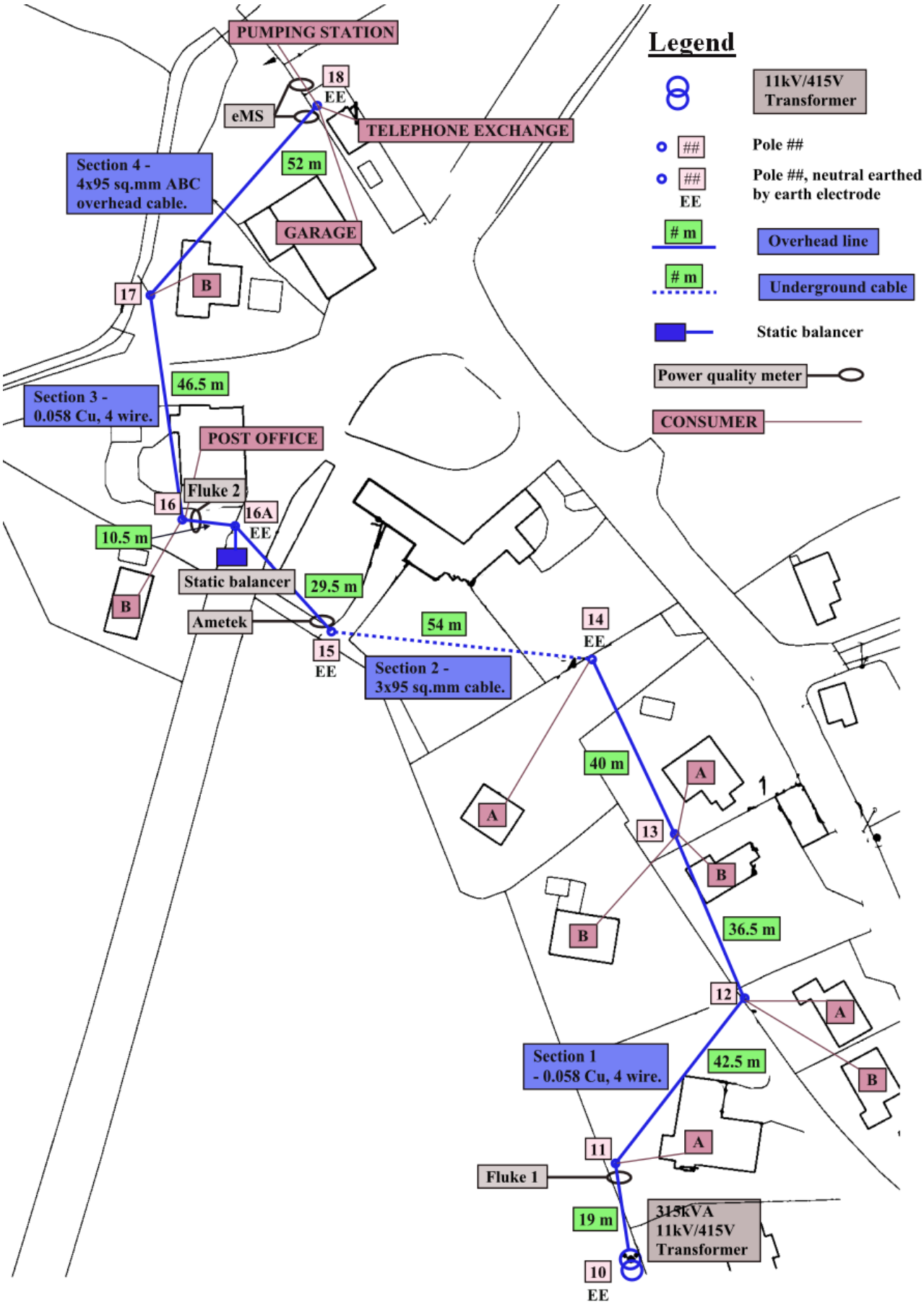

Figure 6.3: Geographic depiction of the rural low-voltage feeder

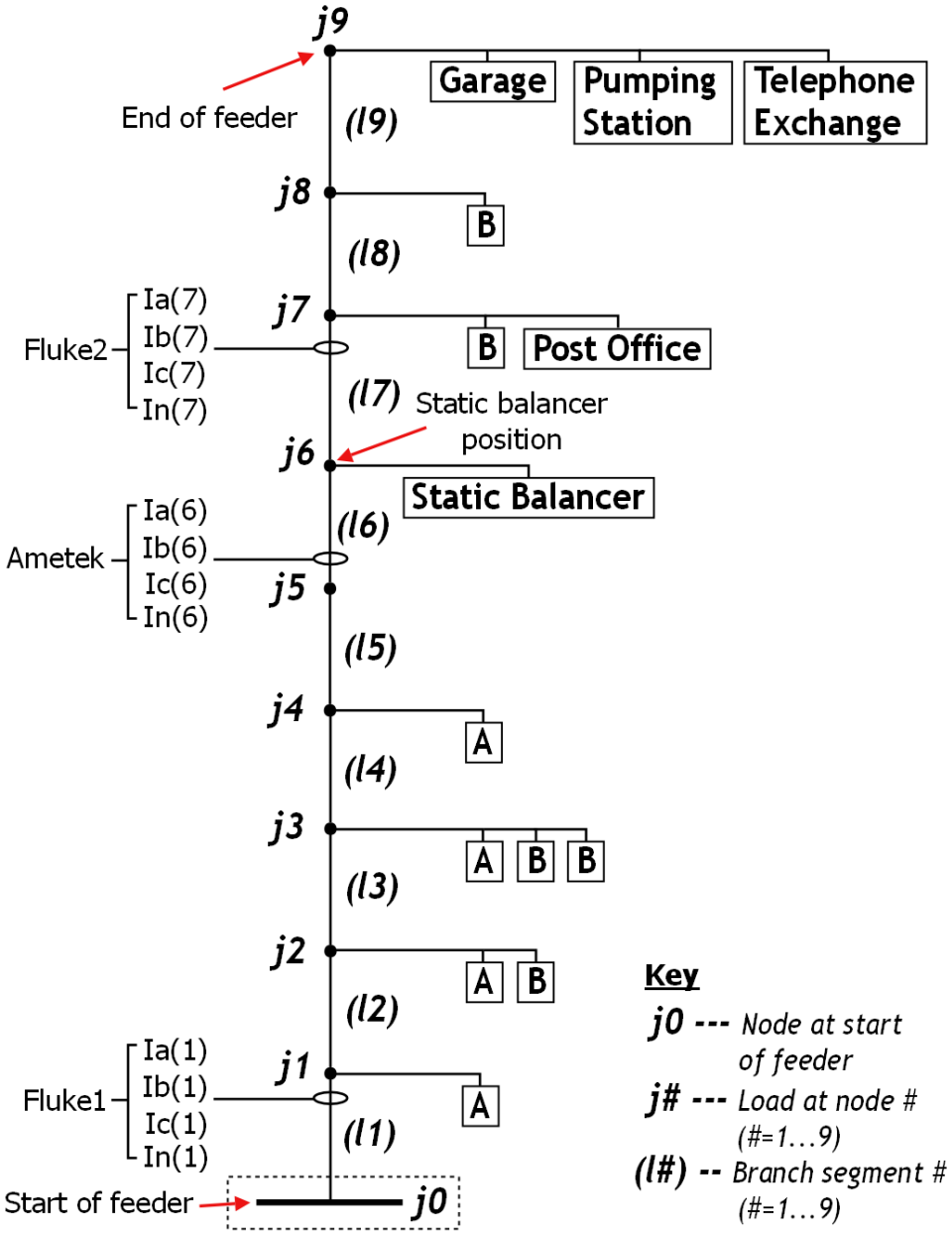

Figure 6.4: Single-line diagram (SLD) of the rural low-voltage feeder

6.3.2 The rural low-voltage feeder was a suitable choice for an initial field trial

In addition to preliminary measurements suggesting that it was unbalanced, the rural low-voltage feeder is suitable for a study on the mitigation of unbalance using the static balancer for several other reasons.

Firstly, it consists of mostly overhead line sections. Compared to an underground cable network, more options are therefore available for the install of power quality meters at

different positions. Also, the phases of all consumers can be determined visually, with no intrusion into consumer premises. Moreover, the static balancer that WPD had in stock was of pole-mounted design. This could be installed easily on a pole without the need for acquiring land space and access.

Secondly, because there are only two cable types and one overhead line type and their design data and lengths were available, it provides a good basis for the accurate modelling of a low-voltage feeder. This will be an advantage to the further validation (against field measurements) of the forward-backward sweep method developed in Chapter 3.

6.3.3 Consumers

As seen from Figure 6.3, the feeder studied supplies nine domestic consumers along with several three-phase consumers including a post office, a garage and a pumping station. From visual inspection it was found that the domestic consumers were unevenly distributed amongst the phases, such that there were – four on the A phase, five on the B phase and zero on the C phase. Two of the domestic consumers connected to the B phase along with all the three-phase consumers are downstream of pole 16A, the position chosen for the static balancer. A small single-phase load – the telephone exchange - is also located at the end of the feeder.

6.3.4 Overhead line and cable types

Also from Figure 6.3, it can be seen that the feeder consists primarily of overhead line sections. Figure 6.5 (a) is a photo of pole #13 showing two single-phase service connections on the B phase and one on the A phase. Although these overhead line sections were constructed decades ago under the Midlands Electricity Board (MEB), based on the experience of the industrial supervisors, it can be assumed that the conductors are 0.058 Cu (open wire) set 0.1524 m apart and the poles are 12 m Stout wooden poles with a planting depth of 1.5 m. A sketch of the construction is shown in Figure 6.5 (b). It would be observed (both from the sketch and from the photo) that the phases are unusually ordered – C-A-B-N – instead of A-B-C-N. The reason for this is that

low-voltage feeders in this part of England had been constructed with the neutral at the top (i.e. the original order was N-A-B-C), then when it became standard for the neutral to be at the bottom, there was a swapping around of the connections made to the top and bottom conductors at all pole positions.

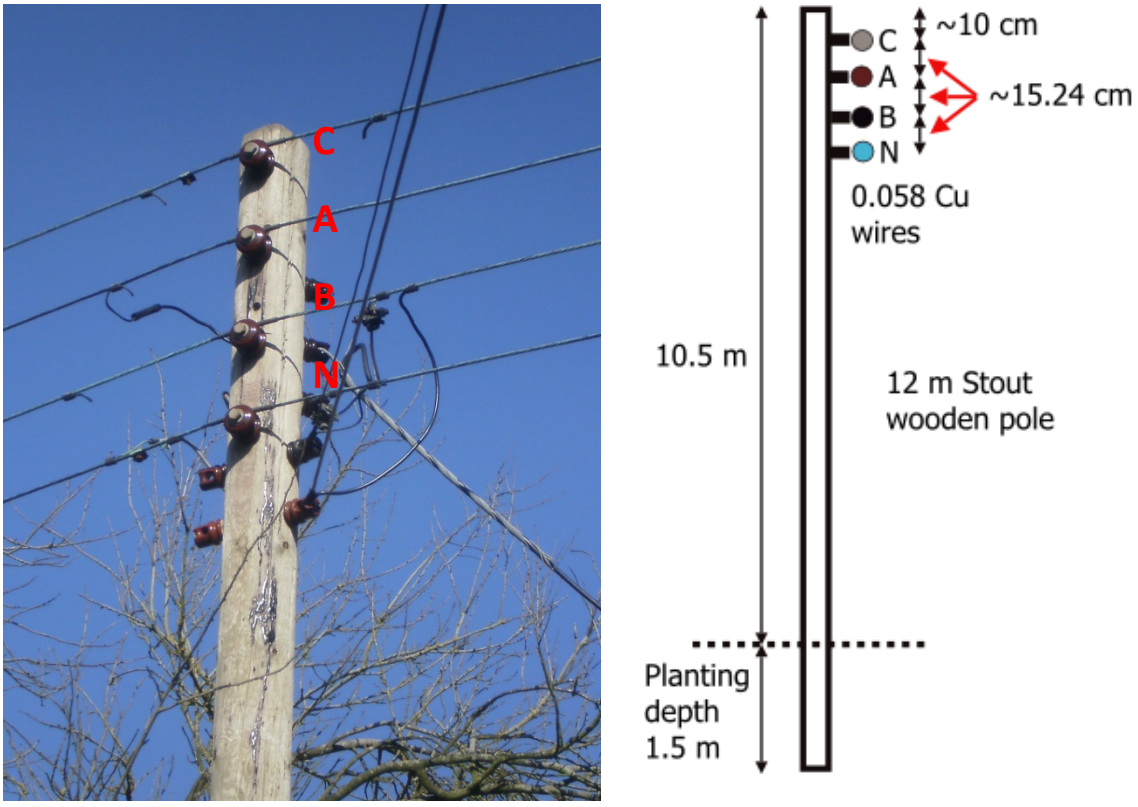

Figure 6.5: Photo of pole #13 and sketch showing its construction details

The rural low-voltage feeder also has a section of 95 sq.mm three-core cable with a concentric neutral between poles 14 and 15 and a section of 95 sq.mm four-core aerial bundled conductors (ABC) overhead cable at the end of the feeder between poles 17 and 18. Photos and sketches of these cable sections are shown in Figure 6.6 and Figure 6.7 respectively.

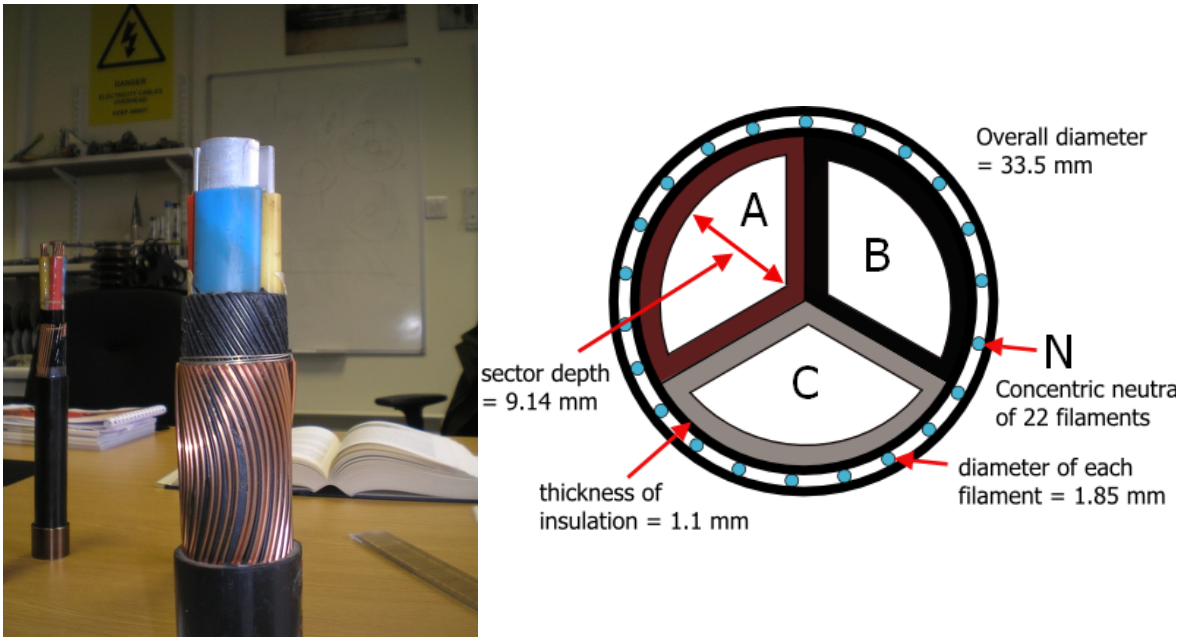

Figure 6.6: Photo of 95 sq.mm three-core cable with concentric neutral and sketch showing its dimensions [80] [84]

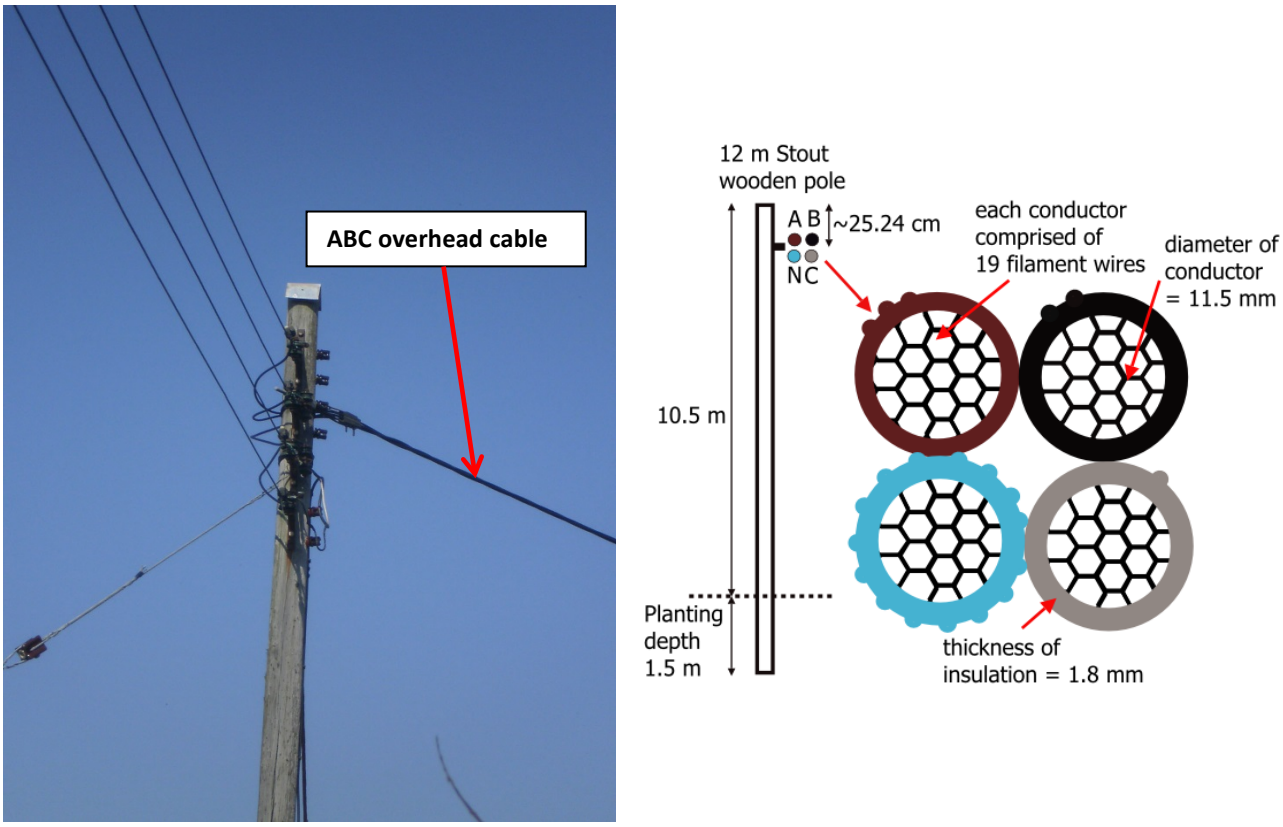

Figure 6.7: Photo of pole #17 95 sq.mm four-core ABC overhead cable and sketch showing its dimensions [85]

6.3.5 A practical example of the unequal distribution of single-phase consumers

As mentioned above there are no domestic consumers connected to phase C. A clue as to why may be in the moving of the neutral to the bottom wire.

Consider the steps that would have been involved in the work to carry out the move. With the rural low-voltage feeder de-energised, the connections from the transformer terminals to the top and bottom wires at the start of the feeder would have been swapped around. At each pole position, the neutral of the consumer cable would have been cut from the top wire and reconnected to the bottom wire. Then, if the consumer's phase wire had originally been connected to the bottom wire (originally the phase C) it would have been cut and reconnected to one of the three phase wires. The top wire, now phase C, may not have necessarily been the most preferable. Because after this work, a visual check would have been necessary before re-energising the feeder and it would have been reassuring to a linesman to not have to see any consumer cables connected to the top wire; as that may mean that a consumer neutral could potentially be connected to what would now be a phase wire. For this reason, the top wire – phase C – may have been given lower preference. This, like the example considered in Figure 2.9 with the four-core cable, is another practical example of how domestic consumers may be unequally distributed amongst the phases.

Another practical reason for the top wire being less favoured is that it is the highest and therefore most difficult to reach.

It should be noted though, that the unequal distribution of domestic consumers on this rural low-voltage feeder may be only one of the reasons for the unbalance. Another could be the distribution of single-phase load equipment within one or more of the three-phase consumers – either at the post office, garage or pumping station.

6.4 Field measurement plan

This section first identifies the intended uses for these field measurements. Next, the rationale behind the need for power quality meters at different locations on the rural low-voltage feeder is explained. The capabilities of the power quality meters available are then presented and their chosen positions identified after discussing several practical challenges.

The section concludes with a summary of the field measurements eventually gathered.

6.4.1 Purpose of field measurements

These field measurements will be used to:

- quantify the benefits of using the static balancer on the rural low-voltage feeder; and
- further validate the forward-backward sweep method developed in Chapter 3 and the static balancer model of Chapter 5.

6.4.2 Rationale for power quality meters at different locations

Measurements are required at three positions: start of feeder; end of feeder; and the static balancer position.

Before and after comparisons at the start and at the end of feeder

The need for measurements at both these locations recognises that current unbalance effects are most onerous at the start of the feeder and voltage unbalance effects are most onerous at the end of the feeder. A comparison of measurements, before and after the static balancer is energised, allows the benefits of the use of the static balancer to be quantified by way of the reduction of the effects of current unbalance (seen at the start of the feeder) and voltage unbalance (seen at the end of the feeder). The measurements required at both locations are identified in Figure 6.8.

Figure 6.8: Measurements required for study of unbalance on a low-voltage feeder

Influence of static balancer

Further measurements at the static balancer position are needed to investigate its influence on unbalance on the low-voltage feeder. Moreover, they will be needed to validate the static balancer model. These are depicted in Figure 6.9.

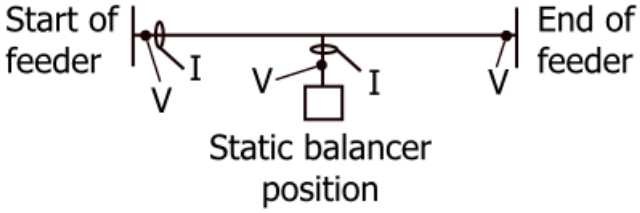

Figure 6.9: Further measurements required to capture the influence of static balancer

Capturing non-domestic consumer demands

In the estimation of the network losses carried out in this chapter and in the validation of the proposed 5 x 5 approach against field measurements later in Chapter 7, the consumer demands will be needed. Ideally, the consumer demands should be individually metered. This however was not a practical option. It would have been costly (as three three-phase meters and nine single-phase meters with logging capabilities would have been required at the non-domestic and domestic consumer premises respectively) and intrusive to consumers (as it would require access to consumers' premises to install; involve temporary loss of supply to consumers; and data privacy issues).

The most practical alternative was to measure small groups of consumers and then estimate the individual consumer demands. This relies on the power quality meters already proposed for the start of the feeder, end of the feeder and static balancer position. In addition to not requiring more meters, this is non-intrusive as all measurements are carried out from the low-voltage network itself. This option would however require further post-processing, as the lumped measurements at different

positions will have to be subtracted to determine the demand of the groups of consumers on the different sections of the feeder.

The initial plan for measurements is depicted in Figure 6.10.

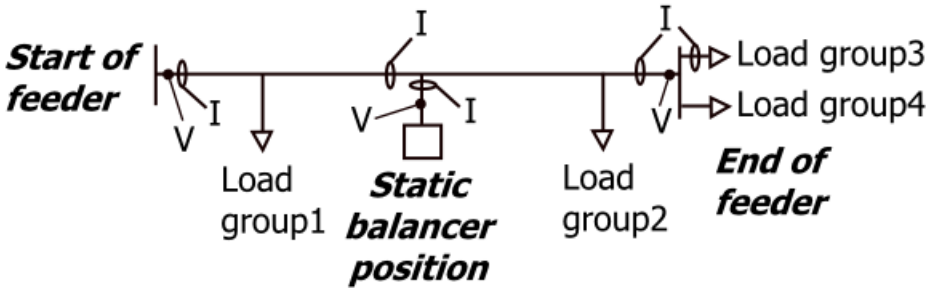

Load group 1: *Domestic consumers - four on phase A and three on phase B.*

Load group 2: *Post Office and two domestic consumers on phase B.*

Load group 3: *Pumping station.*

Load group 4: *Garage and telephone exchange.*

Figure 6.10: Initial plan for measurements on rural low-voltage feeder

6.4.3 Capabilities of power quality meters available

There were five power quality meters available for use. They included two Fluke 1743s, two Ametek PQRs and an eMS meter. Table 6.1 lists the parameters required for an unbalance study on a low-voltage feeder and compares the availability of these parameters from the different power quality meters.

It would have been ideal if, in addition to the phase-neutral voltage and phase current magnitudes, that these meters had also stored phase-neutral voltage and phase current angles as well. This would have provided a ready picture of the phase-neutral voltage and phase current phasors and hence allow the voltage and current unbalance factors to be determined readily. One of the meters though - the Fluke 1743 - stored both phase-neutral and phase-phase voltage magnitudes, thus allowing voltage angles to be calculated. Additionally, it stored the active and reactive power demands per phase, therefore allowing current angles to also be calculated.

Parameters		Fluke 1743	Ametek PQR	eMS
Phase-neutral voltage	Magnitude	S	S	S
	Angle	C		
Phase-phase voltage	Magnitude	S		
	Angle	C		
Phase current	Magnitude	S	S	S
	Angle	C		
Demand per phase	Active	S		
	Reactive	S		
Three-phase demand	Active	S	S	S
	Reactive	S		S
VUF_0		C		S
VUF_2		S	S	S
IUF_0		C		
IUF_2		S		
Legend: S – stored directly. C – calculated from stored values.				

Table 6.1: The availability of parameters from the different power quality meters

6.4.4 Placement of power quality meters

Start of feeder

A Fluke 1743, which requires only a crew with a ladder for its installation, was used at pole #11. The other two meters would have required road access for a lift truck to hoist them onto the pole. This position may have been accessed through the school located just behind the H-pole with the distribution transformer. However, on the day of the installation of the meters, the school was closed and the only access was through a farmer's field.

This power quality meter, shown in Figure 6.11, will be referred to as Fluke 1.

Figure 6.11: Photo showing distribution transformer and Fluke 1 at pole #11 (Start of feeder)

Static balancer position

Two power quality meters were used at this position. An Ametek (shown in Figure 6.12), was placed at pole #15 just upstream of the static balancer. It measures the phase currents upstream of the static balancer.

Figure 6.12: Photo of Ametek PQR at pole #15 (Static balancer position)

Consideration had been given to using the second Ametek PQR meter at pole #16A (the static balancer position). This would have had the following advantages:

- the voltages at the terminals of the static balancer and current drawn by it would be measured directly;
- the current downstream of the static balancer would have been found by finding the difference between two identical power quality meters; and
- the same laptop would have been used to configure both Ametek PQRs and as a result their timestamps could have been synchronised.

The second Ametek PQR however could not be installed. Because pole #16A, was located near to a main road and to position a lift truck to hoist the meter up the pole would have required that the road be partially blocked. In its place a Fluke 1743 was

installed on pole #16. Although the voltages were not measured at the terminals of the static balancer, the distance between pole #16 and #16A was short, being only 10.5 m. Of greater concern was the determination of the currents drawn by the static balancer. Initial plans were for these current measurements to be used to validate the static balancer model. In their absence, an indirect means, discussed later in section 6.7, involving the upstream currents (measured by the Ametek at pole #15) was instead used.

Figure 6.13: Photo of pole #16 (where Fluke 2 was installed) and #16A (with Static balancer installed)

End of feeder

At this position the eMS meter was used. This meter had been designed with nine current input channels and current transformers. Four of them were set to monitor the pumping station and another four to monitor the phase currents on the incoming wires to pole #18 (i.e. the total of pumping station, garage and telephone exchange).

Figure 6.14: Photo of eMS meter at pole #18 (End of feeder)

6.4.5 Summary of measurements taken

All the measurements taken are summarised by the timeline shown in Figure 6.15.

The static balancer was first energised on the 11th November, 2011. Measurements taken two to three weeks before and after this date are referred to as the ***first trial***. Unfortunately data from two of the meters could not be retrieved and it was necessary to take measurements a second time. This was done in February/March 2013. For this, the static balancer was de-energised on the 1st March, 2013. The measurements taken two to three weeks before and after this date are referred to as the ***second trial***. The analysis carried out in this Chapter, which is based solely on field measurements, will be based on this ***second trial***. In this trial, data was retrieved from three of the four meters. The missing measurements are for the meter at the end of the feeder. It would

have allowed the effects of voltage unbalance to be investigated fully up to the end of the feeder. In its place the readings from Fluke 2 will have to be used.

Additionally, there are also ***preliminary*** measurements which had been taken by Fluke 1743s connected to the service cables going to the Post Office and Garage. These measurements were done in March/April 2010.

The static balancer was re-energised after the ***second trial*** and is still in service. It should be noted as well that the Ametek PQR which is also still in service, provided data faithfully in the time period between the two trials. The eMS meter is also in service.

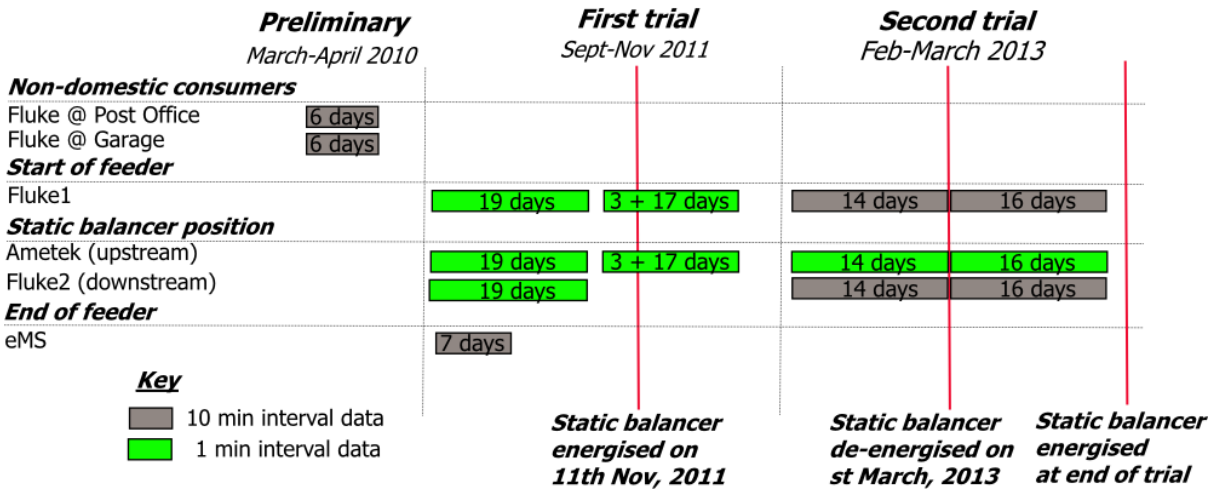

Figure 6.15: Timeline showing all measurements taken on rural low-voltage feeder

6.5 Processing of field measurements

An application, shown in Figure 6.16 was developed in Matlab to view the measurements taken by the different meters. This application also allows the data to be sanitised by performing several checks to ensure that for each meter its:

- Current and voltage readings correspond to the same phase;
- Readings for each phase correspond with the same phase of all other meters;
- Readings are all time-stamped in GMT; and
- Readings are synchronised with those of the other meters. This was necessary as different laptops were used to configure each of the meters. This was done by correlating the phase C current of Fluke 1 with the phase C current readings

of the Ametek and Fluke 2 (as no consumers were connected to this phase between the transformer and the static balancer position).

Several additional processing functions are performed. These are discussed in the sections which follow.

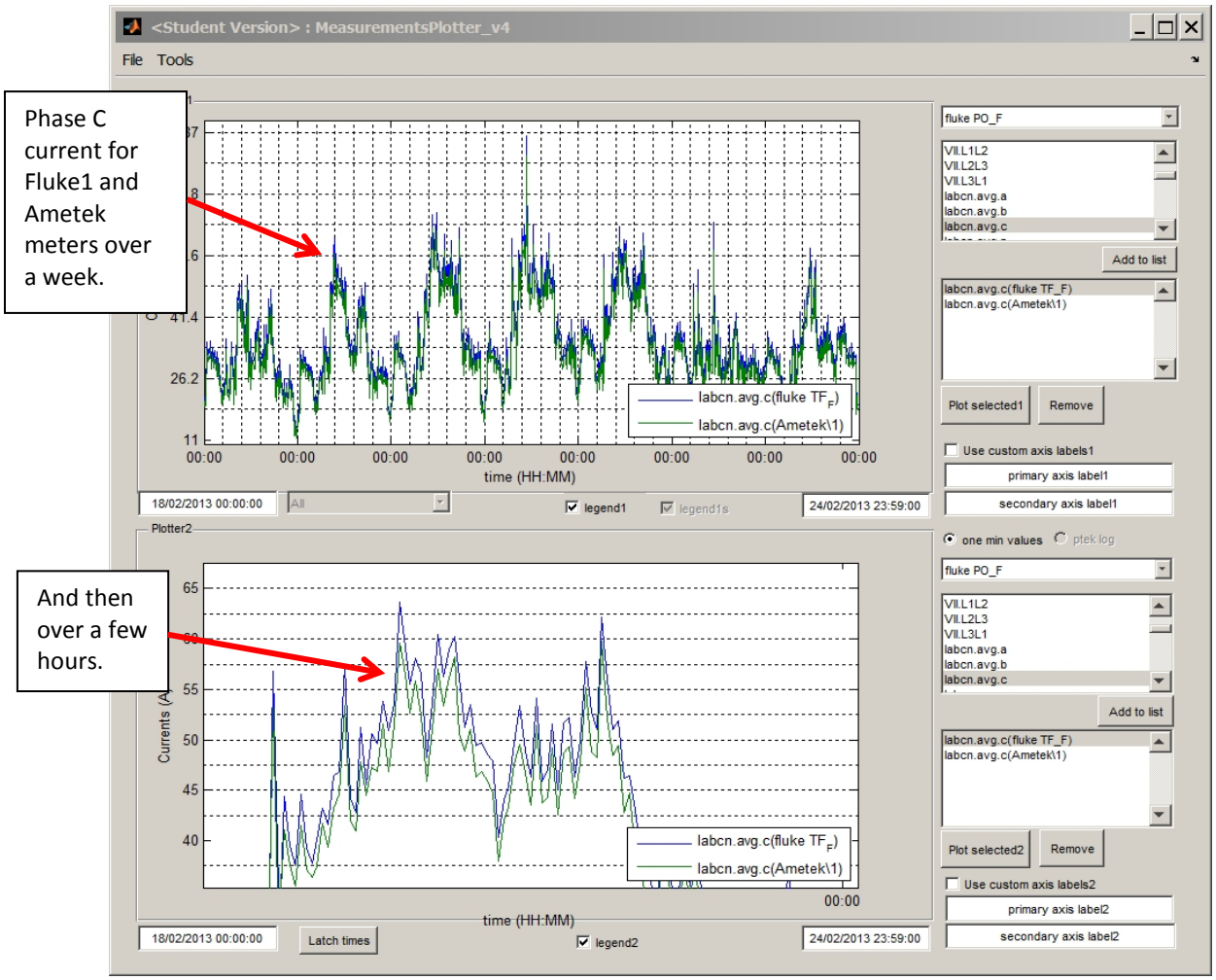

Figure 6.16: Measurements plotter developed in Matlab (phase C currents of Fluke1 and Ametek plotted)

6.5.1 Converting 1 min interval readings to 10 min interval readings

From Figure 6.15 it would be observed that in the first trial the averaging interval for the Ametek and Fluke meters was the same (i.e. one-minute). In the second trial however, the Flukes were configured to their default of ten minutes while the Ametek continued recording at one minute intervals. This meant that for any comparison to be made, it was necessary to convert the Ametek measurements to ten-minute interval values. As depicted in Figure 6.17, this involved finding several ten-minute profiles from

the Ametek data of the phase C current and determining the one that correlated the most to that measured by Fluke1. This method also synchronises the Ametek readings with those of Fluke1 by catering for a clock shift of k minutes between both meters.

The close agreement of the phase C current readings for both meters (after the Ametek data was converted to ten-minute averages) is displayed in the plots given in the snapshot of the measurement plotter (Figure 6.16). The top plot shows an entire week while the bottom plot zooms into a few hours of readings.

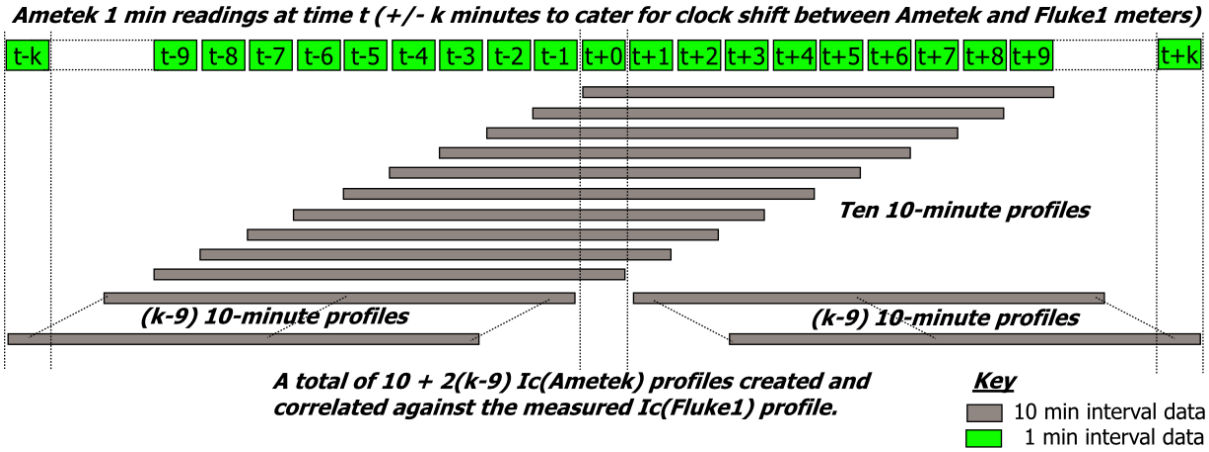

Figure 6.17: Illustration showing the conversion of one minute data into ten minute data

6.5.2 Calculating voltage angles

The exact calculation of the voltage unbalance factors with equations (2.2) and (2.3) requires phase-neutral voltage magnitudes and angles. As Table 6.1 showed, all the meters logged only phase-neutral voltage magnitudes. None of them logged voltage angles. With the Flukes however, because they log phase-phase voltage magnitudes in addition to phase-neutral voltage magnitudes, the voltage angles can be calculated.

To illustrate the method, Figure 6.18 shows a triangle formed from the measured phase-phase and phase-neutral voltage magnitudes.

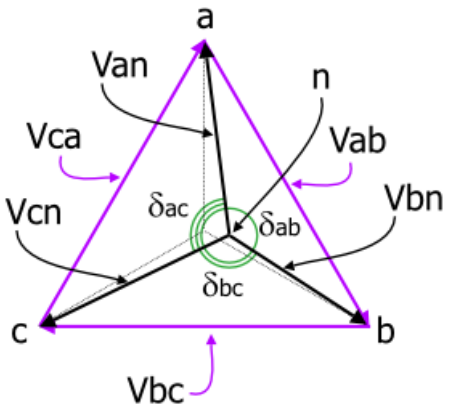

Figure 6.18: Finding voltage angles from average phase-neutral and phase-phase voltage magnitudes

Using the cosine rule, the voltage angles of V_{bn} and V_{cn} can be resolved with respect to V_{an} as:

$$\delta_{bn} = -\delta_{ab} = \cos^{-1}\left(\frac{V_{an}^2+V_{bn}^2-V_{ab}^2}{2V_aV_b}\right) \quad (6.1a)$$

$$\delta_{cn} = \delta_{ca} = \cos^{-1}\left(\frac{V_{cn}^2+V_{an}^2-V_{ca}^2}{2V_cV_a}\right) \quad (6.1b)$$

With these voltage angles, the systems of voltage phasors at the start of the feeder and at the static balancer position will be known.

6.5.3 Calculating current angles

The current angles can also be calculated at the locations with the Flukes installed using the calculated voltage angles and logged active and reactive power demands per phase. They are found using:

$$|I_p|\angle\theta_p = \left(\frac{S_p}{V_{pn}}\right)^* = \frac{|S_p|}{|V_{pn}|}\angle\left(\delta_{pn} - tan(Q_p/P_p)\right) \quad (6.2)$$

where $p = a, b, c$

With these current angles the current unbalance factors can be calculated exactly using equations (2.2) and (2.3).

6.6 Measurement errors

In the first trial, the Flukes and the Ametek meters both took one-minute average readings. The eMS meter took ten-minute average readings, but only one week of data was available from it (before the static balancer was energised as indicated in Figure 6.15). Therefore, with the exception of the eMS data, the first field trial results in essentially a one-minute dataset. Moreover, because it contains only direct measurements, it is subject to the errors inherent to the current and voltage transducers of the respective power quality meters only.

Now, in the second trial, as highlighted in Figure 6.15, the Flukes took ten-minute average readings whilst only the Ametek took one-minute average readings. No data was available from the eMS meter. Therefore, with the exception of the Ametek data, the second field trial results in essentially a ten-minute dataset. Hence, for further analysis, it was necessary to convert the Ametek one-minute averaged readings to ten-minute averaged readings using the method illustrated in Figure 6.17. Because of this necessary post-processing step, the uncertainty in each ten-minute averaged value (denoted by Δx_{ametek}) will combine in quadrature [86] the error of ten independent one-minute readings (denoted by $\Delta x_1, \Delta x_2, \ldots, \Delta x_{10}$), as given by:

$$\Delta x_{ametek} = \pm\left(\sqrt{\sum_{r=1}^{10}(\Delta x_r)^2}\right)/10 \qquad (6.3)$$

The combined error will therefore be less than those of the individual one-minute readings.

The errors anticipated for the voltage and current measurements are presented in Table 6.2 and Table 6.3, respectively. Each table presents the errors anticipated for the datasets of the first and second trials, separately.

	Fluke 1740, $\Delta x_{fluke\,(voltage)}$	**Ametek,** $\Delta x_{ametek\,(voltage)}$	**eMS,** $\Delta x_{eMS(voltage)}$
First trial *(one-minute data)*	**± 0.2 V [+]**	**± 0.6 V [++]**	**Not used**
Second trial *(ten-minute data)*	**± 0.2 V [+]**	**± 0.2 V [+++]**	
[+] 0.1 % of a 230 V input voltage range [87]. **[++] 0.2 % of a 300 V input voltage range [88].** **[+++] After applying equation (6.3) to 10 one-minute readings at 0.2 % of a 300 V input voltage range [88].**			

Table 6.2: Accuracy of voltage measurements for first and second trials

	Fluke 1740, $\Delta x_{fluke(current)}$	Ametek, $\Delta x_{ametek(current)}$	eMS, $\Delta x_{eMS(current)}$
First trial *(one-minute data)*	± 3 A [+]	± 3 A [++]	Not used
Second trial *(ten-minute data)*	± 3 A [+]	± 1 A [+++]	
[+] 2 % of a 150 A range (Flexi Set) [87]. [++] 1 % of a 300 A range (i3000s) [89]. [+++] After applying equation (6.3) to 10 one-minute readings at 1 % of a 300 A range (i3000s) [89].			

Table 6.3: Accuracy of current measurements for first and second trials

The dataset for the second field trial is the more complete; as it has measurements upstream and downstream of the static balancer after it was energised. For that reason, this dataset was used for the analysis. Therefore, the errors related to the Flukes and the Ametek, as presented in the second row of Table 6.2 for voltages and Table 6.3 for currents, should be kept in mind during the analysis.

6.6.1 Looking at the errors more closely

Now there is nothing between the Ametek and Fluke 2 meters except the static balancer; so when that is de-energised, an idea of the absolute difference between current measurements taken by a Fluke and an Ametek following post-processing is visible. This is shown in Figure 6.19.

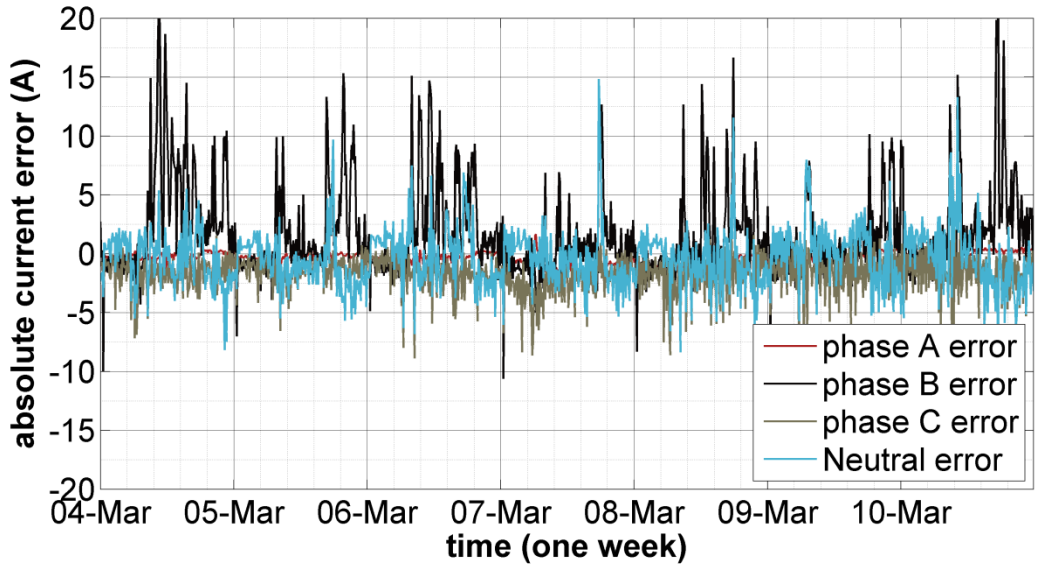

Figure 6.19: Instrument errors between Fluke 2 and Ametek current measurements without static balancer

The error between the Ametek and Fluke 2 current readings are given by:

$$\Delta x_{Ametek(current)-Fluke2} = \pm\sqrt{\left(\Delta x_{ametek(current)}\right)^2 + \left(\Delta x_{fluke(current)}\right)^2} \qquad (6.4)$$

This works out to ± 3.2 A, using the $\Delta x_{fluke(current)}$ and $\Delta x_{ametek(current)}$values in the second row of Table 6.3. For the current errors between the Fluke 2 and Ametek meters shown in Figure 6.19, the means, standard deviations and 95th percentile values are given in Table 6.4. Even though, the mean values are all less than 3.2 A, it can be seen that the phase B current error has a significant spread and its 95th percentile value is twice that of the others. This should be kept in mind when comparisons are done against network simulations later in Chapter 7 because as will be seen later in section 6.10.3, the differences in current measurements taken by Fluke and Ametek meters will be used to estimate the consumer demands which are inputs to the network simulations.

(Ametek – Fluke2)	Mean	Standard deviation	95th percentile value
Phase A	0.4	0.4	1.2
Phase B	2.7	3.4	9.9
Phase C	1.9	1.6	4.8
Neutral	2.0	1.7	5.2

Table 6.4: The mean, standard deviation and 95th percentile values for the difference between Ametek and Fluke2 measurements for all phases and neutral

Continuing, between the two Flukes and between Fluke 1 and the Ametek there will also be errors, as seen in Figure 6.20 for the phase C current measurements. Comparisons between these two sets of meters are only possible on phase C (as there are no consumers connected between these meters on that phase).

Now, the error between the two Flukes, which is seen in Figure 6.20, is given by:

$$\Delta x_{Fluke1-Fluke2(current)} = \pm\sqrt{2\left(\Delta x_{fluke(current)}\right)^2} \quad (6.5)$$

Using the $\Delta x_{fluke(current)}$ value in the second row of Table 6.3, it works out to be ± 4.2 A.

Also, the error between the Fluke 1 and the Ametek is shown in Figure 6.20. This error will be given by:

$$\Delta x_{Fluke1-Ametek(current)} = \pm\sqrt{\left(\Delta x_{fluke(current)}\right)^2 + \left(\Delta x_{ametek(current)}\right)^2} \quad (6.6)$$

It will be the same as that found using equation (6.4), ± 3.2 A.

The mean, standard deviation and 95th percentile values for the differences in phase C measurements between the two Flukes and between Fluke 1 and the Ametek are shown in Table 6.5. In both cases, the mean of errors are not greater than anticipated.

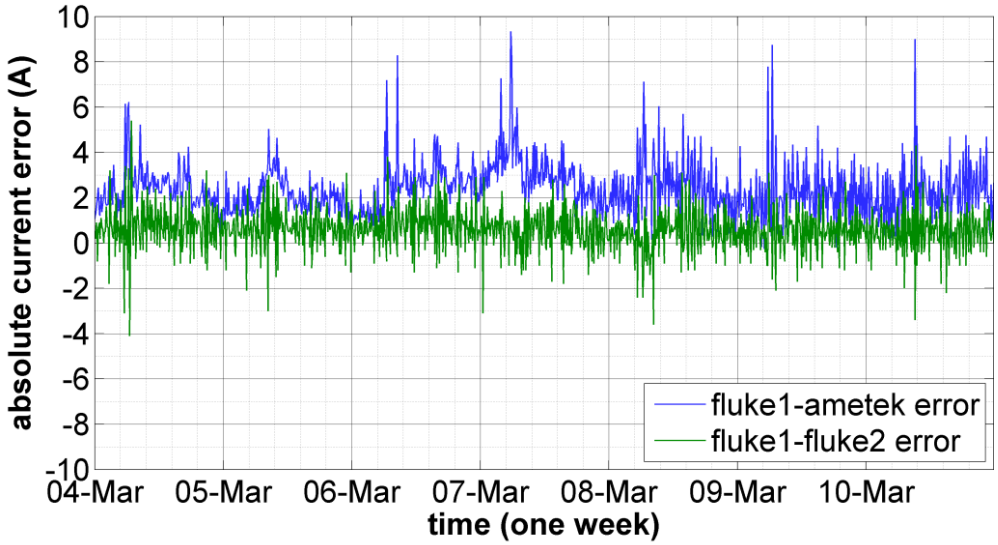

Figure 6.20: Instrument errors between Fluke 1 and Ametek and between Fluke 1 and Fluke 2 phase C current measurements without static balancer

	Mean	Standard deviation	95th percentile value
Phase C (Fluke 1 – Fluke 2)	2.4	1.2	4.4
Phase C (Fluke 1 – Ametek)	0.9	0.7	2.3

Table 6.5: The mean, standard deviation and 95th percentile values for the difference between Fluke 1 and Ametek and between Fluke 1 and Fluke 2 for the phase C current measurements

A similar examination of the voltages could not be done; as no two meters were installed at exactly the same position. There would have been a voltage drop present in such a comparison (if made say between the Ametek and Fluke2).

The following sections present an analysis of the processed field measurements.

6.7 The behaviour of static balancer

This section starts by confirming the static balancer's known behaviour as covered in Section 2.6.6 (G), which was based on the explanation given in the text [8]. After which, it provides some further insight into its behaviour from the field measurements.

6.7.1 Confirmation of the known behaviour

Section 2.6.6 (G) had highlighted that the influence of the static balancer on the low-voltage network was to redistribute some of the downstream neutral current onto the upstream phases, the result of which was more evenly distributed upstream phase currents and lower upstream neutral current. This influence can be confirmed from the currents measured after the static balancer was energised. Figure 6.21 and Figure 6.22 show the downstream and upstream currents measured by the Fluke2 and Ametek meters for one day (20/02/2013). Downstream of the static balancer, it can be seen that:

- the neutral current is, at most times during the day, larger than two of the phase currents; and
- the difference between phase currents is significant. It can, for example, be as high as 70 A between the lightest and heaviest loaded phases.

In contrast, upstream of the static balancer:

- the neutral current is less than all three phase currents; and
- the phase currents are much more evenly distributed. The difference between the lightest and heaviest loaded phases is at most 40 A.

The benefits of this reduction in current unbalance upstream of the static balancer will be quantified in the section 6.10.

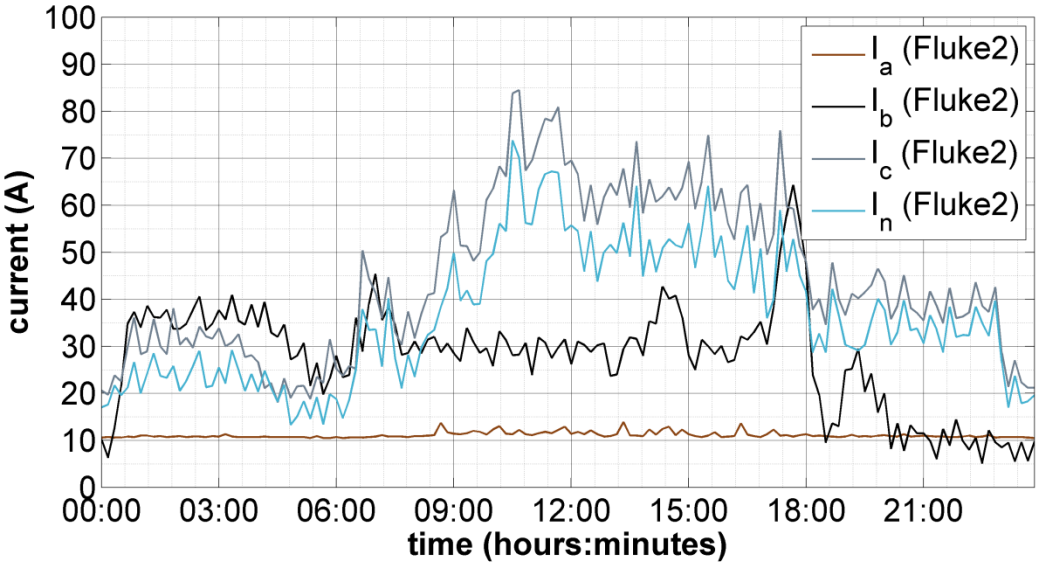

Figure 6.21: Phase and neutral currents downstream of static balancer (Fluke2)

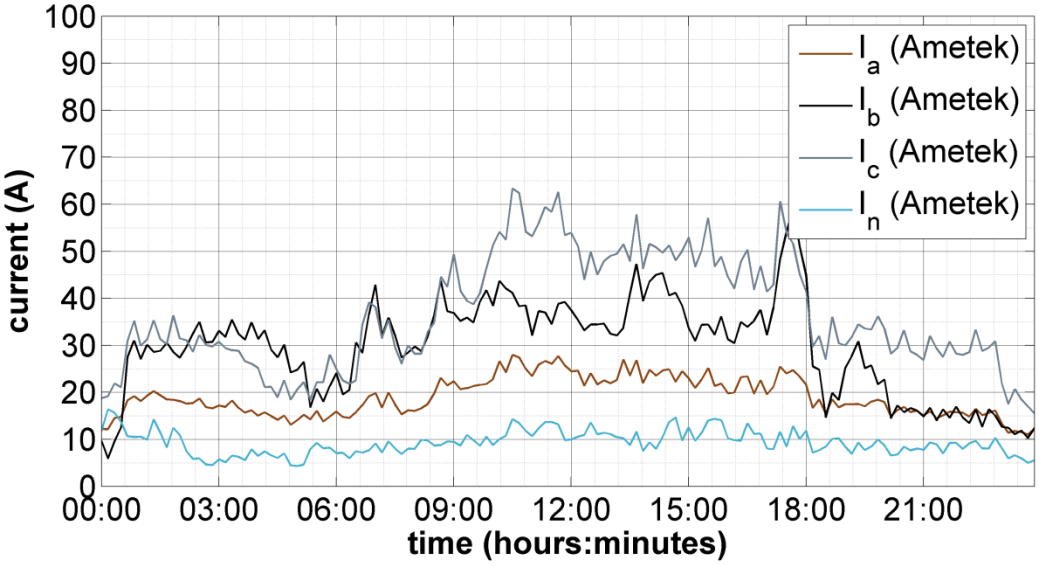

Figure 6.22: Phase and neutral currents upstream of static balancer (Ametek)

6.7.2 Further insight into its behaviour

The static balancer changes not just the current magnitudes upstream of it, as presented in the literature, but also the relative angles of the current phasors. This change is evident in Figure 6.23 (a) and (b) – taken by Fluke1, the only upstream meter for which current angles are available. It can be seen that after the static balancer is energised the angles between current phasors:

- vary considerably more during the week (from a 30° range to a 45°-60° range); and
- fluctuate much more with respect to each other.

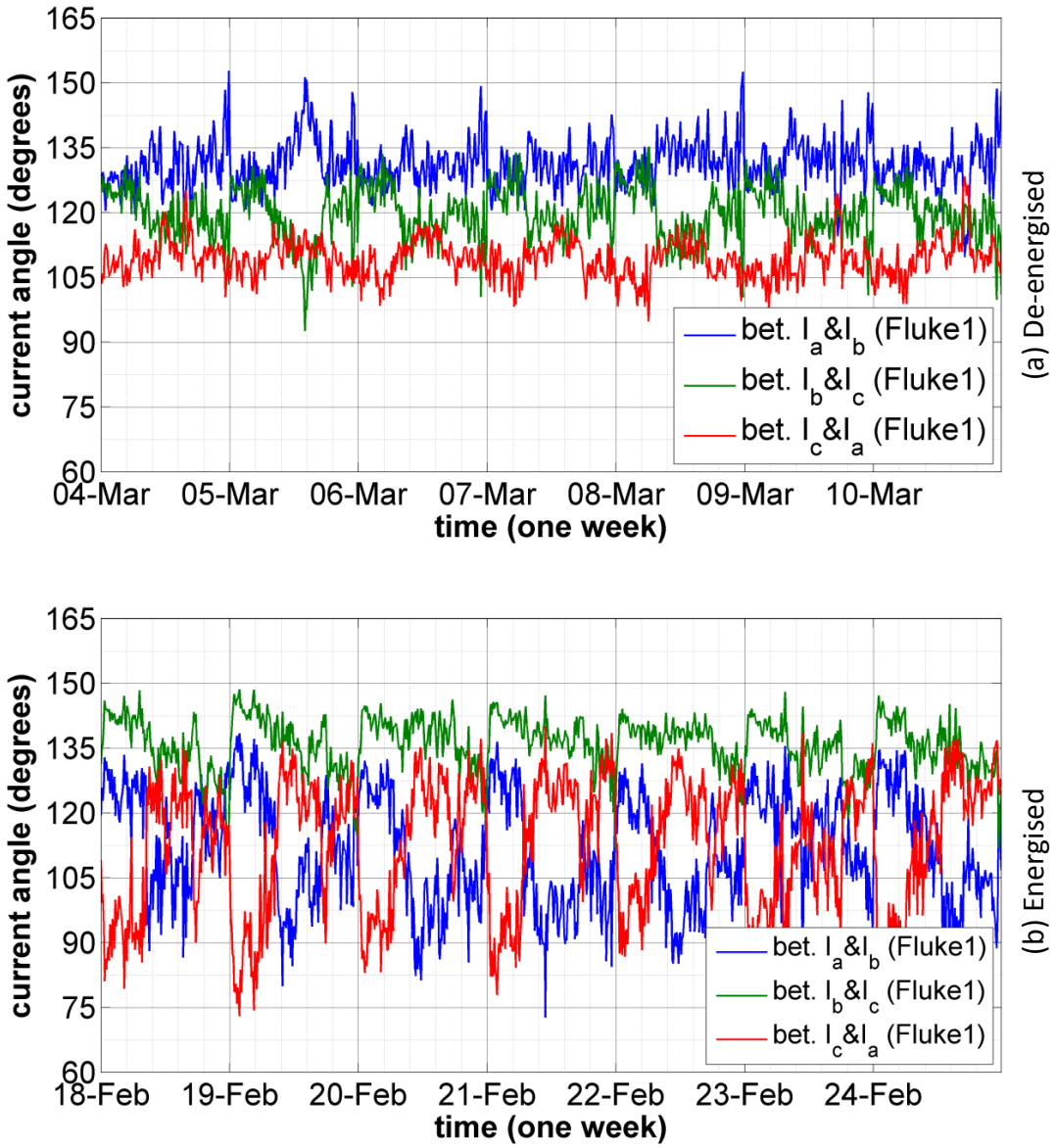

Figure 6.23: Phase currents angles with static balancer (a) de-energised and (b) energised.

This increased variation, which may not be as straightforward to understand as that of the changes in current magnitude, is also reflected in the power transfers and unbalance factors.

The change in active and reactive power transfers per phase

The active and reactive power transfers as measured by Fluke1, with the static balancer de-energised and energised are shown in Figure 6.24 and Figure 6.25, respectively.

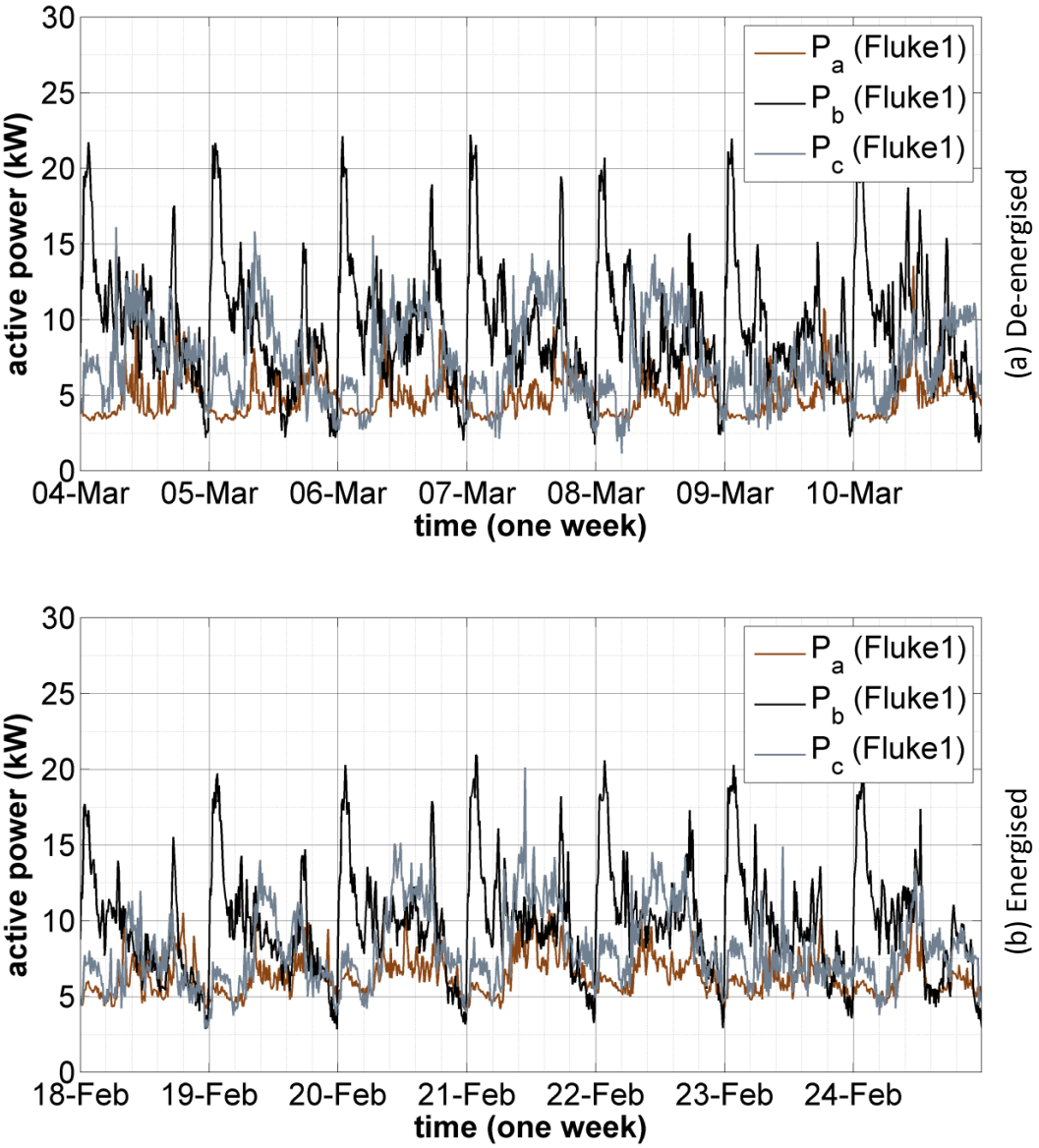

Figure 6.24: Active power transferred per phase as measured directly by Fluke1 with static balancer (a) de-energised and (b) energised.

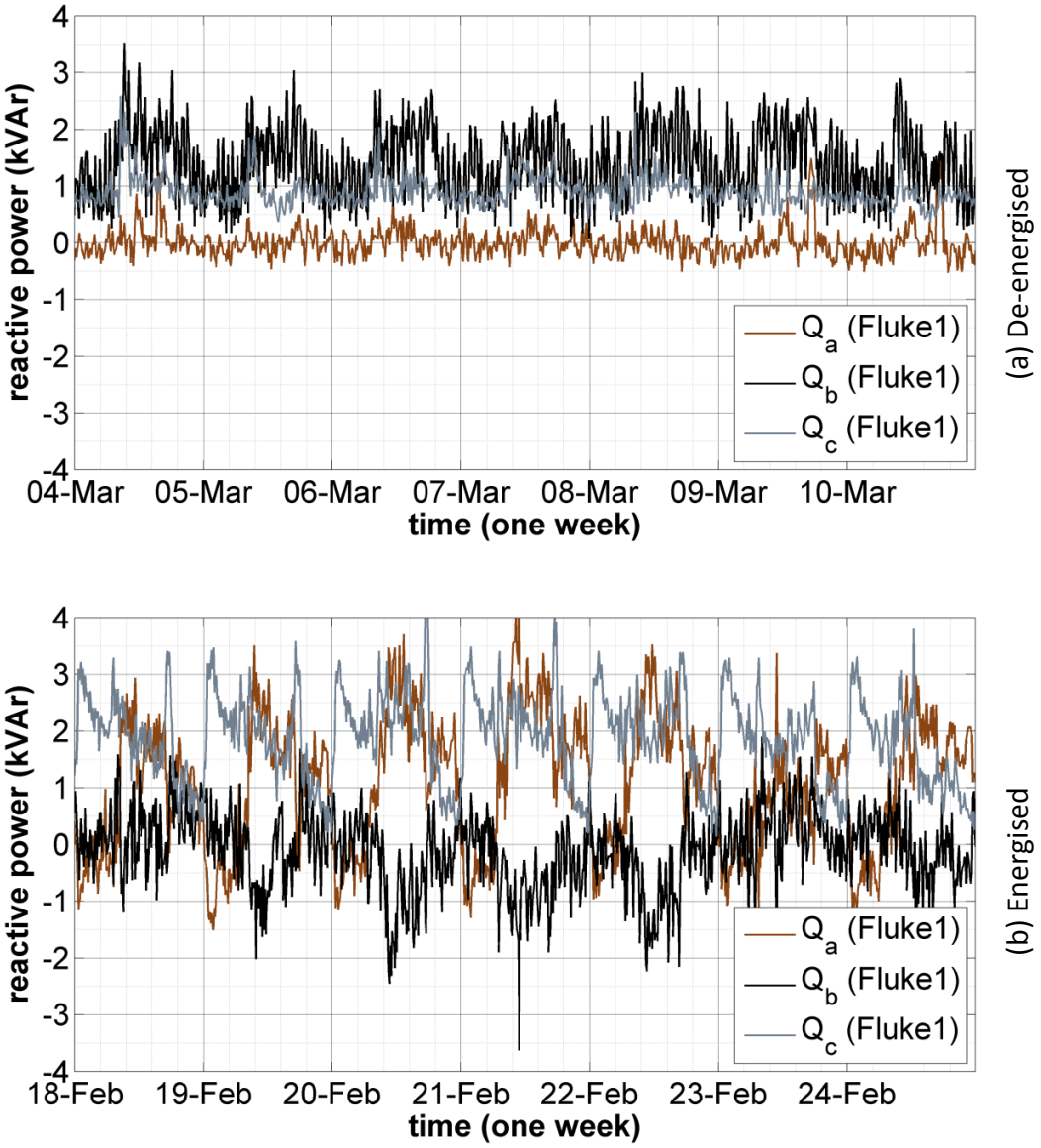

Figure 6.25: Reactive power transferred per phase as measured directly by Fluke1 with static balancer (a) de-energised and (b) energised.

The reactive power transfers are drastically different. With the static balancer de-energised, the power factor on both phases B and C are at all times lagging whilst that of phase A is near unity or at times slightly leading. With the static balancer energised, the reactive power transfer on each phase varies over a wider range throughout the day and seemingly in relation to each other (for instance the more phase A and C lag the more phase B leads). This change is due to the addition of homopolar current phasors by the static balancer to compensate the unbalanced downstream current phasors. The resulting changes to the angles of the upstream current phasors, which occur throughout the day as the current unbalance varies, are reflected in the reactive power transfers of Figure 6.25.

If viewed per phase, these changes in reactive power transfers may be wrongly interpreted as a lowering (or raising) of power factor. Firstly, it must be kept in mind that these are the compensated power transfers (as a result of the static balancer), and not the consumer demand profiles. Secondly, the power factor for unbalanced three-phase power systems, defined previously in section 4.3 as the effective power factor [75], involves finding the effective apparent power using equation (4.2), and is not simply the power factors found from the active and reactive powers of each phase.

There are also changes to the active power transfers per phase; however, they are less observable than those of the reactive power transfers. This is because the active power transfers are much larger in magnitude and so the influence of the homopolar currents will be less prominent. It can be seen though, that the active power transfers on the more heavily loaded phase A decreases slightly, while that on the less loaded phases B and C increase slightly. This is very evident by looking at the peaks.

The change to current unbalance factors

As shown in Figure 6.26 (a) with the static balancer de-energised, the profiles of zero and negative sequence current unbalance factors follow each other closely. The static balancer compensates the zero sequence current and so, when it is energised (Figure 6.26 (b)) the zero sequence current unbalance factor reduces significantly. There is no observable change in the negative sequence current unbalance factor.

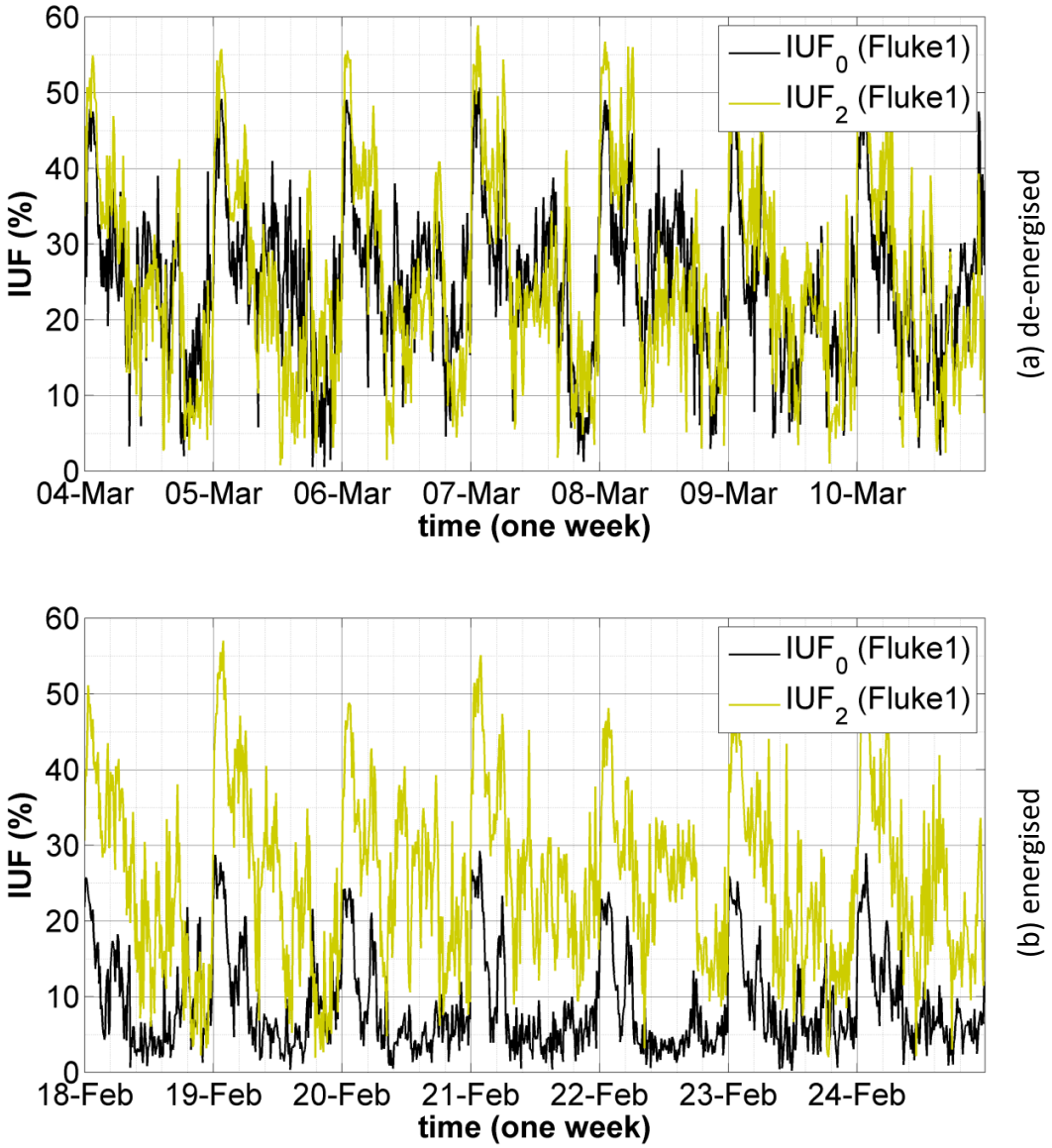

Figure 6.26: Profiles of current unbalance factors with static balancer (a) de-energised and (b) energised

So as to give a better comparison before and after the static balancer was energised; these sequence current unbalance factors can be plotted as duration curves.

The reduction in the zero sequence current unbalance factor is again seen in Figure 6.27 (a). The 95th percentile value, used for comparison, reduced drastically from 44.6 % to 22.8 %.

The duration curves for the negative sequence current unbalance factor are shown in Figure 6.27 (b). The 95th percentile value reduced slightly from 52.0 % to 45.7 %. Any change here though is merely the result of the week to week variations. The static balancer has no influence on this component.

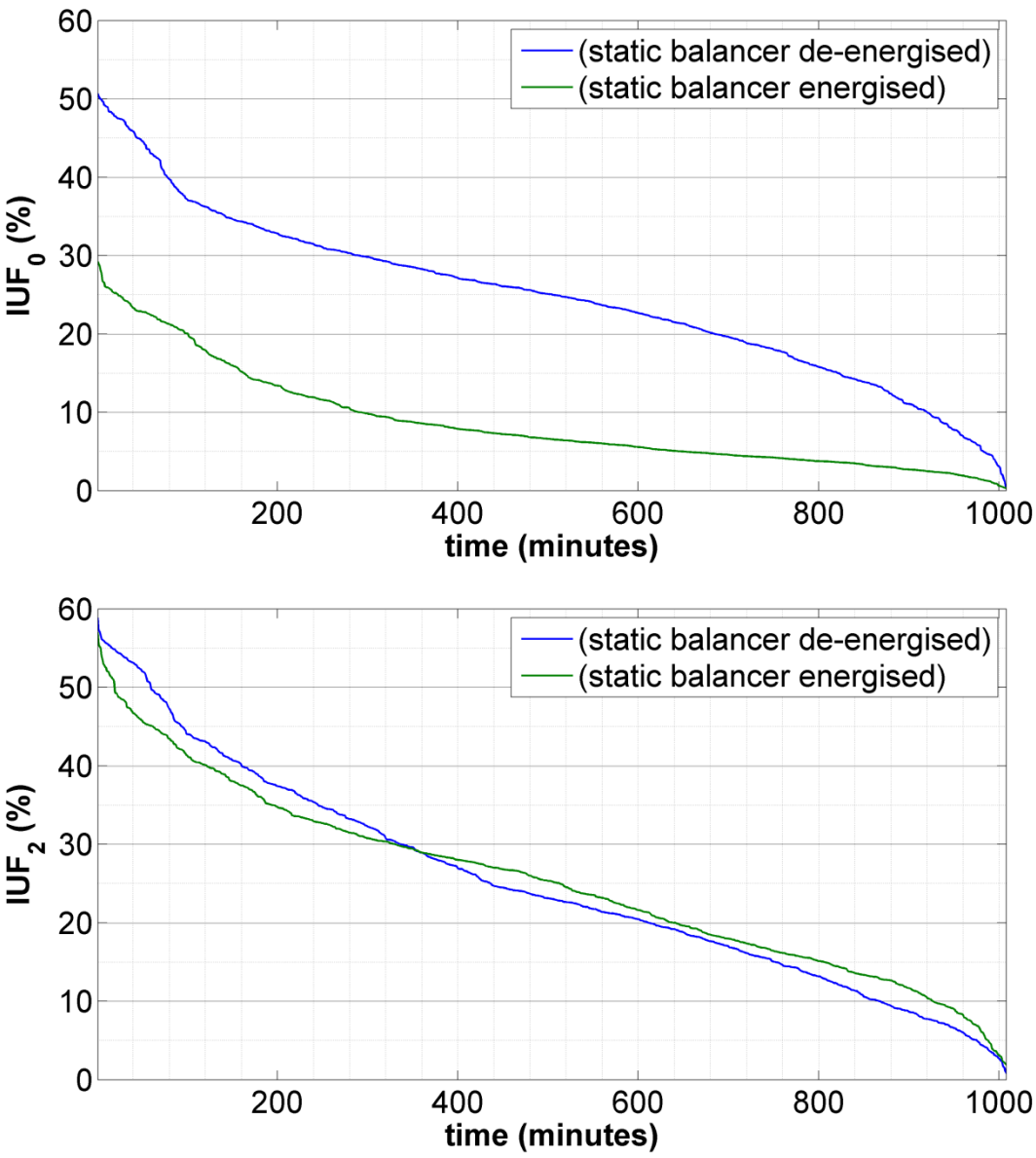

Figure 6.27: Duration curves of (a) zero and (b) negative sequence current unbalance factors

The change to voltage unbalance factors

The profiles of both sequence voltage unbalance factors are shown in Figure 6.28. It can be seen that they appear to vary independently of each other regardless of whether the static balancer is de-energised or energised.

With the static balancer energised (Figure 6.28 (b)) there is a marked reduction in the zero sequence voltage unbalance factor. The negative sequence voltage unbalance factor appears unchanged.

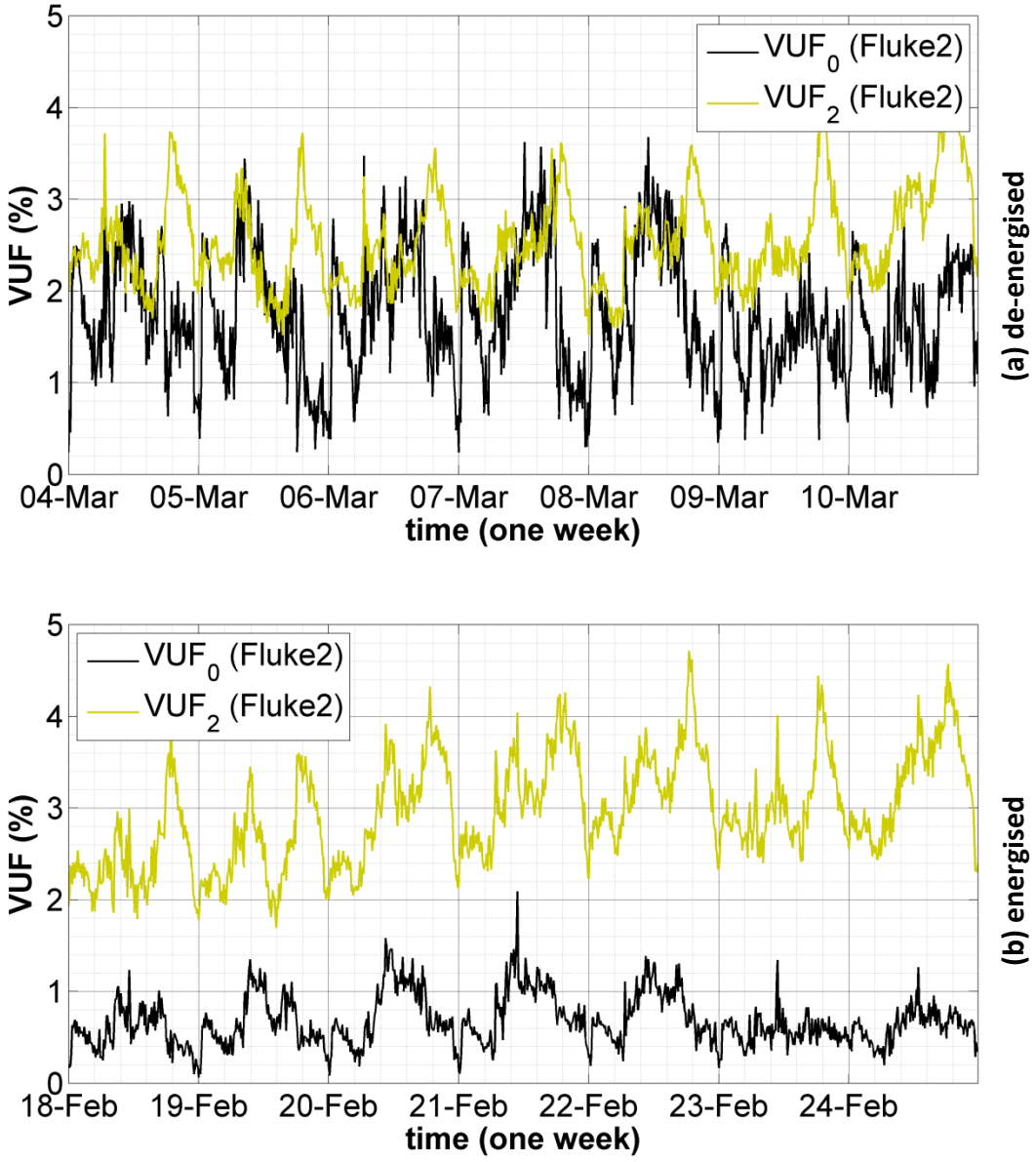

Figure 6.28: Profiles of voltage unbalance factors with static balancer (a) de-energised and (b) energised

The sequence voltage unbalance factors are plotted as duration curves in Figure 6.29.

From Figure 6.29 (a), it was found that the 95th percentile value of zero sequence voltage unbalance factor reduced from 2.9 % to 1.2 %.

The duration curves for the negative sequence voltage unbalance factor are shown in Figure 6.29 (b). The 95th percentile value increased slightly from 3.6 % to 3.9 %. Again, any change here is not due to the static balancer but merely the result of the week to week variations.

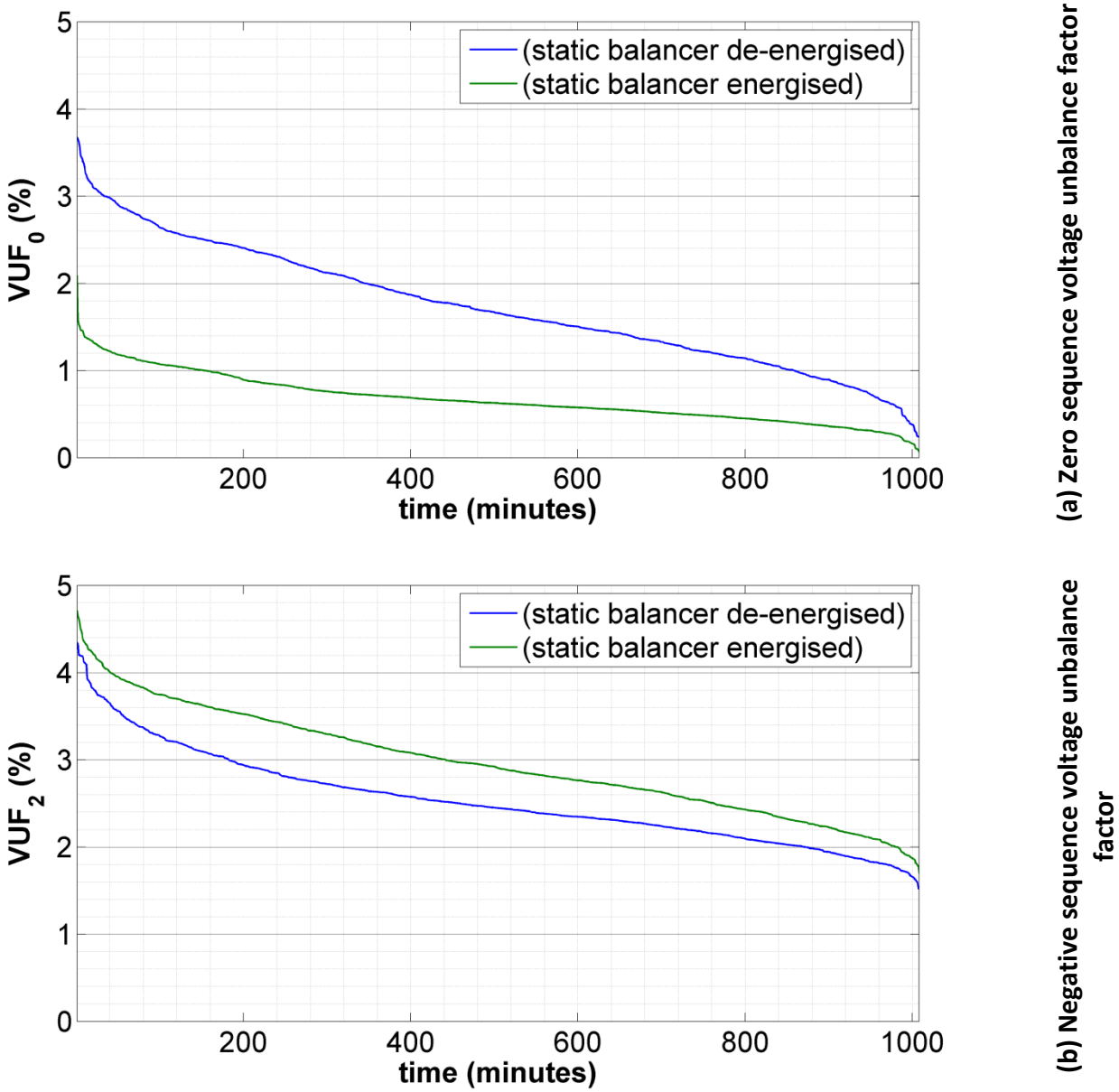

Figure 6.29: Duration curves of (a) zero and (b) negative sequence voltage unbalance factors

6.8 Validation of static balancer model by field measurements

The static balancer model can be validated by using the Fluke2 measurements of the downstream currents and the phase-neutral voltages at the static balancer's terminals to calculate the upstream currents. These calculated upstream currents can then be compared to the measured upstream currents from the Ametek meter.

Firstly, the currents drawn by the static balancer are calculated from the voltages at its terminals (measured by Fluke2) using equation (5.11) and the short-circuit impedance calculated from the design sheets (Table 5.2). Then the upstream currents are found by the sum of these currents and the downstream currents (also measured by Fluke2). These calculated upstream phase and neutral currents closely matched those measured by the Ametek meter. Figure 6.30 presents a comparison for one day (20th February, 2013). Even though the model does not account for harmonics, which are present in the measured currents, and the short-circuit impedance of the installed static balancer was not measured but assumed values calculated from the design sheets, the average percentage error was only ± 8.3 % and the average absolute error was ± 1.4 A. This is good enough for unbalanced power flow simulations, since the error from other models needed for network simulations, such as consumer demands, will be subject to perhaps even greater error due to the number of assumptions made to model them.

It can be observed that the largest error occurs on phase B. This can be accounted for by the higher error on the current transformer connected to that phase, as identified in Figure 6.19.

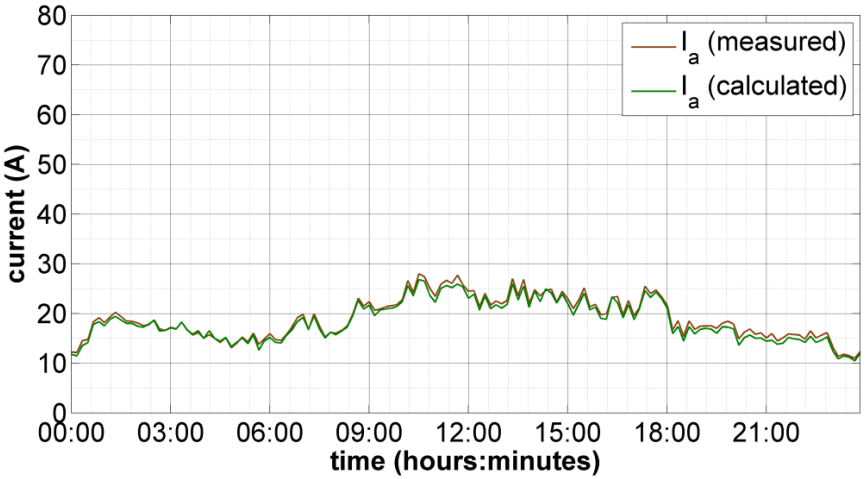

Phase A

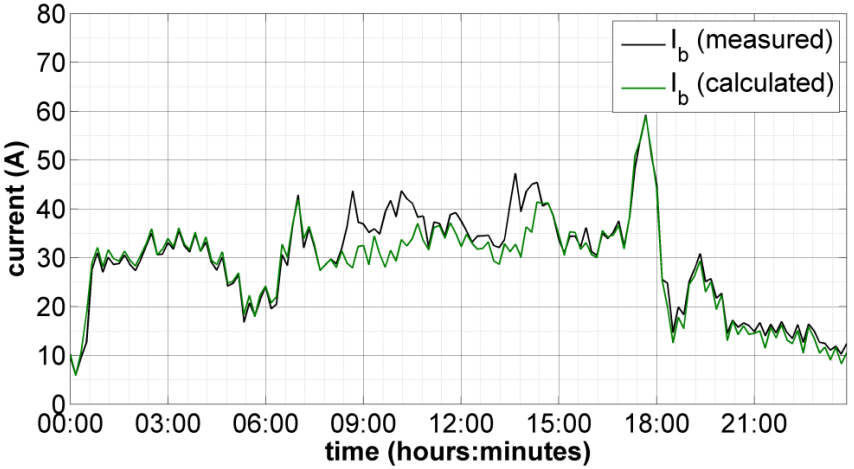

Phase B

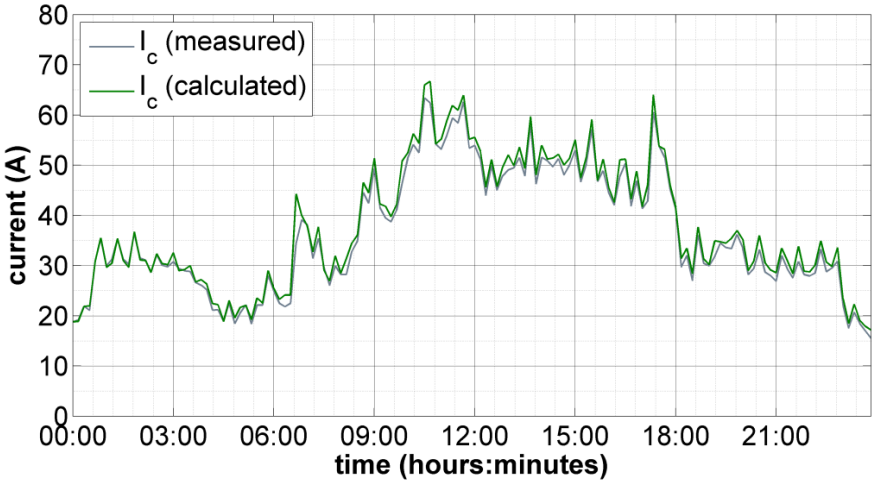

Phase C

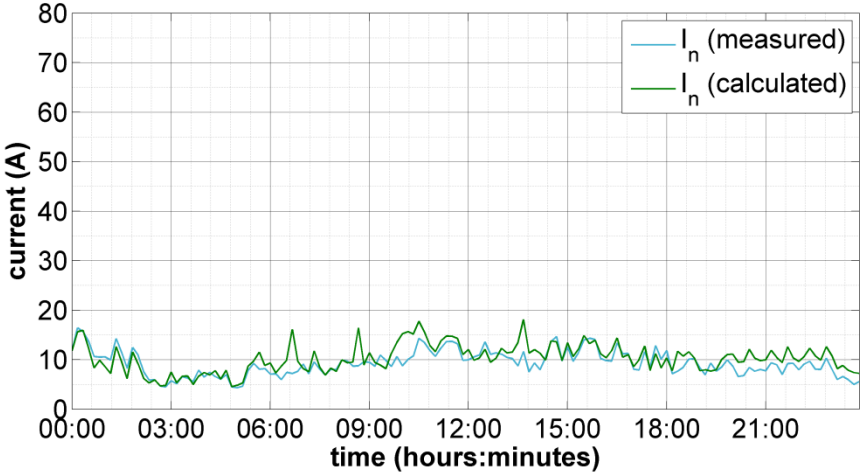

Neutral

Figure 6.30: Comparison of measured (Ametek) and calculated upstream current magnitudes

6.9 The sequence unbalance factors

This section discusses observations made about the sequence unbalance factors on the rural feeder without the static balancer.

6.9.1 Sequence current unbalance factors and current angle unbalance

The relationship between the sequence unbalance factors (i.e. $IUF_0 > IUF_2$ and vice-versa), is directly related to the relative angles between the current phasors. Previously, this was seen in Chapter 4, where three cases of current unbalance were examined. The first case considered current magnitude unbalance only, the second current angle unbalance only and the third a combination of both current magnitude and angle unbalance. The relationships between zero and negative sequence current phasors in these three cases were depicted in Figure 4.7, Figure 4.9 and Figure 4.11 respectively. They showed that the negative and zero sequence currents were:

- equal when the angles between current phasors were nearly 120° apart (regardless of current magnitude unbalance); and
- unequal when the angle between two current phasors were bigger (or smaller) than those between the other two.

To demonstrate this dependence on current angles, which is also evident in the field measurements, Figure 6.31 shows a plot of IUF_2 versus IUF_0. Highlighted in black are the readings for which the angles were close to 120 °, in green are those for which the angle between two current phasors were greater than 123 ° (*one big, two small angles*) and in orange those for which the angle between two current phasors were less than 117 ° (*one small, two big angles*). There is a clear pattern. The black readings follow a path in which $IUF_0 \cong IUF_2$, the green, a path in which $IUF_0 > IUF_2$ and the orange, a path in which $IUF_2 > IUF_0$.

Now the groupings – (*one big, two small angles*) and (*one small, two big angles*) – result in $IUF_0 > IUF_2$ and $IUF_2 > IUF_0$ only when combined with the current magnitude

unbalance usually present on this feeder (i.e. a very lightly loaded A phase accompanied by more heavily loaded B and C phases). It should not be construed as a general expectation as other feeders will not necessarily have the same current magnitude unbalance. The principal idea here is that the difference between IUF_0 and IUF_2 can be explained by looking at the relative angles between the current phasors and by extension the relative power factors of loads on each phase.

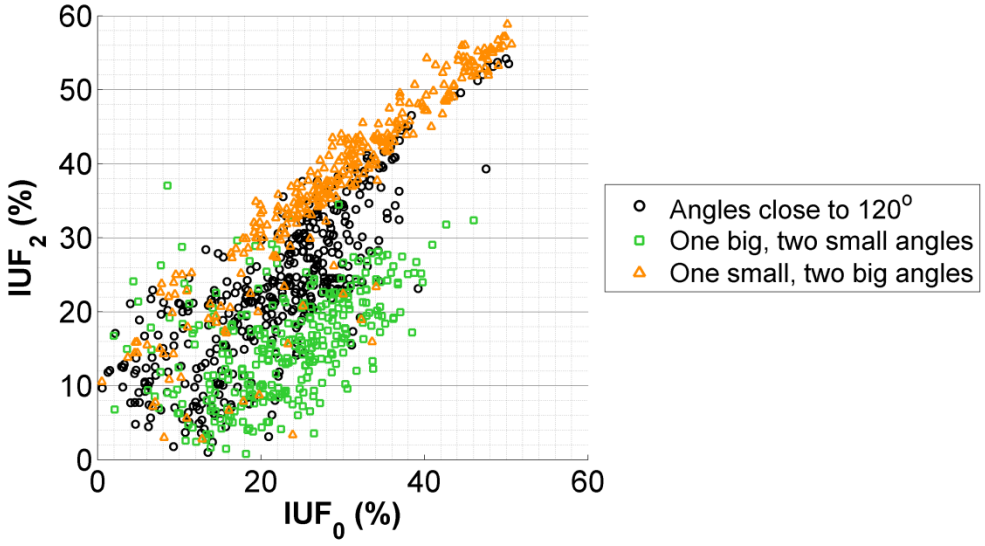

Figure 6.31: Relationship between negative and zero sequence current unbalance factors (static balancer de-energised)

6.9.2 Localised indicators of unbalance

The concept of localised indicators of unbalance was introduced in Chapter 2 as a difference between the consumer and network perspectives to unbalance. The ideas put forward there can be observed in relationships between the sequence voltage unbalance factors and the other sequence unbalance factors.

Relationship between zero voltage unbalance factor and other sequence unbalance factors

The plot of Figure 6.32 shows the dependence of the zero sequence voltage unbalance to the zero sequence current unbalance factor of the rural feeder. It demonstrates that:

- there is a positive correlation between the zero sequence current unbalance factor and the zero sequence voltage unbalance factors at the start and at the end of the feeder; and

- at the end of the feeder, the zero sequence voltage unbalance factor is more measureable and so can be used as a localised indicator of unbalance.

No similar relationship was evident either between VUF_0 and IUF_2 or between VUF_0 and VUF_2.

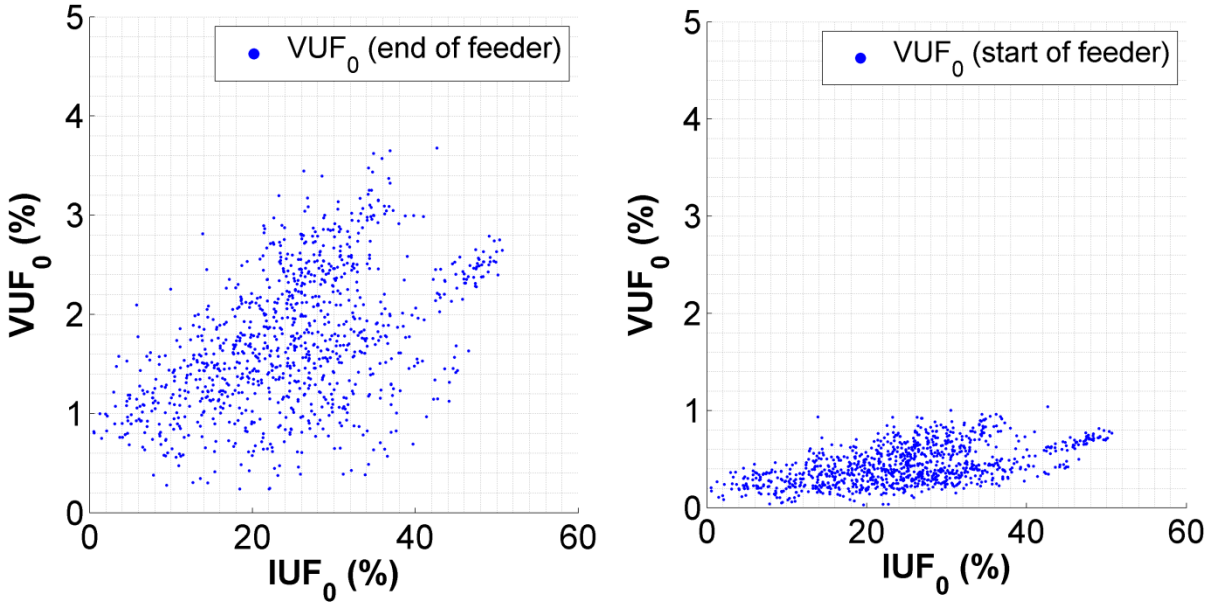

Figure 6.32: Relationship between zero sequence voltage and current unbalance factors at the (a) end and (b) start of the feeder

Relationship between negative sequence voltage unbalance factor and other sequence unbalance factors

Plots of negative sequence voltage unbalance factor versus either zero or negative sequence current unbalance factors (not shown) displayed no correlation. The negative sequence voltage unbalance factor was also found to vary independently of the zero sequence voltage unbalance factor.

Therefore, from these measurements the negative sequence voltage unbalance factor is not a localised indicator of unbalance.

6.9.3 Similarities to consumer demand profiles

The daily profiles of the sequence voltage unbalance factors were shown in Figure 6.28.

Interestingly, both show strong resemblance to typical demand profiles – a domestic load profile in the case of VUF_2 and a commercial load profile in the case of VUF_0.

This may be the result of a peculiarity with this feeder, in that commercial consumers are all located at the end of the feeder where the VUF_0 will be at its highest. This observation is important as it indicates that the behaviour of consumers may influence the profile shapes of the sequence voltage unbalance factors.

6.9.4 Phase-neutral voltage magnitudes and the zero sequence current unbalance factor

A histogram of all the phase-neutral voltage magnitudes (i.e. all three phases) is shown in Figure 6.33. Each bar is subdivided to show the number of readings to which either $IUF_0 > IUF_2$ (black portion) or $IUF_2 > IUF_0$ (yellow portion).

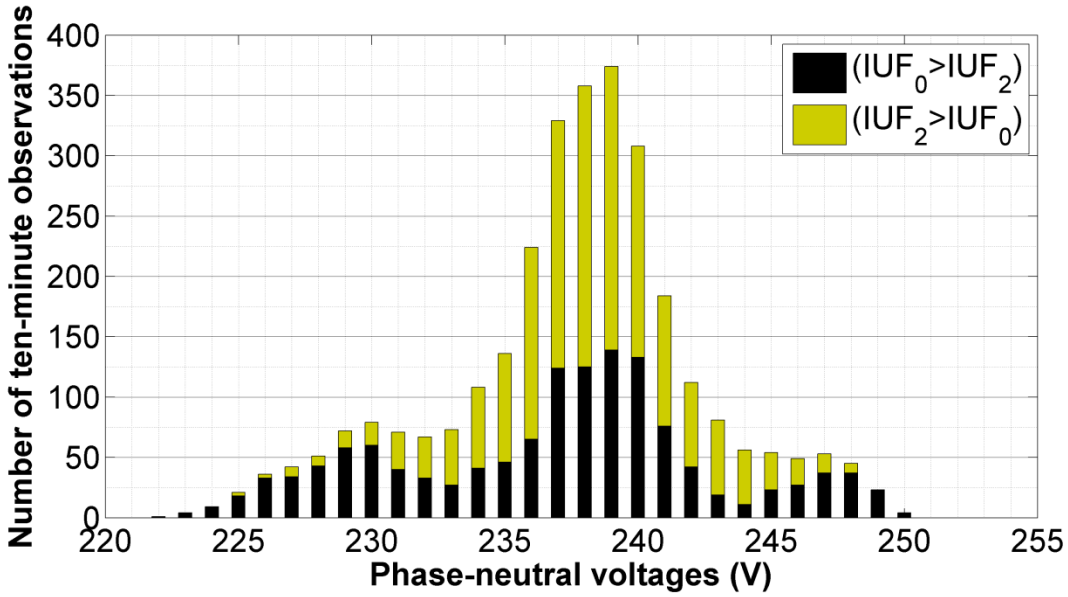

Figure 6.33: Stacked histogram of all phase-neutral voltages over a week showing voltages at extremities are more likely because of higher zero sequence current unbalance (static balancer de-energised)

For this distribution there are several peaks evident. The most prominent being the middle peak close to nominal voltage. There are also two smaller peaks at the higher and lower voltage extremities.

The middle peak – near to nominal voltage – can be associated with readings in which $IUF_2 > IUF_0$. This is seen by the widening of the yellow bars towards the middle of the distribution. The two smaller peaks on the other hand, can be associated with instances in which there are a greater portion of readings in which $IUF_0 > IUF_2$. This is seen by the widening of the black bars towards the extremities.

The mean and standard deviations are presented in Table 6.6. These values also show that the phase-neutral voltage magnitudes are on average closer to nominal and have less variation when $IUF_0 < IUF_2$. This demonstrates the importance of reducing IUF_0.

Phase-neutral voltage magnitudes:	Mean (V)	Standard deviation (V)
$IUF_0 > IUF_2$ (black portion)	236.9	±6.0
$IUF_0 < IUF_2$ (yellow portion)	238.1	±3.7
All readings	237.6	±4.8

Table 6.6: Means and standard deviations of phase-neutral voltage magnitudes (static balancer de-energised)

6.10 Quantified benefits of using a static balancer on this rural feeder

The benefits of using the static balancer can be quantified by comparing the effects of unbalance as identified in Figure 2.13 for the weeks with it de-energised and energised. It is difficult however, to make this comparison a fair one, as the consumer demand profiles over one week to another will not be the same (both in terms of the total across the three phases and in terms of the individual phases). The effects therefore cannot simply be quantified over one week and then compared to the next.

In the sections which follow, quantification of the effects is carried out either with respect to IUF_0 of the total consumer current ($I_{consumers}$) or to the total active power delivered to the consumers ($P_{consumers}$). The preference though, was to quantify the effects with respect to the former. The choice of using either $I_{consumers}$ or $P_{consumers}$ was contingent upon whether or not there was a strong correlation to the network effect. Both $I_{consumers}$ and $P_{consumers}$ must be calculated and will be explained as they are used.

The quantified benefits are summarised in Table 6.7. They are discussed in depth in the sections which follow.

			Static balancer		Meters used
			De-energised	Energised	
			4th to 10th March, 2013	18th to 24th February, 2013	
Unbalance indicators (95th percentile values from section 6.7):					
Current unbalance factors	IUF_0		44.6 %	22.8 %	Fluke1
	IUF_2		52.0 %	45.7 %	
Voltage unbalance factors	VUF_0		2.9 %	1.2 %	Fluke2
	VUF_2		3.6 %	3.9 %	
Effects of unbalance:					
(a) Network utilisation	NU_PRCC	(at $max(I_{p(1)})$)	20.7 %	12.3 %	Fluke1
		(when $IUF_0 = 100\%$)	26.9 %	15.0 %	
	pf_e (when $IUF_0 = 100\%$)		0.42	0.81	
(b) Neutral currents	I_n (when $IUF_0 = 100\%$)		97 A	28 A	
(c) Ground currents	I_g		*Not measured but as seen in section 4.5 I_g like I_n is directly proportional to IUF_0.*		
(d) Losses	Network energy lost as a percentage of energy delivered to all consumers.		1.5 %	1.4 %	All meters
	Total energy lost as a percentage of energy delivered to all consumers.		3.6 %	4.0 %	
(e) Neutral-point shifting	Using V_0 as $V_{n/g}$ cannot be measured directly.	(at $mean(\mathrm{IUF_0})$)	4.2 V	1.4 V	Fluke2
		(when $IUF_0 = 100\%$)	15.2 V	5.1 V	
(f) Phase-neutral voltages	V_{an}(mean)		238.4 V	235.1 V (-3.2 V)	Fluke2
	V_{bn}(mean)		241.2 V	242.5 V (+1.3 V)	
	V_{cn}(mean)		233.1 V	231.9 V (-1.2 V)	
(g) Voltage regulation	$VR_{indicator}$(95th percentile)		14.6 %	12.9 % (-1.7 %)	
Key: Improvement (of more than 40 %) ; No real change observed ; Degradation (of more than 40%). Note this key does not apply to (f). All voltages were within UK statutory limits (230 V -6%/+10%).					

Table 6.7: Effects of unbalance with the static balancer de-energised and energised

6.10.1 Network utilisation

The improvement in network utilisation was quantified for the entire feeder load by using the Fluke1 meter readings. The following sections look at the potential released current capacity and the effective power factor.

Potential released current capacity (NU_PRCC)

The NU_PRCC, which was explained in section 4.3 and depicted in Figure 4.2, represents how far off the available headroom is from the ideal headroom (balanced phase currents) at any point in time. It is defined by equation (4.1) as the difference between maximum and average (or ideal) current flows with respect to the feeder rating (220 A). Therefore a lower value indicates that the feeder is operating nearer to the ideal.

The daily profiles of NU_PRCC are shown in Figure 6.34 (a) and Figure 6.34 (b) for the weeks where the static balancer was de-energised and energised, respectively. It is clear that there is a reduction when the static balancer is energised, indicating an improvement in network utilisation and therefore a release in capacity.

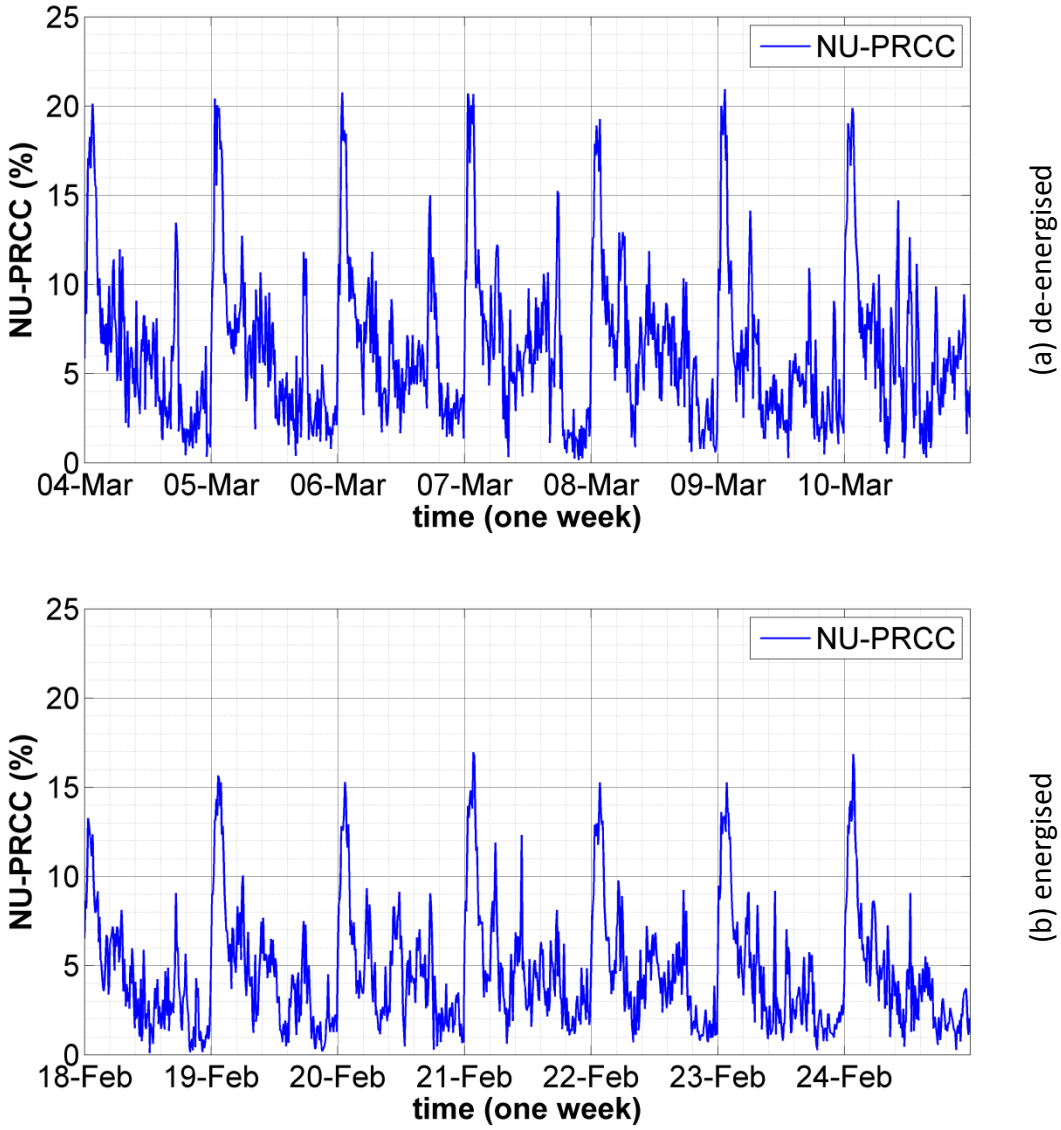

Figure 6.34: NU_PRCC daily profiles for weeks with static balancer (a) de-energised and (b) energised.

Now, to quantify the improvement in NU_PRCC, it can be plotted with respect to the IUF_0 of the total consumer current ($I_{consumers}$). This current refers to the total phase and neutral currents drawn by all the consumers on the feeder. It is measured directly by the Fluke1 meter (at the start of the feeder) only when the static balancer is de-energised. With the static balancer energised however, the homopolar currents introduced by it are included in the readings of the Fluke1 meter. In that case, the total consumer current may be calculated using the measurements from all three meters:

$$I_{consumers}(t) = I_{p(7)}(t) + \left(I_{p(1)}(t) - I_{p(6)}(t)\right) \quad (6.7)$$

where $p = a, b, c$ and $t = 1 \ldots 1008$ 10-minute readings.

The IUF_0 of $I_{consumers}$ is then found using equation (2.3).

The plots of NU_PRCC versus IUF_0 of the total consumer current ($I_{consumers}$) are shown in Figure 6.35.

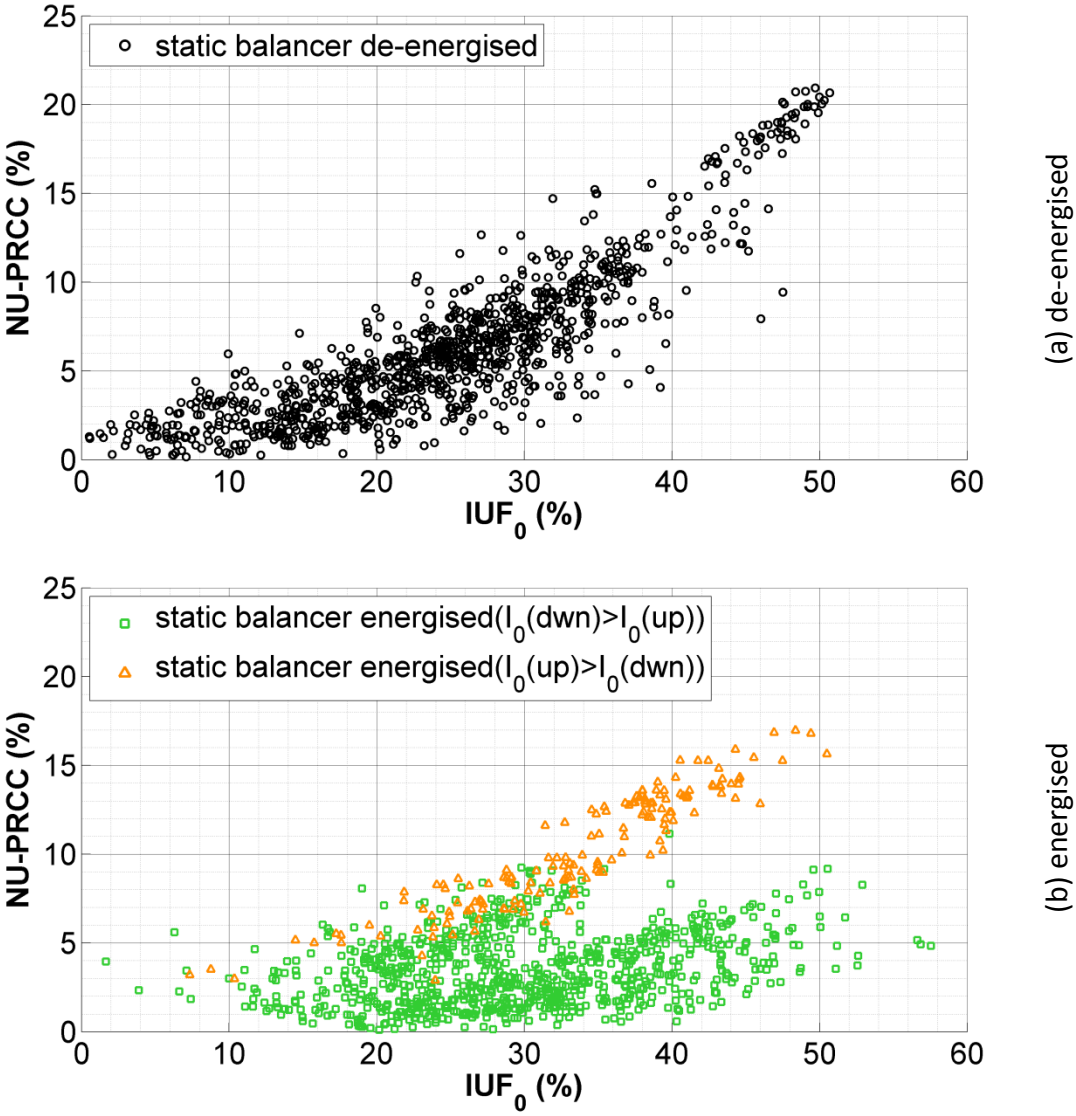

Figure 6.35: Scatter plots of NU_PRCC versus IUF_0 for weeks with static balancer (a) de-energised and (b) energised.

The black dots of Figure 6.35 (a) give readings taken with the static balancer de-energised and the green and orange dots of Figure 6.35 (b) with it energised. The green dots are those readings (with the static balancer energised) for which the zero sequence current drawn by the downstream consumers was greater than that drawn by those upstream (the opposite is true for the orange dots).

It can be observed that the black and orange readings are both higher than the green readings. These differences can be quantified by finding the gradients of the lines formed by each set of readings. For each set, the NU_PRCC appears directly proportional to IUF_0 such that they follow straight lines of the form:

$$NU\_PRCC = m_1(IUF_0/100) \quad (6.8)$$

This equation has been expressed such that, the gradient m_1, gives the NU_PRCC when $IUF_0 = 100\ \%$. They are given in Table 6.8 for each line.

	m_1
Static balancer de-energised	**26.9**
Static balancer energised	**15.0**
- Green dots ($I_{0(down)} > I_{0(up)}$)	**11.5**
- Orange dots ($I_{0(up)} > I_{0(down)}$)	**30.7**

Table 6.8: Gradients expressed to give NU_PRCC when $IUF_0 = 100\ \%$.

With the static balancer energised the NU_PRCC at $IUF_0 = 100\ \%$ reduced significantly from 26.9 % to 15 % (gradient of orange and green readings combined). This quite significant drop of 11.9 % means that the difference between maximum and average (or ideal) current flows with respect to the feeder rating (220 A) reduces by 26.2 A. This is quite significant, considering the maximum feeder currents are in the neighbourhood of 90 A.

Also, from the lower gradient of the green readings (11.5 % compared to 30 % of the orange readings) it appears that the static balancer may be better at compensating the downstream loads than the upstream ones.

Quantifying the difference at times of heavy loading

The NU_PRCC is of greater significance when the network is at most risk i.e. when the phase conductors are most heavily loaded. Table 6.9 shows the improvement in NU_PRCC at these times using two approaches.

The first is to look at the reduction in NU_PRCC at the time of maximum feeder current (seen at Fluke1). Again, the reduction is quite significant (20.7 % to 12.3 %). This is a drop of 8.4 % which works out to be a difference of 18.5 A between the maximum and average current flows.

The second is a more statistical approach. It involves sorting all the phase currents (seen by Fluke1) in descending order so as to produce a duration curve, and then finding the average of the corresponding NU_PRCC values above the 95th percentile (this is illustrated in Figure 6.36). It can be seen that with the static balancer there is a reduction in both the average and standard deviation of the NU_PRCC.

	NU_PRCC		
	Above 95th percentile		At time of maximum current
	Mean	Standard deviation	
Static balancer de-energised	13.7 %	±4.1 %	20.7 % (@ 90.9 A)
Static balancer energised	10 %	±3.5 %	12.3 % (@ 86.2 A)

Table 6.9: NU_PRCC at times of heavy loading with static balancer de-energised and energised.

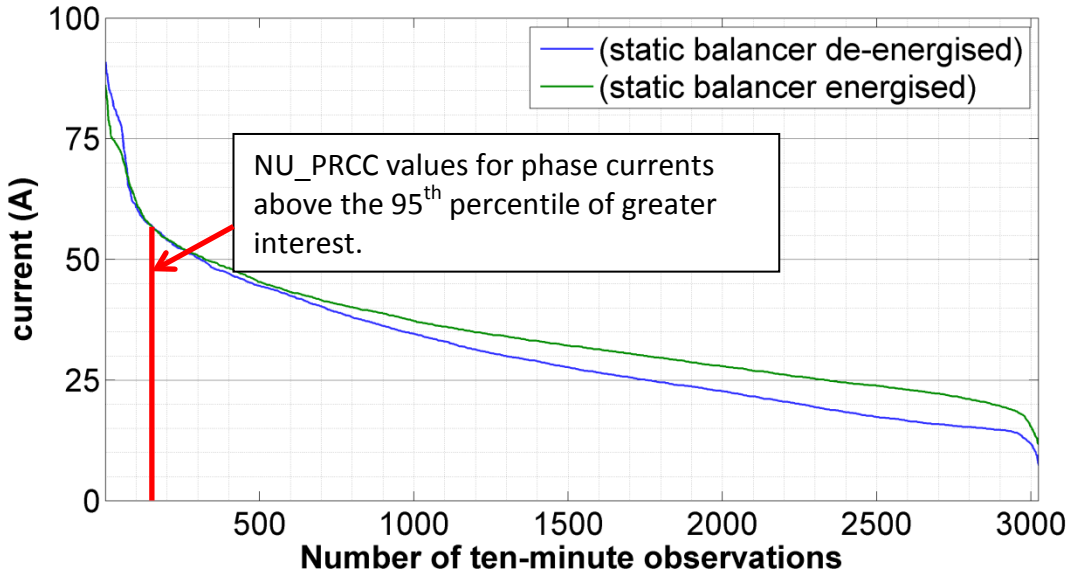

Figure 6.36: Duration curve of all phase currents

Effective power factor

The effective power factor was explained in section 4.3 and depicted in Figure 4.3. Its definition comes from the IEEE 1459 [75]. It is the ratio of the active power to effective apparent power. The latter, given by equation (4.2), equates to an active power that if transmitted, would result in the same current impact (i.e. losses) and voltage impact (i.e. insulation effects and no-load losses).

The daily profiles of the effective power factor are shown in Figure 6.37. With the static balancer energised, there is a significant improvement in effective power factor,

especially during the day. As can be seen, before it ranged between 0.75 and 0.99 and after between 0.90 and 0.99. It also appears to fluctuate less.

Also, it can be observed that just after midnight, there are one or two drops which occur recurrently day after day. These drops still occurred after the static balancer was energised but were much less - 0.66 before and 0.79 after.

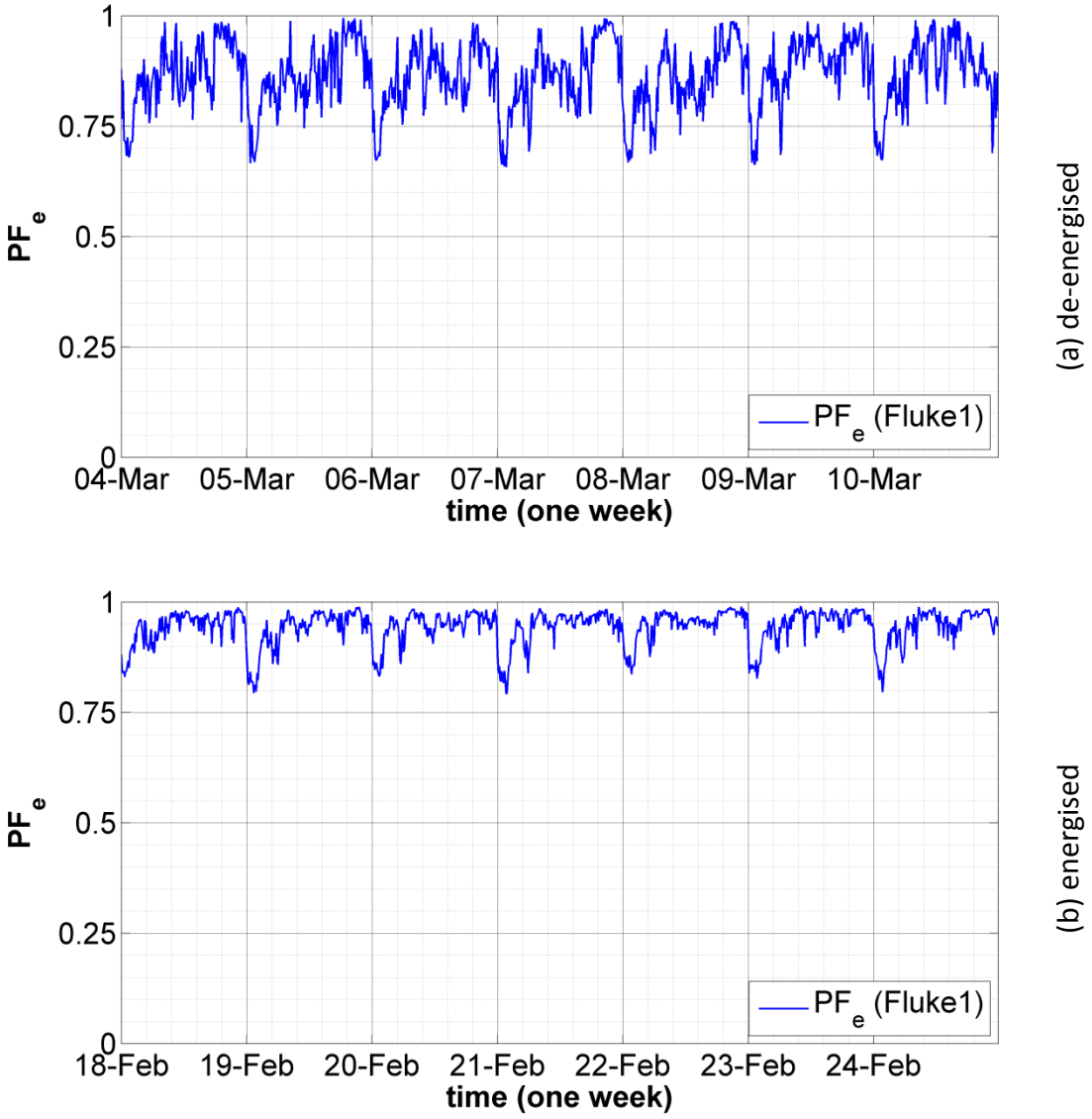

Figure 6.37: Effective power factor profiles for weeks with static balancer (a) de-energised and (b) energised.

The improvement in PF_e can be quantified by plotting it against IUF_0 as shown in Figure 6.38. Again, green and orange dots are readings taken with the static balancer energised and black dots with it de-energised. Also, the green readings highlight when

the zero sequence current drawn by downstream consumers was greater than that drawn by the upstream consumers (for the orange readings the opposite is true).

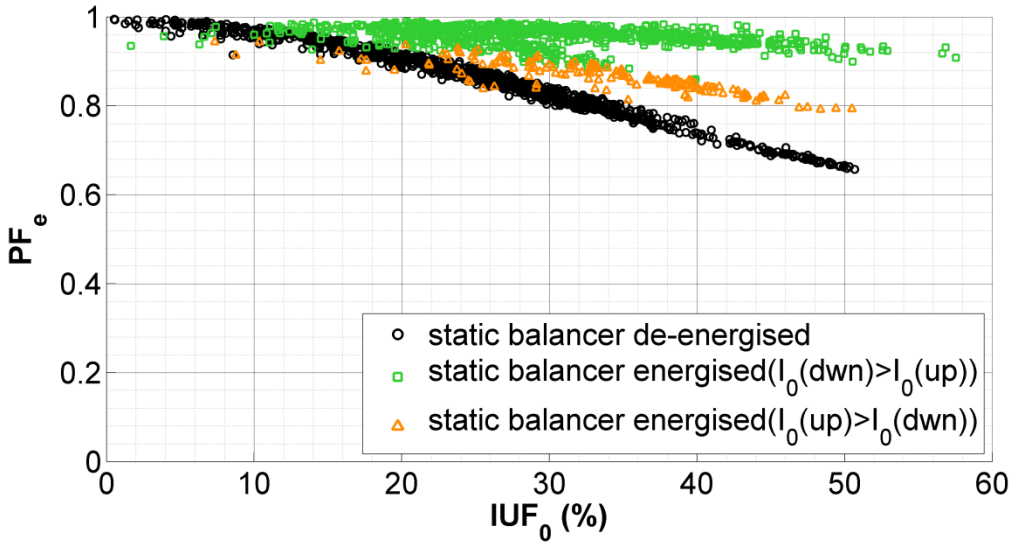

Figure 6.38: Scatter plots of pf_e versus IUF_0

It is clear, from the much gentler gradients of the green and orange dots, that there is a significant improvement in PF_e with IUF_0 when the static balancer was energised. Further, like the plots of NU_PRCC shown previously in Figure 6.35, the improvement appears to be maximised if the zero sequence currents are greater downstream of the static balancer (seen by the even gentler gradient of green readings compared to orange ones).

Now, these differences may be quantified by approximating, for each set of readings, linear relationships of the form:

$$PF_e = 1 - m_2(IUF_0/100) \qquad (6.9)$$

This equation has been expressed such that the gradients m_2 (which are given in Table 6.10) will correspond to give the drop in PF_e (from unity) when $IUF_0 = 100\ \%$. The effective power factors at $mean\ (IUF_0)$ are also given.

	m_2	PF_e when $IUF_0 = 100\%$	PF_e at $mean(IUF_0)$
Static balancer de-energised	**0.58**	**0.42**	**0.84**
Static balancer energised	**0.19**	**0.81**	**0.95**
- Green dots ($I_{0(down)} > I_{0(up)}$)	**0.14**	**0.86**	**0.96**
- Orange dots ($I_{0(up)} > I_{0(down)}$)	**0.40**	**0.60**	**0.89**

Table 6.10: Gradients expressed to give drop in PF_e when $IUF_0 = 100\ \%$ and PF_e at $mean(IUF_0)$.

With the static balancer energised the PF_e drops to only 0.81 at $IUF_0 = 100\ \%$ and 0.95 at $mean(IUF_0)$. This is significantly better than the corresponding values of 0.42 and 0.84 without the static balancer.

Also, the difference between the green and orange readings is significant. The PF_e drops to only 0.86 at $IUF_0 = 100\ \%$ and 0.96 at $mean(IUF_0)$ if there is greater unbalance downstream of the static balancer.

6.10.2 Neutral current

The neutral current between the start of the feeder and the static balancer position is significantly less with the static balancer energised. This can be seen by comparing the daily profiles taken from the Fluke1 measurements shown in Figure 6.39 (a) with the static balancer de-energised, to Figure 6.39 (b) with the static balancer energised.

In addition to a reduction in neutral current (average value was reduced from 23.4 A to 9 A) there also appears to be less variability during the day.

Also, shortly after midnight, there are brief increases in the neutral current which occur; these are reduced with the static balancer energised. It should be noted these brief increases coincide with the observed drops in the effective power factor mentioned previously.

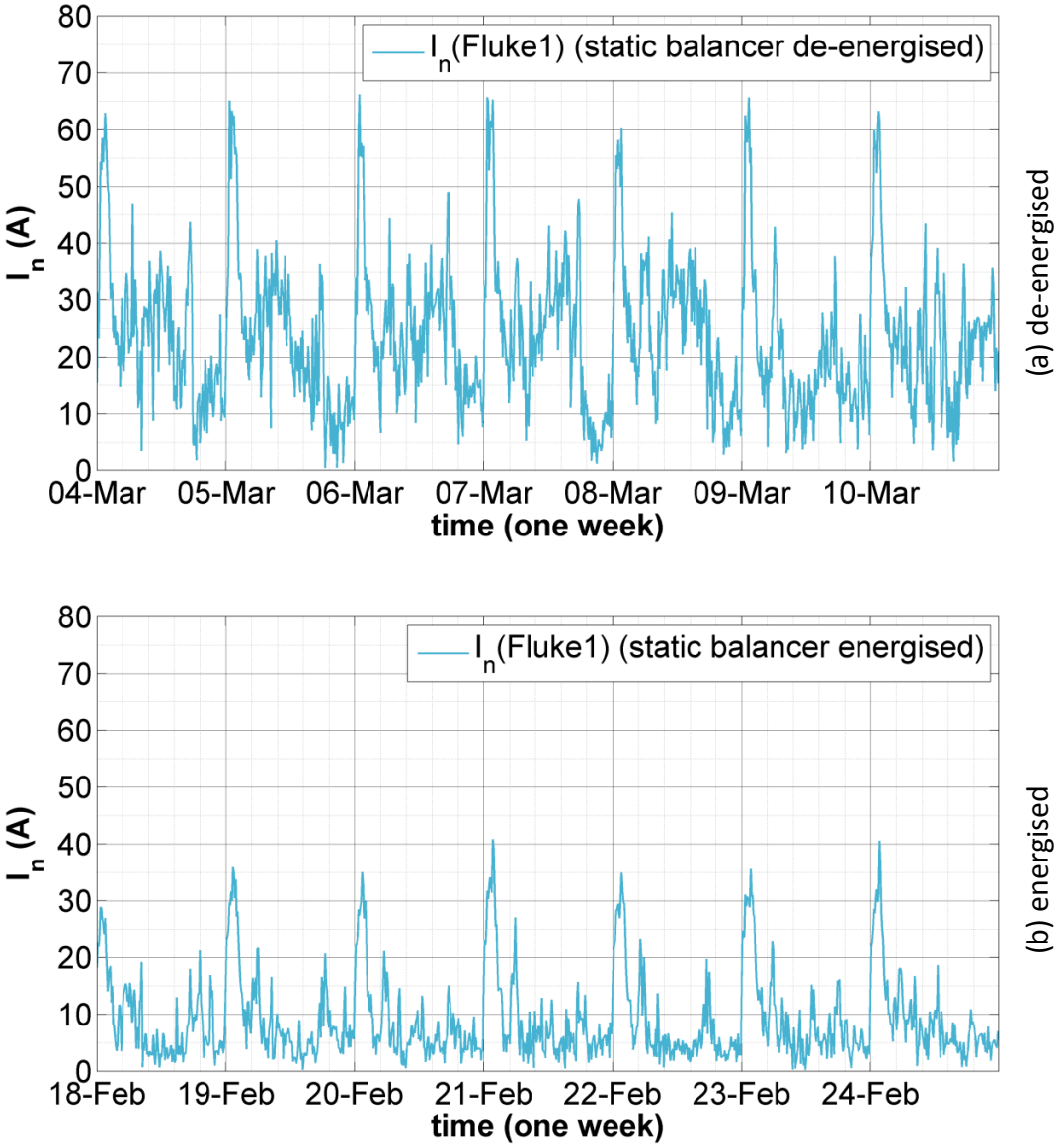

Figure 6.39: Profiles of neutral current (Fluke1) for weeks with static balancer (a) de-energised and (b) energised.

The reduction in neutral current can be quantified by plotting it against IUF_0 as shown in Figure 6.40. As before, the black readings are with the static balancer de-energised and the green and orange readings are with it energised.

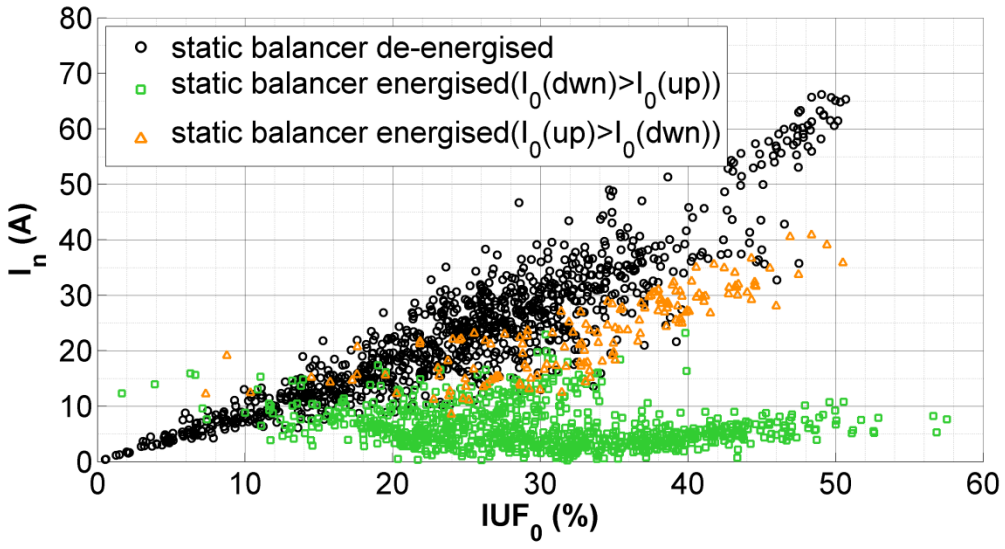

Figure 6.40: Scatter plots of I_n versus IUF_0

Now, it is known that the neutral current is directly proportional to the zero sequence current and likewise to the zero sequence current unbalance factor. Therefore, each set of readings will follow a line passing through the origin:

$$I_n = m_3(IUF_0/100) \tag{6.10}$$

The values of m_3 given in Table 6.11, are the neutral current at $IUF_0 = 100\ \%$. Also given are the neutral current at $mean\ (IUF_0)$.

	m_3	I_n at $mean(IUF_0)$
Static balancer de-energised	**97.3 A**	**26.8 A**
Static balancer energised	**28.2 A**	**7.8 A**
- Green dots ($I_{0(down)} > I_{0(up)}$)	**18.8 A**	**5.2 A**
- Orange dots ($I_{0(up)} > I_{0(down)}$)	**70.2 A**	**19.3 A**

Table 6.11: Gradients expressed to give I_n when $IUF_0 = 100\ \%$ and I_n at $mean(IUF_0)$.

With the static balancer energised, the neutral current at most times (green readings) is kept below 20 A, even with very high IUF_0. It goes beyond this mostly when the zero sequence current of upstream consumers is greater than those downstream (orange readings). At $IUF_0 = 100\ \%$, the neutral current for the green and orange readings are 18.8 A and 70.2 A respectively. With the static balancer de-energised, it is much greater, 97.3 A.

6.10.3 Losses

The losses on the feeder can be estimated from the measurements taken by all three meters. The following sections present the approach and assumptions made in doing this.

Estimating network power losses

To estimate the network power losses, knowledge of the consumers – their placement and phases connected – is tied to the location of the meters on the feeder. This information was presented earlier in Figure 6.4 as a single-line diagram of the feeder using the nomenclature described in Chapter 3. The following expressions are with reference to that single-line diagram.

The network power loss (kW), averaged over each ten minute interval of a week (i.e. $t = 1 \ldots 1008$ ten minute averages), is given by:

$$Network\ power\ loss\ (t) = \left(\sum_{l=1\ldots9}\left(\sum_{p=a,b,c,n}\left(\left|I_{p(l)}(t)\right|\right)^2 R_{pp(l)}\right)\right)/1000 \qquad (6.11)$$

where

$R_{pp(l)}$ are the resistances of the phase and neutral wires ($p = a, b, c, n$) of branch segment (l). The impedances for all these overhead line and cable types are calculated in Appendix A.

$I_{p(l)}$ are the currents flowing on the phase and neutral wires ($p = a, b, c, n$) of branch segment (l).

The network energy loss (kWh) over the week can then be found from the area under this power loss curve given by:

$$Network\ energy\ loss\ = \sum_{t=1}^{1008}\big(Network\ power\ losses(t)\big)(1/6) \qquad (6.12)$$

From equation (6.11) it is clear that the currents on each branch segment will be needed. However, the currents on only four of the nine branch segments ($(l1)$, $(l5)$, $(l6)$ and $(l7)$) are known directly from measurements taken by the Fluke

and Ametek meters (as shown in Figure 6.4). The current flows on the remaining branch segments must be estimated. To do this it is assumed that:

- For $(l2)$ to $(l4)$, as there are four domestic consumers connected to phase A between Fluke1 and the Ametek, the current drawn by each domestic consumer on phase A is given by:

  $$I_{L(domestic-A)} = \frac{I_{a(1)} - I_{a(6)}}{4} \quad (6.13)$$

  And similarly, as there are three domestic consumers on phase B, the current drawn by each domestic consumer on phase B is given by:

  $$I_{L(domestic-B)} = \frac{I_{b(1)} - I_{b(6)}}{3} \quad (6.14)$$

- For $(l8)$ and $(l9)$, the current drawn by the Post Office and the group of consumers at $j9$ are assumed equal and the current drawn by the two domestic consumers on phase B are assumed to be the same as $I_{L(domestic-B)}$. Using these assumptions and the Fluke2 current measurements, the current drawn by the Post Office is given by:

  $$I_{La(PO)} = I_{a(7)}/2 \quad (6.15a)$$

  $$I_{Lb(PO)} = \left(I_{b(7)} - 2I_{L(domestic-B)}\right)/2 \quad (6.15b)$$

  $$I_{Lc(PO)} = I_{c(7)}/2 \quad (6.15c)$$

Now, for these equations the current angles of branch segment $(l6)$ are needed. This segment is measured by the Ametek meter though, which as mentioned previously, stores only current magnitudes. Therefore, further assumptions must be made. They will depend on whether the static balancer is energised or de-energised. If it is de-energised, it can be assumed that these angles will be the same as those measured by Fluke 2 (as there are no consumers between the meters). If however, the static balancer is energised, the angles of the calculated upstream currents found in section 6.8 are assumed.

Following these assumptions, the current flows on branch segments can be approximated using the equations presented in Table 6.12. These assumptions are expected to have little effect to the approximation of losses done here (as well as the network simulations done later in chapter 7), since the currents seen on four of the

nine branch segments will exactly match those measured. Moreover, this is a relatively short feeder. The more significant source of error will be in the measurement errors, as discussed earlier in section 6.6.

Segment number	Phase and neutral currents	
1	$\boldsymbol{I_{p(1)}}$ where $\boldsymbol{p = a, b, c, n}$	***Fluke 1***
2	$\boldsymbol{I_{a(1)} - I_{L(domestic-A)}}$ $\boldsymbol{I_{b(1)}}$ $\boldsymbol{I_{c(1)}}$ $\boldsymbol{I_{n(1)} + I_{L(domestic-A)}}$	
3	$\boldsymbol{I_{a(1)} - 2I_{L(domestic-A)}}$ $\boldsymbol{I_{b(1)} - I_{L(domestic-B)}}$ $\boldsymbol{I_{c(1)}}$ $\boldsymbol{I_{n(1)} + 2I_{L(domestic-A)} + I_{L(domestic-B)}}$	
4	$\boldsymbol{I_{a(1)} - 3I_{L(domestic-A)}}$ $\boldsymbol{I_{b(1)} - 3I_{L(domestic-B)}}$ $\boldsymbol{I_{c(1)}}$ $\boldsymbol{I_{n(1)} + 3I_{L(domestic-A)} + 3I_{L(domestic-B)}}$	
5	$\boldsymbol{I_{p(5)}}$ where $\boldsymbol{p = a, b, c, n}$	***Ametek***
6	$\boldsymbol{I_{p(6)}}$ where $\boldsymbol{p = a, b, c, n}$	***Ametek***
7	$\boldsymbol{I_{p(7)}}$ where $\boldsymbol{p = a, b, c, n}$	***Fluke 2***
8	$\boldsymbol{I_{a(7)} - I_{La(PO)}}$ $\boldsymbol{I_{b(7)} - I_{Lb(PO)} - I_{L(domestic-B)}}$ $\boldsymbol{I_{c(7)} - I_{Lc(PO)}}$ $\boldsymbol{I_{n(7)} + I_{La(PO)} + I_{Lb(PO)} + I_{Lc(PO)} + I_{L(domestic-B)}}$	
9	$\boldsymbol{I_{a(7)} - I_{La(PO)}}$ $\boldsymbol{I_{b(7)} - I_{Lb(PO)} - 2I_{L(domestic-B)}}$ $\boldsymbol{I_{c(7)} - I_{Lc(PO)}}$ $\boldsymbol{I_{n(7)} + I_{La(PO)} + I_{Lb(PO)} + I_{Lc(PO)} + 2I_{L(domestic-B)}}$	

Table 6.12: Summary of measured and approximated phase and neutral currents

The other power losses include those on the static balancer and the distribution transformer. They are presented next before giving the tally of total power losses.

Estimating static balancer losses

If the static balancer is energised, then its own losses must be taken into account. This is given (in kW) by:

$$Static\ balancer\ power\ loss\ (t) = \left(\sum_{p=a,b,c}\left(\left|I_{Cp(l)}(t)\right|\right)^2 R_T + Iron\ losses_T\right)/1000 \quad (6.16)$$

where

$I_{Cp(l)}$ is current drawn by the static balancer. They are determined using equation (5.11) from the phase-neutral voltages measured by Fluke2 (as mentioned in section 6.8).

$Iron\ Losses_T$ is provided in design sheets from the manufacturer [81] - 118.2 W.

R_T is the winding resistance of the static balancer (from Table 5.2 – 0.1379 Ω).

Also, the additional energy losses due to the static balancer over a week (in kWh) will be given by:

$$Static\ balancer\ energy\ loss\ = \sum_{t=1}^{1008}\big(Static\ balancer\ power\ losses\ (t)\big)(1/6) \quad (6.17)$$

Estimating distribution transformer power losses

The power losses on the distribution transformer will reduce if the currents through it are more balanced. Now, to find this power loss, the total current through the distribution transformer is required. Estimating this total current however, is not possible, as the other two rural feeders were not measured. Therefore, assumptions must be made. One approach, which will give a very conservative estimate (in kW), is to assume that the distribution transformer supplies only this feeder:

$$Distribution\ transformer\ power\ loss\ (t) = \Big(\sum_{p=a,b,c}\big(\big|I_{p(1)}(t)\big|\big)^2 R_{DT} + Iron\ Losses_{DT}\Big)/1000 \quad (6.18)$$

where

$I_{p(1)}$ is total feeder current measured by Fluke1.

R_{DT} is the winding resistance of the distribution transformer. The winding resistance of the 315 kVA (11 kV / 415 V) is given in [10] as 0.009 Ω.

$Iron\ Losses_{DT}$ is also provided in [10] as 425 W.

The energy losses due to the distribution transformer over a week (in kWh) will be given by:

$$Distribution\ transformer\ energy\ loss\ = \sum_{t=1}^{1008}\big(Distribution\ transformer\ power\ loss\ (t)\big)(1/6) \quad (6.19)$$

Total power losses

Finally, the total power losses (in kW) comprise the power losses on the network plus that of distribution transformer and the static balancer (if it is energised):

$$Total\ power\ losses(t) = Network\ power\ losses(t) + Static\ balancer\ power\ losses(t) + Distribution\ transformer\ power\ losses(t) \quad (6.20)$$

And the total energy losses over the week (in kWh) is given by:

$$Total\ energy\ losses\ = \sum_{t=1}^{1008}(Total\ power\ losses(t))(1/6) \quad (6.21)$$

Estimated losses

Daily profiles of the power losses with the static balancer de-energised and energised are shown in Figure 6.41 (a) and (b), respectively. In Figure 6.41 (b) the static balancer power losses are also shown.

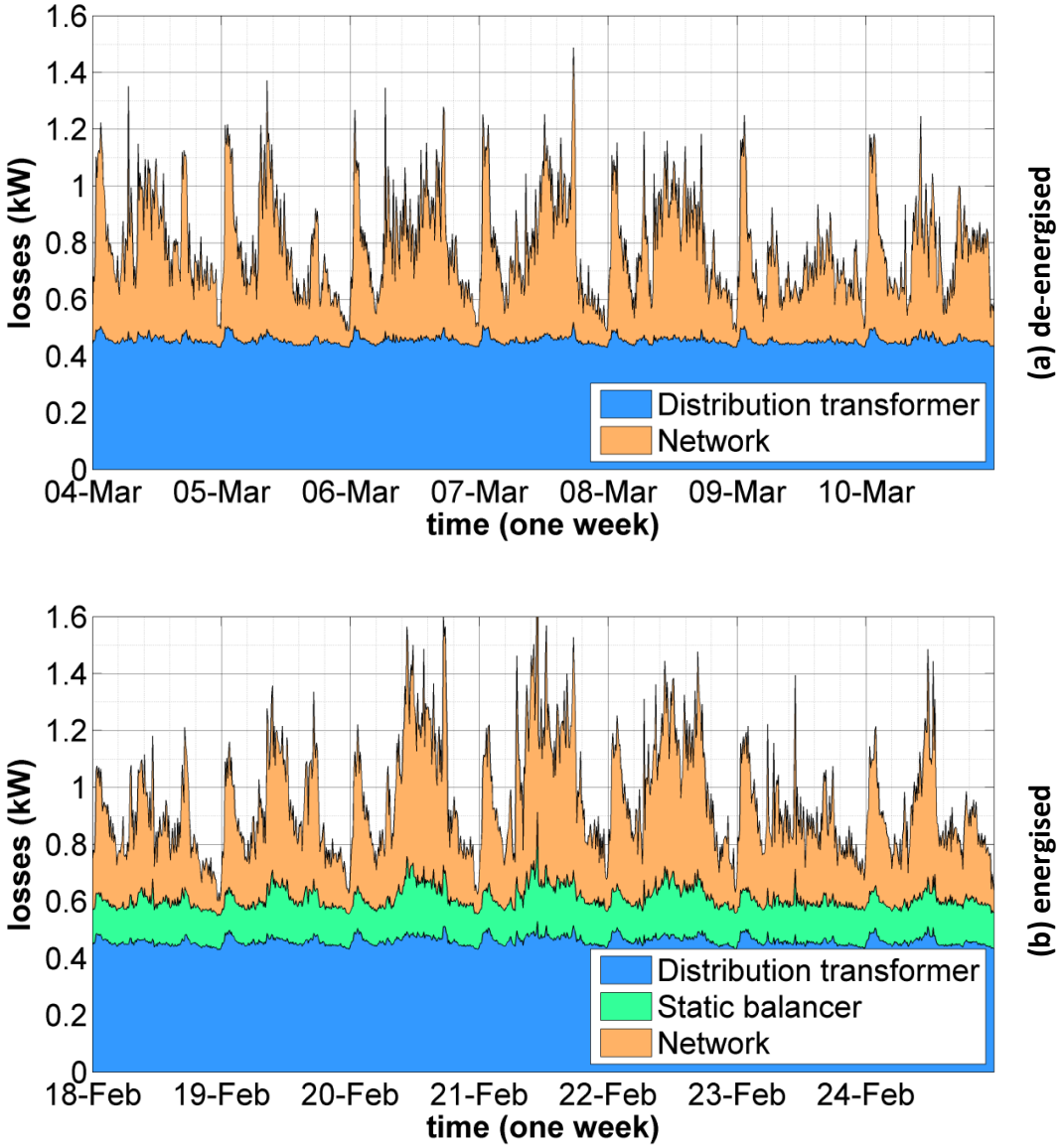

Figure 6.41: Profiles of power losses for weeks with static balancer (a) de-energised and (b) energised.

With the static balancer energised, there appears to be an overall increase in the total power losses. The static balancer power losses seem to contribute towards this. Also, it is clear that the total power losses are dominated by the distribution transformer. A significant portion of the losses in the static balancer and the distribution transformer can be attributed to their iron losses (118.2 W and 425 W respectively).

The benefit (if any) of using the static balancer to reduce losses can be quantified by finding the difference in the total energy lost as a percentage of the energy delivered, before and after the static balancer was energised. Ideally, for this to be a fair comparison, the profiles of power delivered to each consumer and therefore the total

energy delivered to all consumers should be the same for both weeks. Such a comparison is however, impossible when examining an actual feeder.

From these field measurements though, some assessment of the total energy lost as a percentage of the energy delivered can still be done.

The calculation of energy losses – network, static balancer and distribution transformer – was covered in the previous section. The calculated values are summarised in Table 6.13. Although there is an increase in the total energy losses with the static balancer energised, no real conclusions can be drawn from that as yet, since the energy delivered to all the consumers in each week would have differed.

	Energy lost (kWh)			
	Distribution transformer	Static balancer	Network	Total
Static balancer de-energised	77	0	55	132
Static balancer energised	77	25	57	159

Table 6.13: Energy delivered and energy lost

Now, the energy delivered must be found from the profile of active power delivered to all the consumers ($P_{consumers}$). This is found by subtracting network and static balancer power losses from the active power transfer seen by Fluke1:

$$P_{consumers}(t) = \sum_{p=a,b,c} re\left(V_{pn(1)}(t).I^{*}_{p(1)}(t)\right) - Network\ power\ losses(t) - Static\ balancer\ power\ losses(t) \quad (6.22)$$

where $p = a, b, c$ and $t = 1 \ldots 1008$ averaged ten-minute readings.

The energy delivered to all the consumers is then:

$$Energy\ delivered\ to\ all\ consumers\ = \sum_{t=1}^{1008}(P_{consumers}(t))(1/6) \quad (6.23)$$

The network and total energy lost as percentages of the energy delivered are presented in Table 6.14. The differences before and after the static balancer was energised for both of them are clearly very small.

	Energy delivered to all consumers (kWh)	Network energy lost as a percentage of energy delivered	Total energy lost as a percentage of energy delivered
Static balancer de-energised	**3654**	**1.5 %**	**3.6 %**
Static balancer energised	**4009**	**1.4 %**	**4.0 %**

Table 6.14: Network and total energy lost as percentages of energy delivered

The reason for such little change in the total energy lost as a percentage of the energy delivered is that the distribution transformer losses dominate the total losses. This is mainly due to its iron losses, which amounts to 71.4 kWh ($0.425 \times 24 \times 7$) of the 77 kWh given in Table 6.13 for both weeks. This is about half the total losses.

Additionally, the reason for the slight increase is due to the static balancer's losses. This too is mainly due to iron losses, 20 kWh ($0.1182 \times 24 \times 7$) of the 25 kWh given in Table 6.13.

Lastly, the network power losses as a percentage of the energy delivered decreased slightly. This was due to the reduction in current unbalance brought about by the static balancer. It is useful to investigate the static balancer's influence on the network power losses further by plotting it against $P_{consumers}$, as shown in Figure 6.42. The following observations can be made from this plot:

- the reduction in network power losses when the static balancer is energised is indeed very modest. This is seen by the slightly lower paths followed by the green and orange dots compared to that followed by the black dots; and
- unlike previous plots, where the green readings are associated with a greater reduction in effects of unbalance compared to the orange readings, it appears that in the case of network power losses, the opposite is true; if the zero sequence current of upstream consumers is greater than those downstream, the network losses are lower.

This last observation hints that the position of the static balancer in relation to the consumers can influence the network power losses.

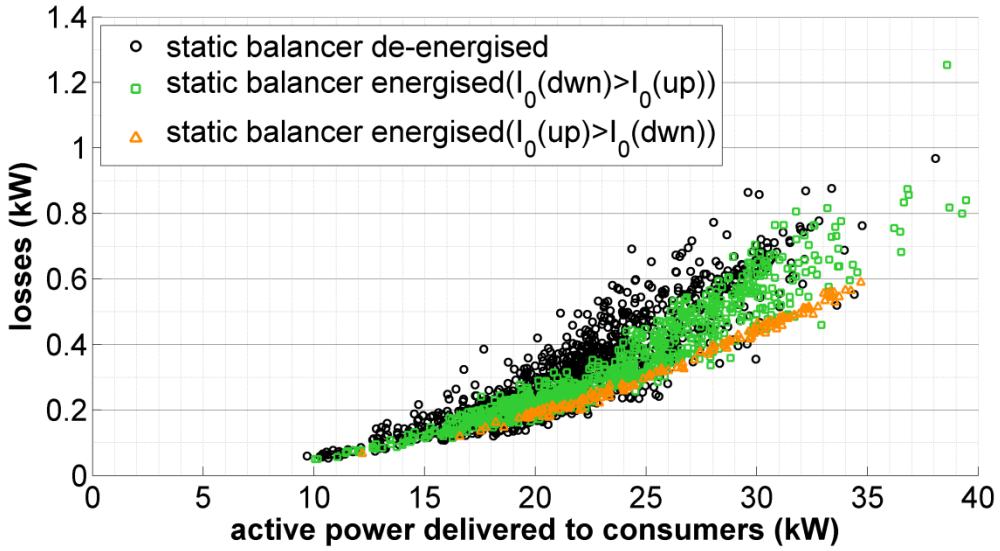

Figure 6.42: Network power losses versus active power delivered to consumers

6.10.4 Neutral-point shifting

As mentioned in section 4.3.4, the displacement of the neutral voltage $V_{n'g}$ cannot be measured directly but in its place the zero sequence voltage as given by equation (4.8) using phase-neutral voltages may be used. The relationship between them and the zero sequence current unbalance factor was seen in Figure 4.19.

The daily profiles of the zero sequence voltage seen at the Fluke1 and Fluke2 positions are shown in Figure 6.43 (a) with the static balancer de-energised and in Figure 6.43 (b) with the static balancer energised. There is a clear reduction at both positions but the more significant is that observed at the end of the feeder (Fluke2).

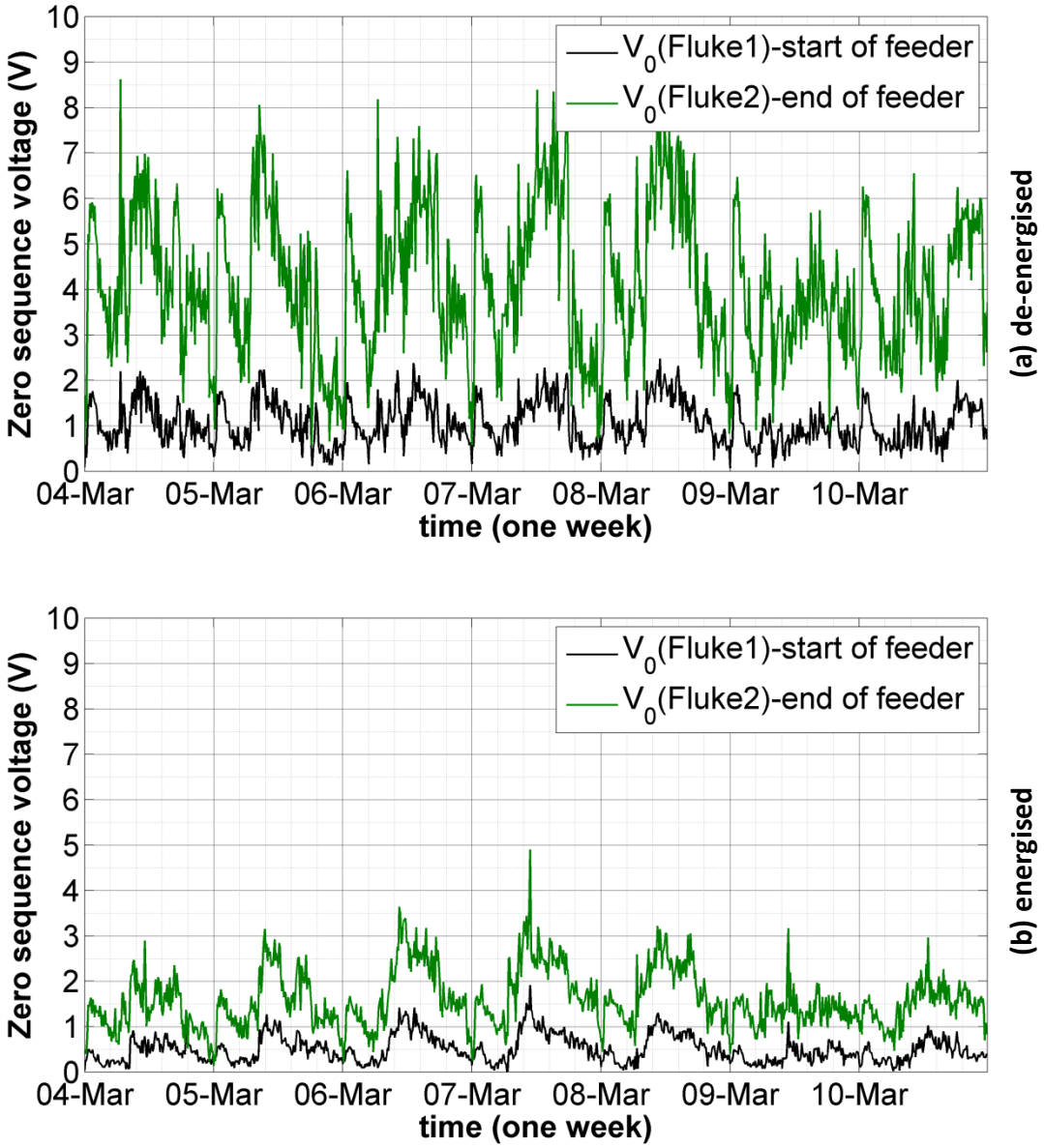

Figure 6.43: Profiles of zero sequence voltage (Fluke2) for weeks with static balancer (a) de-energised and (b) energised.

The reduction of the zero sequence voltage at the Fluke2 position can be quantified by plotting it against IUF_0 as shown in Figure 6.44. Again, the black readings are with the static balancer de-energised and the green and orange readings are with it energised. Like Figure 6.42 for network power losses, it appears that there is a greater reduction in zero sequence voltages when the zero sequence current of upstream consumers is greater than those downstream (as can be seen by the lower gradient of the orange readings).

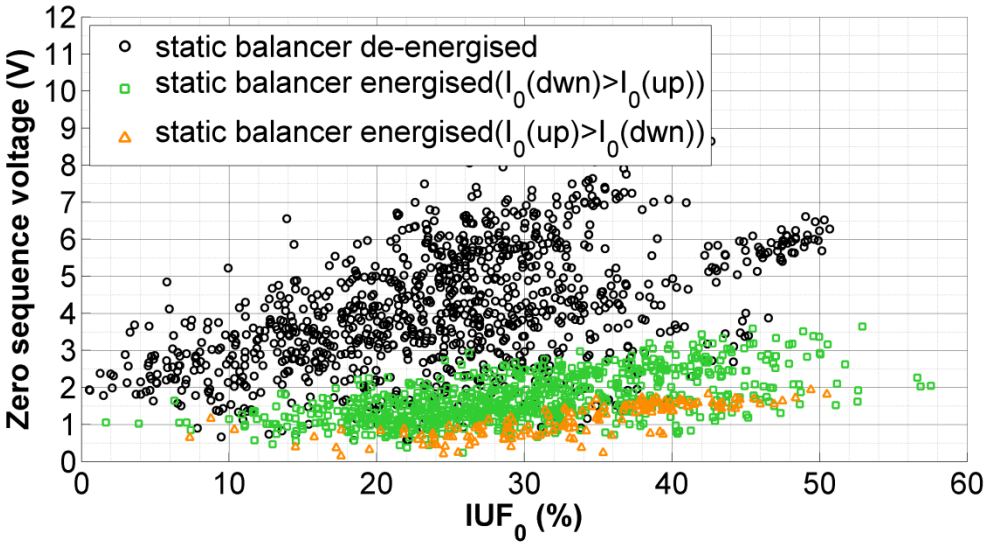

Figure 6.44: Scatter plots of $V_{0(j7)}$ versus IUF_0

Continuing, from Figure 6.44, it can be seen that the zero sequence voltage is directly proportional to the zero sequence current unbalance factor. Therefore, each set of readings can be approximated by a line passing through the origin:

$$V_{0(j7)} = m_4(IUF_0/100) \tag{6.24}$$

The values of m_4 given in Table 6.15 are the zero sequence voltage $V_{0(j7)}$ at $IUF_0 = 100$ % for each of set of readings. Also given are $V_{0(j7)}$ at $mean(IUF_0)$.

	m_4	$V_{0(j7)}$ at $mean(IUF_0)$
Static balancer de-energised	**15.2**	**4.2**
Static balancer energised	**5.1**	**1.4**
- Green dots ($I_{0(down)} > I_{0(up)}$)	**5.5**	**1.5**
- Orange dots ($I_{0(up)} > I_{0(down)}$)	**3.4**	**0.9**

Table 6.15: Gradients expressed to give $V_{0(j7)}$ when $IUF_0 = 100$ % and $V_{0(j7)}$ at $mean(IUF_0)$.

With the static balancer, the zero sequence voltage at $IUF_0 = 100$ % is 5.1 V, which is significantly less than the 15.2 V without it. There is also a very significant reduction in the zero sequence voltage at $mean(IUF_0)$, 1.4 V as opposed to 4.2 V.

6.10.5 Phase-neutral voltages

All phase-neutral voltage magnitudes measured by all three meters were within acceptable limits for weeks both before and after the static balancer was energised. There were therefore no violations in terms of low phase-neutral voltages on more heavily loaded phases (for this feeder phase C and then phase B) or high phase-neutral voltages on lightly loaded phases (for this feeder phase A). The effect of the very

unbalanced phase currents may have been averted because of the short length and therefore lower voltage drops along the feeder.

6.10.6 Voltage regulation

The 95th percentile values of the voltage regulation indicators ($VR_{indicator}$) were presented in Table 6.7. There was a reduction after the static balancer was energised but because of the short length of the feeder it was not very significant.

6.10.7 Summary of quantified benefits

The static balancer was very beneficial at improving network utilisation, reducing neutral current and neutral-point shifting. Improvements to all other effects of unbalance were either marginal or non-discernible.

Additionally, it was observed that the reduction to some network effects was dependent on the zero sequence currents of upstream consumers relative to that of downstream consumers.

6.11 Chapter conclusions

The gathering of measurements for the field trial involved a considerable amount of planning. And even with a measurement plan in place, solutions and assumptions were still needed to overcome practical limitations related to the capabilities and placement of various power quality meters. Such data on an actual low-voltage feeder at various positions are invaluable and well worth the effort, even if it were to be carried out not as a trial of the static balancer.

In this chapter, the analysis of the field measurements has led to the following outcomes:

- The validation of the static balancer model against field measurements;
- Further insight gained into the behaviour of the static balancer on the low-voltage network, particularly with regard to it influence on the relative angles

between current phasors, active and reactive power transfers and unbalance factors;

- The identification of the relative angles between current phasors as the reason for differing magnitudes of zero and negative sequence current unbalance factors; and
- The quantification of the benefits of using the static balancer (as summarised by Table 6.7). This adds practical numbers to its strengths and weaknesses, which can only be gained from a field trial.

7. Validation of proposed 5 x 5 approach to forward-backward sweep method against field measurements

7.1 Objectives

This chapter completes ***Objective (a)*** and ***Objective (c)***:

Objective (a): *To accurately model and solve very unbalanced low-voltage feeders.*

Objective (c): *To investigate the behaviour and quantify the benefits of the static balancer to low-voltage networks.*

By fulfilling the following tasks:

Objective (a)

Task (a.2): Model an actual low-voltage feeder (cables and lines) and validate network simulation results (voltages and currents) against field measurements.

Objective (c)

Task (c.6): Compare the benefits found from network simulations with the static balancer model to those from field measurements.

7.2 Overview

This chapter validates the proposed 5 x 5 approach to the forward-backward sweep method, covered in Chapter 3, against the field measurements taken on the rural

feeder with and without the static balancer. An overview of the chapter, showing the linkages to previous chapters, is depicted in Figure 7.1.

Now, this is actually the second validation of the proposed 5 x 5 approach. Previously, in Chapter 3, it had been validated using the test network of Figure 3.12, to ensure that it satisfied Kirchhoff's voltage and current laws and matched Matlab Simulink SimPowerSystems. This second validation, it should be noted, is rare in that it will be done against field measurements. This further emphasizes the value of these field measurements.

Previously, in Chapter 3, using the test network it had been shown that the 3 x 3 approach to the forward-backward sweep method produced differing phase-neutral voltages and zero sequence voltage unbalance factors from the proposed 5 x 5 approach. Additional differences, though minor, were also noted between neutral currents and losses found with the two approaches. This chapter investigates whether or not these differences are significant when compared against actual field measurements.

Most of the information needed to model the rural feeder has already been introduced in Chapter 6. Presented were - the single-line diagram and the overhead line and cable design data. The calculation of overhead line and cable impedances from the design data is covered in Appendix A. Also given were assumptions needed to estimate the current profiles of consumers on each phase (expressed in equations (6.13) to (6.15)).

Two additional aspects of the network model however are still needed – earth resistance values and load model type - and these are considered in the next section.

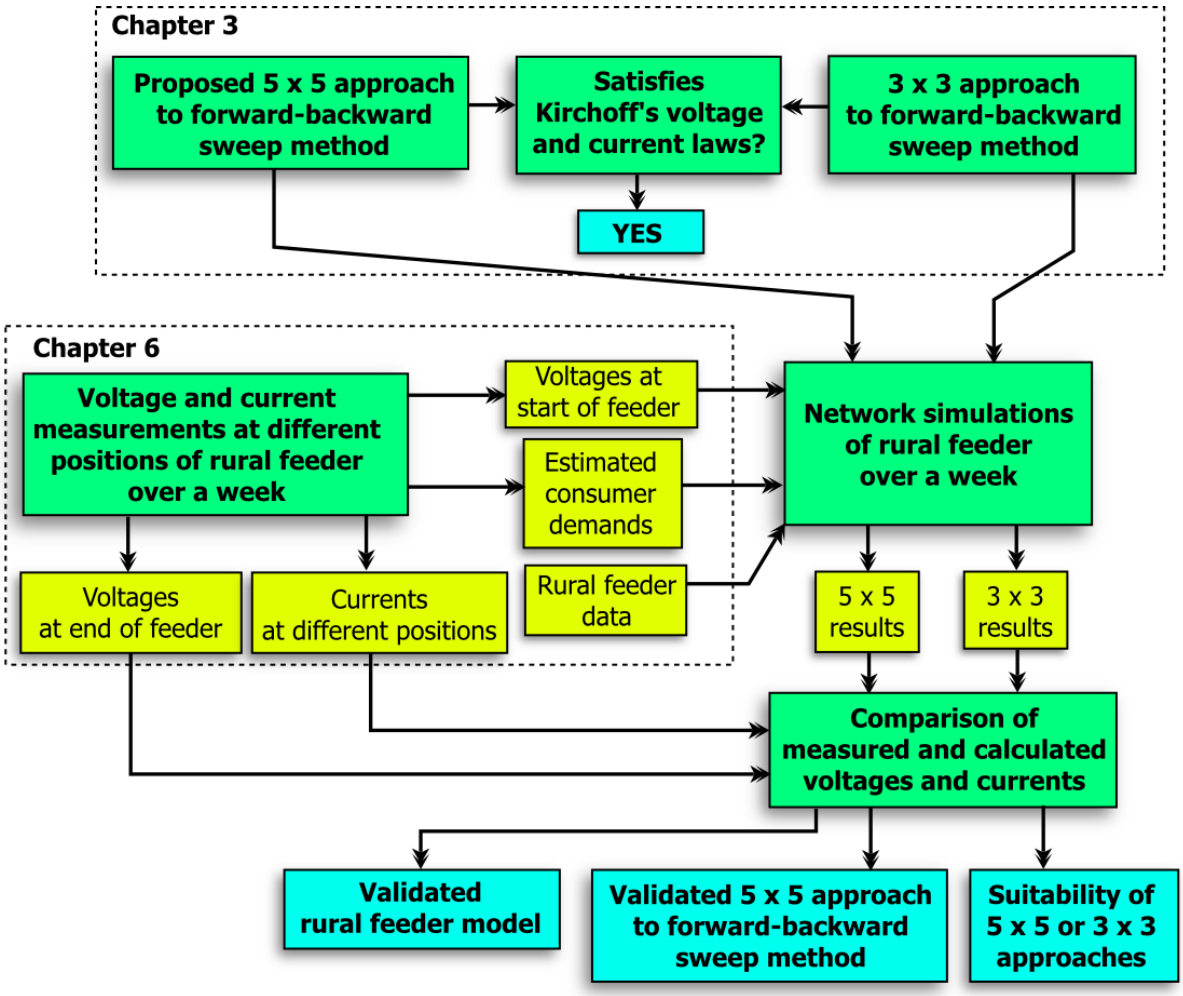

Figure 7.1: Overview of Chapter 7

7.3 Modelling aspects

Both of these aspects – earth resistance values and load model types - are not easily known unless very specific measurements are taken. The approach here will be to carry out the validation assuming earth resistance values (taken from a practical range in the literature) and constant power loads.

7.3.1 Earthing resistance values

The neutral is connected to earth at multiple points along the feeder. These connections are made either to driven earth electrodes on the network or to metal work (water and gas pipes) at consumer premises. Suitable resistances for each are discussed in the sections which follow.

Earth electrode resistances

Tests results for sixteen earth electrodes were reported for rural low-voltage feeders in 1957 by the North West Electricity Board on their PME systems [90]. The average resistance was $6\ \Omega$ and the minimum and maximum values were $2\ \Omega$ and $10\ \Omega$. For the validation, $6\ \Omega$ will be assumed.

Although these values are from tests carried out on rural English villages decades ago, they give an idea of the practical range for these earth resistances. Also, as noted in [90] the Board's earth electrodes had been regularly tested in the 1950s and showed no variation.

It should be noted as well that these values more than satisfy the requirement of Engineering Recommendation G12/3 [1] which states that:

"The combined resistance of all LV neutral earth electrodes shall not exceed 20 ohms (before the connection of consumers' earthing terminals to the neutral)."

In the case of this rural feeder, with five earth electrodes, each assumed to be $6\ \Omega$, the combined resistance works out to be $1.2\ \Omega$.

Metal pipework resistances

Fewer measurements for water pipes at consumer premises were reported in [90] (only five measurements). With the exception of one consumer's water pipe which was reported to be in very good condition, the lowest value however was $6\ \Omega$ and the highest $16.5\ \Omega$.

For the validation, a value of $10\ \Omega$ will be assumed.

7.3.2 Load model type – constant impedance, constant current or constant power models

The profiles of current drawn by domestic and non-domestic consumers, taken from current measurements, were presented in Chapter 6 by equations (6.13) to (6.15). Load models for unbalanced power flow methods however, typically require active and reactive power as inputs and not current. Equation (3.25) presented in Chapter 3 for a constant power load model is an example of this. Similar equations for the constant current and constant impedance load models can be found in [51].

Therefore, equations similar to (6.13) to (6.15) were derived in terms of the active and reactive power measurements and used to find the power demands per phase at each pole position.

For the validation, presented in the next section, constant power load models are assumed using those power demands at each pole position.

7.4 Validation against field measurements

7.4.1 Overview of the validation

Both approaches to the forward-backward sweep method are validated by comparing their results to field measurements taken over a period of a week. An overview of the validation is illustrated in Figure 7.2. This was done at ten-minute intervals over the weeks before and after the static balancer was energised. The validation of the results for each week is presented in the next two sections. The main focus is the validation of the proposed 5 x 5 approach. The results from the 3 x 3 approach are presented only if they differ significantly from that obtained by the proposed 5 x 5 approach.

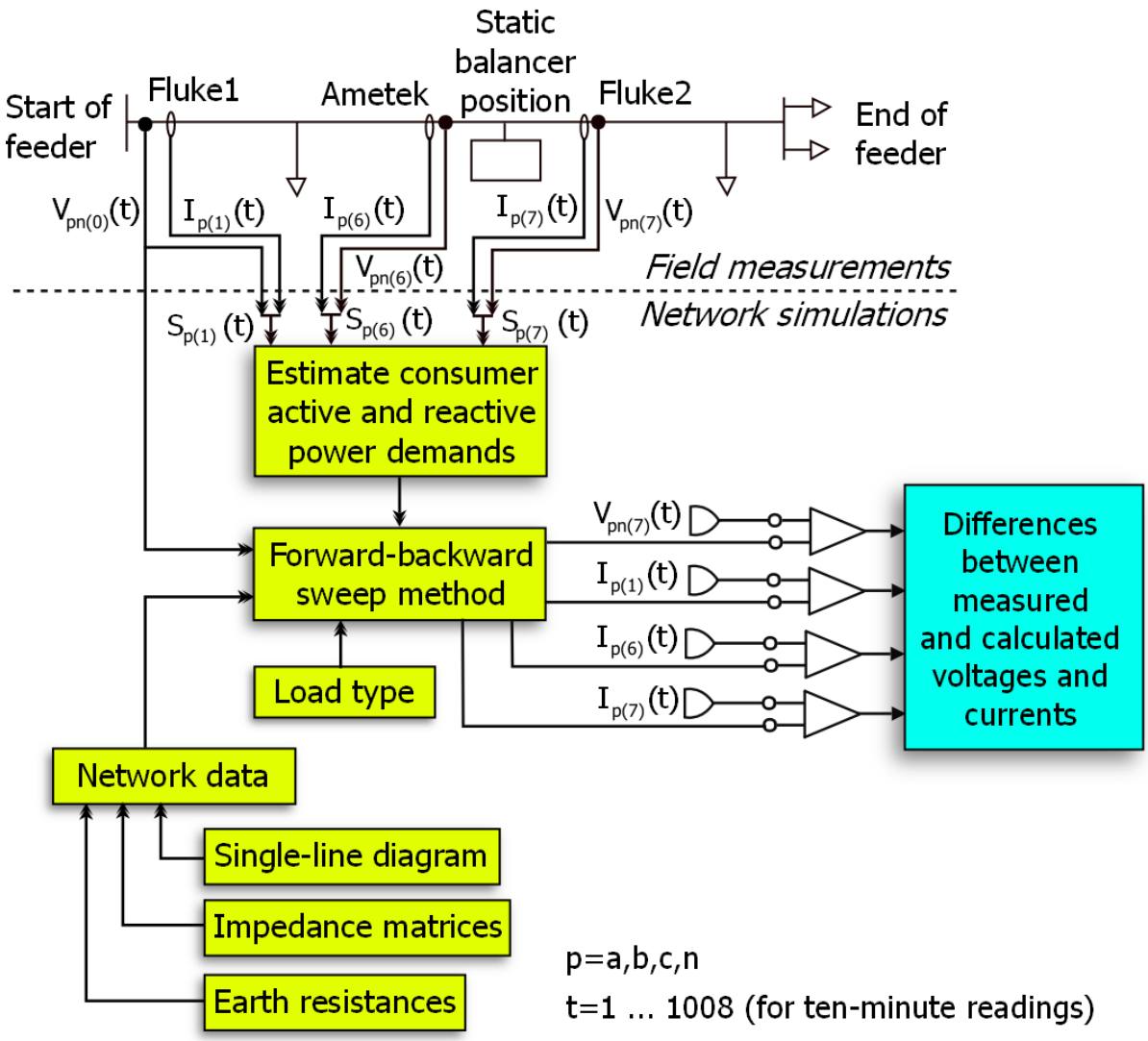

Figure 7.2: Overview of the validation against field measurements

7.4.2 Without static balancer

Phase-neutral voltages

In Figure 7.3, the measured phase-neutral voltages at the Fluke2 position ($V_{pn(7)}$) are plotted alongside the calculated values from the 5 x 5 and 3 x 3 approaches. The results from the proposed 5 x 5 approach are in very good agreement with the measured values and those from the 3 x 3 approach are less of a match. Similar plots can be shown at the Ametek position.

The mean absolute difference (in volts) between calculated phase-neutral voltages from both approaches and the measured values are given in Table 7.1. They are less when the phase-neutral voltages are found using the proposed 5 x 5 approach.

Approach to forward-backward sweep method:	Metering position:	
	Ametek	Fluke2
Proposed 5 x 5 approach	1.11 V	0.56 V
3 x 3 approach	1.29 V	1.43 V

Table 7.1: Mean absolute difference (in volts) between measured values and those calculated by 5 x 5 and 3 x 3 approaches (over a week without static balancer) assuming constant power loads and an earth electrode resistance of 6 Ω.

The mean absolute differences are of the order of 3 to 8 times the voltage measurement errors shown in Table 6.2 for the second field trial, which for both meters was ± 0.2 V. These mean absolute differences, being less than 1 % of the nominal 230 V, are relatively small; considering that assumptions were made to calculate the network impedances (covered in Appendix A) and that the consumer loads given by equations (6.13) to (6.15) involved finding a difference in readings from different meters and so would have a measurement error associated with them as was seen in Table 6.4 and Table 6.5.

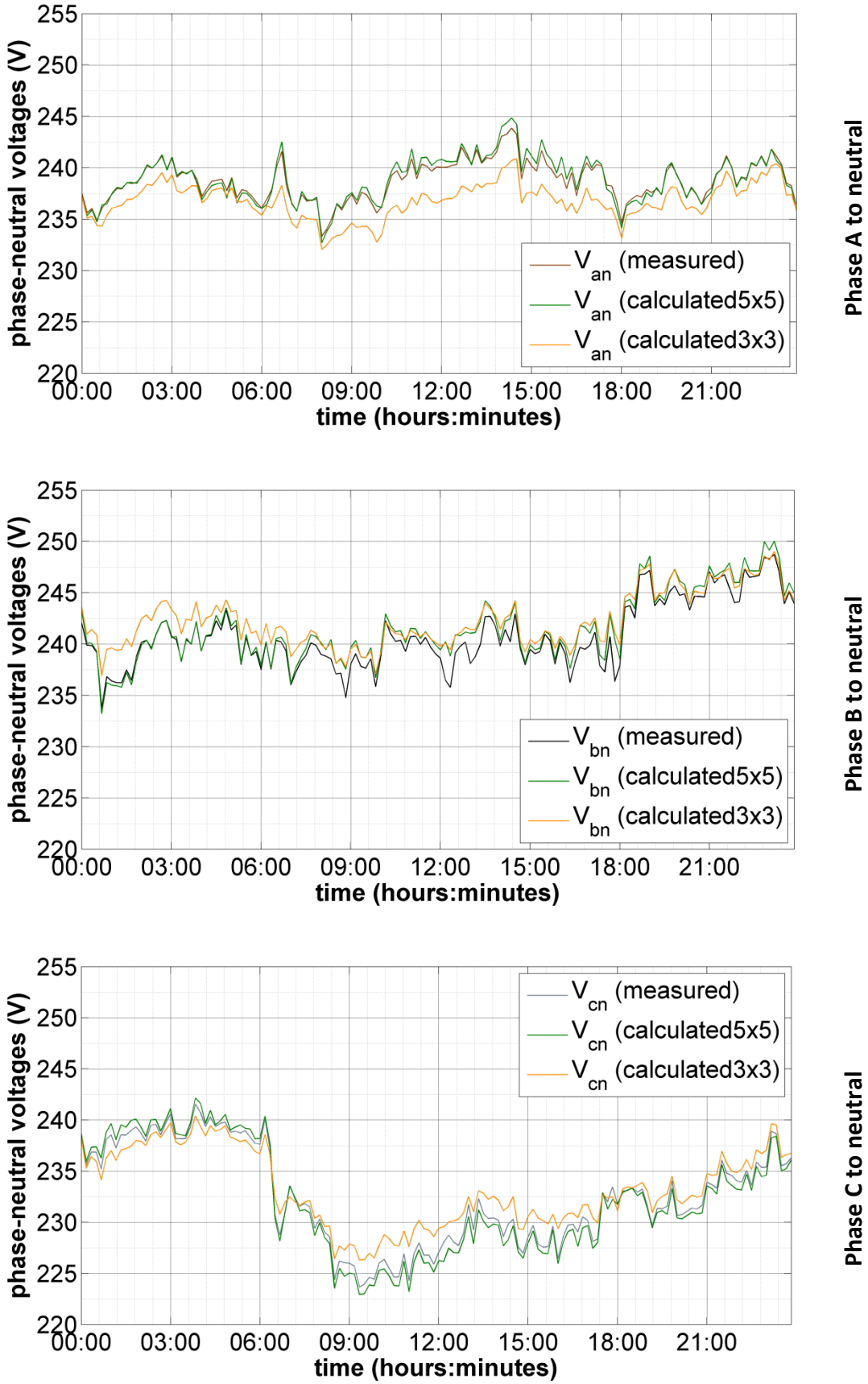

Figure 7.3: Calculated and measured phase-neutral voltages at end of feeder (Fluke2) assuming constant current load models (for the 8th March 2013)

Phase and neutral currents

The calculated phase and neutral currents from both approaches were in good agreement with the measured values at all three metering positions. Figure 7.4 shows the measured values at the Fluke1 position along with those calculated using the proposed 5 x 5 approach and the 3 x 3 approach. As can be seen, better agreement could have been reported, if not for some minor differences which can be observed in the phase B currents. The minor differences on this phase also accounts for minor differences observed on the neutral current.

The mean percentage differences and the mean absolute differences between the measured and the calculated phase and neutral currents for both approaches are given in Table 7.2 and Table 7.3, respectively. For the phase currents they are similar regardless of the approach used but for the neutral current, the 3 x 3 approach produced slightly better agreement. Also, from Table 7.3 it can be seen that for both approaches the mean absolute differences do not exceed ± 3 A. This is in order with the current measurement error of the Fluke meter, which was the higher of the two meters, as shown in Table 6.3 for the second field trial.

It should be noted that the higher mean percentage differences for the neutral current of Fluke1 (indicated in the shaded boxes) are not considered because they were not measured directly by a current transformer. Instead they are the phasor sum of the measured phase currents and so would include the instrument error of three other current transformers. All other phase and neutral currents were measured directly.

Approach to forward-backward sweep method:		Metering position:		
		Fluke1	Ametek	Fluke2
Proposed 5 x 5 approach	Phases	5.9 %	8.3 %	3.6 %
	Neutral	14.4 %	13.7 %	12.3 %
3 x 3 approach	Phases	6.0 %	8.3 %	3.9 %
	Neutral	14.0 %	12.8 %	11.2 %

Table 7.2: Mean percentage differences between measured values and those calculated by 5 x 5 and 3 x 3 approaches (over a week without static balancer) assuming constant power loads and an earth electrode resistance of 6 Ω.

Approach to forward-backward sweep method:		Metering position:		
		Fluke1	Ametek	Fluke2
Proposed 5 x 5 approach	Phases	1.8 A	1.7 A	0.6 A
	Neutral	2.3 A	3.0 A	2.6 A
3 x 3 approach	Phases	1.8 A	1.6 A	0.7 A
	Neutral	2.1 A	2.8 A	2.4 A

Table 7.3: Mean absolute differences between measured values and those calculated by 5 x 5 and 3 x 3 approaches (over a week without static balancer) assuming constant power loads and an earth electrode resistance of 6 Ω.

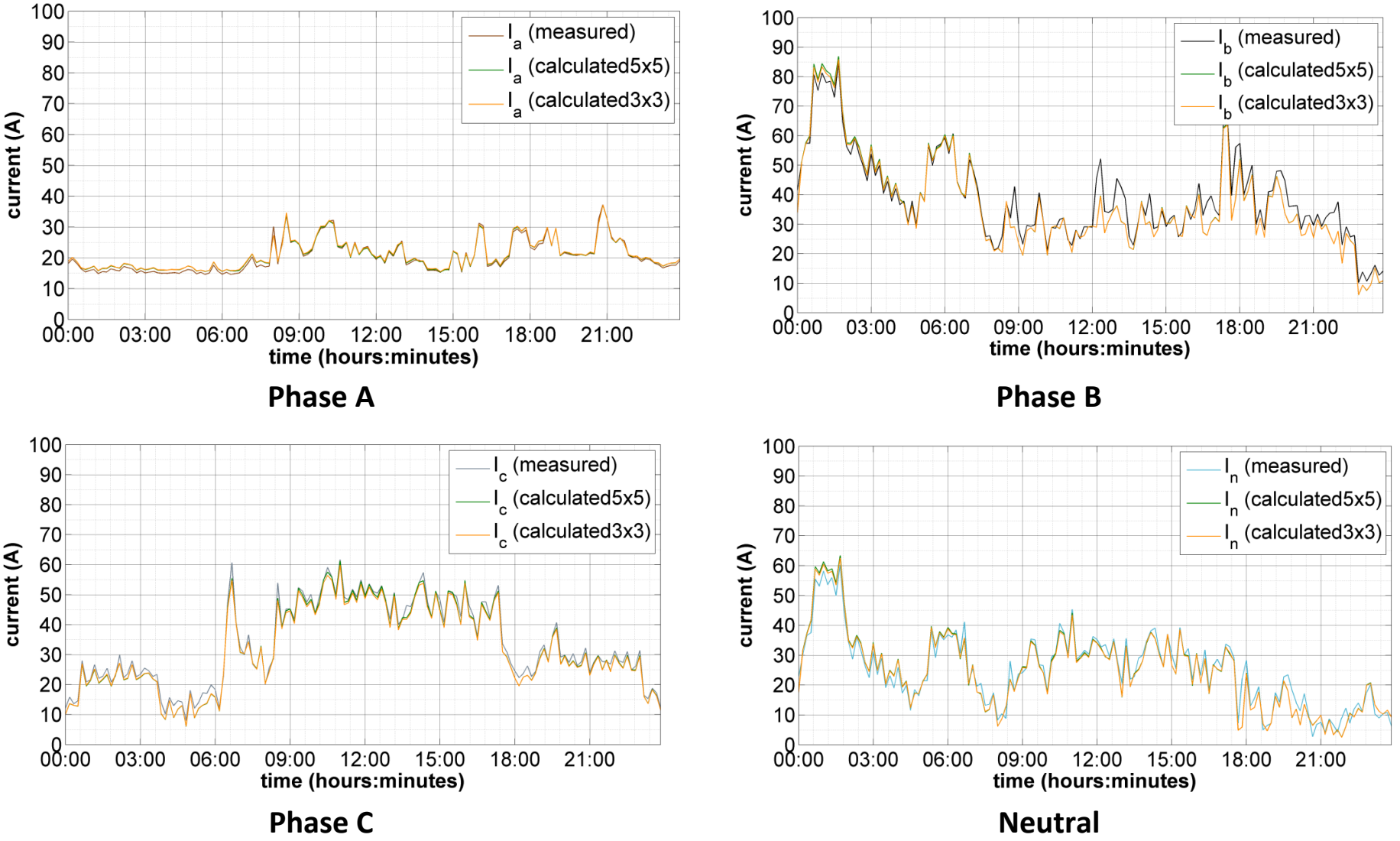

Figure 7.4: Calculated and measured phase and neutral currents at the start of the feeder (Fluke1)

7.4.3 With static balancer energised

Phase-neutral voltages

The phase-neutral voltages calculated using both approaches were in very good agreement with measured values. The mean absolute difference, presented in Table 7.4, for both approaches were between 2 to 6 times the voltage measurement error of ± 0.2 V for both meters, as was given in Table 6.2 for the second field trial.

Approach to forward-backward sweep method:	Metering position:	
	Ametek	Fluke2
Proposed 5 x 5 approach	1.09 V	0.35 V
3 x 3 approach	1.11 V	0.44 V

Table 7.4: Mean absolute difference (in volts) between measured values and those calculated by 5 x 5 and 3 x 3 approaches (over a week with static balancer) assuming constant power loads and an earth electrode resistance of 6 Ω.

Phase and neutral currents

The measured phase currents were again in good agreement with the calculated values from both approaches at all three metering positions. As before, minor differences between the measured and calculated phase B currents were observed for both approaches.

The measured neutral current upstream of the static balancer however, was in agreement only with that calculated using the proposed 5 x 5 approach. As shown in Figure 7.5, for the Ametek position, the upstream neutral currents calculated using the 3 x 3 approach are much higher than those measured.

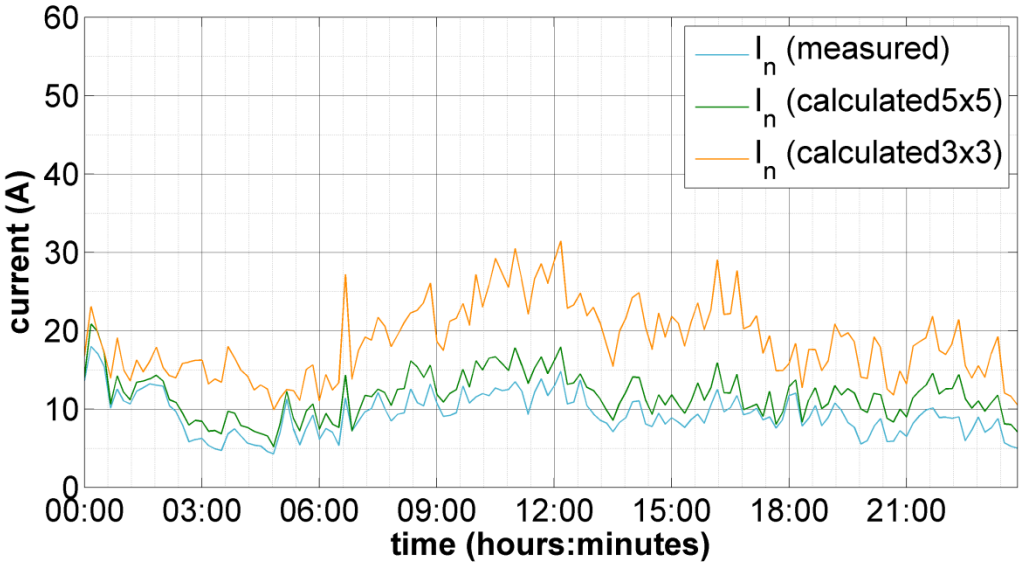

Figure 7.5: Calculated and measured neutral currents at just upstream of the static balancer (Ametek)

The differences seen in results for the upstream metering positions (Ametek and Fluke1) are visible in the mean percentage differences given in Table 7.5 and in the mean absolute differences given in Table 7.6. For the 3 x 3 approach, they are very significant on the neutral – as high as 173 % and 7.5 A at the Fluke 1 position (keep in mind that the neutral at this position was not measured directly). Although the corresponding difference from the results of the proposed 5 x 5 approach is not insignificant (64 %) it is far less and from Figure 7.6, it is still a very reasonable fit to the measured values. Further, the mean absolute difference, as seen in Table 7.6, is less than ± 3 A.

Approach to forward-backward sweep method:		Metering position:		
		Fluke1	Ametek	Fluke2
Proposed 5 x 5 approach	Phases	5.7 %	7.1 %	3.0 %
	Neutral	64.1 %	23.3 %	6.7 %
3 x 3 approach	Phases	8.7 %	12.8 %	3.0 %
	Neutral	172.7 %	95.4 %	6.0 %

Table 7.5: Mean percentage differences between measured values and those calculated by 5 x 5 and 3 x 3 approaches (over a week with static balancer) assuming constant power loads and an earth electrode resistance of 6 Ω.

Approach to forward-backward sweep method:		Metering position:		
		Fluke1	Ametek	Fluke2
Proposed 5 x 5 approach	Phases	1.8 A	1.6 A	0.5 A
	Neutral	2.9 A	1.9 A	1.8 A
3 x 3 approach	Phases	2.7 A	2.9 A	0.5 A
	Neutral	7.5 A	7.8 A	1.6 A

Table 7.6: Mean absolute differences between measured values and those calculated by 5 x 5 and 3 x 3 approaches (over a week with static balancer) assuming constant power loads and an earth electrode resistance of 6 Ω.

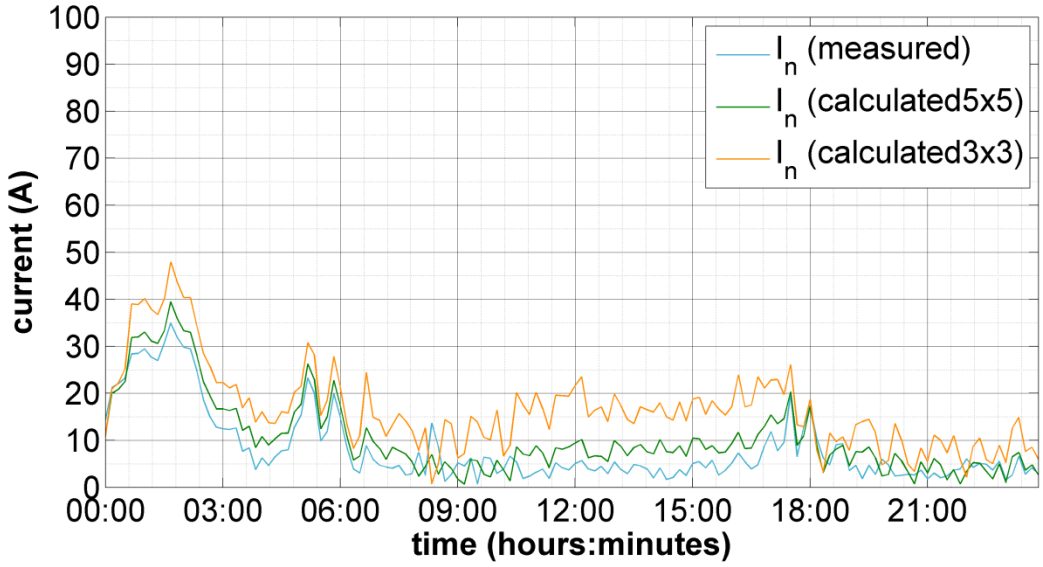

Figure 7.6: Calculated and measured neutral currents at the start of the feeder (Fluke 1)

Though less noticeable if plotted, there is also less agreement in the upstream phase currents calculated by the 3 x 3 approach. The mean percentage differences presented in Table 7.5 and the mean absolute differences presented in Table 7.6 both make this clear. At the upstream metering positions, both the mean percentage differences and the mean absolute differences of the phase currents found by the 3 x 3 approach are higher than those found using the proposed 5 x 5 approach.

7.4.4 Summary

- The proposed 5 x 5 approach produced voltages and currents which were in good agreement with the measured values both with and without the static balancer.
- The results from the 3 x 3 approach were also in good agreement but only without the static balancer.

The following section accounts for observations made from the results of both methods.

7.5 Accounting for the differences between the approaches

The proposed 5 x 5 approach produced more accurate results than the 3 x 3 approach. In particular, the phase-neutral voltages and the upstream neutral currents (with the static balancer energised) were a closer match. The following sections explain these observations.

7.5.1 Calculated voltages are related to the current unbalance of consumer demands

The 3 x 3 approach is less accurate when the zero sequence current unbalance factor of the total consumer current ($I_{consumers}$) (as defined in section 6.10) is higher than the negative sequence current unbalance factor. This is seen in Figure 7.7, which shows the distribution of the absolute voltage difference between phase-neutral voltage magnitudes measured by Fluke2 to those calculated using the 3 x 3 approach. It is clear that the black bars, which indicate instances where $IUF_0 > IUF_2$, are skewed to right of the distribution towards higher absolute voltage differences. The difference between both sequence current unbalance factors, as recognised in Chapters 4 and 6, are because of the power factors of the single-phase loads relative to each other (i.e. current angle unbalance). This indicates a weakness of the 3 x 3 approach in that it will be subject to greater error if used to simulate feeders with loads in which $IUF_0 > IUF_2$.

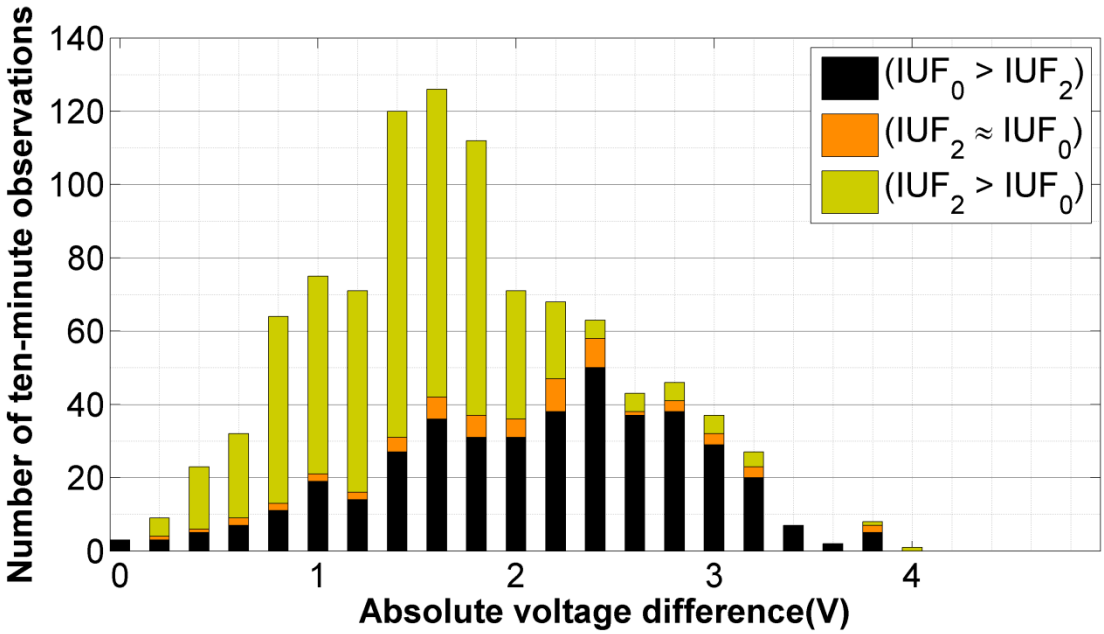

Figure 7.7: Absolute voltage difference between phase-neutral voltage magnitudes measured by Fluke2 to those calculated using the 3 x 3 approach showing significance of the relative magnitudes of the two sequence current unbalance factors of the total consumer current

A plot similar to Figure 7.7 but for the results from the proposed 5 x 5 approach is shown in Figure 7.8. Apart from the absolute voltage differences being lower, there appears to be less dependence on the relationship between IUF_0 and IUF_2 of the $I_{consumers}$. This is a strength of the proposed 5 x 5 approach.

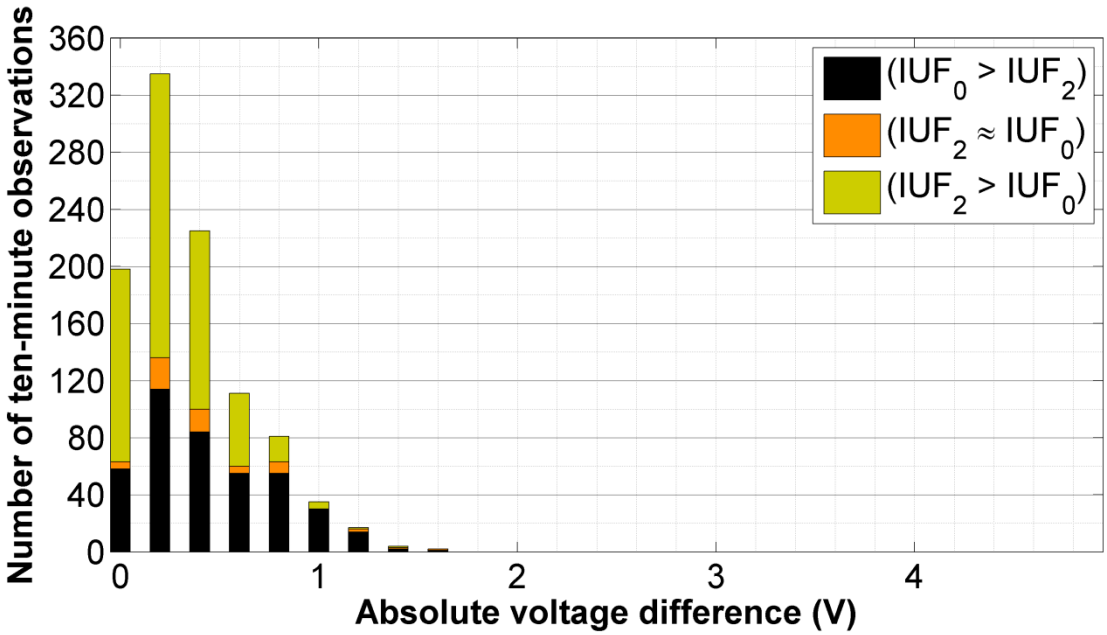

Figure 7.8: Absolute voltage difference between phase-neutral voltage magnitudes measured by Fluke2 to those calculated using the proposed 5 x 5 approach

Greater absolute voltage difference is not necessarily due to the magnitude of the zero sequence current unbalance factor

It is interesting to point out that from the results of the 3 x 3 approach, it is not the magnitude of the zero sequence current unbalance which affected the absolute voltage difference, but the magnitude of it relative to that of the negative sequence current unbalance. This can be appreciated from Figure 7.9 which shows the same distribution but with the bars stratified into four ranges of IUF_0. From this plot, it cannot be easily concluded that a high IUF_0 results in a high absolute voltage difference (since to the left of the histogram there are many wide green and orange bars representing instances of high IUF_0 and lower absolute voltage differences).

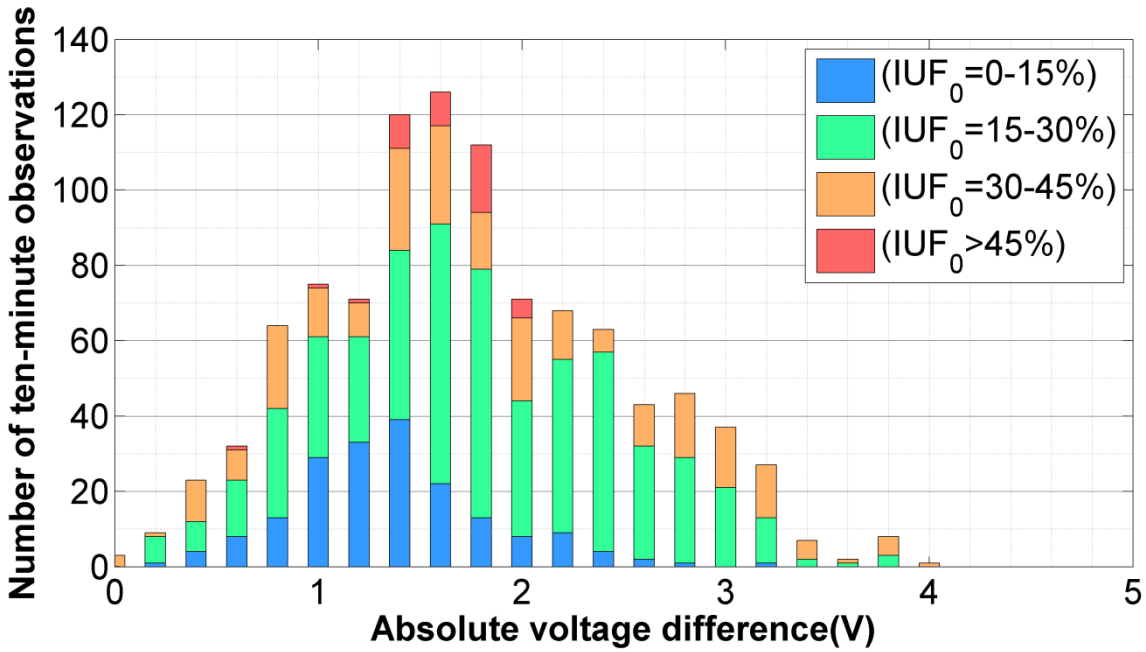

Figure 7.9: Absolute voltage difference between phase-neutral voltage magnitudes measured by Fluke2 to those calculated using the 3 x 3 approach showing number of observations for different ranges of zero sequence current unbalance factor

7.5.2 Upstream neutral currents and calculated phase-neutral voltages

With the static balancer energised, only the upstream neutral currents calculated using the proposed 5 x 5 approach were a good enough match to the measured values.

Recalling from equation (5.11), the current drawn by the static balancer depends largely on the voltages at its terminals or more specifically, on one third of the phasor sum of the phase-neutral voltages (i.e. the zero sequence voltage). Therefore any inaccuracy in the approach used to calculate these voltages will be reflected in the calculated upstream currents.

The higher upstream neutral currents calculated by the 3 x 3 approach are therefore because of its less accurate phase-neutral voltages. As evidence of this, Figure 7.10 compares the zero sequence voltage measured at the terminals of the static balancer (i.e. Fluke 2) to those calculated using both approaches. It is clear that the result from the proposed 5 x 5 approach is a much better match.

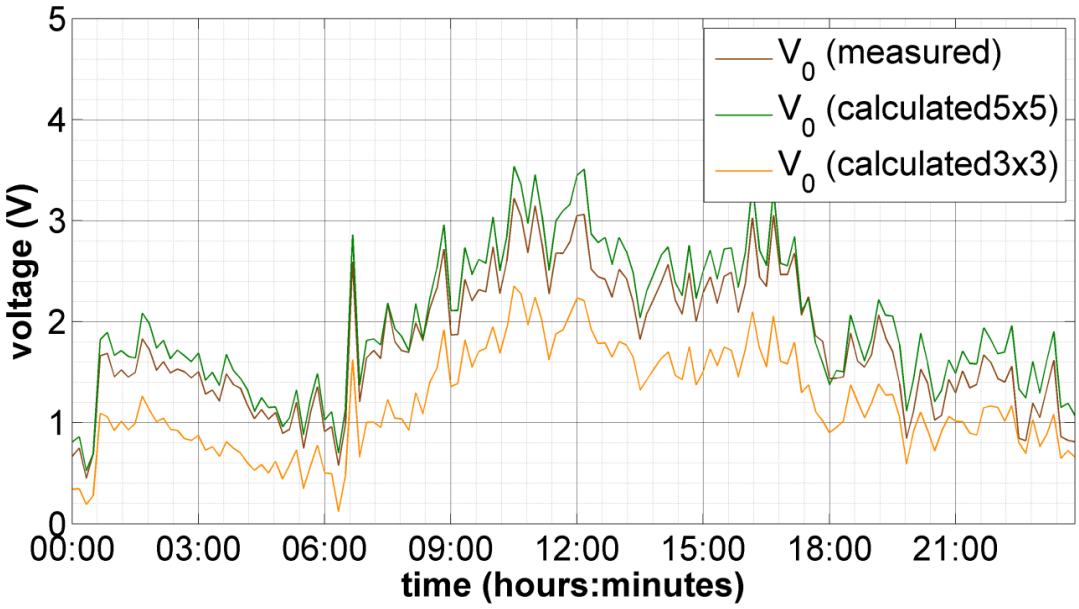

Figure 7.10: Calculated and measured zero sequence voltages at Fluke 2 (static balancer position)

7.6 Comparison of benefits calculated by network simulations to those quantified by field measurements

The sequence unbalance factors and network effects are quantified in Table 7.7 from the results of both approaches and compared to those presented earlier in Table 6.7 from the field measurements. Results identified in dark blue and orange are either *very comparable* or *comparable* to the measurements and those highlighted and in purple were less comparable to the measurements.

The results from the proposed 5 x 5 approach were mostly *very comparable* to the measurements. Its results accurately captured the effects of unbalance on the rural feeder with and without the static balancer. Moreover, both zero and negative sequence unbalance factors were computed very accurately. The only results which were *less comparable* to the measurements were the NU_PRCC(at $max(I_{p(1)})$) and $VR_{indicator}$.

The results from the 3 x 3 approach were mostly *less comparable* to the measurements. Its main weakness, the calculation of the zero sequence voltages, which was identified in section 7.5.2, accounts for much of the differences. This includes the differences seen in the zero sequence voltage unbalance factors, neutral-point shifting (which cannot be measured directly and so is the zero sequence voltage itself), effective power factor, NU_PRCC (when $IUF_0 = 100\ \%$)) and the zero sequence current unbalance factor (with the static balancer).

Notably, the 3 x 3 approach accurately calculates the negative sequence unbalance factors.

			MEASURED		SIMULATED USING PROPOSED 5 x 5 APPROACH		SIMULATED USING 3 x 3 APPROACH	
			Static balancer		Static balancer		Static balancer	
			De-energised 4th to 10th March, 2013	Energised 18th to 24th February, 2013	De-energised	Energised	De-energised	Energised
Unbalance indicators (95th percentile values from section 6.7):								
Current unbalance factors	IUF_0		44.6 %	22.8 %	47.1 %	25.4 %	46.7 %	30.4 %
	IUF_2		52.0 %	45.7 %	53.3 %	46.3 %	52.3 %	46.0 %
Voltage unbalance factors	VUF_0		2.9 %	1.2 %	3.1 %	1.3 %	1.5 %	0.8 %
	VUF_2		3.6 %	3.9 %	3.5 %	4.0 %	3.5 %	3.9 %
Effects of unbalance:								
(a) Network utilisation	NU_PRCC	(at $max(I_{p(1)})$)	20.7 %	12.3 %	20.5 %	16.6 %	20.0 %	17.9 %
		(when $IUF_0 = 100\%$)	26.9 %	15.0 %	25.5 %	15.0 %	25.0 %	17.4 %
	pf_e (when $IUF_0 = 100\%$)		0.42	0.81	0.40	0.79	0.40	0.71
(b) Neutral currents	I_n (when $IUF_0 = 100\%$)		97 A	28 A	97 A	27 A	96 A	27 A
(c) Ground currents	I_g Values can only be given for proposed 5 x 5 approach. They were calculated for the Fluke2 position.		*Not measured but as seen in section 4.5 I_g like I_n is directly proportional to IUF_0.*		*1 mA*	*256 mA*	*As explained in section 3.6, I_g is not computed by this approach.*	
(d) Losses	Network energy lost as a percentage of energy delivered to all consumers.		1.5 %	1.4 % (-0.1 %)	1.5 %	1.4 % (-0.1 %)	1.1 %	1.3 % (+0.2 %)
	Total energy lost as a percentage of energy delivered to all consumers.		3.6 %	4.0 % (+ 0.4 %)	3.6 %	4.0 % (+0.4 %)	3.3 %	3.9 % (+0.6 %)
(e) Neutral-point shifting	Using V_0 as $V_{n'g}$ cannot be measured directly.	(at $mean(\mathrm{IUF}_0)$)	4.2 V	1.4 V	4.4 V	1.6 V	2.1 V	1.0 V
		(when $IUF_0 = 100\%$)	15.2 V	5.1 V	16.0 V	5.7 V	7.5 V	3.5 V
(f) Phase-neutral voltages	V_{an}(mean)		238.4 V	235.1 V (-3.2 V)	238.5 V	235.5 V (-3.0 V)	236.7 V	234.8 V (-1.9 V)
	V_{bn}(mean)		241.2 V	242.5 V (+1.3 V)	242.0 V	242.9 V (+0.9 V)	242.8 V	243.3 V (+0.5 V)
	V_{cn}(mean)		233.1 V	231.9 V (-1.2 V)	233.1 V	232.1 V (-0.9 V)	233.9 V	232.3 V (-1.5 V)
(g) Voltage regulation	$VR_{indicator}$(95th percentile)		14.6 %	12.9 % (-1.7 %)	17.1 %	14.4 % (-2.7 %)	15.1 %	14.0 % (-1.1 %)

Key: Improvement (of more than 40 %) ; No real change observed ; Degradation (of more than 40 %).
Very comparable to measurements (± 6 %) ; Comparable to measurements (± 12 %) ; Less comparable to measurements (not within ± 12 %)

Note this key does not apply to (f). All voltages were within UK statutory limits (230 V -6%/+10%).

Table 7.7: Comparison of quantified benefits from measurements and simulations

7.7 Computation time of both approaches

The proposed 5 x 5 approach is intended for the planning of very unbalanced low-voltage feeders. As was seen in Chapter 3, its derivation gave emphasis to accuracy and not computation time, and so did not involve any unnecessary assumptions. The 3 x 3 approach on the other hand, involved assumptions and so will have an advantage in computation time. It is used in real-time unbalanced power flow applications.

The computational times of both approaches are compared in Table 7.8 without the static balancer and in Table 7.9 with the static balancer. It can be seen that per solution, both approaches solve very quickly (less than 0.1 seconds). Also, the 3 x 3 approach is about two times faster than the proposed 5 x 5 approach but only for simulations without the static balancer. For simulations with the static balancer, it appears to be two times slower.

Approach to forward-backward sweep method:	Total (for all 1008 solutions over the entire week)		Average per solution	
	Number of iterations	Computation time	Number of iterations	Computation time
Proposed 5 x 5 approach	27562	42 s	27	0.04 s
Standard 3 x 3 approach	4032	17 s	4	0.02 s

Table 7.8: Computation times without static balancer

Approach to forward-backward sweep method:	Total (for all 1008 solutions over the entire week)		Average per solution	
	Number of iterations	Computation time	Number of iterations	Computation time
Proposed 5 x 5 approach	18137	32 s	18	0.03 s
Standard 3 x 3 approach	14625	63 s	15	0.06 s

Table 7.9: Computation times with static balancer

For these simulations, it should be noted that the convergence criterion, expressed by equations (3.32) and (3.33) of Chapter 3, were set to the same tolerances for both approaches. The power mismatches were set to 5 W, voltages magnitudes to 0.01 V and voltage angles to 0.01 °. Also, a laptop with an Intel Core i7 processor, 16 Gb of memory and a solid state drive was used.

7.8 Chapter conclusions

The proposed 5 x 5 approach produces results which are in very good agreement with the measured values, both with and without the static balancer. This was evident both in the validation of the voltages and currents as well as in the comparison of the quantified benefits.

The 3 x 3 approach produces good results but its calculated phase-neutral voltages are not as accurate as that from the proposed 5 x 5 approach. This was particularly important in the simulations with the static balancer. Since the current drawn by the static balancer depends on the voltages at its terminals, the less accurate phase-neutral voltages found at its terminals (i.e. Fluke 2 position) resulted in the significant differences between measured and calculated upstream phase and neutral currents. This makes the 3 x 3 approach unsuitable for any analysis of low-voltage feeders with the static balancers.

Additionally, it was shown that for the 3 x 3 approach, the absolute voltage difference in the phase-neutral voltages can be attributed to the instances in which the zero sequence current unbalance factor of the total consumer current was higher than its negative sequence current unbalance factor.

8. Conclusions

8.1 Guidelines for monitoring unbalance on low-voltage feeders

There is a need to recognise the differences between the consumer and the low-voltage network perspectives to unbalance. Standards such as the BS EN 50160 [83] are written from a consumer perspective and place emphasis on concerns over consumer three-phase equipment such as induction machines. From this thesis, which took the low-voltage network perspective to unbalance, the following proposals are made to guide the monitoring of unbalance on low-voltage feeders. This is especially important now to distribution network operators, in light of increasing penetrations of low-carbon technologies.

8.1.1 Greater importance be placed on sequence current unbalance factors

The importance placed on the different sequence unbalance factors should be reflective of the effects of unbalance. This will not be the same for both perspectives. From the low-voltage network, the effects are driven by current unbalance (as made clear in Figure 2.13), whilst for consumer three-phase equipment, they are driven by voltage unbalance.

The standards, being written with a consumer perspective, therefore direct attention towards the sequence voltage unbalance factors, with more emphasis placed on the negative sequence voltage unbalance factor. This is reflected in the approximations and recommended limits for the negative sequence voltage unbalance factor given in the standards. Understandably, concern over the zero sequence voltage unbalance is not stressed, because consumer three-phase equipment is typically supplied without a neutral.

With a low-voltage network perspective, attention should be directed towards the sequence current unbalance factors. Of them, greater emphasis, as argued in Chapter 4 theoretically and then in Chapter 6 by field measurements, should be placed on the zero sequence current unbalance factor. This was seen in the stronger correlation between this unbalance factor and the effects identified in Figure 2.13 throughout the theoretical and field analyses. The negative sequence current unbalance factor did have an influence on these effects but to a much lesser extent.

8.1.2 Sequence unbalance factors be used to locate the source of the unbalance

A further difference with the low-voltage network perspective is that when sequence unbalance factors are measured on a studied feeder, it is important to know where the unbalance was created. It is useful to categorise each sequence unbalance factor as either localised, that is, they are due to unbalanced loads on the studied feeder itself, or non-localised, that is, they may include unbalance from other parts of the network.

Of the four sequence unbalance factors, only the current unbalance factors are necessarily localised. This is not the case for the voltage unbalance factors.

The negative sequence voltage unbalance factor is non-localised and that was confirmed by the field measurements on the rural feeder. This is because it can include negative sequence voltage unbalance originating from the higher voltage network (propagated across the delta-star winding of the distribution transformer) and from other low-voltage feeders fed from the same distribution transformer.

Now, the zero sequence voltage unbalance factor, though not influenced by the higher voltage network (typically in delta and so has no zero sequence voltages), need not be considered localised as it can still include the zero sequence unbalance from the other feeders supplied from the same distribution transformer. The field measurements however showed that it was directly related to the zero sequence current unbalance

factor, and so was to a great extent a localised indicator. This is particularly the case towards the end of the feeder (Figure 6.32 (b)), where the zero sequence voltage is more dependent on the unbalanced loads on the studied feeder itself.

8.1.3 Greater importance be placed on the zero sequence voltage unbalance factor

From the low-voltage network perspective, greater emphasis should be placed on the zero sequence voltage unbalance factor rather than the negative sequence voltage unbalance factor. From the theoretical and field analysis, there are several arguments for this:

- The negative sequence voltage unbalance factor did not provide an adequate reflection of the effects of unbalance on the network. To highlight this, in the theoretical analysis of Chapter 4, it was shown that even with all the load on one phase, the negative sequence voltage unbalance factor remained less than even the recommended 2 % limit (Figure 4.25). Also, in the field analysis of Chapter 6, the improvements in the effects of unbalance seen on the rural feeder with the static balancer energised were reflected in a reduction in the zero sequence voltage unbalance factor and not in the negative sequence voltage unbalance factor (Table 6.7).
- There was a positive correlation between the zero sequence voltage unbalance factor and the zero sequence current unbalance factor. The effects on the network being influenced more by this current unbalance factor.
- Unlike the negative sequence voltage unbalance factor, the zero sequence voltage unbalance factor was a localised indicator of unbalance, particularly at the end of the feeder.

The negative sequence voltage unbalance factor still remains important though, but more in the interests of three-phase consumers and concerns over propagation onto other parts of the network.

8.1.4 Importance of where measurements are taken

With the low-voltage network perspective, the most meaningful locations to take current and voltage unbalance measurements differs. This is very different from the consumer perspective, where only voltage unbalance measurements are needed and only at the point of supply to the consumer.

Current unbalance measurements, taken at the start of the feeder, give a picture of the unbalance on the entire feeder.

In the case of voltage unbalance measurements, they should be taken at the end of the feeder. This is because at this location, the zero sequence voltage unbalance factor is higher and more reflective of the unbalance on the feeder itself.

It should also be appreciated that recommended limits on the sequence unbalance factors should be with respect to the location in which the measurements are taken. That is, limits on sequence current unbalance factors should be specified at the start of the feeder and limits on the sequence voltage unbalance factors should be specified at the end of the feeder.

8.2 Reasons for unbalance

8.2.1 Systematic reasons for the uneven distribution of consumers amongst phases

The uneven distribution of consumers amongst the three phases is not just random as reported in the literature, it can also be systematic. Two examples have been described in this thesis but there are certainly more.

One example, explained in section 6.3.5, was recognised on the rural feeder, a mostly overhead line network. It had been deduced after putting together information from the industrial supervisors as to the unusual ordering of the phases (C-A-B-N) and after

identifying the phases to which each consumer was connected to. The top conductor – phase C - was the least preferred because it had previously been used as the neutral.

Another example, explained by industrial supervisors, was described by Figure 2.9. It had applied to underground networks with four-core cables and had to do with the tendency to connect to one of the phase wires closest to the neutral.

8.2.2 Identification of additional cause of unbalance

In the theoretical analysis on the representative feeder of Chapter 4, it was recognised that the power factors of the loads on each phase relative to each other, governs the relative angles between current phasors. This is the fundamental cause of current angle unbalance.

This fundamental cause of unbalance is not one of the widely recognised causes that are mentioned in the literature and which were organised and presented in Figure 2.8.

It can be explained by taking a practical example of three loads – Load 1 (15 kW), Load 2 (15 kVA, 0.866 lagging) and Load 3 (15 kVA, 0.7 lagging). On the face of it, one might not expect that it would make any difference which of the phases each of the three loads was connected to. However, calculating the neutral current (assuming nominal and balanced voltages) will reveal that the neutral current is less (40 A) when Load 2 and 3 are connected to phase B and C respectively and more (49 A) when the connected phases are swapped around.

This was demonstrated more onerously by the current angle unbalance case of Chapter 4 where one of the swapped phases had a leading power factor. It was seen that this influenced all the quantified effects. The most noticeable difference was with the neutral current, which was pointed out in Figure 4.16.

8.3 Explanation of why sequence unbalance factors differ

An observation was made in [6] from field measurements on low-voltage feeders in Germany that on some of them the negative sequence voltage unbalance factor was higher than the zero sequence voltage unbalance factor while on others they were equal. This is answered first by looking at the current unbalance factors.

8.3.1 Sequence current unbalance factors

Current angle unbalance, due to the relative power factors of loads on each phase, accounts for differences between sequence current unbalance factors. The theoretical analyses of Chapter 4 examined the linkages between current phasors and sequence current phasors. It was recognised that:

- where there was current magnitude unbalance only, the negative and zero sequence current phasors were of equal magnitudes and thus so too would be the respective unbalance factors. Only if there was any current angle unbalance did they differ;
- where the relative current angles differed similarly (e.g. *one big, two small angles* or *one small, two big angles*) then depending on current magnitude unbalance either $IUF_0 > IUF_2$ or $IUF_2 > IUF_0$; and
- when current angle unbalance and current magnitude unbalance combined, it was theoretically possible to have no negative sequence current unbalance and only zero sequence current unbalance (the opposite is also true).

These relationships were also clearly evident in the field analyses of section 6.9.1 (Figure 6.31).

8.3.2 Sequence voltage unbalance factors

The differences between sequence voltage unbalance factors is indirectly related to current angle unbalance, through the resulting differences in sequence current unbalance factors that it causes. Each sequence voltage unbalance factor is mostly dependent on its respective sequence current unbalance factor only. This was recognised from the representative feeder which showed that the sequence networks

were to a great extent independent of each other, even though the cable impedance was an asymmetrical four-core cable.

Now, from field analysis of Chapter 6, this direct relationship between each sequence voltage unbalance factor and its respective sequence current unbalance factor was evident only in the case of the zero sequence unbalance factors (Figure 6.32). It could not be proven for the negative sequence unbalance factors because, as mentioned previously, this component is non-localised and so included variations in negative sequence voltage unbalance originating from other parts of the network.

8.4 Quantifying the effects of unbalance

Several mathematical expressions, presented in Chapter 4, were derived specifically for the purpose of quantifying a potential unbalance effect. They include the potential released current capacity (equation (4.1)) and the voltage regulation indicator (equation (4.16)). The suitability of these mathematical expressions to quantify these effects of unbalance was evident in the theoretical and field analyses of Chapters 4 and 6 respectively.

Others, such as the effective power factor (equation (4.6)) were selected from the literature and applied to the analysis.

8.5 A new 5 x 5 approach to solve low-voltage networks

A new approach was proposed for the solution of multi-grounded low-voltage networks represented by 5 x 5 matrices. The general circuit solved is as described in section 3.3 and depicted in Figure 3.3. This general circuit was the starting point for a review of existing approaches and the derivation of the proposed approach. It made only the following assumptions:

- All voltages and currents are perfectly sinusoidal and at 50 Hz; and
- The assumed earth wire is based on Carson's papers [68] [69], where the earth is assumed to be an infinite solid with uniform resistivity.

It was shown that the standard 3 x 3 solution [51] as well as a popular 5 x 5 solution [73] given in the literature, both involve several assumptions and approximations, particularly with regard to the neutral and earth return paths.

The new approach however, made no further assumptions beyond those listed above. Moreover, there were no approximations as to the sharing of the neutral and ground currents. Instead, it used Kirchhoff's voltage and current laws to find these currents.

This new approach was validated first in Chapter 3 by a series of tests, using the test network shown in Figure 3.12, to ensure that its results satisfied Kirchhoff's voltage and current laws. Also, these results, presented in Appendix B, are in very good agreement to those of Matlab Simulink SimPowerSystems. Additionally, in Chapter 7, a second validation was done - this time against actual measurements of voltage and current on the rural feeder. The calculated voltages and currents were in very good agreement, considering that assumptions were made to account for the individual consumer demands. Moreover, the quantified effects of unbalance were also in good agreement with those measured.

In Chapter 7, the computation time of the new 5 x 5 approach was compared to that of the standard 3 x 3 approach. It was observed that for simulations without the static balancer, the standard 3 x 3 approach was faster but for simulations with the static balancer, the new 5 x 5 approach was faster. Regardless, both approaches solve the rural feeder model in less than 0.1 seconds.

8.6 Strengths of the new 5 x 5 approach

8.6.1 The new 5 x 5 approach is needed when investigating static balancers on low-voltage feeders

The current drawn by the static balancer depends largely on the voltages at its terminals; any inaccuracy in the approach used to calculate these voltages will be

reflected in the calculated upstream currents. In Chapter 7, it was seen that even though the results from the 3 x 3 approach are good enough for most applications of an unbalanced power flow method, its phase-neutral voltages were not a very close match to the measured values and this became especially critical when the static balancer was energised.

The proposed 5 x 5 approach on the other hand, produces phase-neutral voltages which are in much better agreement to the measured values, especially when viewed in terms of calculated zero sequence voltages (which as seen from equation (5.11) chiefly determines the current drawn). And this resulted in it producing much more accurate upstream phase and neutral currents than those found with the 3 x 3 approach. For this reason, the more accurate new 5 x 5 approach developed here is needed when investigating static balancers on low-voltage feeders.

8.6.2 The new 5 x 5 approach is preferable when studying feeders with higher zero sequence current unbalance factors

In Chapter 7 it was recognised that the higher absolute voltage difference in results found using the 3 x 3 approach, was related to instances in which the zero sequence current unbalance factor of the total consumer current was higher than the negative sequence current unbalance factor (Figure 7.7). This was not the case for the results found using proposed 5 x 5 approach (Figure 7.8) and so is one of its strengths.

8.7 Grounds for investigating the re-introduction of the static balancer

There are practical and theoretical arguments in favour of the static balancer. Its practical selling points, which were compared to other mitigation methods in Table 2.4, were its simplicity and that it is a retrofit (as opposed to a network replacement).

Additionally, the static balancer reduces the zero sequence currents only, which, as was made evident in the theoretical analysis of section 4.5.3 using the representative

feeder, is of greater importance to the low-voltage network. The incremental benefit of also reducing negative sequence currents and achieving perfect current balance was relatively small.

8.8 Modelling the static balancer

The static balancer was represented in a form suitable for use in the forward-backward sweep method by equation (5.11). The basis for this representation is its very low zero sequence impedance as a result of having an interconnected-star winding. With this equation, the currents drawn by the static balancer are homopolar and will depend on the short-circuit impedance of the static balancer and the zero sequence voltage at its terminals.

After determining the short-circuit impedance by a short-circuit test (the results of which were a very close match to values calculated from manufacturer design sheets) this representation was validated first in the laboratory by applying unbalanced voltages at the terminals of a static balancer. The average difference between measured and calculated phase and neutral currents were found to be fairly small, 0.7 A and 1.7 A respectively.

A second validation against field measurements was carried out in Chapter 6. This was done using the model to calculate the currents upstream of the static balancer from measurements taken by a meter located downstream. The calculated upstream currents were found to be in close agreement (8.3 %) to the measured values, which is adequate for unbalanced power flow simulations.

8.9 Further insight into the behaviour of the static balancer

There is more going on with regard to the behaviour of the static balancer than is explained in [8]. There, the attention is on its ability to redistribute the downstream

neutral currents onto the upstream phases with the result being more evenly balanced upstream phase currents and lower upstream neutral currents.

The field measurements gave an opportunity for insight into other changes, which are also the result of the compensating currents from the static balancer being homopolar. They are as follows.

Firstly, as observed in Figure 6.23, there was considerably more variation in the upstream phase current angles. Now, a change in current angle unbalance may actually be beneficial, as the neutral current – sum of the phase current phasors – may be reduced, depending on the phase current magnitudes. This was evident in the field measurements.

Second, there was a change in the upstream active and reactive power transfers per phase. This was seen in Figure 6.24 and Figure 6.25. The variations across phases were relative to one another. They were the result of the compensation by the static balancer of the zero sequence component of the unbalanced power delivered to the consumers.

The third observation was that the upstream zero sequence current and voltage unbalance factors were considerably reduced (Figure 6.26 and Figure 6.28 respectively). The negative sequence unbalance factors, as anticipated, remained unchanged.

8.10 Strengths and weakness of the static balancer

The field trial of the static balancer revealed its strengths and weaknesses through a comparison of the quantified effects of unbalance for the weeks before and after it was energised.

It was found that the static balancer was very beneficial at improving network utilisation (in terms of both potential release current capacity and effective power factor), reducing neutral current and neutral-point shifting. Improvements to the other

effects such as phase-neutral voltage magnitudes and voltage regulation were not discernible, given the short length of the rural feeder.

With regard to a reduction in total losses (due to reduced current unbalance), it was recognised the total energy losses as a percentage of the energy delivered, increased slightly with the static balancer. This was because of its iron losses.

9. Future work

9.1 Deployment of static balancers for urban feeders

The MEB Notes on the static balancer [9] recommends that the static balancer be positioned at the end of the feeder. However, the field analyses of Chapter 6 revealed that several network effects were dependent on the relative magnitudes of the zero sequence current drawn by consumers upstream and downstream of static balancer. Specifically, if:

- the zero sequence current drawn by consumers downstream is higher then there is a greater improvement in the potential release current capacity, effective power factor and neutral current.
- the zero sequence current drawn by consumers upstream is higher then there is a greater improvement in network losses and neutral-point shifting (its change was seen in zero sequence voltage).

Therefore, the positioning of the static balancer may not be as straightforward as implied in [9] and some further investigation is needed to ensure the best use of static balancers on urban feeders. This thesis provides the foundation for that investigation with a validated new 5 x 5 approach to the forward-backward sweep method as well as a validated rural feeder model, in which the influence of its position can be readily recognised.

9.2 Specification of static balancers for urban feeders

The impedances of urban and rural feeders differ (in terms of feeder lengths and R/X ratios of the cable and overhead lines). The impedance of the static balancer in relation to the network impedance may influence the benefits seen on the network. This sensitivity should be investigated.

9.3 Investigation of a 4 x 4 approach to the forward-backward sweep method based on the assumption of the earth as a perfect conductor

In Chapter 7, the computation time of the proposed 5 x 5 approach was found to be longer that of the standard 3 x 3 approach for network simulations without the static balancer. Now, even though the proposed 5 x 5 approach was developed for the planning of very unbalanced feeders and research into the impact of high penetrations of low-carbon technologies, it may be simplified to give a new 4 x 4 approach which may be suited to the accurate real-time solution of very unbalanced feeders as well. This simplification will involve making the assumption that the earth is a perfect conductor.

Now, if the earth is assumed to be a perfect conductor, it has zero impedance and shares no mutual inductances to the phase and neutral wires. This can be expressed by setting Z_{pg}, Z_{ng} and Z_{gg} (where $p = a, b, c, n$), which appear in the Z'_{pn} terms of equation (3.23) to zero. Also, the only current flowing to ground would be $I_{z(l-1)}$ and $I_{z(l)}$ ($I_{g(l-1)}$ and $I_{g(l)}$ would be zero as both ends of the perfect earth conductor are at zero volts). Using KVL and KCL only, as was done in section 3.7.1, the exact equation for the sharing of the out-of-balance current can be found:

$$I_{n(l)} = \frac{\left(I_{n(l+1)} + I_{Labc(j)}\right)Z_{gr(l)} - \left[\left(Z_{an} + Z_{gr(l-1)}\right)I_{a(l)} + \left(Z_{bn} + Z_{gr(l-1)}\right)I_{b(l)} + \left(Z_{cn} + Z_{gr(l-1)}\right)I_{c(l)}\right]}{\left(Z_{nn} + Z_{gr(l)} + Z_{gr(l-1)}\right)} \quad (9.1)$$

This equation is general and would apply to any branch segment on the network. The following simplifications should be noted if:

- l is the only branch: $I_{La(j)} = I_{a(l)}$,$I_{Lb(j)} = I_{b(l)}$,$I_{Lc(j)} = I_{c(l)}$ and $I_{Labc(j)} = I_{n(l)}$ (9.2a)
- l is the last branch: $I_{n(l+1)} = 0$ (9.2b)
- l is the first branch: $I_{n(l-1)} = 0$ and $Z_{gr(l-1)} = Z_{gr(0)}$. (9.2c)

The current $I_{z(l)}$ flowing to earth is given by:

$$I_{z(l)} = I_{n(l+1)} - I_{n(l)} + I_{Labc(j)} \quad (9.3)$$

These equations must first be validated in the same manner as the proposed 5 x 5 approach. With them the influence of the assumption of the earth as a perfect conductor can be studied. Moreover, the computation time of the new 4 x 4 approach can be compared to that of the proposed 5 x 5 approach and the standard 3 x 3 approach.

9.4 Isolating the negative sequence voltage unbalance on a low-voltage feeder from that originating at the higher voltage network

From this thesis it has been recognised that:

- Each sequence voltage unbalance factor is directly proportional to its own sequence current unbalance factor;
- Even with asymmetrical cable impedances, the negative sequence voltage unbalance is not very dependent on the zero sequence current unbalance factor (and likewise the zero sequence voltage unbalance factor is not very dependent on the negative sequence current unbalance factor); and
- Current angle unbalance accounts for the differences between the negative and zero sequence current unbalance factors.

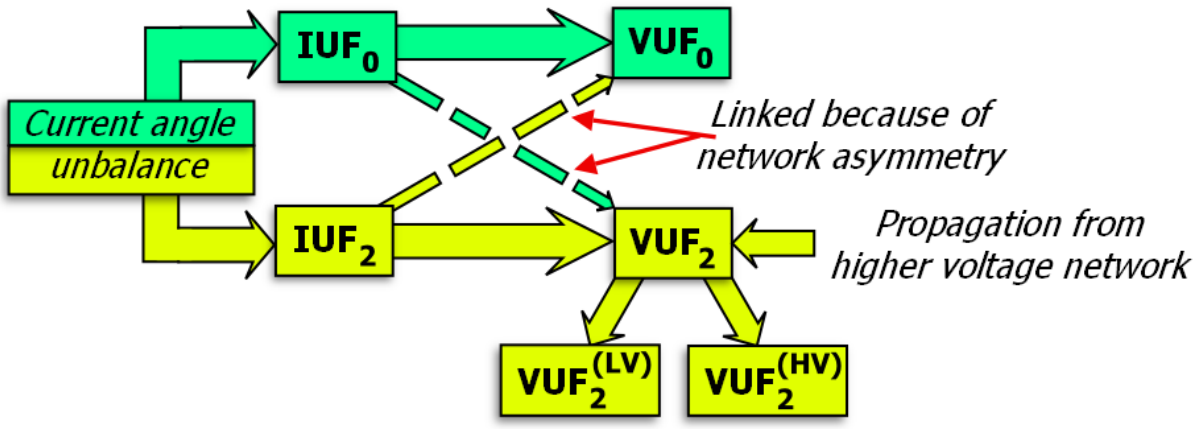

Figure 9.1: The relationships between the four sequence unbalance factors

The relationships between the four sequence unbalance factors are illustrated in Figure 9.1. Using them, it is possible to determine estimates for the negative sequence voltage unbalance factor due to:

- the loads on the low-voltage feeder itself ($VUF_2^{(LV)}$); and
- the higher voltage network ($VUF_2^{(HV)}$).

Therefore, if measurements are taken at the start of a low-voltage feeder of the four sequence unbalance factors and all phase current magnitudes and angles, it would be possible for a utility field engineer to determine the origin of a high negative sequence voltage unbalance factor. Such a feature, once validated against field measurements, can be programmed into power quality meters.

9.5 The mitigation of harmonics using static balancers

In addition to the benefits presented in Chapter 6, the static balancer also reduces voltage and current harmonics. This additional benefit is advantageous because low-carbon technologies using inverter systems may potentially worsen the harmonics on the low-voltage network.

During the first field trial a full harmonic record was downloaded from the Ametek meter. This gives an opportunity to examine this benefit.

The harmonic voltages, as defined as in [91], were found for a week with and without the static balancer. They are the rms amplitude of the harmonic voltage of order h given as a percentage of the rms amplitude of the fundamental component. The spectrum of these harmonic voltages up to the 24th harmonic component is shown in Figure 9.2. For each component, the bottom of the red bar indicates the value below which 95 % observations are contained. Similarly, the bottom of the blue bar indicates the value below which 50 % of the observations are contained.

Figure 9.2 (a) shows the harmonic voltages without the static balancer. It indicates that the rural feeder had significant levels of odd harmonics – particularly 3rd, 5th, 7th, 9th, 11th and 13th – with the 5th being the highest. With the static balancer energised, Figure

9.2 (b), it was observed that the 3rd, 5th, 9th and 11th harmonic components were reduced whilst the 7th and 13th harmonic components remained relatively unchanged.

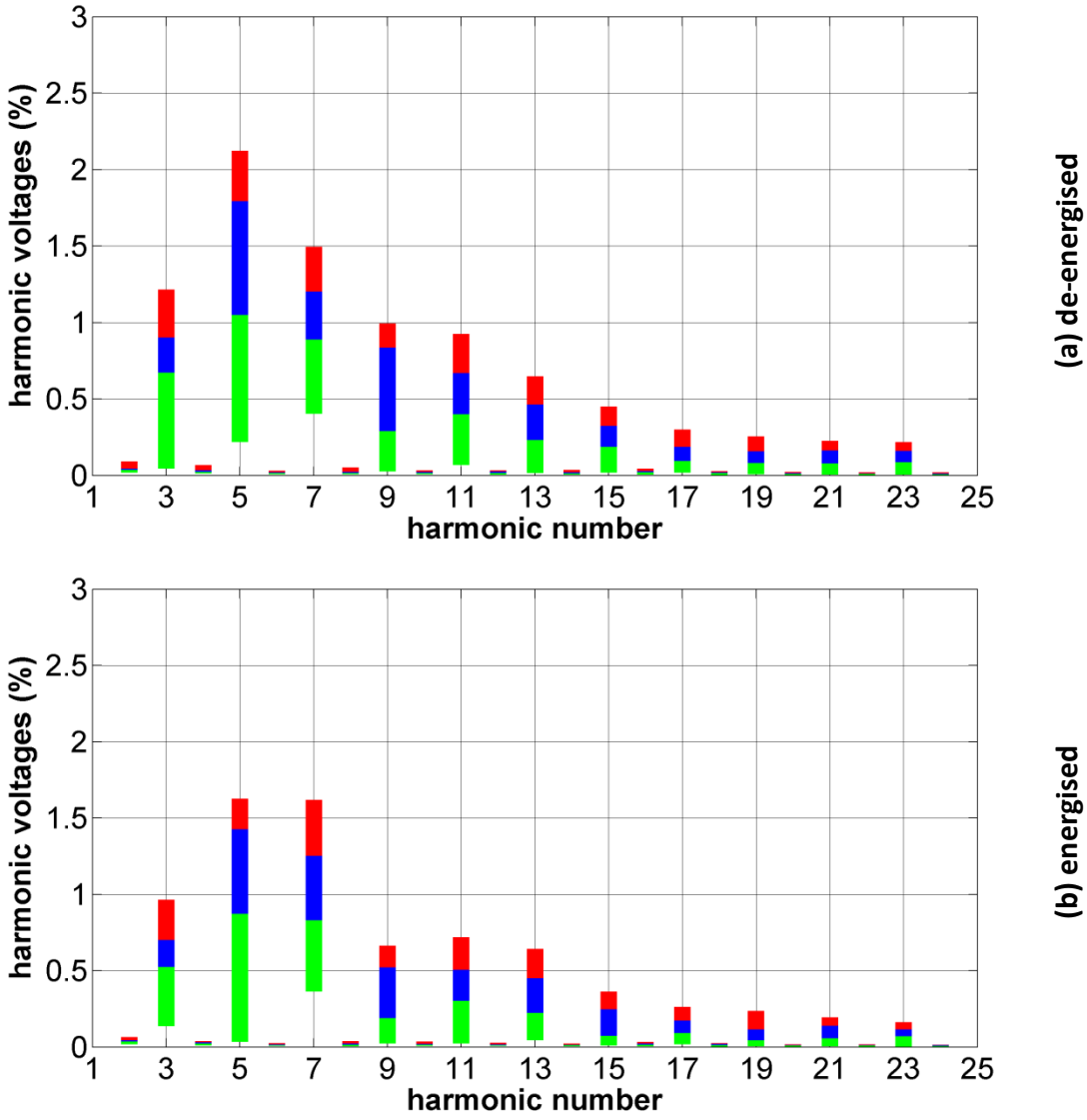

Figure 9.2: Harmonic voltages as seen on all phases for the weeks with the static balancer (a) de-energised and (b) energised.

The spectrum of the harmonic currents during a week with and without the static balancer is shown in Figure 9.3. The harmonic currents are the rms amplitude of the harmonic currents of order h as a percentage of the rms amplitude of the fundamental component.

Figure 9.3 (a) shows that on the rural feeder, the 3rd harmonic component is the most significant and is followed by the 5th, 7th, 9th, 11th and 13th harmonics components. With the static balancer energised, Figure 9.3 (b), there is a noticeable reduction in the 3rd,

5th, 11th and 13th harmonic components and to a less noticeable degree the 9th harmonic component as well.

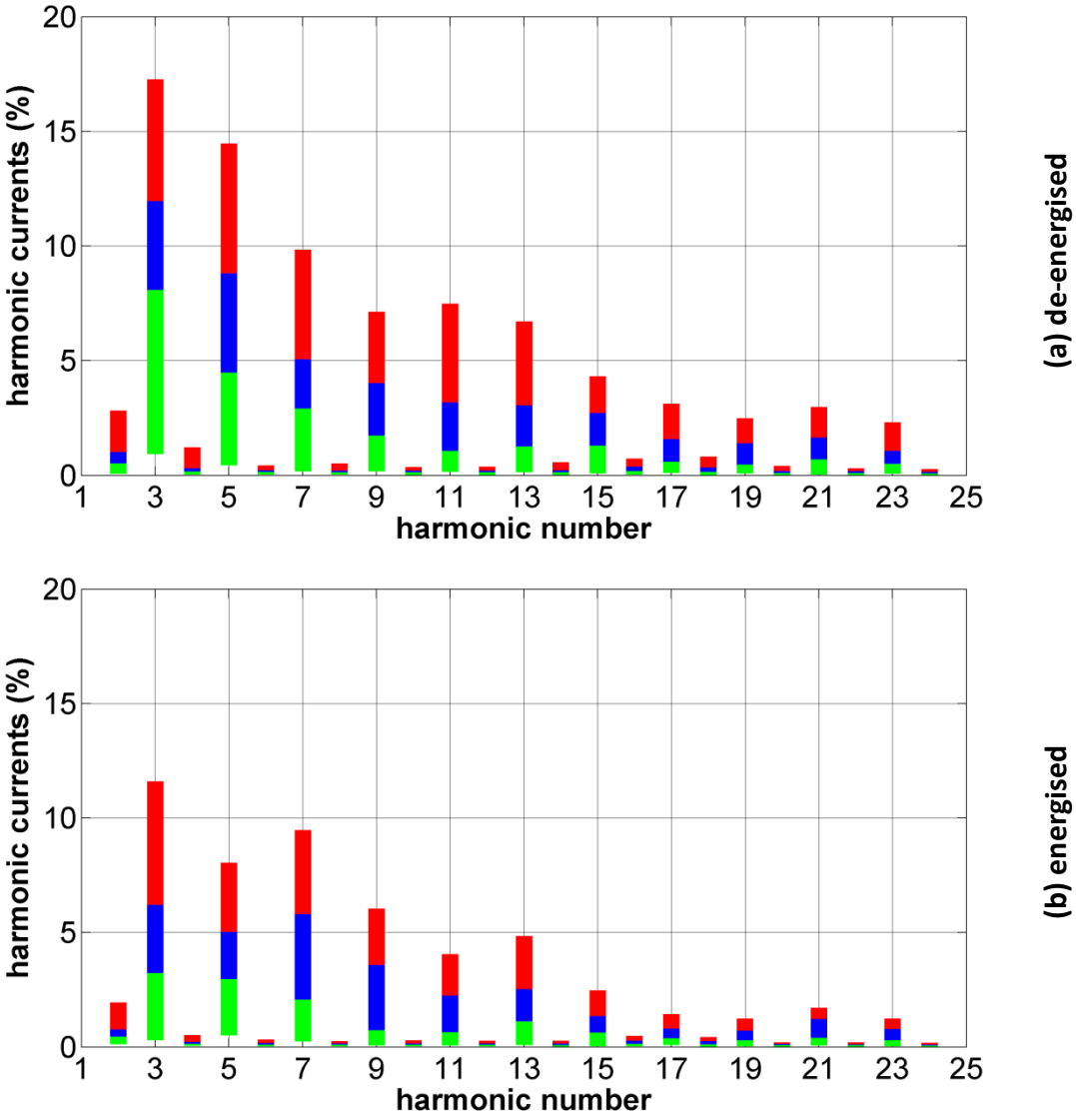

Figure 9.3: Harmonic currents as seen on all phases for the weeks with the static balancer (a) de-energised and (b) energised.

Now, it was expected that the static balancer would reduce the triplen harmonic components as they are zero sequence components [92]. Further investigation is needed to explain how it deals with the odd harmonics like the 5th, 7th, 11th and 13th harmonic components, as the observations made about these components are not immediately evident. Further work in this topic should also include more field measurements or laboratory experiments to quantify this benefit.

10. References

[1] Energy Networks Association, “Engineering Recommendation G12/3: Requirements for the Application of Protective Multiple Earthing to Low Voltage Networks,” Energy Networks Association, London.

[2] Scottish and Southern Energy Power Distribution, “LCNF Tier 1 Close-Down report: Demonstrating the benefits of monitoring LV networks with embedded PV panels and EV charging point,” 2012. [Online]. Available: http://www.ssepd.co.uk/uploadedFiles/Controls/Lists/Innovation/LV_network_monitoring/SSET1002LV_NetworkMonitoringCloseDownReport130228.pdf.

[3] P. Bale, Western Power Distribution, “PV impacts on suburban networks,” in *2012 Low Carbon Network Fund Annual Conference*, Cardiff, 2012.

[4] D. Randles, Electricity North West, “Low Voltage Network Solutions,” in *2012 Low Carbon Network Fund Annual Conference*, Cardiff, 2012.

[5] Energy Networks Association, “ENA - 2012 Low Carbon Networks Fund Annual Conference,” Energy Networks Association, 2012. [Online]. Available: http://www.energynetworks.org/electricity/smart-grid-portal/lcnf/2012-low-carbon-networks-fund-annual-conference.html. [Accessed 07/11/2012 November 2012].

[6] J. Meyer, S. Hahle, P. Schegner and C. Wald, “Impact of electrical car charging on unbalance in public low voltage grids,” in *Electrical Power Quality and Utilisation (EPQU), 2011 11th International Conference on*, Lisbon, 2011.

[7] A. Stigant, “A device for the rapid determination of the current distribution of the line side of a three-phase inter-connected-star static balancer operating on a four wire system,” *Electrical Engineers, Journal of the Institution of,* pp. 57(2), 201-208, 1919.

[8] S. A. Stigant and H. M. Lacey, The J & P Transformer Book being a Practical Technology of the Power Transformer, London: Johnson & Philips Ltd, 1935.

[9] Midlands Electricity Board, Notes on Static Balancers, circa 1960s.

[10] E.ON Central Networks, “Network Design Manual,” December 2006.

[11] C. Wagner and R. Evans, Symmetrical Components as Applied to the Analysis of Unbalanced Electrical Circuits, New York and London, U.K.: McGraw-Hill, 1933.

[12] C. L. Fortescue, “Method of symmetrical co-ordinates applied to the solution of polyphase networks,” *34th Annual Convention of the American Institute of Electricaal Engineers, Atlantic City, N.J.,* pp. 1027-1140, 1918.

[13] H. Akagi, Y. Kanazawa and A. Nabae, “Generalized theory of instantaneous reactive power and its applications,” *Transactions of the IEE-Japan,* Vols. Part B, vol. 103, no. 7, pp. 483-490, 1983.

[14] H. Akagi, S. Ogasawara and H. Kim, “The theory of instantaneous power in three-phase four-wire systems and its applications,” *Electrical Engineering in Japan,* vol. 135, no. 3, pp. 74-86, 2001.

[15] L. S. Czarnecki, “On some misinterpretations of the instantaneous reactive power p-q theory,” *IEEE Transactions on Power Electronics,* vol. 19, no. 3, pp. 828-836, 2004.

[16] J. L. Willems, “Critical analysis of different current decomposition and compensation schemes,” in *International School on Nonsinusoidal Currents and Compensation*, Łagów, Poland, 2008.

[17] J. J. Grainger and W. D. J. Stevenson, Power System Analysis, New York: McGraw-Hill, 1994.

[18] P. Pillay and M. Manyage, “Definitions of Voltage Unbalance,” *IEEE Power Engineering Review,* vol. 21, no. 5, pp. 49-51, 2001.

[19] M. H. J. Bollen, “Definitions of Voltage Unbalance,” *IEEE Power Engineering Review,* vol. 22, no. 11, pp. 49-50, 2002.

[20] A. K. Singh, G. K. Singh and R. Mitra, “Some Observations on Definitions of Voltage Unbalance,” *39th North American Power Symposium, NAPS '07.,* pp. 473-479, 2007.

[21] British Standards Institute, BS EN 50160: Voltage characteristics of electricity supplied by public electricity networks, London: British Standards Institute, 2010.

[22] British Standards Institute, BS EN 61000-2-2: Electromagnetic compatibility

(EMC). Environment. Compatibility levels for low-frequency conducted disturbances and signalling in public low-voltage power supply systems, London: British Standards Institute, 2002.

[23] IEEE Power & Energy Society, IEEE Std 1159: Recommended Practice for Monitoring Electric Power Quality, New York: IEEE, 2009.

[24] J. A. L. Ghijselen and Z. P. M. Van den Bossche, "Exact voltage unbalance assessment without phase measurements," *IEEE Transactions on PowerSystems,* vol. 20, no. 1, pp. 519-520, 2005.

[25] Energy Networks Association, Engineering Recommendation P29: Planning limits for voltage unbalance in the United Kingdom, London: Energy Networks Association, 1990.

[26] I. Richardson, Integrated High-resolution Modelling of Domestic Electricity Demand and Low Voltage Electricity Distribution Networks, Ph.D. Thesis. Loughborough University., 2010.

[27] C. Tsai-Hsiang and Y. Wen-Chih, "Analysis of multi-grounded four-wire distribution systems considering the neutral grounding," *Power Delivery, IEEE Transactions on,* vol. 16(4), pp. pp. 710-717, 2001.

[28] M. A. Taghikhani and M. Rafiei, "Thermal coefficient measurements of typical distribution transformers operating under imbalance conditions," in *Electrical Power Distribution Networks (EPDC), 2011 16th Conference on*, Bandar Abbas, Iran, 2011.

[29] J. Desmet, D. Putman, F. D'hulster and R. Belmans, "Thermal analysis of the influence of nonlinear, unbalanced and asymmetric loads on current conducting capacity of LV-cables," in *Power Tech Conference Proceedings, 2003 IEEE*, Bologna, 2003.

[30] L. Degroote, B. Renders, B. Meersman and L. Vandevelde, "Neutral-point shifting and voltage unbalance due to single-phase DG units in low voltage distribution networks," in *2009 IEEE PowerTech*, Bucharest, 2009.

[31] M. Chindris, A. Cziker, A. Miron and H. Bălan, "Propagation of Unbalance in Electric Power Systems," in *Electrical Power Quality and Utilisation, 9th*

International Conference on, Barcelona, Spain., 2007.

[32] A. S. Anderson and R. C. Ruete, "Voltage Unbalance in Delta Secondaries Serving Single-Phase and 3-Phase Loads," *Power Apparatus and Systems, Part III. Transactions of the American Institute of Electrical Engineers,* vol. 73, no. 2, pp. 928-932, 1954.

[33] A. Von Jouanne and B. Banerjee, "Assessment of voltage unbalance," *Power Delivery, IEEE Transactions on,* vol. 16(4), pp. pp. 782-790, 2001.

[34] British Standards Institute, BS EN 61000-4-27: Electromagnetic compatibility (EMC) - Part 4-27: Testing and measurement techniques - Unbalance, immunity test, London: British Standards Institute, 2001.

[35] W. H. Kersting and W. H. Phillips, "Phase frame analysis of the effects of voltage unbalance on induction machines," *IEEE Transactions on Industry Applications,* vol. 33, no. 2, pp. 415-420, 1997.

[36] National Electrical Manufacturers Association (NEMA), MG 1-1998: Motors and Generators, Rosslyn: NEMA Standards Publication, 1998.

[37] British Standards Institute, BS EN 60034-1: Rotating electrical machines, Part 1: Rating and performance, London: British Standards Institute, 2010.

[38] S.-G. Jeong and J.-Y. Choi, "Line Current Characteristics of Three-Phase Uncontrolled Rectifiers Under Line Voltage Unbalance Condition," *IEEE Transactions of Power Electronics,* vol. 17, no. 6, pp. 935-945, 2002.

[39] O. Wasynczuk, "Analysis of line-commutated converters during unbalanced operating conditions," *IEEE Transactions on Energy Conversion,* vol. 9, no. 2, pp. 420-426, 1994.

[40] M. Chomat and L. Schreier, "Control method for DC-link voltage ripple cancellation in voltage source inverter under unbalanced three-phase voltage supply conditions," *Electric Power Applications, IEE Proceedings,* vol. 152, no. 3, pp. 494-500, 2005.

[41] J.-K. Kang and S.-K. Sul, "Control of unbalanced voltage PWM converter using instantaneous ripple power feedback," in *28th Annual IEEE Power Electronics Specialists Conference*, St. Louis, 1997.

[42] O. Ojo and I. Bhat, “Influence of input supply voltage unbalances on the performance of AC/DC buck rectifiers,” *25th Annual IEEE Power Electronics Specialists Conference, PESC '94 Record.,* vol. 2, pp. 777-784, 1994.

[43] J. Carr and L. V. McCall, “Divergent evolution and resulting characteristics among the world's distribution systems,” *IEEE Transactions on Power Delivery,* vol. 7, no. 3, pp. 1601-1609, 1992.

[44] M. W. Siti, D. V. Nicolae and A. A. Jimoh, “Reconfiguration and Load Balancing in the LV and MV Distribution Networks for Optimal Performance,” *IEEE Transactions on power delivery,* vol. 22, no. 4, pp. 2534-2540, 2007.

[45] S. Civanlar, J. J. Grainger, H. Yin and S. S. Lee, “Distribution feeder reconfiguration for loss reduction,” *IEEE Transactions on power delivery,* vol. 3, no. 3, pp. 1217-1223, 1988.

[46] D. V. Nicolae, M. W. Siti and A. A. Jimoh, “LV self balancing distribution network reconfiguration for minimum losses,” in *IEEE* , Bucharest, 2009 IEEE Bucharest PowerTech.

[47] S. W. Heunis and R. Herman, “A load reconfiguration algorithm for optimizing LV residential feeders with voltage performance as the criterion,” in *Power Engineering Society Summer Meeting*, 2001.

[48] W. H. Kersting and W. H. Phillips, “Modeling and analysis of unsymmetrical transformer banks serving unbalanced loads,” *IEEE Transactions on Industry Applications,* vol. 32, no. 3, pp. 720-725, 1996.

[49] W. H. Kersting, “Causes and effects of unbalanced voltages serving an induction motor,” *IEEE Transactions on Industry Applications,* vol. 37, no. 1, pp. 165-170, 2001.

[50] A. Baggini, Handbook of Power Quality, London: United Kingdom: Wiley, 2008.

[51] W. Kersting, Distribution System Modeling and Analysis, New York: CRC Press, 2002.

[52] W. E. M. Ayres, “The application of the induction voltage regulator,” *Electrical Engineers, Journal of the Institution of,* vol. 69, no. 418, pp. 1208-1218, 1931.

[53] D. Randles, Electricity North West, “Voltage management of low voltage (LV)

busbars," in *2012 Low Carbon Network Fund Annual Conference*, Cardiff, 2012.

[54] T. J. Reynal, "Load balancing transformer". United States of America Patent 5 557 249, 17 September 1996.

[55] D. Ahmadi, M. Bina and M. Golkar, "A Critical Cross-Examination on Load-Balancing Transformers for Distribution Systems," *Power Delivery, IEEE Transactions on,* pp. 25(3), 1645-1656, 2010.

[56] D. Ahmadi, M. Bina and M. Golkar, "A comprehensive comparison between three practical topologies of the load-balancing transformers," in *1st Power Electronic & Drive Systems & Technologies Conference (PEDSTC)*, Tehran, 2010.

[57] H. Beltrán, N. Aparicio, E. Belenguer and C. C. Garcia, "Fuel cell connection inverters used for unbalance compensation in low voltage distribution systems," in *The International Conference on Renewable Energies and Power Quality*, Santander, 2008.

[58] B. Meersman, B. Renders, L. Degroote, T. Vandoorn and L. Vandevelde, "DC-bus voltage controllers for a three-phase voltage-source inverter for distributed generation," in *International Conference on Renewable Energies and Power Quality (ICREPQ09)*, Valencia, 2009.

[59] B. Meersman, B. Renders, L. Degroote, T. Vandoorn and L. Vandevelde, "Three-phase inverter-connected DG-units and voltage unbalance," *Electric Power Systems Research,* vol. 81, no. 4, pp. 899-906, 2011.

[60] F. Shahnia, A. Ghosh, G. Ledwich and F. Zare, "An approach for current balancing in distribution networks with rooftop PVs," in *2012 IEEE Power and Energy Society General Meeting*, San Diego, 2012.

[61] F. Shahnia, R. Majumder, A. Ghosh, G. Ledwich and F. Zare, "Voltage imbalance analysis in residential low voltage distribution networks with rooftop PVs," *Electric Power Systems Research,* vol. 81, no. 9, pp. 1805-1814, 2011.

[62] K. H. Chua, Y. S. Lim, J. Wong, P. Taylor, E. Morris and S. Morris, "Voltage unbalance mitigation in low voltage distribution networks with photovoltaic systems," *Journal of Electronic Science and Technology,* vol. 10, no. 1, pp. 1-6, 2012.

[63] Y. Hu, Z. Chen and P. Excell, “Power quality improvement of unbalanced power system with distributed generation units,” *Electric Utility Deregulation and Restructuring and Power Technologies (DRPT), 2011 4th International Conference on,* pp. 417-423, 2011.

[64] Scottish and Southern Energy Power Distribution, “Design Drivers for an Energy Storage and Management Unit for connection to a DNOs low-voltage network,” in *provided via email from Martin Lee on the 14th February, 2014.*, Nottingham, 2013.

[65] Scottish and Southern Energy Power Distribution, “Specification for the provision of Energy Storage and Management Units for SSEPD.,” in *provided via email from Martin Lee on the 14th February, 2014.*, Nottingham, 2013.

[66] Claude Lyons Limited, “3rd Harmonic Rejection Transformers,” 20 July 2001. [Online]. Available: http://www.claudelyons.co.uk/pdf/hrt.pdf. [Accessed 31 May 2013].

[67] The Transformer & Electrical Co Ltd, “Neutral Current Trap (3rd harmonic rejection transformer),” [Online]. Available: http://www.teccoltd.com/hrt1.html. [Accessed 31 May 2013].

[68] J. R. Carson, “Wave propogation in overhead wires with ground return,” *Bell System Technical Journal,* vol. 5(4), pp. 539-554, 1926.

[69] J. R. Carson, “Ground return impedance: Underground wire and earth return,” *Bell System Technical Journal,* vol. 8(1), pp. 94-98, 1929.

[70] P. M. Anderson, Analysis of faulted power systems, New York: IEEE Press, 1995.

[71] J. Horak, “Zero sequence impedance of overhead transmission lines,” in *59th Annual Conference for Protective Relay Engineers, 2006*, College Station, 2006.

[72] W. H. Kersting, “The Whys of Distribution System Analysis,” *IEEE Industry Applications Magazine,* vol. 17, no. 5, pp. 59-65, 2011.

[73] R. Ciric, A. Feltrin and L. Ochoa, “Power flow in four-wire distribution networks-general approach,” *Power Systems, IEEE Transactions on,* vol. 18(4), pp. pp. 1283-1290, 2003.

[74] The MathWorks, Inc., SimPowerSystems for use with Simulink - User's Guide

(Version 3), Natick: The MathWorks, Inc., 2003.

[75] IEEE Std 1459-2010, IEEE Standard Definitions for the Measurement of Electric Power Quantities Under Sinusoidal, Nonsinusoidal, Balanced, or Unbalanced Conditions., IEEE, 2010.

[76] A. E. Emanuel, "On the definition of power factor and apparent power in unbalanced polyphase circuits with sinusoidal voltage and currents," *Power Delivery, IEEE Transactions on,* vol. 8(3), pp. pp. 841-852, 1993.

[77] L. S. Czarnecki, "Power related phenomena in three-phase unbalanced systems," *Power Delivery, IEEE Transactions on,* vol. 10(3), pp. pp. 1168-1176, 1995.

[78] J. L. Willems, J. A. Ghijselen and A. E. Emanuel, "The apparent power concept and the IEEE Standard 1459-2000," *Power Delivery, IEEE Transactions on,* vol. 20 (2), pp. pp. 876-884, 2005.

[79] Electric Utility Engineers of the Westinghouse Electric Corporation, Electric Utility Engineering Reference Book : Distribution Systems, East Pittsburgh, PA.: Westinghouse Electric Corporation, 1959.

[80] "Prysmian Cables and Systems," 2009. [Online]. Available: http://www.prysmian.co.uk/export/sites/prysmian-enGB/attach/pdf/Low_Voltage_Cables/Low_Voltage_Utility/Waveform_Cable_2012.pdf. [Accessed 14 April 2012].

[81] The Transformer & Electrical Co Ltd, *Design sheet for 100 amp balancers (attachment (100AMP BALANCER058) to email dated 28.06.2010),* 2010.

[82] N. Oliver-Taylor, "Voltage unbalance in low-voltage distribution networks (MEng project)," Department of Electronic and Electrical Engineering, Loughborough University, 2011.

[83] BS EN 50160, Voltage characteristics of electricity supplied by public electricity networks, BSI, 2010.

[84] BS 3988, Specification for wrought aluminium for electrical purposes - Solid conductors for insulated cables, BSI, 1970.

[85] G P U Power Distribution, "Overhead Lines Material Manual," 1980-2000s.

[86] J. R. Taylor, An Introduction to Error Analysis: The study of uncertainties in

physical measurements, Sausalito: University Science Books, 1982.

[87] Fluke, “Disturbance Analyzer: Fluke 1740 Series Three-Phase Power Quality Loggers,” Fluke, [Online]. Available: http://www.fluke.com/fluke/m3en/Power-Quality-Tools/Logging-Power-Meters/Fluke-1740-Series.htm?PID=56029. [Accessed 09 02 2014].

[88] AMETEK Power Instruments, *P&QR Power & Quality Recorder,* New York: AMETEK Power Instruments, 2004.

[89] Fluke, “Fluke i3000 Flex AC Current Clamp. Flex-24.,” Fluke, 03 2006. [Online]. Available: http://media.fluke.com/documents/i3000s__iseng0000.pdf. [Accessed 03 2014].

[90] F. Mather, “Earthing of low- and medium-voltage distribution systems and equipment,” *Proceedings of the IEE - Part A: Power Engineering,* vol. 105, no. 20, pp. 97-104, 1958.

[91] The Electricity Association, Engineering Recommendation G5/4: Planning levels for harmonic voltage distortion and the connection of non-linear equipment to transmission systems and distribution networks in the United Kingdom, London: The Electricity Association Services Limited, 2001.

[92] C. Sankaran, Power Quality, Boca Raton: CRC Press, 2002.

A. Overhead line and cable impedance calculations

A.1 Primitive impedance matrix and equations

Carson's papers [68] and [69] are the basis for the calculation of the impedances for cables with an assumed ground return. In Carson's approach, the earth is assumed to be an infinite solid with constant resistivity and all wires are grounded at the remote end. His method is covered in texts such as [70] and [51]. The equations used here follow that of [70]. The primitive self and mutual impedances, as defined in [70], are used to represent all phase, neutral and assumed ground wires for both cable and overhead line designs.

The cable designs and circuits for a three-core and a four-core cable with assumed ground wires are given in Figure A.1. It can be seen that with the three-core cable, representation by a 5 x 5 matrix is direct; as it is comprised of five conductors - three phase wires, a concentric neutral and an assumed ground wire. For the four-core cable however, there are two neutral conductors – a neutral wire and a concentric neutral – and so six conductors. Therefore, an additional step – Kron reduction, which assumes that both neutrals are in parallel - is required for its 5 x 5 matrix representation. The following are the steps for calculating the impedances for both cables. The four-core cable is used as an example.

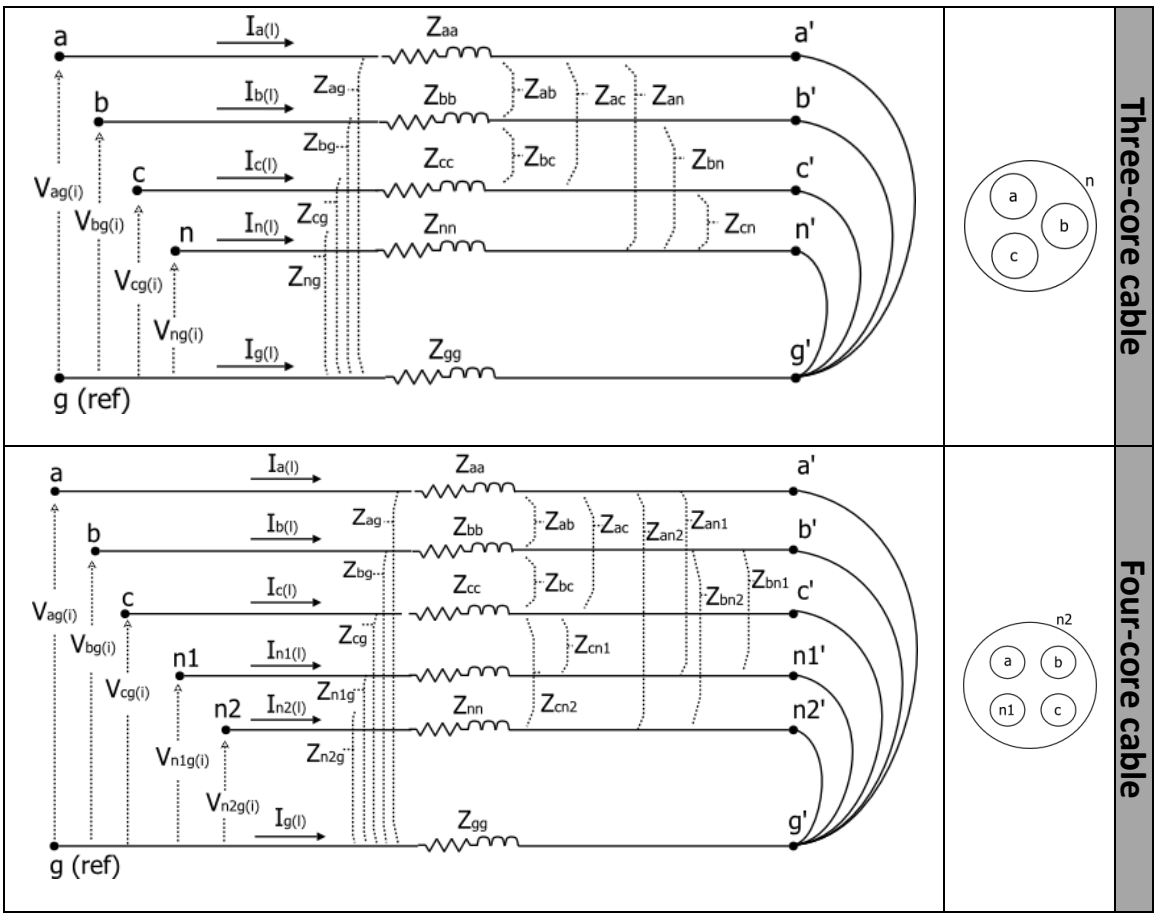

Figure A.1: Cable designs and circuits for both cables.

Referring to Figure A.1, the voltage drop equations are:

$$\begin{bmatrix} V_{aa'} \\ V_{bb'} \\ V_{cc'} \\ V_{n1n1'} \\ V_{n2n2'} \\ V_{gg'} \end{bmatrix} = \begin{bmatrix} \bar{z}_{aa} & \bar{z}_{ab} & \bar{z}_{ac} & \bar{z}_{an1} & \bar{z}_{an2} & \bar{z}_{ag} \\ \bar{z}_{ab} & \bar{z}_{bb} & \bar{z}_{bc} & \bar{z}_{bn1} & \bar{z}_{bn2} & \bar{z}_{bg} \\ \bar{z}_{ac} & \bar{z}_{bc} & \bar{z}_{cc} & \bar{z}_{cn1} & \bar{z}_{cn2} & \bar{z}_{cg} \\ \bar{z}_{an1} & \bar{z}_{bn1} & \bar{z}_{cn1} & \bar{z}_{n1n1} & \bar{z}_{n1n2} & \bar{z}_{n1g} \\ \bar{z}_{an2} & \bar{z}_{bn2} & \bar{z}_{cn2} & \bar{z}_{n1n2} & \bar{z}_{n2n2} & \bar{z}_{n2g} \\ \bar{z}_{ag} & \bar{z}_{bg} & \bar{z}_{cg} & \bar{z}_{n1g} & \bar{z}_{n2g} & \bar{z}_{gg} \end{bmatrix} \begin{bmatrix} I_{a(l)} \\ I_{b(l)} \\ I_{c(l)} \\ I_{n1(l)} \\ I_{n2(l)} \\ I_{g(l)} \end{bmatrix} \quad \text{(A.1)}$$

The primitive impedances given in this 6 x 6 matrix are found using the standard formulae for the self and mutual inductance between two parallel cylindrical wires [70]. For the phase and neutral conductors, they are given by:

Primitive self impedances (Ω/km)

$$\bar{z}_{pp} = r_p + j\omega k \left(\ln \frac{2s}{D_{sp}} - 1 \right) \quad \text{(A.2)}$$

$$p = a, b, c, n1, n2$$

Primitive mutual impedances (Ω/km)

$$\bar{z}_{pq} = j\omega k\left(\ln\frac{2s}{D_{pq}} - 1\right) \quad \text{(A.3)}$$

$p, q = a, b, c, n1, n2$

$p \neq q$

where

$r_p =$ resistance of phase conductor or neutral p. (Ω/km)

$s =$ length of wire (1000 m). (m)

$D_{sp} =$Geometric mean radius of phase or neutral conductor p. (m)

$\omega = 2 \cdot \pi \cdot f\ (rad/sec)$

$f =$ frequency. (Hz)

$k = 2 \cdot 10^{-4}.\ (constant)$

$D_{pq} =$Geometric mean distance between conductor p and q. (m)

Further, the primitive ground self and mutual impedances, as given in [70], are:

Primitive ground self impedance (Ω/km)

$$\bar{z}_{gg} = r_d + jwk\left(\ln\frac{2s}{D_{sd}} - 1\right) \quad \text{(A.4)}$$

Primitive ground mutual impedances (Ω/km)

$$\bar{z}_{pg} = jwk\left(\ln\frac{2s}{D_{ad}} - 1\right) \quad \text{(A.5)}$$

$p = a, b, c, n1, n2$

where

$r_d = 9.869 \cdot 10^{-4} \cdot f\ (\Omega/km)$

$D_{sd} =$ Geometric mean radius of assumed ground wire g. Set to one metre.

$D_{ad} =$Distance between conductor p and assumed ground wire g.

Approximated in [70] by:

$$D_{ad} = \sqrt{\left(658.368 \cdot \sqrt{\rho/f}\right) \cdot D_{sd}} \qquad (m)$$

$$D_{ad} = 25.658 \cdot (\rho/f)^{1/4} \qquad (m) \quad \text{(A.6)}$$

where $\rho =$ earth resistivity. Assumed to be 100 ohm-metre.

Equations (A.2) to (A.6) can be used to find all the primitive impedances for both cables.

The following describes the additional step needed to convert the 6 x 6 matrix of (A.1) into a 5 x 5 matrix (applicable only to the four-core cable). Firstly, the assumption that the neutral conductor and the concentric neutral and ground wires are connected in parallel implies that $\mathrm{V_{n1n1'} = V_{n2n2'}}$. This means that subtracting the fourth row from the fifth row of equation (A.1) gives a new equation:

$$\begin{bmatrix} V_{aa'} \\ V_{bb'} \\ V_{cc'} \\ V_{n1n1'} \\ 0 \\ V_{gg'} \end{bmatrix} =$$

$$\begin{bmatrix} \bar{z}_{aa} & \bar{z}_{ab} & \bar{z}_{ac} & \bar{z}_{an1} & \bar{z}_{an2} & \bar{z}_{ag} \\ \bar{z}_{ab} & \bar{z}_{bb} & \bar{z}_{bc} & \bar{z}_{bn1} & \bar{z}_{bn2} & \bar{z}_{bg} \\ \bar{z}_{ac} & \bar{z}_{bc} & \bar{z}_{cc} & \bar{z}_{cn1} & \bar{z}_{cn2} & \bar{z}_{cg} \\ \bar{z}_{an1} & \bar{z}_{bn1} & \bar{z}_{cn1} & \bar{z}_{n1n1} & \bar{z}_{n1n2} & \bar{z}_{n1g} \\ \bar{z}_{an2} - \bar{z}_{an1} & \bar{z}_{bn2} - \bar{z}_{bn1} & \bar{z}_{cn2} - \bar{z}_{cn1} & \bar{z}_{n1n2} - \bar{z}_{n1n1} & \bar{z}_{n2n2} - \bar{z}_{n1n2} & \bar{z}_{n2g} - \bar{z}_{n1g} \\ \bar{z}_{ag} & \bar{z}_{bg} & \bar{z}_{cg} & \bar{z}_{n1g} & \bar{z}_{n2g} & \bar{z}_{gg} \end{bmatrix} \begin{bmatrix} I_{a(l)} \\ I_{b(l)} \\ I_{c(l)} \\ I_{n1(l)} \\ I_{n2(l)} \\ I_{g(l)} \end{bmatrix}$$

(A.7)

Replacing $\mathrm{I_{n1(l)}}$ by $\mathrm{I_{n1(l)} + I_{n2(l)}}$ and the replacing the fifth column by the difference between the fifth and fourth columns leaves the equations unchanged:

$$\begin{bmatrix} V_{aa'} \\ V_{bb'} \\ V_{cc'} \\ V_{n1n1'} \\ 0 \\ V_{gg'} \end{bmatrix} =$$

$$\begin{bmatrix} \bar{z}_{aa} & \bar{z}_{ab} & \bar{z}_{ac} & \bar{z}_{an1} & \bar{z}_{an2} - \bar{z}_{an1} & \bar{z}_{ag} \\ \bar{z}_{ab} & \bar{z}_{bb} & \bar{z}_{bc} & \bar{z}_{bn1} & \bar{z}_{bn2} - \bar{z}_{bn1} & \bar{z}_{bg} \\ \bar{z}_{ac} & \bar{z}_{bc} & \bar{z}_{cc} & \bar{z}_{cn1} & \bar{z}_{cn2} - \bar{z}_{cn1} & \bar{z}_{cg} \\ \bar{z}_{an1} & \bar{z}_{bn1} & \bar{z}_{cn1} & \bar{z}_{n1n1} & \bar{z}_{n1n2} - \bar{z}_{n1n1} & \bar{z}_{n1g} \\ \bar{z}_{an2} - \bar{z}_{an1} & \bar{z}_{bn2} - \bar{z}_{bn1} & \bar{z}_{cn2} - \bar{z}_{cn1} & \bar{z}_{n1n2} - \bar{z}_{n1n1} & \hat{z}_{n2n2} & \bar{z}_{n2g} - \bar{z}_{n1g} \\ \bar{z}_{ag} & \bar{z}_{bg} & \bar{z}_{cg} & \bar{z}_{n1g} & \bar{z}_{n2g} - \bar{z}_{n1g} & \bar{z}_{gg} \end{bmatrix} \begin{bmatrix} I_{a(l)} \\ I_{b(l)} \\ I_{c(l)} \\ I_{n1(l)} + I_{n2(l)} \\ I_{n2(l)} \\ I_{g(l)} \end{bmatrix}$$

(A.8)

where $\hat{z}_{n2n2} = \bar{z}_{n2n2} - \bar{z}_{n1n2} - \bar{z}_{n1n2} + \bar{z}_{n1n1}$

This matrix can be expressed in the form:

$$\begin{bmatrix} \Delta V_{abcng} \\ 0 \end{bmatrix} = \begin{bmatrix} \hat{z}_1 & \hat{z}_2 \\ \hat{z}_3 & \hat{z}_4 \end{bmatrix} \begin{bmatrix} I_{abcng(l)} \\ I_{n2(l)} \end{bmatrix} \tag{A.9}$$

This can be reduced to:

$$\Delta V_{abcng} = (\hat{z}_1 - \hat{z}_2 \cdot \hat{z}_4^{-1} \cdot \hat{z}_3) I_{abcng(l)} \tag{A.10}$$

where

$$\hat{z}_1 = \begin{bmatrix} \bar{z}_{aa} & \bar{z}_{ab} & \bar{z}_{ac} & \bar{z}_{an1} & \bar{z}_{ag} \\ \bar{z}_{ab} & \bar{z}_{bb} & \bar{z}_{bc} & \bar{z}_{bn1} & \bar{z}_{bg} \\ \bar{z}_{ac} & \bar{z}_{bc} & \bar{z}_{cc} & \bar{z}_{cn1} & \bar{z}_{cg} \\ \bar{z}_{an1} & \bar{z}_{bn1} & \bar{z}_{cn1} & \bar{z}_{n1n1} & \bar{z}_{n1g} \\ \bar{z}_{ag} & \bar{z}_{bg} & \bar{z}_{cg} & \bar{z}_{n1g} & \bar{z}_{gg} \end{bmatrix}$$

$$\hat{z}_2 = \begin{bmatrix} \bar{z}_{an2} - \bar{z}_{an1} \\ \bar{z}_{bn2} - \bar{z}_{bn1} \\ \bar{z}_{cn2} - \bar{z}_{cn1} \\ \bar{z}_{n1n2} - \bar{z}_{n1n1} \\ \bar{z}_{n2g} - \bar{z}_{n1g} \end{bmatrix}$$

$$\hat{z}_3 = [\bar{z}_{an2} - \bar{z}_{an1} \quad \bar{z}_{bn2} - \bar{z}_{bn1} \quad \bar{z}_{cn2} - \bar{z}_{cn1} \quad \bar{z}_{n1n2} - \bar{z}_{n1n1} \quad \bar{z}_{n2g} - \bar{z}_{n1g}]$$

$$\hat{z}_4 = \hat{z}_{n2n2}$$

A.2 Cable design data and calculated values

The calculations of the impedance matrices of a 95 sq. mm three-core cable with concentric neutral and a 95 sq. mm four-core cable with concentric neutral, which are both used in the thesis, are presented in three tables. Table A.1 identifies some of the cable design data typically available either from manufacturers or cable standards. Table A.2 presents the geometric mean distances and radii calculated from these data. These values were calculated using equations found in textbooks such as [51]. Then, from these values the 5 x 5 impedance matrices given in Table A.3, for both cables were found using equations (A.2) to (A.6).

	Three-core cable	Four-core cable
Overall cable dimensions		
Cable diameter, d_{cable}	**33.5 mm**	**37.5 mm**
Number of cores	**3**	**4**
Thickness of oversheath, t_{sheath}	**2.1 mm**	**2.2 mm**
Phase and neutral conductors (sector-shaped)		
Nominal cross-sectional area, x_{area}	**95 mm^2**	**95 mm^2**
Maximum DC resistance of phase and neutral wires	**0.32 Ω/km**	**0.32 Ω/km**
Average thickness of insulation	**1.1 mm**	**1.1 mm**
Sector depth, s_d *(taken from BS 3988* [84]*)*	**9.14 mm**	**10.35 mm**
Back radius, b_r *(taken from BS 3988* [84]*)*	**10.24 mm**	**12 mm**
Concentric ground and neutral wires		
Maximum DC resistance of concentric ground and neutral wires	**0.32 Ω/km**	**0.32 Ω/km**
Number of filaments, k	**22**	**22**
Radius of conductor filament, $r_{filament}$	**0.925 mm**	**0.925 mm**

Table A.1: Input data for cable impedances of the three-core and four-core cables.

Apart from the dimensions of the sector shaped conductors - b_r and s_d - which were taken from BS 3988, all other values given in Table A.1 came from a cable manufacturer's data sheet [80]. Approximations were however used to find the distance from the centre of the cable to the centres of:

- the phase and neutral conductors. (R_1)
- the filaments of the concentric neutral wire. (R_2)

These distances R_1 and R_2 were approximated using equations (A.11) and (A.12) respectively.

$$R_1 = (b_r - s_d) + (s_d/2) \quad \text{(A.11)}$$

$$R_2 = (d_{cable}/2) - t_{sheath} - r_{filament} \quad \text{(A.12)}$$

These distances are used to calculate the geometric mean distances, which are given by equations (A.13) and (A.14) for the four-core cable and by equation (A.15) for the three-core cable.

$$D_d = 2 \cdot R_1 \qquad \textit{(four-core only)} \qquad \text{(A.13)}$$

$$D_{hv} = \left(\sqrt{2}\right) \cdot R_1 \qquad \textit{(four-core only)} \qquad \text{(A.14)}$$

$$D_d = \left(\sqrt{3}\right) \cdot R_1 \qquad \textit{(three-core only)} \qquad \text{(A.15)}$$

D_{cng_cond} was found by taking the geometric mean of the distances of each conductor (in turn) to each surrounding concentric neutral filament.

Further, the geometric mean radii of the sector-shaped conductors were found by approximating them to solid round conductors using:

$$GMR_{cond} \approx 0.779 \cdot \left(r_{equiv}\right) \approx 0.779 \cdot \left(\sqrt{x_{area}/\pi}\right) \qquad \text{(A.16)}$$

The geometric mean radius of the concentric neutral (its filaments represented as a single conductor) were found using a standard formula normally applied with bundled conductors [51]:

$$GMR_{cng} = \sqrt[k]{GMR_{filament} \cdot k \cdot R_2^{k-1}} \qquad \text{(A.17)}$$

where $GMR_{filament} = 0.779 \cdot \left(r_{filament}\right)$

Table A.2 gives the values found from equations (A.11) to (A.17). The calculated 5 x 5 impedance matrices are shown in Table A.3 for the three-core and four-core cables.

	Three-core cable	Four-core cable
Approximated dimensions	**mm**	**mm**
Distance from centre of cable to centre of phase conductor, R_1	5.67	6.825
Distance from cable centre to centre of a filament, R_2	13.725	15.625
Geometric mean distances		
Horizontal or vertical separation between phase conductors, D_{hv}	-	9.652
Diagonal separation between phase conductors, D_d	9.821	13.650
Geometric mean distance between phase conductors and concentric neutral and ground wires, D_{cng_cond}	13.725	15.625
Geometric mean radii		
Geometric mean radius of phase and neutral conductors, GMR_{cond}	4.2838	4.2838
Geometric mean radius of concentric ground and neutral wires, GMR_{cng}	13.8152	15.6353

Table A.2: GMRs, GMDs and approximated distances for the three-core and four-core cables.

Cable C1 (three-core cable, Ω/km)

$$\begin{bmatrix} 0.3200 + 0.7873i & 0.7352i & 0.7352i & 0.7142i & 0.2672i \\ 0.7352i & 0.3200 + 0.7873i & 0.7352i & 0.7142i & 0.2672i \\ 0.7352i & 0.7352i & 0.3200 + 0.7873i & 0.7142i & 0.2672i \\ 0.7142i & 0.7142i & 0.7142i & 0.3200 + 0.7138i & 0.2672i \\ 0.2672i & 0.2672i & 0.2672i & 0.2672i & 0.0493 + 0.5193i \end{bmatrix}$$

Cable C2 (four-core cable, Ω/km)

$$\begin{bmatrix} 0.5855 + 0.2016i & 0.2655 + 0.1506i & 0.2655 + 0.1288i & 0.2655 + 0.1506i & 0.1005 + 0.0455i \\ 0.2655 + 0.1506i & 0.5855 + 0.2016i & 0.2655 + 0.1506i & 0.2655 + 0.1288i & 0.1005 + 0.0455i \\ 0.2655 + 0.1288i & 0.2655 + 0.1506i & 0.5855 + 0.2016i & 0.2655 + 0.1506i & 0.1005 + 0.0455i \\ 0.2655 + 0.1506i & 0.2655 + 0.1288i & 0.2655 + 0.1506i & 0.5855 + 0.2016i & 0.1005 + 0.0455i \\ 0.1005 + 0.0455i & 0.1005 + 0.0455i & 0.1005 + 0.0455i & 0.1005 + 0.0455i & 0.0874 + 0.4354i \end{bmatrix}$$

Table A.3: Cable impedance matrices for a three-core and a four-core cable.

This method was used to calculate the impedance matrices needed to model the rural feeder presented in chapter 6. The rural feeder model uses the cable C1 of Table A.3 as well as an overhead line (Figure 6.5) and ABC cable (Figure 6.7), both of which are given in Table A.4.

ABC overhead line cable shown in Figure 6.7 (Ω/km)

$$\begin{bmatrix} 0.3200 + 0.7863i & 0.7082i & 0.6864i & 0.7082i & 0.2672i \\ 0.7082i & 0.3200 + 0.7863i & 0.7082i & 0.6864i & 0.2672i \\ 0.6864i & 0.7082i & 0.3200 + 0.7863i & 0.7082i & 0.2672i \\ 0.7082i & 0.6864i & 0.7082i & 0.3200 + 0.7863i & 0.2672i \\ 0.2672i & 0.2672i & 0.2672i & 0.2672i & 0.0493 + 0.5193i \end{bmatrix}$$

Overhead line shown in Figure 6.5 (Ω/km)

$$\begin{bmatrix} 0.4312 + 0.8093i & 0.5629i & 0.5629i & 0.5193i & 0.2672i \\ 0.5629i & 0.4312 + 0.8093i & 0.5193i & 0.5629i & 0.2672i \\ 0.5629i & 0.5193i & 0.4312 + 0.8093i & 0.4939i & 0.2672i \\ 0.5193i & 0.5629i & 0.4939i & 0.4312 + 0.8093i & 0.2672i \\ 0.2672i & 0.2672i & 0.2672i & 0.2672i & 0.0493 + 0.5193i \end{bmatrix}$$

Table A.4: ABC Cable and overhead line impedance matrices for rural feeder

B. Results of KVL and KCL checks

The following sections, present the simulation results of the test network of Figure 3.12 for three sets of test input data. The results given in the tables of each section confirm that the proposed 5 x 5 approach passed the KVL and KCL checks. They were performed with convergence tolerances of P_{tol} set to 0.00005 W, Q_{tol} set to 0.00005 VAr, $Vmag_{tol}$ set to 0.00005 V and $Vang_{tol}$ set to 0.00005 °.

B.1 Test input data 1

Test input data 1 gives a network with balanced loads, balanced voltages at the start of the feeder, symmetric three-core cables and low earth resistances at the start and at the end of the feeder.

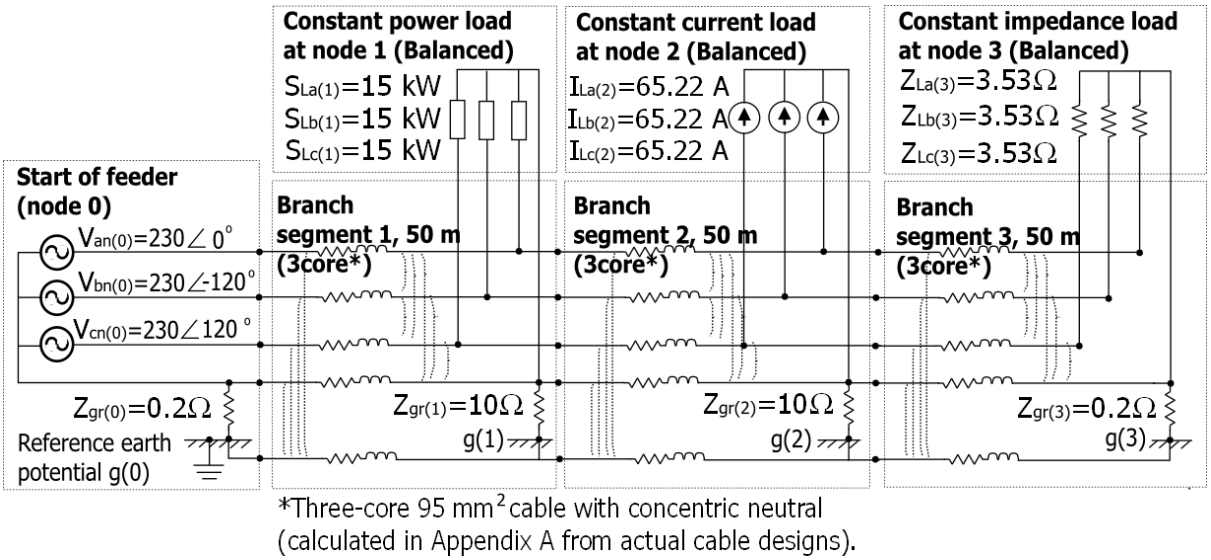

Figure B.1: Test network input data 1.

Results found using proposed 5 x 5 approach

KVL check

	Phase A loop	
	Mag (A)	Ang (°)
$-V_{an(0)}$	230	180
$-V_{ng(0)}$	0	0
$+V_{aa'(1)}$	3.15777	9.05840
$+V_{aa'(2)}$	2.08601	9.02269
$+V_{aa'(3)}$	1.02877	9.00136
$+V_{an(3)}$	223.80747	-0.25223
$+V_{ng(3)}$	0	0
$-V_{gg'(3)}$	0	0
$-V_{gg'(2)}$	0	0
$-V_{gg'(1)}$	0	0
Sum	0	0

Table B.1: KVL check of phase A loop (Test input data 1)

KCL check 1

	Branch segment 1		Branch segment 2		Branch segment 3	
	Mag (A)	Ang (°)	Mag (A)	Ang (°)	Mag (A)	Ang (°)
I_a	194.79255	-0.19495	128.67906	-0.23065	63.46168	-0.25199
I_b	194.79255	-120.19495	128.67906	-120.23065	63.46168	-120.25199
I_c	194.79255	119.80505	128.67906	119.76935	63.46168	119.74801
I_n	0	0	0	0	0	0
I_g	0	0	0	0	0	0
Sum	0	0	0	0	0	0

Table B.2: KCL check 1 of sum of branch currents (Test input data 1)

KCL check 2

	Node 1 a'			Node 1 b'	
	Mag (A)	Ang (°)		Mag (A)	Ang (°)
$I_{a(1)}$	194.79255	-0.19495	$I_{b(1)}$	194.79255	-120.19495
$-I_{La(1)}$	66.11356	179.87455	$-I_{Lb(1)}$	66.11356	59.87455
$-I_{a(2)}$	128.67906	179.76935	$-I_{b(2)}$	128.67906	59.76935
Sum	0	0	Sum	0	0
	Node 1 c'				
	Mag (A)	Ang (°)			
$I_{c(1)}$	194.79255	119.80505			
$-I_{Lc(1)}$	66.11356	-60.12545			
$-I_{c(2)}$	128.67906	-60.23065			
Sum	0	0			
	Node 1 n'			Node 1 g'	
	Mag (A)	Ang (°)		Mag (A)	Ang (°)
$I_{n(1)}$	0	0	$I_{g(2)}$	0	0
$-I_{Labc(1}$	0	0	$-I_{g(1)}$	0	0
$-I_{n(2)}$	0	0			
Sum	0	0	=	0	0

Table B.3: KCL check 2 of sum of phase, neutral and earth currents at node 1 (Test input data 1)

Results found using Matlab Simulink SimPowerSytems

KVL check

	Phase A loop	
	Mag (A)	Ang (°)
$-V_{an(0)}$	230	180
$-V_{ng(0)}$	0	0
$+V_{aa'(1)}$	3.15777	9.05840
$+V_{aa'(2)}$	2.08601	9.02269
$+V_{aa'(3)}$	1.02877	9.00136
$+V_{an(3)}$	223.80747	-0.25223
$+V_{ng(3)}$	0	0
$-V_{gg'(3)}$	0	0
$-V_{gg'(2)}$	0	0
$-V_{gg'(1)}$	0	0
Sum	0	0

Table B.4: KVL check of phase A loop (Test input data 1)

KCL check 1

	Branch segment 1		Branch segment 2		Branch segment 3	
	Mag (A)	Ang (°)	Mag (A)	Ang (°)	Mag (A)	Ang (°)
I_a	194.79255	-0.19495	128.67906	-0.23065	63.46168	-0.25199
I_b	194.79255	-120.19495	128.67906	-120.23065	63.46168	-120.25199
I_c	194.79255	119.80505	128.67906	119.76935	63.46168	119.74801
I_n	0	0	0	0	0	0
I_g	0	0	0	0	0	0
Sum	0.0	0	0	0	0	0

Table B.5: KCL check 1 of sum of branch currents (Test input data 1)

KCL check 2

	Node 1 a'			Node 1 b'	
	Mag (A)	Ang (°)		Mag (A)	Ang (°)
$I_{a(1)}$	194.79255	-0.19495	$I_{b(1)}$	194.79255	-120.19495
$-I_{La(1)}$	66.11356	179.87455	$-I_{Lb(1)}$	66.11356	59.87455
$-I_{a(2)}$	128.67906	179.76935	$-I_{b(2)}$	128.67906	59.76935
Sum	0	0	Sum	0	0
	Node 1 c'				
	Mag (A)	Ang (°)			
$I_{c(1)}$	194.79255	119.80505			
$-I_{Lc(1)}$	66.11356	-60.12545			
$-I_{c(2)}$	128.67906	-60.23065			
Sum	0	0			
	Node 1 n'			Node 1 g'	
	Mag (A)	Ang (°)		Mag (A)	Ang (°)
$I_{n(1)}$	0	0	$I_{g(2)}$	0	0
$-I_{Labc(1}$	0	0	$-I_{g(1)}$	0	0
$-I_{n(2)}$	0	0			
Sum	0	0	=	0	0

Table B.6: KCL check 2 of sum of phase, neutral and earth currents at node 1 (Test input data 1)

Computation times

	Computation time
Proposed 5 x 5 approach	**0.03 s**
Matlab Simulink SimPowerSystems	**5.34 s**

Table B.7: Computation times (Test input data 1)

B.2 Test input data 2

Test input data 2 reflects a more realistic network with unbalanced loads, unbalanced voltages at the start of the feeder, differing earth resistances and different cable types.

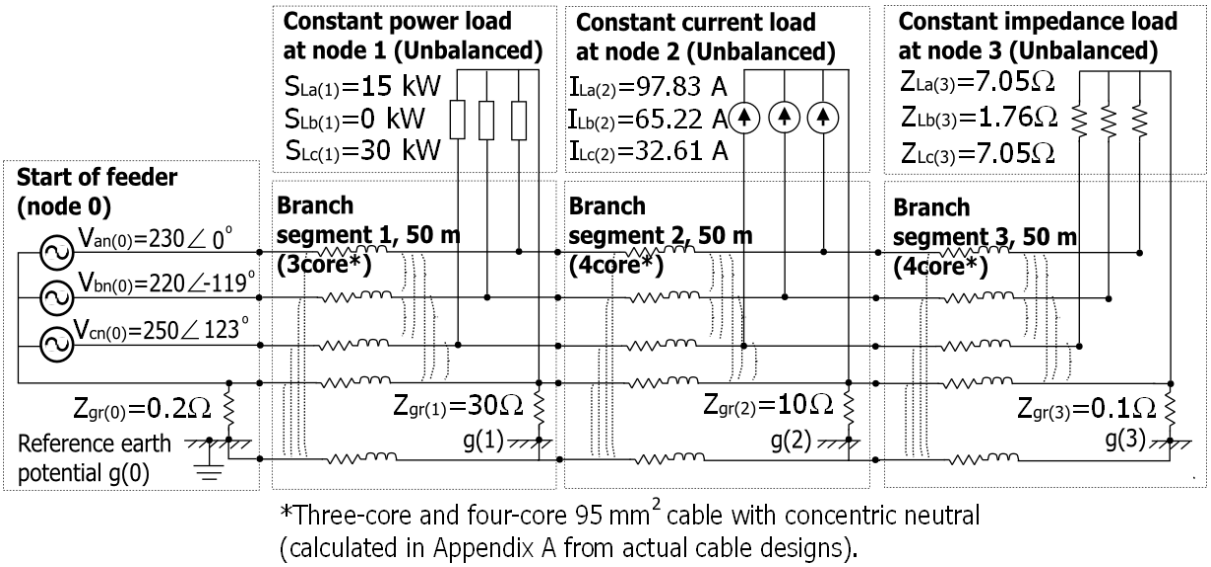

Figure B.2: Test network input data 2.

Results found using proposed 5 x 5 approach

KVL check

	Phase A loop	
	Mag (A)	Ang (°)
$-V_{an(0)}$	230	180
$-V_{ng(0)}$	1.64157	-102.50452
$+V_{aa'(1)}$	3.34496	8.20819
$+V_{aa'(2)}$	2.18317	7.96566
$+V_{aa'(3)}$	0.56823	2.93203
$+V_{an(3)}$	224.09796	0.43642
$+V_{ng(3)}$	0.83370	-103.22254
$-V_{gg'(3)}$	0.16203	-10.76471
$-V_{gg'(2)}$	0.16127	-10.51913
$-V_{gg'(1)}$	0.10543	-23.57672
Sum	0	0

Table B.8: KVL check of phase A loop (Test input data 2)

KCL check 1

	Branch segment 1		Branch segment 2		Branch segment 3	
	Mag (A)	Ang (°)	Mag (A)	Ang (°)	Mag (A)	Ang (°)
I_a	195.73147	0.09192	129.59771	0.22057	31.77192	0.43642
I_b	184.27030	-119.68714	184.27030	-119.68714	119.05309	-119.74645
I_c	189.24589	122.80681	67.74170	122.61339	35.13318	122.48771
I_n	8.19383	-116.93006	94.51953	92.18614	79.00354	55.85450
I_g	8.20785	77.49548	8.26748	77.55417	8.30678	77.30859
Sum	0	0	0	0	0	0

Table B.9: KCL check 1 of sum of branch currents (Test input data 2)

KCL check 2

	Node 1 a'			Node 1 b'	
	Mag (A)	Ang (°)		Mag (A)	Ang (°)
$I_{a(1)}$	195.73147	0.09192	$I_{b(1)}$	184.27030	-119.68714
$-I_{La(1)}$	66.13473	179.83982	$-I_{Lb(1)}$	0	0
$-I_{a(2)}$	129.59771	-179.77943	$-I_{b(2)}$	184.27030	60.31286
Sum	0	0	Sum	0	0
	Node 1 c'				
	Mag (A)	Ang (°)			
$I_{c(1)}$	189.24589	122.80681			
$-I_{Lc(1)}$	121.50479	-57.08536			
$-I_{c(2)}$	67.74170	-57.38661			
Sum	0	0			
	Node 1 n'			Node 1 g'	
	Mag (A)	Ang (°)		Mag (A)	Ang (°)
$I_{n(1)}$	8.19383	-116.93006	$I_{g(2)}$	8.26748	77.55417
$-I_{Labc(1)}$	101.81613	89.93804	$-I_{g(1)}$	8.20785	-102.50452
$-I_{n(2)}$	94.51953	-87.81386			
Sum	0.06022	85.57951	$=$	0.06022	85.57951

Table B.10: KCL check 2 of sum of phase, neutral and earth currents at node 1 (Test input data 2)

Results found using Matlab Simulink SimPowerSytems

KVL check

	Phase A loop	
	Mag (A)	Ang (°)
$-V_{an(0)}$	230.00000	180.00000
$-V_{ng(0)}$	1.64213	-102.65783
$+V_{aa'(1)}$	3.34484	8.19992
$+V_{aa'(2)}$	2.18296	7.96377
$+V_{aa'(3)}$	0.56803	2.92301
$+V_{an(3)}$	224.09697	0.43642
$+V_{ng(3)}$	0.83097	-102.84343
$-V_{gg'(3)}$	0.16209	-10.91673
$-V_{gg'(2)}$	0.16132	-10.67244
$-V_{gg'(1)}$	0.10547	-23.73003
Sum	0	0

Table B.11: KVL check of phase A loop (Test input data 2)

KCL check 1

	Branch segment 1		Branch segment 2		Branch segment 3	
	Mag (A)	Ang (°)	Mag (A)	Ang (°)	Mag (A)	Ang (°)
I_a	195.73096	0.09193	129.59729	0.22058	31.77178	0.43642
I_b	184.27091	-119.68734	184.27069	-119.68734	119.05339	-119.74668
I_c	189.24612	122.80690	67.74183	122.61355	35.13326	122.48790
I_n	8.20106	-117.06349	94.52238	92.19869	78.99330	55.86813
I_g	8.21065	77.34217	8.27030	77.40087	8.30967	77.15657
Sum	0	0	0	0	0	0

Table B.12: KCL check 1 of sum of branch currents (Test input data 2)

KCL check 2

	Node 1 a'			Node 1 b'	
	Mag (A)	Ang (°)		Mag (A)	Ang (°)
$I_{a(1)}$	195.73096	0.09193	$I_{b(1)}$	184.27091	-119.68734
$-I_{La(1)}$	66.13463	179.83983	$-I_{Lb(1)}$	0.00022	60.88383
$-I_{a(2)}$	129.59729	-179.77942	$-I_{b(2)}$	184.27069	60.31266
Sum	0	0	Sum	0	0
	Node 1 c'				
	Mag (A)	Ang (°)			
$I_{c(1)}$	189.24612	122.80690			
$-I_{Lc(1)}$	121.50489	-57.08530			
$-I_{c(2)}$	67.74183	-57.38645			
Sum	0	0			
	Node 1 n'			Node 1 g'	
	Mag (A)	Ang (°)		Mag (A)	Ang (°)
$I_{n(1)}$	8.20106	-117.06349	$I_{g(2)}$	8.27030	77.40087
$-I_{Labc(1)}$	101.81597	89.93824	$-I_{g(1)}$	8.21065	-102.65783
$-I_{n(2)}$	94.52238	-87.80131			
Sum	0.06025	85.42667	$=$	0.06025	85.42667

Table B.13: KCL check 2 of sum of phase, neutral and earth currents at node 1 (Test input data 2)

Computation times

	Computation time
Proposed 5 x 5 approach	0.27 s
Matlab Simulink SimPowerSystems	4.80 s

Table B.14: Computation times (Test input data 2)

B.3 Test input data 3

The test input data 3 was chosen to see if the proposed 5 x 5 approach would satisfy the KVL and KCL checks even with very unrealistic input data (very unbalanced voltages at start of feeder and unrealistic branch segment impedances as given in Table B.15).

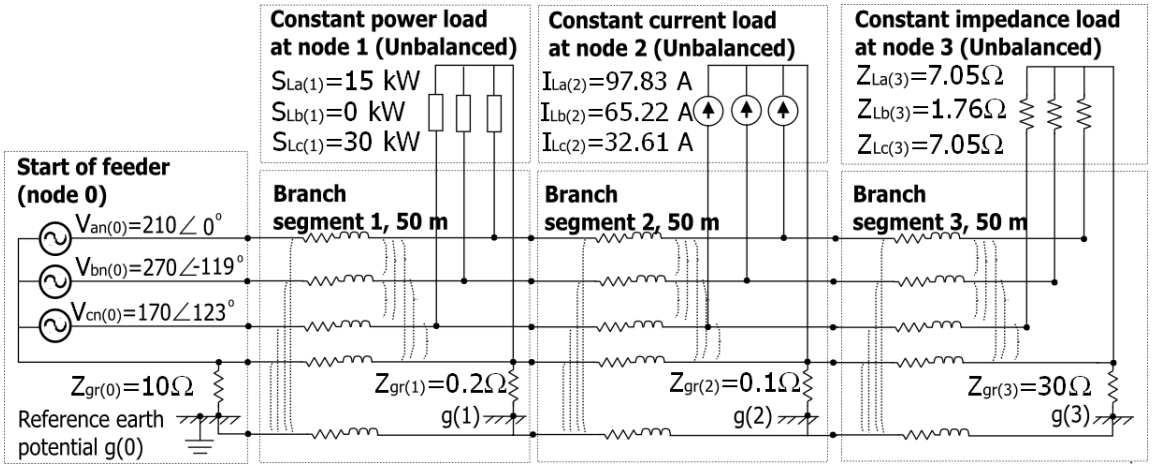

Figure B.3: Test network input data 3.

Branch segments 1 and 3
$\begin{bmatrix} 1 & 0 & 1 & 0 & 1 \\ 0 & 1 & 0 & 1 & 0 \\ 1 & 0 & 1 & 0 & 1 \\ 0 & 1 & 0 & 1 & 0 \\ 1 & 0 & 1 & 0 & 1 \end{bmatrix}$
Branch segment 2
$\begin{bmatrix} 2i & 0.5 & 0.5 & 0.5 & 1 \\ 0.5 & 2i & 0.5 & 0.5 & 1 \\ 0.5 & 0.5 & 2i & 0.5 & 1 \\ 0.5 & 0.5 & 0.5 & 2i & 1 \\ 1 & 1 & 1 & 1 & 2i \end{bmatrix}$

Table B.15: Branch segment impedances for test input data 3

Results found using proposed 5 x 5 approach

KVL check

	Phase A loop	
	Mag (A)	Ang (°)
$-V_{an(0)}$	210.00000	180.00000
$-V_{ng(0)}$	14.88905	35.41824
$+V_{aa'(1)}$	8.86183	75.43866
$+V_{aa'(2)}$	14.10984	100.26323
$+V_{aa'(3)}$	0.97602	52.22316
$+V_{an(3)}$	194.78059	-7.65193
$+V_{ng(3)}$	5.76967	-27.05414
$-V_{gg'(3)}$	0.97609	-127.78391
$-V_{gg'(2)}$	6.43388	70.03429
$-V_{gg'(1)}$	8.86197	-104.56771
Sum	0	0

Table B.16: KVL check of phase A loop (Test input data 3)

KCL check 1

	Branch segment 1		Branch segment 2		Branch segment 3	
	Mag (A)	Ang (°)	Mag (A)	Ang (°)	Mag (A)	Ang (°)
I_a	198.12176	-6.35059	125.44068	-7.26643	27.61540	-7.65193
I_b	221.91968	-126.62508	221.91968	-126.62508	156.70229	-126.62508
I_c	246.14951	127.87383	56.97696	128.34507	24.36912	128.70634
I_n	88.06272	4.28436	135.76532	52.36782	137.18702	53.53978
I_g	1.48891	-144.58176	57.54637	133.46923	0.19232	152.94588
Sum	0	0	0	0	0	0

Table B.17: KCL check 1 of sum of branch currents (Test input data 3)

KCL check 2

	Node 1 a'			Node 1 b'	
	Mag (A)	Ang (°)		Mag (A)	Ang (°)
$I_{a(1)}$	198.12176	-6.35059	$I_{b(1)}$	221.91968	-126.62508
$-I_{La(1)}$	72.72475	175.22924	$-I_{Lb(1)}$	0	0
$-I_{a(2)}$	125.44068	172.73357	$-I_{b(2)}$	221.91968	53.37492
Sum	0	0	Sum	0	0
	Node 1 c'				
	Mag (A)	Ang (°)			
$I_{c(1)}$	246.14951	127.87383			
$-I_{Lc(1)}$	189.17505	-52.26810			
$-I_{c(2)}$	56.97696	-51.65493			
Sum	0	0			
	Node 1 n'			Node 1 g'	
	Mag (A)	Ang (°)		Mag (A)	Ang (°)
$I_{n(1)}$	88.06272	4.28436	$I_{g(2)}$	57.54637	133.46923
$-I_{Labc(1)}$	149.95334	106.78200	$-I_{g(1)}$	1.48891	35.41824
$-I_{n(2)}$	135.76532	-127.63218			
Sum	57.35679	131.99641	=	57.35679	131.99641

Table B.18: KCL check 2 of sum of phase, neutral and earth currents at node 1 (Test input data 3)

Results found using Matlab Simulink SimPowerSytems

KVL check

	Phase A loop	
	Mag (A)	Ang (°)
$-V_{an(0)}$	210.00000	180.00000
$-V_{ng(0)}$	14.88905	35.41825
$+V_{aa'(1)}$	8.86184	75.43867
$+V_{aa'(2)}$	14.10984	100.26321
$+V_{aa'(3)}$	0.97602	52.22320
$+V_{an(3)}$	194.78058	-7.65193
$+V_{ng(3)}$	5.76968	-27.05415
$-V_{gg'(3)}$	0.97609	-127.78390
$-V_{gg'(2)}$	6.43388	70.03425
$-V_{gg'(1)}$	8.86198	-104.56771
Sum	0	0

Table B.19: KVL check of phase A loop (Test input data 3)

KCL check 1

	Branch segment 1		Branch segment 2		Branch segment 3	
	Mag (A)	Ang (°)	Mag (A)	Ang (°)	Mag (A)	Ang (°)
I_a	198.12176	-6.35059	125.44068	-7.26643	27.61540	-7.65193
I_b	221.91993	-126.62508	221.91967	-126.62509	156.70228	-126.62509
I_c	246.14951	127.87382	56.97696	128.34506	24.36912	128.70634
I_n	88.06285	4.28448	135.76529	52.36782	137.18700	53.53978
I_g	1.48891	-144.58173	57.54634	133.46922	0.19232	152.94585
Sum	0	0	0	0	0	0

Table B.20: KCL check 1 of sum of branch currents (Test input data 3)

KCL check 2

	Node 1 a'			Node 1 b'	
	Mag (A)	Ang (°)		Mag (A)	Ang (°)
$I_{a(1)}$	198.12176	-6.35059	$I_{b(1)}$	221.91993	-126.62508
$-I_{La(1)}$	72.72475	175.22924	$-I_{Lb(1)}$	0.00027	60.95713
$-I_{a(2)}$	125.44068	172.73357	$-I_{b(2)}$	221.91967	53.37491
Sum	0	0	Sum	0	0
	Node 1 c'				
	Mag (A)	Ang (°)			
$I_{c(1)}$	246.14951	127.87382			
$-I_{Lc(1)}$	189.17506	-52.26811			
$-I_{c(2)}$	56.97696	-51.65494			
Sum	0	0			
	Node 1 n'			Node 1 g'	
	Mag (A)	Ang (°)		Mag (A)	Ang (°)
$I_{n(1)}$	88.06285	4.28448	$I_{g(2)}$	57.54634	133.46922
$-I_{Labc(1)}$	149.95315	106.78207	$-I_{g(1)}$	1.48891	35.41827
$-I_{n(2)}$	135.76529	-127.63218			
Sum	57.35676	131.99640	$=$	57.35676	131.99640

Table B.21: KCL check 2 of sum of phase, neutral and earth currents at node 1 (Test input data 3)

Computation times

	Computation time
Proposed 5 x 5 approach	**0.01 s**
Matlab Simulink SimPowerSystems	**4.82 s**

Table B.22: Computation times (Test input data 3)

C. Direct matrix solutions

C.1 Direct matrix solution of representative low-voltage network with constant impedance loads

The voltages at the end of the representative low-voltage feeder shown in Figure C.1 can be solved once the currents flowing on the branch segment 1 are known. This can be done directly given 1) the phase-neutral voltages at the start of the feeder and 2) the impedances of the loads at the end of the feeder. The direct solution involves finding an expression for the phase-neutral voltages at the start of the feeder in terms of the network impedances and currents flowing on the branch segment 1. The following gives the derivation of this expression in three parts: 1) start of the feeder, 2) the branch segment 1 and 3) the end of the feeder.

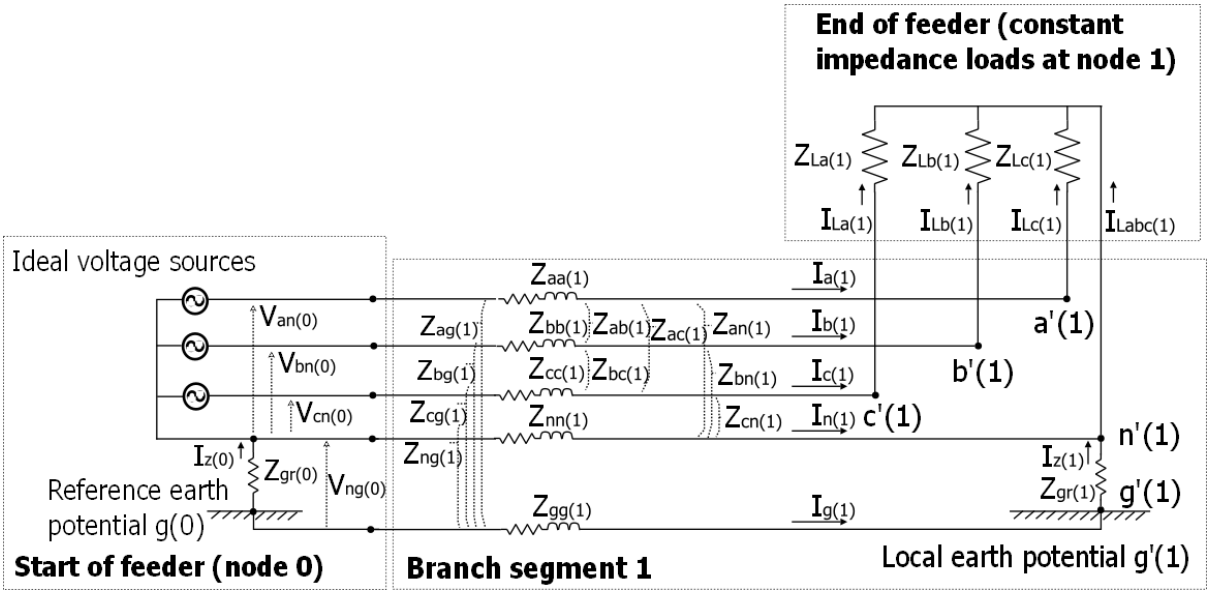

Figure C.1: An representative low-voltage network with constant impedance loads

C.1.1 Start of the feeder

The phase-ground voltages are expressed in terms of the phase-neutral voltages by:

$$\begin{bmatrix} V_{ag(0)} \\ V_{bg(0)} \\ V_{cg(0)} \\ V_{ng(0)} \end{bmatrix} = \begin{bmatrix} V_{an(0)} \\ V_{bn(0)} \\ V_{cn(0)} \\ 0 \end{bmatrix} + \begin{bmatrix} V_{ng(0)} \\ V_{ng(0)} \\ V_{ng(0)} \\ V_{ng(0)} \end{bmatrix} \quad \text{(C.1)}$$

But as $V_{ng} = I_{g(1)} Z_{gr(0)}$ and $I_{g(1)} = -\left(I_{a(1)} + I_{b(1)} + I_{c(1)} + I_{n(1)}\right)$ (Kirchhoff's current law), this can be expressed as:

$$\begin{bmatrix} V_{ag(0)} \\ V_{bg(0)} \\ V_{cg(0)} \\ V_{ng(0)} \end{bmatrix} = \begin{bmatrix} V_{an(0)} \\ V_{bn(0)} \\ V_{cn(0)} \\ 0 \end{bmatrix} - \left[Z'_{gr(0)}\right] \begin{bmatrix} I_{a(1)} \\ I_{b(1)} \\ I_{c(1)} \\ I_{n(1)} \end{bmatrix} \quad \text{(C.2)}$$

where:

$$\left[Z'_{gr(0)}\right] = Z_{gr(0)} \begin{bmatrix} 1 & 1 & 1 & 1 \\ 1 & 1 & 1 & 1 \\ 1 & 1 & 1 & 1 \\ 1 & 1 & 1 & 1 \end{bmatrix}$$

C.1.2 The branch segment 1

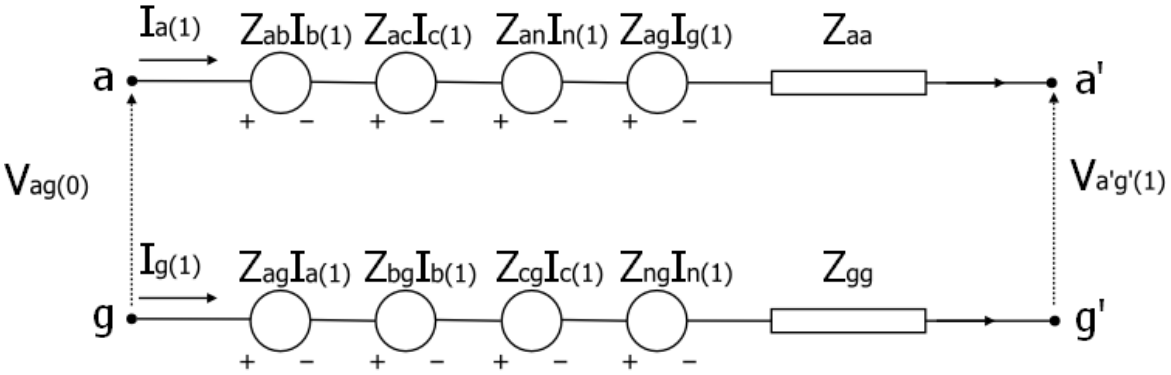

Figure C.2: Loop circuit formed of phase A and assumed ground wire

Looking at the loop circuit shown in Figure C.2 for the voltages induced on phase A and assumed ground wires and applying Kirchhoff's voltage law:

$$V_{ag(0)} = V_{aa'(1)} + V_{a'g'(1)} - V_{gg'(1)} \quad \text{(C.3)}$$

$$V_{ag(0)} = Z_{aa} I_{a(1)} + Z_{ab} I_{b(1)} + Z_{ac} I_{c(1)} + Z_{an} I_{n(1)} + Z_{ag} I_{g(1)} + V_{a'g'(1)} - \left(Z_{ag} I_{a(1)} + Z_{bg} I_{b(1)} + Z_{cg} I_{c(1)} + Z_{ng} I_{n(1)} + Z_{gg} I_{g(1)}\right) \quad \text{(C.4)}$$

Using Kirchhoff's current law ($I_{a(1)} + I_{b(1)} + I_{c(1)} + I_{n(1)} + I_{g(1)} = 0$) to eliminate $I_{g(1)}$ gives:

$$V_{ag(0)} = (Z_{aa} - 2Z_{ag} + Z_{gg})I_{a(1)} + (Z_{ab} - Z_{ag} - Z_{bg} + Z_{gg})I_{b(1)} + (Z_{ac} - Z_{ag} - Z_{cg} + Z_{gg})I_{c(1)} + (Z_{an} - Z_{ag} - Z_{ng} + Z_{gg})I_{n(1)} + V_{a'g'(1)} \quad \text{(C.5)}$$

Similarly for phases B, C and neutral:

$$V_{bg(0)} = (Z_{ab} - Z_{ag} - Z_{bg} + Z_{gg})I_{a(1)} + (Z_{bb} - 2Z_{bg} + Z_{gg})I_{b(1)} + (Z_{bc} - Z_{bg} - Z_{cg} + Z_{gg})I_{c(1)} + (Z_{bn} - Z_{bg} - Z_{ng} + Z_{gg})I_{n(1)} + V_{b'g'(1)} \quad \text{(C.6)}$$

$$V_{cg(0)} = (Z_{ac} - Z_{ag} - Z_{cg} + Z_{gg})I_{a(1)} + (Z_{bc} - Z_{bg} - Z_{cg} + Z_{gg})I_{b(1)} + (Z_{cc} - 2Z_{cg} + Z_{gg})I_{c(1)} + (Z_{cn} - Z_{cg} - Z_{ng} + Z_{gg})I_{n(1)} + V_{c'g'(1)} \quad \text{(C.7)}$$

$$V_{ng(0)} = (Z_{an} - Z_{ag} - Z_{ng} + Z_{gg})I_{a(1)} + (Z_{bn} - Z_{bg} - Z_{ng} + Z_{gg})I_{b(1)} + (Z_{cn} - Z_{cg} - Z_{ng} + Z_{gg})I_{c(1)} + (Z_{nn} - 2Z_{ng} + Z_{gg})I_{n(1)} + V_{n'g'(1)} \quad \text{(C.8)}$$

This can be written in matrix form:

$$\begin{bmatrix} V_{ag(0)} \\ V_{bg(0)} \\ V_{cg(0)} \\ V_{ng(0)} \end{bmatrix} - \begin{bmatrix} V_{a'g'(1)} \\ V_{b'g'(1)} \\ V_{c'g'(1)} \\ V_{n'g'(1)} \end{bmatrix} = [Z'_{abcn}] \begin{bmatrix} I_{a(1)} \\ I_{b(1)} \\ I_{c(1)} \\ I_{n(1)} \end{bmatrix} \quad \text{(C.9)}$$

where the elements of $[Z'_{abcn}]$ are given by:

$$Z_{pq} = (Z_{pq} - Z_{pg} - Z_{qg} + Z_{gg})$$

$$p, q = a, b, c, n$$

C.1.3 End of the feeder

The phase-ground voltages expressed in terms of the phase-neutral voltages are given by:

$$\begin{bmatrix} V_{a'g'(1)} \\ V_{b'g'(1)} \\ V_{c'g'(1)} \\ V_{n'g'(1)} \end{bmatrix} = \begin{bmatrix} V_{a'n'(1)} \\ V_{b'n'(1)} \\ V_{c'n'(1)} \\ 0 \end{bmatrix} + \begin{bmatrix} V_{n'g'(1)} \\ V_{n'g'(1)} \\ V_{n'g'(1)} \\ V_{n'g'(1)} \end{bmatrix} \quad \text{(C.10)}$$

Now the phase-neutral voltages are given in terms of the load impedances by:

$$\begin{bmatrix} V_{a\prime n\prime(1)} \\ V_{b\prime n\prime(1)} \\ V_{c\prime n\prime(1)} \\ 0 \end{bmatrix} = \begin{bmatrix} Z_{La(1)} & 0 & 0 & 0 \\ 0 & Z_{Lb(1)} & 0 & 0 \\ 0 & 0 & Z_{Lc(1)} & 0 \\ 0 & 0 & 0 & 0 \end{bmatrix} \begin{bmatrix} I_{a(1)} \\ I_{b(1)} \\ I_{c(1)} \\ I_{n(1)} \end{bmatrix} \quad \text{(C.11)}$$

Also since $V_{n\prime g\prime(1)} = -I_{g(1)}Z_{gr(1)}$ and $I_{g(1)} = -\left(I_{a(1)} + I_{b(1)} + I_{c(1)} + I_{n(1)}\right)$ (Kirchhoff's current law), equation (C.11) can be expressed as:

$$\begin{bmatrix} V_{a\prime g\prime(1)} \\ V_{b\prime g\prime(1)} \\ V_{c\prime g\prime(1)} \\ V_{n\prime g\prime(1)} \end{bmatrix} = \left[Z'_{Labcgr(1)}\right] \begin{bmatrix} I_{a(1)} \\ I_{b(1)} \\ I_{c(1)} \\ I_{n(1)} \end{bmatrix} \quad \text{(C.12)}$$

where:

$$\left[Z'_{Labcgr(1)}\right] = \begin{bmatrix} Z_{La(1)} + Z_{gr(1)} & Z_{gr(1)} & Z_{gr(1)} & Z_{gr(1)} \\ Z_{gr(1)} & Z_{Lb(1)} + Z_{gr(1)} & Z_{gr(1)} & Z_{gr(1)} \\ Z_{gr(1)} & Z_{gr(1)} & Z_{Lc(1)} + Z_{gr(1)} & Z_{gr(1)} \\ Z_{gr(1)} & Z_{gr(1)} & Z_{gr(1)} & Z_{gr(1)} \end{bmatrix}$$

C.1.4 Direct solution of branch currents

Substituting equations (C.2) and (C.12) into (C.9) gives:

$$\begin{bmatrix} V_{an(0)} \\ V_{bn(0)} \\ V_{cn(0)} \\ 0 \end{bmatrix} - \left[Z'_{gr(0)}\right] \begin{bmatrix} I_{a(1)} \\ I_{b(1)} \\ I_{c(1)} \\ I_{n(1)} \end{bmatrix} - \left[Z'_{Labcgr(1)}\right] \begin{bmatrix} I_{a(1)} \\ I_{b(1)} \\ I_{c(1)} \\ I_{n(1)} \end{bmatrix} = \left[Z'_{abcn}\right] \begin{bmatrix} I_{a(1)} \\ I_{b(1)} \\ I_{c(1)} \\ I_{n(1)} \end{bmatrix}$$

$$\begin{bmatrix} V_{an(0)} \\ V_{bn(0)} \\ V_{cn(0)} \\ 0 \end{bmatrix} = \left[Z'_{gr(0)} + Z'_{abcn} + Z'_{Labcgr(1)}\right] \begin{bmatrix} I_{a(1)} \\ I_{b(1)} \\ I_{c(1)} \\ I_{n(1)} \end{bmatrix} \quad \text{(C.13)}$$

Using equation (C.13) the branch currents can be found.

C.1.5 Direct solution of voltages at the end of the feeder

Firstly, the branch currents are used to find the phase-ground voltages at the start of the feeder. This is found using equation (C.2). Following this, the voltages at the end of the feeder can be found with reference to the ground g at the start of the feeder by:

$$\begin{bmatrix} V_{a'g(1)} \\ V_{b'g(1)} \\ V_{c'g(1)} \\ V_{n'g(1)} \\ V_{g'g(1)} \end{bmatrix} = \begin{bmatrix} V_{ag(0)} \\ V_{bg(0)} \\ V_{cg(0)} \\ V_{ng(0)} \\ 0 \end{bmatrix} - [Z_{abcng}] \begin{bmatrix} I_{a(1)} \\ I_{b(1)} \\ I_{c(1)} \\ I_{n(1)} \\ -(I_{a(1)} + I_{b(1)} + I_{c(1)} + I_{n(1)}) \end{bmatrix} \quad \text{(C.14)}$$

where $[Z_{abcng}]$ is the primitive 5 x 5 impedance matrix for the branch segment 1 given by:

$$[Z_{abcng}] = \begin{bmatrix} Z_{aa} & Z_{ab} & Z_{ac} & Z_{an} & Z_{ag} \\ Z_{ab} & Z_{bb} & Z_{bc} & Z_{bn} & Z_{bg} \\ Z_{ac} & Z_{bc} & Z_{cc} & Z_{cn} & Z_{cg} \\ Z_{an} & Z_{bn} & Z_{cn} & Z_{nn} & Z_{ng} \\ Z_{ag} & Z_{bg} & Z_{cg} & Z_{ng} & Z_{gg} \end{bmatrix}$$

C.2 Direct matrix solution of representative low-voltage network with constant current loads

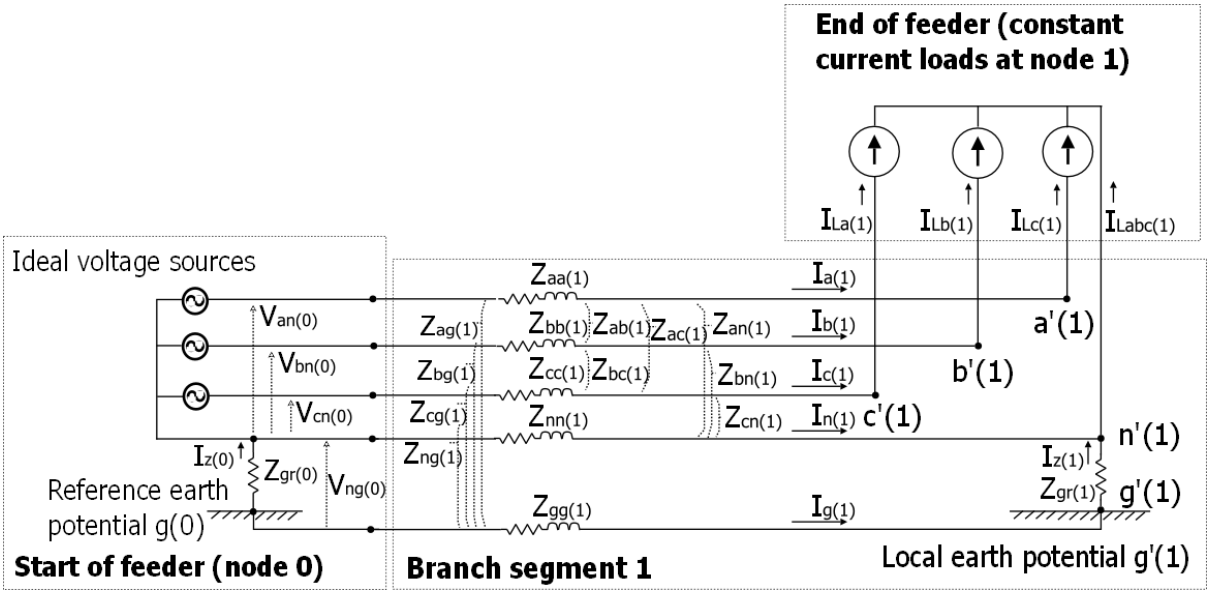

Figure C.3: Representative low-voltage feeder with constant current loads

C.2.1 Direct solution of branch currents

On the phase wires, the branch currents equal the load currents:

$$I_{a(1)} = I_{La(1)}, I_{b(1)} = I_{Lb(1)}, I_{c(1)} = I_{Lc(1)} \quad \text{(C.15)}$$

The sharing of the out-of-balance current between the neutral and ground wires can be found directly by applying all the conditions of equation (3.24) to equation (3.23). For the neutral wire, this gives:

$$I_{n(1)} = \frac{-[(Z'_{an}+Z_{gr(1)}+Z_{gr(0)})I_{a(1)}+(Z'_{bn}+Z_{gr(1)}+Z_{gr(0)})I_{b(1)}+(Z'_{cn}+Z_{gr(1)}+Z_{gr(0)})I_{c(1)}]}{(Z'_{nn}+Z_{gr(1)}+Z_{gr(0)})} \quad \text{(C.16)}$$

where $Z'_{pn} = Z_{pn(1)} - Z_{pg(1)} - Z_{ng(1)} + Z_{gg(1)}; p = a, b, c, n$

Substituting equation (C.15) into equation (C.16) and including $I_{g(1)} = -\big(I_{a(1)} + I_{b(1)} + I_{c(1)} + I_{n(1)}\big)$, the branch currents can be found directly by:

$$\begin{bmatrix} I_{a(1)} \\ I_{b(1)} \\ I_{c(1)} \\ I_{n(1)} \\ I_{g(1)} \end{bmatrix} =$$

$$\begin{bmatrix} 1 & 0 & 0 \\ 0 & 1 & 0 \\ 0 & 0 & 1 \\ \frac{-(Z'_{an}+Z_{gr(1)}+Z_{gr(0)})}{(Z'_{nn}+Z_{gr(1)}+Z_{gr(0)})} & \frac{-(Z'_{bn}+Z_{gr(1)}+Z_{gr(0)})}{(Z'_{nn}+Z_{gr(1)}+Z_{gr(0)})} & \frac{-(Z'_{cn}+Z_{gr(1)}+Z_{gr(0)})}{(Z'_{nn}+Z_{gr(1)}+Z_{gr(0)})} \\ \frac{(Z'_{an}+Z_{gr(1)}+Z_{gr(0)})}{(Z'_{nn}+Z_{gr(1)}+Z_{gr(0)})} - 1 & \frac{(Z'_{bn}+Z_{gr(1)}+Z_{gr(0)})}{(Z'_{nn}+Z_{gr(1)}+Z_{gr(0)})} - 1 & \frac{(Z'_{cn}+Z_{gr(1)}+Z_{gr(0)})}{(Z'_{nn}+Z_{gr(1)}+Z_{gr(0)})} - 1 \end{bmatrix} \begin{bmatrix} I_{La(1)} \\ I_{Lb(1)} \\ I_{Lc(1)} \end{bmatrix}$$

(C.17)

C.2.2 Direct solution of voltages at the end of the feeder

With the branch currents found by equation (C.17), the voltages at the end of the feeder can be found with reference to the ground g at the start of the feeder using equation (C.14) as before.